THE SIMULATION OF TRANSPORT AND DIFFUSION PROCESSES USING NETWORK THERMODYNAMICS AND BOND GRAPH TECHNIQUES

A thesis submitted to The University of Glasgow
for the degree of Ph.D.

by

David Albert Williams.

Faculty of Science.
Chemistry Department.

September 1988.

CONTENTS

ACKNOWLEDGEMENTS

I would like to thank the following for their support and invaluable assistance in the course of this research:

Dr Russell Paterson for excellent supervision, encouragement and patience, all of which have helped to make this a most enjoyable and stimulating period of study.

My colleagues, in particular Sam McFadzean, Donald Young and Ann Smith for giving every possible assistance from the outset.

My family for their understanding and practical support.

I would also like to thank Prof. Graham, Dr McNeill (both University of Strathclyde) and Prof. Spiro (Imperial College) for their help in providing useful information and discussion on swelling-diffusion systems.

Thanks are also due to the staff of the University of Glasgow for their friendly cooperation.

Finally I must acknowledge financial support in the form of a quota award from the Science and Engineering Research Council.

LIST OF SYMBOLS

ROMAN SYMBOLS

A	Chemical affinity. Chapter 1.
A	Area.
A_j	Local area of a lump. Chapter 4.
A_o	Dry area. Chapter 4.
a, b	Exchanging ions, also used as subscripts. Chapter 3.
C	Capacitance.
c	Solution concentration.
$\bar{c}$	Concentration within diffusing medium.
c_a, c_b	Concentrations of ions a and b respectively. Chapter 3.
$\bar{c}_a$, $\bar{c}_b$	Concentrations of ions a and b in exchanger respectively. Chapter 3.
$\bar{c}_f$	Concentration of fixed charge within resin. Chapter 3.
c_o	Initial concentration.
c_{se}	Source effort concentration Chapter 6.
c_s	Concentration at saturation. Chapter 6.
D	Diffusion coefficient.
D^j	Local diffusion coefficient. Chapter 4.
D_a, D_b	Self diffusion coefficients of ions a and b respectively. Chapter 3.
D_{ab}	Mutual diffusion coefficient. Chapter 3.
D^j_{ab}	Local mutual diffusion coefficient in a lump. Chapter 3.
D^*	Intrinsic diffusion coefficient of solute in non-tortuous medium. Chapter 4.
D_s	Diffusion coefficient from steady state measurements Chapter 6.

D_L	Diffusion coefficient from time lag. Chapter 6.
d	Depth.
e	Effort.
F	The Faraday. Chapter 3.
f	Flow.
f_q, f_i, f_v, f_r	Flows of heat, matter, volume, and chemical reaction rate. Chapter 1.
f_s	Fractional swelling. Chapter 4.
f_s^o	Fractional swelling at centre of membrane. Chapter 4.
f_m	Maximum fractional swelling. Chapter 4.
H	Step time for integration.
$I_1()$, $K_1()$	Modified Bessel functions. Chapter 6.
i	Electric current. Chapter 1.
J	Flux.
J_a, J_b	Flux of ions a and b. Chapter 3.
$J_o()$	Bessel function. Chapter 2.
J_o	Theoretical flux for no edge. Chapter 6.
j	Lump number, also used as subscript. Chapters 1-4.
K'^a_b	Molar selectivity coefficient. Chapter 3.
K, K_c, K_p	Rates in kinetic models of swelling. Chapter 4.
L	Conductance. Chapter 1.
l	Length or thickness.
l_j	Local thickness of a lump. Chapter 4.
l_o	Dry membrane thickness. Chapter 4.
l_d	Thickness of dry membrane remaining. Chapter 4.
m_1, m_2	Coefficients in state space equations.
$\bar{N}_a$, $\bar{N}_b$	Mole fractions of ions a and b in exchanger respectively. Chapter 3.

N_x, N_y	Number of lumps in R-C plane model of Universe. Chapter 5.
N_x, N_y, N_z	Number of lumps in R-C network model of Universe. Chapter 6.
n	Number of moles. Chapter 2.
n	Reticulation number. Chapters 2-4.
n_c	Number of rows of lumps modelling clamped region (edge effect). Chapter 6.
n_s	Number of fully swollen lumps. Chapter 4.
n_x, n_y, n_z	Degrees of reticulation in x, y and z directions respectively. Chapters 5-7.
P	Pressure. Chapter 1.
q	Charge.
q_j	Charge in lump j. Chapters 2-4.
q_o	Initial loading in uniformly loaded polymer.
$q_{x,y}$	Charge in 2D model. Chapters 5-6.
$q_{x,y,z}$	Charge in 3D model. Chapter 7.
R	The Gas Constant. Chapter 3.
R	Resistance.
R_j	Bond graph resistance. Chapters 2-4.
$R_{x,y}$	2D bond graph resistance. Chapter 5.
$R_{x,y,z}$	3D bond graph resistance. Chapter 7.
r	Radius.
r_e	Radius of exposed face Chapter 6.
r_j	Radius to volume centre of lump j.
r^e_j	Radius of outer edge of lump j.
r^e_y	Radius to outer edge of lump y (for all values of x,y). Chapter 6.
r_o	Total radius of sphere or cylinder.
r_y	Radius to volume centre of lump y (for all values of x,y). Chapters 5-6.
r'_o, r'_e	Parameters, $\pi r_o/l$, $\pi r_e/l$. Chapter 6.

S	Entropy. Chapter 1.
S	Summation to infinity. Chapter 6.
dS_e	Entropy change due to reversible exchanges. Chapter 1.
dS_i	Entropy change due to irreversible processes. Chapter 1.
T	Temperature. Chapters 1 and 3.
t	Time
t_c	Time for penetrating water fronts to meet in centre. Chapter 4.
t_L	Time lag. Chapter 6.
V	Volume of system.
V_o	Dry volume of membrane. Chapter 4.
v	Volume of a lump.
v_e	Volume of external solution. Chapter 3.
v_r	Volume enclosed by radius r.
v_o	Dry volume of a lump. Chapter 4.
v_w	Volume fraction of water. Chapter 4.
w	Empirical constant in Kielland's equation. Chapter 3.
w	Total width of sheet. Chapter 6.
w_e	Half width of exposed sheet face. Chapter 6.
x	Axis of diffusion.
z	Factor of increase in each dimension. Chapter 4.
z_a, z_b	Signed valencies of ions a and b respectively. Chapter 3

GREEK SYMBOLS

α	Distribution coefficient.
β_k	Bessel function roots. Chapters 2 and 5.
γ_a, γ_b	Activity coefficients of ions a and b respectively. Chapter 3.

Δ	Indicating a step.
Φ	Dissipation function. Chapter 1.
θ	Tortuosity factor. Chapter 4.
$N_{\kappa}{}^{a}{}_{b}$	Rational thermodynamic equilibrium constant. Chapter 3.
μ	Chemical potential. Chapters 1 and 2.
ψ	Electric potential. Chapter 1.
Σ	Summation sign.
σ	Rate of change of entropy. Chapter 1.
τ	Dimensionless time parameter. Chapter 3.
ν_a, ν_b	Stoicheometric coefficients of ions a and b respectively. Chapter 3.

SUMMARY

A theoretical framework for the computer simulation of all uncoupled diffusion processes was developed using network thermodynamics and bond graph techniques. Applications in the areas of membrane science and drug diffusion studies are illustrated.

A new method of numerical analysis based on the bond graph model was developed employing a single exponential function. This was tested for several simple linear one dimensional diffusion problems.

This method of integration was then used to produce computer simulations of ion exchange diffusion and swelling-diffusion systems based on non-linear bond graph models.

A bond graph model for two dimensional diffusion was developed and validated for plane sheet diffusion and release from a limited cylinder. Several useful applications of these models are illustrated.

A bond graph model for the simulation of three dimensional diffusion processes was also developed, therefore allowing the quantitative study of diffusion systems with complete assymetry. This bond graph model was tested for the simple example of diffusion from a cube.

INTRODUCTION.

Many diffusion problems are, in mathematical terms, extremely complex. The mathematics of diffusion are dependant on the strict definition of the boundary conditions in addition to the initial concentrations within the system, [1]. As a result most problems can only be solved for certain simple boundary conditions and initial concentration profiles, which must be uniform or at least smooth. Mathematical solutions are therefore specific for a set of strictly defined conditions and are limited to that application. Any modification of these requires reformulation of the mathematics. For some problems, approximate solutions are available, [1], [2], these are still limited to the description of one particular system.

The study of complex diffusion phenomena, which cannot be solved mathematically, is aided by numerical analysis. This has been facilitated in recent years by the advent of powerful desktop micro computers and high level computer languages, reducing the restrictions of computation time and programming effort. These are characteristically applied to isolated problems and are therefore extremely inflexible and typically of an **ad hoc** nature.

The major aim of this research was to develop a flexible theoretical framework for the computer simulation of all uncoupled chemical diffusion systems. This required that the computer models be able to simulate diffusion systems, including non-linear phenomena, of any geometry, with no restrictions on the initial and boundary conditions.

The methods developed in this thesis for solving diffusion problems are based on the description of the system using network thermodynamics and the bond graph technique. Network thermodynamics is a rigorous discipline that can be used to describe all non-steady behaviour and as it incorporates the theories of reversible and non-equilbrium thermodynamics, it also reproduces the results predicted by these for equilibrium and steady states, [3], [4], [5]. The bond graph, using the methods of Paynter, [6], is a technique for representing the network thermodynamic model, and is used as a basis for computer simulation of the system dynamics. These are therefore also referred to as bond graph models. The bond graph is an extremely flexible tool and so these modelling techniques are extremely convenient and powerful.

The theory required to produce a bond graph model of uncoupled diffusion is discussed in Chapter 1, in which the concepts of the generalised resistor and capacitor are introduced. In addition, a new method for numerical analysis based on the bond graph model is developed using a single exponential function. This technique was successfully tested for the 'C-C' bond graph model of one dimensional Fickian diffusion, the results are given in Chapter 2.

In Chapters 3 to 7, methods for using bond graph modelling techniques to solve non-linear and 2D and 3D diffusion problems are developed. The examples presented in these chapters illustrate the lack of restrictions on system geometry and boundary conditions. Specifically, the topic of Chapter 3 is bi-ionic exchange diffusion which

serves to develop the C-C bond graph model for non-linear diffusion coefficients and variable selectivity. The problem of bi-ionic non-isotopic exchange is one for which an **ad hoc** numerical analysis has been applied previously for a simple example, [7]. The bond graph model was shown to reproduce these results and a variety of more complex boundary conditions were considered, these are presented in Chapter 3.

Chapter 4 examines the most complex boundary conditions possible in the development of a computer model of drug release from a swelling polymer membrane. In these problems the local dimensions and the diffusion coefficient are both functions of time and position. This was a potentially useful application of bond graph modelling since release devices employing these functions are currently being designed as highly reliable vehicles for drug delivery, [8]. The simulation of diffusion under these conditions is an excellant example of the power and flexibility of the bond graph model.

In Chapters 5 and 6 a new bond graph model of diffusion in two dimensions is developed and applied to a variety of problems in membrane science. Using this 2D model the 'edge effect', a classic problem in membrane characterisation, [9], was solved, (Section 6.2) and the effects of non-uniform initial concentration distributions in two dimensions were examined, in particular on release rates, (Section 6.3). This leads logically to the development of a bond graph model for diffusion in three dimensional space, thus allowing the simulation of

diffusion systems with complete assymetry, both in geometry and diffusional properties. This is the topic of the final chapter.

The aims of this research have indeed been met, with the flexibility and sucess of the computer models developed clearly demonstrated by a variety of applications. This thesis contains the theoretical basis on which any uncoupled diffusional problem may be solved by computer simulation, provided the fundamental system parameters are known.

REFERENCES FOR INTRODUCTION.

[1]. J.Crank. The Mathematics of Diffusion, Clarendon Press, Oxford, England (1959).

[2]. F.Helfferich, Ion Exchange, J. Wiley, New York (1962).

[3]. G.Oster, A.Perelson and A.Katchalsky, Nature, **234**, (1971) 393.

[4]. R.Paterson. Network thermodynamics, Chapter 1 in Membranes Structure and Function, E. E. Bittar (Ed.), J.Wiley and Sons, New York (1980).

[5]. R.Paterson and Lutfullah in, Ion Exchange Technology, D.Naden and M.Streat (Eds.). Ellis Horwood, Chichester, England (1982).

[6]. H.Paynter. Analysis and Design of Engineering Systems, MIT, Cambridge, MA, (1961).

[7]. F.Helfferich and M.S.Plesset, J. Chem. Phys. **28** (1952) 418.

[8]. N.B Graham and M.E. McNeill, Hydrogels for controlled drug delivery. Biomaterials, **5** (1984) 27-36.

[9]. R.M. Barrer, J.A.Barrie and M.G.Rogers, Trans. Faraday Soc. **58**, (1962) 2473.

CHAPTER ONE

THERMODYNAMICS OF NON-STEADY STATE PHENOMENA

1.1 INTRODUCTION

The methods for computer simulation of chemical diffusion processes discussed in this thesis, are based on the quantitative analysis of bond graph models. The bond graph is used for representing the nonequlibrium processes which may occur in a system. In order to discuss the construction of this bond graph, the fundamental principles on which network thermodynamics and the bond graph are founded must be explored. Essentially, a global description of non-steady state phenomena is facilitated by a study of the reversible and irreversible processes which can occur simultaneously in any discrete volume element within the system to be studied. This chapter describes the concept of a material's resistance to chemical flow, using the rigorous theory of irreversible thermodynamics, [1]. This is then incorporated into the general theory of network thermodynamics and a discussion of bond graph symbolism and techniques. A basic bond graph model for one dimensional chemical diffusion is then introduced as an example of the general techniques more fully investigated in the bulk of this thesis.

1.2 IRREVERSIBLE THERMODYNAMICS

Some idealised processes may be described as entirely reversible and may therefore be studied using equilibrium thermodynamics alone. All natural phenomena however are observed to proceed spontaneously in one direction only: towards the equilibrium state. Since irreversible processes are more complex mathematically than those which can be regarded as reversible, many of the transport problems

solved in this thesis are without mathematical solution. Detailed knowledge of the internal parameters are required to describe the dynamics of a non-equilibrium system. It is not sufficient to define only the external forces. In chemical diffusion, which is the main topic of this thesis, the local distributions of concentrations must be known.

1.2.1 Entropy Changes in Spontaneous Processes.

In thermodynamics entropy changes provide the criteria for distinguishing between reversible and irreversible phenomena. Clausius' statement is well suited for our purposes: "Die Energie der Welt ist konstant die Entropie der Welt strebt einem maximum zu." [2]. (The energy in any process is conserved but entropy tends to a maximum value.) The entropy change for any system may be written as the sum of two seperate terms, eqn(1.1).

$$dS = dS_e + dS_i \qquad (1.1)$$

dS_e is the change resulting from reversible exchange of energy between the system and its surroundings and dS_i is that due to irreversible processes occuring within the system itself. Classical thermodynamics states that this latter function is always greater than or equal to zero. If zero then the system is undergoing a reversible change only. Irreversible processes always result in entropy production, eqn(1.2).

$$dS_i \geq 0 \qquad (1.2)$$

The rate of change of entropy per unit time σ, eqn(1.3),

$$\sigma = \frac{dS_i}{dt} \tag{1.3}$$

multiplied by the temperature T, has the dimensions of free energy per unit time. It is a measure of the rate of local dissipation of free energy, or power dissipation, and is therefore an important thermodynamic quantity. It is known as the dissipation function.

1.2.2 Dissipation function.

Irreversible thermodynamic theory defines the dissipation function explicitly as a sum of a number of products, eqn(1.4).

$$T\sigma = \Phi = f_q\left(\frac{-dT}{T}\right) + \sum f_i\left(-d\mu_i\right) + f_v(-dP) + i(-d\psi) + \sum f_r A \geq 0 \tag{1.4}$$

Each product in the sum consists of a flow multiplied by a conjugate force for each energy domain. The flows f_q, f_i, f_v, i and f_r are the flows of heat, matter, volume, electric current and rate of chemical reaction respectively. Each is multiplied by its conjugate force, or effort. These are respectively, temperature difference, (divided by the temperature itself), chemical, pressure and electric potential differences and in the final term, the conjugate force to the rate of chemical reaction is the chemical affinity. Since there may be several chemical species in the system and indeed several chemical reactions the flow and force products must be summed for each. Eqn(1.4) may be written in completely general terms as:

$$\Phi = \sum^{k} f_k \, e_k \qquad \geq 0 \tag{1.5}$$

The effort conjugate to each flow f_k is now denoted simply as e_k. The dissipation function is of fundamental importance to the study of non-equilibrium processes as it defines all thermodynamic flows and forces, accounting for all irreversible phenomena that may occur within a system. By itself however it is of little practical use. For further development relationships between flows and forces are required.

1.2.3 Phenomenological equations.

Lord Rayleigh in his famous treatise on the theory of sound [3], used a set of equations, that expressed the linear dependance of all mechanical flows on all mechanical forces operating in a system. Onsager later extended this theory to cover all thermodynamic flows and forces, f_k and e_k, [4]. The result was a symmetrical set of phenomonological equations, eqns(1.6).

$$\begin{aligned}
f_1 &= L_{11}e_1 + L_{12}e_2 + L_{13}e_3 + \ldots + L_{1k}e_k \\
f_2 &= L_{21}e_1 + L_{22}e_2 + L_{23}e_3 + \ldots + L_{2k}e_k \\
&\vdots \\
f_k &= L_{k1}e_1 + L_{k2}e_2 + L_{k3}e_3 + \ldots + L_{kk}e_k
\end{aligned} \tag{1.6}$$

or equivalently,

$$f_k = \sum_{j=1}^{n} L_{jk}\, e_k \qquad (k = 1,2,\ldots,n) \qquad (1.7)$$

Each of the flows and forces must be as defined in the dissipation function. Alternatively we may rearrange eqn(1.6) to express the efforts as functions of flow, eqns(1.8).

$$\begin{aligned} e_1 &= R_{11}f_1 + R_{12}f_2 + R_{13}f_3 + \ldots + R_{1k}f_k \\ e_2 &= R_{21}f_1 + R_{22}f_2 + R_{23}f_3 + \ldots + R_{2k}f_k \\ &\vdots \\ e_k &= R_{k1}f_1 + R_{k2}f_2 + R_{k3}f_3 + \ldots + R_{kk}f_k \end{aligned} \qquad (1.8)$$

and again equivalently,

$$e_k = \sum_{j=1}^{n} R_{jk}\, f_k \qquad (k = 1,2,\ldots,n) \qquad (1.9)$$

The L coefficients are flows per unit force and are therefore generalised mobilities or conductances. Conversely R coefficients are forces per unit flow, and are generalised resistances.

Since each flow is defined as a linear function of all the forces in a system, irreversible thermodynamics provides a natural and rigorous theory for describing coupled diffusion. In this thesis however we will not discuss coupled phenomena but will concentrate on uncoupled chemical diffusion, except for the special case of

electrical coupling in ion exchange diffusion. For systems where there is only one flow and one effort eqn(1.9) reduces to a single phenomenological equation written here simply without subscripts, eqn(1.10).

$$e = R f \tag{1.10}$$

or as the inverse:

$$f = R^{-1} e \tag{1.11}$$

It may be noted that eqn(1.11) is identical in form to that of the classical transport laws. By substituting the appropriate flows and efforts one can obtain re-statements of the Laws of Fourier, Fick, Darcy (or Poisseuille), and Ohm. There is however no corresponding classical law for steady chemical reactions.

The theory of irreversible thermodynamics alone, allows treatment of a large range of phenomena, but these are restricted to sufficiently slow steady state processes occuring when the system is close to equilibrium. The thermodynamics of the steady state is simplified by the fact that it is time invariant and the local effort gradients are therefore constant with time also. By combining network theory with the general principles of irreversible thermodynamics a theory for all dynamic processes is obtained in which these restrictions are removed, [5], [6]; network thermodynamics.

1.3 NETWORK THERMODYNAMICS AND THE BOND GRAPH TECHNIQUE.

In network thermodynamics a diffusion system under study is conceptually divided into a number of small but finite volume elements or lumps, within each lump local

equilibrium is assumed. This greatly simplifies the mathematics and any inherent error can be compensated for by using a large number of these volumes/lumps. The theoretical description of not only the dissipative processes described above, but also reversible exchanges of energy which may occur in parallel, allows quantitative models of non-steady state phenomena. The construction of the bond graph model using the methods of Paynter, [7], leads to a quantitative computer simulation of the system's dynamics.

The term lump, although not particularly elegant is derived from electric circuit theory and is used extensively in network thermodynamics. In this text both terms lump and volume element are employed and have identical meaning.

1.3.1 The bond graph and power flow.

The bond graph is a device for representing the power processing properties of each volume element (or lump) of the network and the way in which these are connected. Power flow throughout the system is shown by means of a 'power bond' with the direction of flow indicated by means of a half arrow fig(1.1a). Each bond has associated with it an effort and a flow variable, as defined in the dissipation function, where necessary the bonds may be labelled and the flows and efforts annotated on each bond as in fig(1.1).

1.3.2 The generalised resistor and capacitor.

From the theory of irreversible thermodynamics, outlined above, any flow through the system will be met by

a resistance to that flow. This leads to the concept of a generalised resistor, a power processing element at which eqn(1.11) relates the effort and flow variables. Eqn(1.11) then is the constitutive relationship for this element. In bond graph terms this function is represented by the '1-port' resistor element, symbol R. Ports in the bond graph are positions where power may enter or leave power processing elements. The resistor is a 1-port device with only one point of entry for power flow and therefore one connecting power bond. In particular, a chemical resistor is that which accounts for the resistance to the flow of matter, driven by chemical potential gradients as defined by the dissipation function. Fig(1.1b) shows the representation of this dissipative function in the bond graph.

Of special interest in chemical diffusion is the ability of a volume element to store matter reversibly. This leads us to the concept of another 1-port device, the generalised capacitor, which stores or releases energy reversibly. In the general terms of network thermodynamics the capacitor is an element, symbol C, for which the constitutive relation exists between an effort and the corresponding charge, q, eqn(1.12).

$$e = C^{-1} q \qquad (1.12)$$

With q defined as the time integral of flow, eqn(1.13).

$$q \equiv \int f \, dt \qquad (1.13)$$

For a diffusion system q is simply the number of moles of diffusant in each volume element. The capacitor, like the resistor derives its name from the familiar electrical

example for which the displacement is electric charge. Fig(1.1c) is the representation of capacitive function in the bond graph.

There is one other one port power processing device in bond graph theory, the inductor but this has no chemical analogue and is not relevant to this work.

In addition there are three, two port elements, the transformer, transducer and the gyrator, [8]. The transducer is required in the bond graphs of multicomponent coupled diffusion but are outwith this application.

1.3.3 0- and 1-junctions.

In nature the roles of capacitor and resistor are combined in each volume but in a bond graph model they are separated both conceptually and mathematically as described above. The 'junctions' of the bond graph control the way power flows are divided and enter the power processing elements of the model. These junctions are 3-port devices and neither dissipate energy (as the resistor element), nor store it (as the capacitor). That is, energy is conserved. Fig(1.1) shows the two types of junctions employed, the 1-junction, and the 0 junction.

At all junctions power is conserved, therefore eqn(1.14) follows.

$$e_1 f_1 - e_3 f_3 = e_2 f_2 \qquad (1.14)$$

In the 0-junction (also known as the common effort junction), the efforts of the three component power bonds are equal, eqn(1.15).

$$e_1 = e_2 = e_3 \tag{1.15}$$

This is equivalent to a parallel junction in electrical circuits. By combining eqns(1.14) and (1.15) the flows of the connecting power bonds may be related by eqn(1.16).

$$f_1 - f_3 = f_2 \tag{1.16}$$

The common flow or 1-junction is the converse of the 0-junction. Now the flows of the three power bonds connected to it are equal, eqn(1.17).

$$f_1 = f_2 = f_3 \tag{1.17}$$

This is equivalent to a serial junction in an electrical circuit. Again by combining eqns(1.14) and now eqn(1.14) a relationship between the efforts of the connecting power bonds is derived, eqn(1.18).

$$e_1 - e_3 = e_2 \tag{1.18}$$

The resistor is a series element connected to the bond graph by a 1-junction, fig(1.2a). The difference between the power entering and leaving, given by eqn(1.14), is that directed towards, and dissipated by, the resistor. Conversely the lump capacitor is connected to the bond graph via a 0-junction, fig(1.2b). The difference in power entering and leaving this junction given by eqn(1.14) is in this case that stored reversibly.

1.3.4 Causality and the Causal stroke.

To enable the use of the bond graph as a complete algorithm for quantitative analysis one futher concept must be introduced, that of causality. At each port both an effort and a flow variable exist, one can control either

but not both simultaneously. We use the notation that one of these variables is the input and the other the output. It may be noticed that we chose to write the constitutive equation for the capacitor above using the inverse of the capacitance, eqn(1.12). This equation may equally be written as:

$$f = C \frac{de}{dt} \tag{1.19}$$

We use the convention that, as in high level computer languages, the variable on the left hand side of the equation is the output variable. Therefore eqns(1.11) and (1.12) have the reversed implied causality from eqns(1.10) and (1.19). For the resistor, which has an apparent linear constitutive equation, the distinction is unimportant. For the capacitor however we can distinguish between the two as 'integral causality' with e given as a static function of the time integral of flow, and 'derivative causality' where e is the input and f is given as a time derivative of a static function of e.

The natural causal assignment for a bond graph capacitor is integral since steps in effort, which are present in a network model, would require power to become infinite using the derivative formulation. We may then refer to the capacitors of the bond graph as defining the distribution of energy, or the efforts, throughout the system, these in turn drive the chemical flows which may then be integrated with respect to time. In addition to the requirements of the capacitors, causality must be assigned at the junctions sensibly, for example only one effort

should be input to a common effort or 0-junction. (Since lump capacitors are connected via the 0-junctions this single input effort will in fact be that output from the capacitor.) Similarly only one flow should be input to the 3-port 1-junction.

Causality is indicated in the bond graph by means of a causal stroke. This is a line drawn perpendicular to the power bond at either the bond's 'head', (next to the half arrow) or tail. The position of the stroke indicates the side to which the effort signal is being directed. By this method an assigned integral causality at a capacitor element requires that the power bond connected to it should have a causal stroke drawn at it's tail, indicating effort being output and flow as the input variable. For the purposes of this work it is only important that causality be assigned sensibly throughout the bond graph. If inconsistencies in the causal arguements were to arise it would indicate that the model required revision. The normal practise is to assign causality at the capacitors, then at the junctions and finally to the resistor elements for which either causality will suffice.

1.3.5 The C-C Linear bond graph.

It is useful to illustrate the construction of a complete bond graph using the aforementioned components by considering a simple example. Perhaps the simplest diffusion problem to choose is that of a planar membrane held between two well stirred solutions of different concentration. (A system of this type is considered in Chapter 3 for an ion exchange membrane). We will examine

initially a one lump bond graph model of this system. A one lump model is one in which only one only volume element is used to model the membrane phase, fig(1.3). The thermodynamics of the problem dictate that the membrane will have resistive and capacitive functions, being able not only to resist the flow of matter from one solution to the other but also store within itself an amount of diffusant. These are represented in the bond graph by a single capacitor placed at the volume centre of the lump, C_2 in fig(1.3), and two resistors at each of the lump's edges, accounting for the resistance to flow from the edges to the centre of the membrane. The resistances are therefore equal. The contacting solutions are considered to be well stirred, with no diffusional gradients in these and consequently each may be represented in the the bond graph by capacitors; C_1 and C_3 in fig(1.3). Since this graph is characterised by two capacitors at either end, we refer to it as a C-C model. Note that the assignments of causality are self consistent as required.

1.3.6 Reticulation of bond graph models.

We would not expect a one lump model to be suitable for quantitative predictions and to obtain adequate precision we require to split the system into a much larger number of volume elements. Normally equal volume lumps are chosen and fig(1.4) shows a three lump model of the previous C-C example. The two terminal capacitors, (solution volumes), are now relabelled C_1 and C_5 (identical to C_1 and C_3 of fig(1.3)), but the membrane capacitances and resistances will have suitably rescaled values, as described in

Chapter 2. The central portion of the bond graph from R_1 to R_4, the membrane phase, is often referred to as an R-C chain due to the repetition. The resistors within the chain R_2 and R_3 now account for the resistance to diffusion between adjacent lump centres and will have different resistances to R_1 and R_4.

1.3.7 State-Space Equations.

The bond graph may be used as an algorithm to set up the characteristic state-space equations for the membrane system which give the flow into each of the capacitors, [9], [10]. These state-space equations define the flows into each capacitor, dq/dt, as functions of the local state variables R, C and q of the bond graph elements. As an aid to the illustration of this technique the state-space equation for the central capacitor C_3 of the bond graph in fig(1.4) is derived as an example. For this purpose we have arbitrarily numbered the bonds around this capacitor from 1 to 9, fig(1.5). Each effort and flow component may be labelled for each bond. In this way the flow f_5 may be related to the flows f_4 and f_6 since the three power bonds 4, 5, and 6 connect to the 3-port junction at which flow must be conserved, eqn(1.20):

$$\frac{dq_3}{dt} \equiv f_5 = f_4 - f_6 \qquad (1.20)$$

(cf eqn(1.16)). Since power bonds 4 and 6 are both connected to 0-junctions we can equate the flows to the flow components of power bonds 3 and 7 respectively, eqns(1.21) and (1.22).

$$f_4 = f_3 \qquad (1.21)$$

$$f_6 = f_7 \tag{1.22}$$

The flows f_3 and f_7 are both output from the resistors R_2 and R_3 respectively and so we may relate these to the input efforts using the constitutive relationships at each (from eqn(1.11)) to produce:

$$\frac{dq_3}{dt} = R_2^{-1} e_3 - R_3^{-1} e_7 \tag{1.23}$$

From the two 1-junctions to which the power bonds 3 and 7 are connected we can use the principle of power conservation (eqn(1.18)) to expand the equation further:

$$\frac{dq_3}{dt} = R_2^{-1} \left(e_2 - e_4 \right) - R_3^{-1} \left(e_6 - e_8 \right) \tag{1.24}$$

All efforts in this equation may be equated to those output from the capacitors using the relationship of equal effort at the appropriate 0-junctions, eqns(1.25) to (1.28).

$$e_2 = e_1 \tag{1.25}$$

$$e_8 = e_9 \tag{1.26}$$

$$e_4 = e_5 \tag{1.27}$$

$$e_6 = e_5 \tag{1.28}$$

Since they are output from the C elements each effort may be related to the respective charges on the capacitors by the constitutive equations (from eqn(1.12)):

$$e_1 = C_2^{-1} q_2 \tag{1.29}$$

$$e_5 = C_3^{-1} q_3 \tag{1.30}$$

$$e_9 = C_4^{-1} q_4 \qquad (1.31)$$

Making these substitutions and rearranging gives the desired state-space equation.

$$\frac{dq_3}{dt} = -\left(C_3^{-1} R_2^{-1} + C_3^{-1} R_3^{-1} \right) q_3 + \left(\left(C_2^{-1} R_2^{-1} \right) q_2 + \left(C_4^{-1} R_3^{-1} \right) q_4 \right) \qquad (1.32)$$

The state-space equation for any capacitor within an R-C chain of any length is identical in form to this and we can write in general terms the flow into the j^{th} capacitor as, eqn(1.33).

$$\dot{q}_j = -\left(C_j^{-1} R_{j-1}^{-1} + C_j^{-1} R_j^{-1} \right) q_j + \left(\left(C_{j-1}^{-1} R_{j-1}^{-1} \right) q_{j-1} + \left(C_{j+1}^{-1} R_j^{-1} \right) q_{j+1} \right) \qquad 1 > j < n+1 \qquad (1.33)$$

Where n is the number of lumps in the linear bond graph. Therefore the power bonds need not be labelled. Capacitors C_1 and C_{n+2}, (C_5 in our example 3 lump bond graph), are end capacitors and have different state-space equations but only in the number of terms, eqns(1.34) and (1.35) respectively.

$$\dot{q}_1 = -\left(C_1^{-1} R_1^{-1} \right) q_1 + \left(C_2^{-1} R_1^{-1} \right) q_2 \qquad (1.34)$$

$$\dot{q}_{n+2} = -\left(C_{n+2}\ R_{n+1}\right)q_{n+2} + \left(C_{n+1}\ R_{n+1}\right)q_{n+1} \qquad (1.35)$$

1.3.8 Computer simulation and integration procedure.

The state-space equations may be regarded as first order differential equations of the form,

$$\dot{q}_j = \frac{dq_j}{dt} = -m_1 q_j + m_2 \qquad \text{for } j=1 \text{ to } n+2 \qquad (1.36)$$

By integrating each of the equations in turn, with respect to time, updated charges in each of the capacitors may be obtained. The accomplishment of this task forms the basis of a computer program for quantitative simulation based on the bond graph model. It is not possible to integrate each of the equations in one step since the coefficients m_1 and m_2 are not simple constants but are themselves functions of the charge values (in the case of m_2), and R and C coefficients which may also be time variant. Instead integration must be made over finite step times H, small enough that we can justify the simplifying assumption that over the period of time H, all parameters other than the principle q_j may be considered constant. Under these limitations m_1 and m_2 become pseudo-constants. Integration over the step time period, H, leads to an equation for the new charge value on capacitor j after time H, q_j^H.

Using this method numerical integration procedures can be omitted and a replacement exponential expression is

obtained, eqn(1.44) below. This has proved to be an invaluable aid to this research since it results in substantial reductions in computational time, (at least three times faster than the Runge-Kutta method) allowing much larger and therefore more precise models to be handled. This proved especially important for solving 2D and 3D systems, Chapters 5-7. The method may be applied to any bond graph on appropriate substitution of m_1 and m_2, it will facilitate future work.

Rewriting eqn(1.36).

$$\frac{dq_j}{(-m_1 q_j + m_2)} = t^0\, dt \qquad (1.37)$$

A function U is defined, eqn(1.38).

$$U = -m_1 q_j + m_2 \qquad (1.38)$$

$$\Rightarrow dU = -m_1 dq_j \qquad (1.39)$$

Substituting in eqn(1.37) and integrating from times t to t+H:

$$\int_t^{t+H} \frac{dU}{-m_1 U} = \int_t^{t+H} t^0\, dt \qquad (1.40)$$

$$\Rightarrow -\frac{1}{m_1} \left[\ln(U) \right]_t^{t+H} = H \qquad (1.41)$$

$$\Rightarrow \quad \ln\left[\frac{U_{t+H}}{U_t}\right] = -H\, m_1 \qquad (1.42)$$

Take exponential:

$$U_{t+H} = U_t \exp(-Hm_1) \qquad (1.43)$$

By substituting back for U, using q_j^H to denote the charge in capacitor j after time H, leads to eqn(1.44).

$$q_j^H = \frac{m_2 - \exp(-Hm_1).(-m_1 q_j + m_2)}{m_1} \qquad (1.44)$$

This equation applied to each capacitor of the model in turn yields an updated charge distribution at t=t+H. The evolution of the process may be predicted by repetition of the entire process, for as many cycles as required. This method of combined temporal with spatial reticulation is fundamental and allows these bond graph models to simulate non-linear, time dependant processes with ease. This will be illustrated in Chapter 3, in ion exchange and in Chapter 4 in which swelling/diffusion systems are modelled.

FIGURE 1.1.

Bond graph symbols.

a). The power bond.

b). Resistor.

c). Capacitor.

d). 3-port 1-junction.

e). 3-port 0-junction.

SYMBOL	REPRESENTING
a) 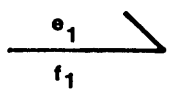	power bond
b) 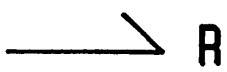	resistor
c) 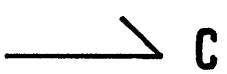	capacitor
d) 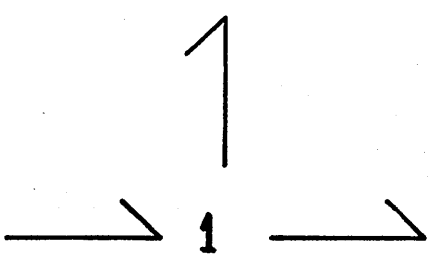	1-junction
e) 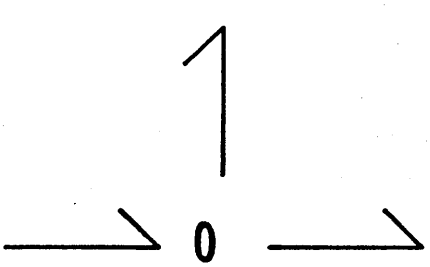	0-junction

FIGURE 1.2.

Resistance and capacitance as represented in bond graph.

a) Resistive function: Power directed towards resistor port, e_2f_2, is dissipated irreversibly.

b) Capacitive function: Power directed towards capacitor port, e_2f_2, is reversibly stored as energy (effort).

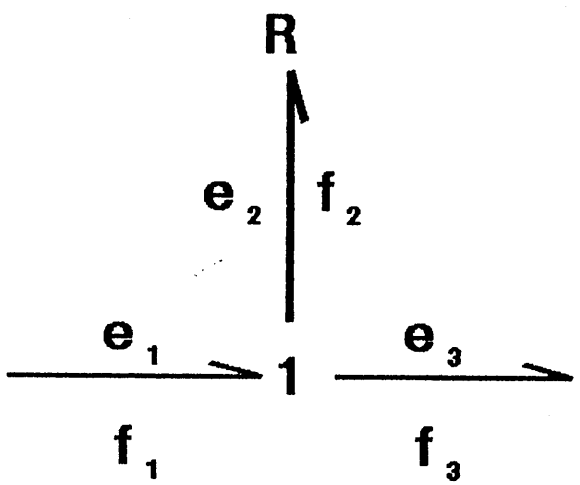

a)

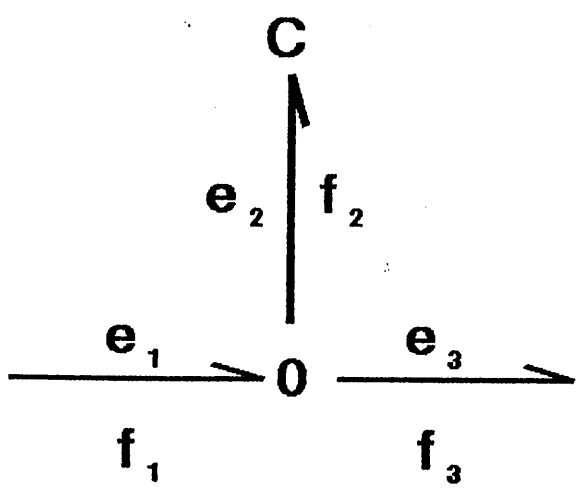

b)

FIGURE 1.3.

Example of a 1-lump C-C bond graph model. This uses only one volume element to model resistive and capacitive functions of membrane. Total resistance of membrane divided into two separate resistances, R_1 and R_2. C_1 and C_3 represent the (well stirred) external solutions as capacitors.

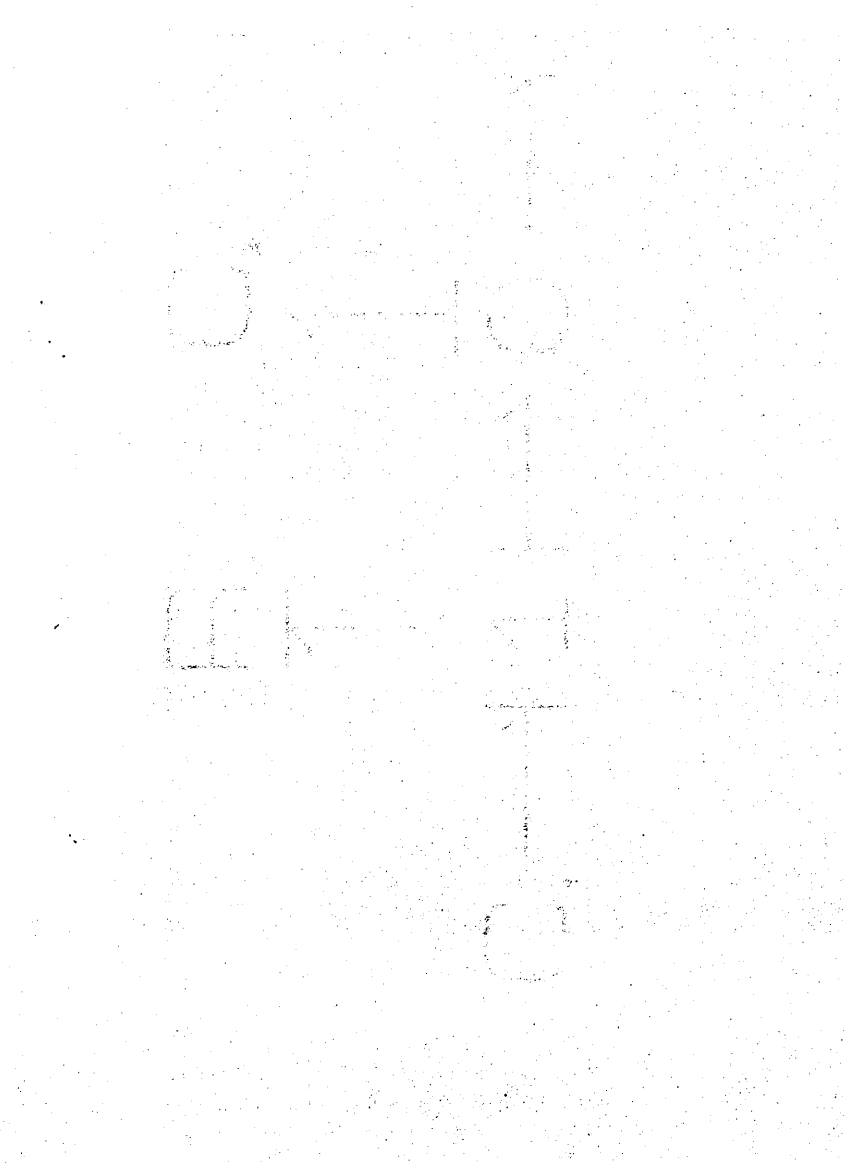

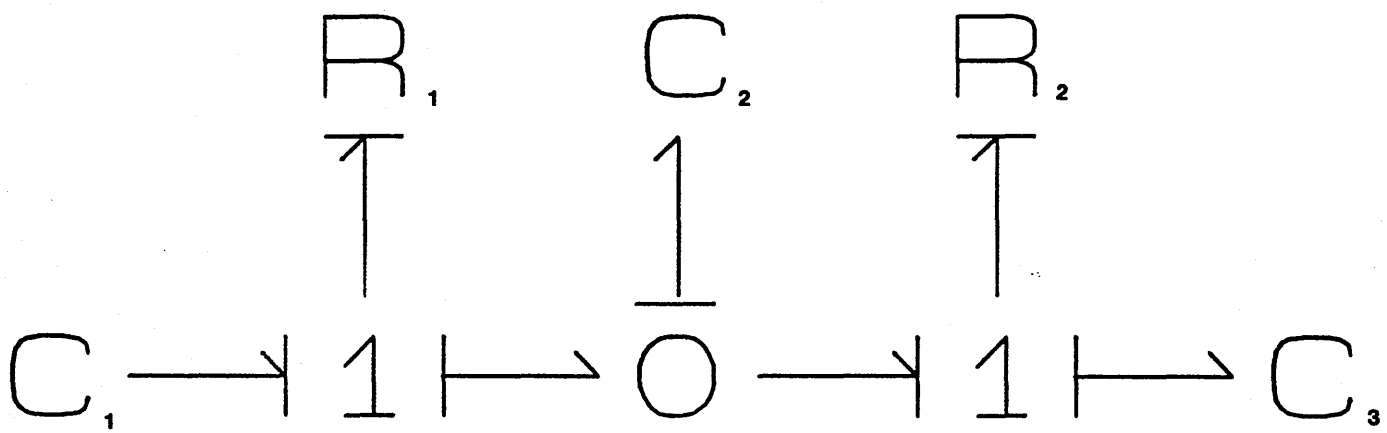
R1
C2
R2
C1
1
0
1
C3

FIGURE 1.4.

Three lump C-C bond graph used for resistor/capacitor model of membrane, with consecutive labelling of capacitors and resistors. This one bond graph is in effect an algorithm which may be used to simulate all one dimensional diffusion phenomena, including membrane composites, and spherical or cylindrical diffusional models.

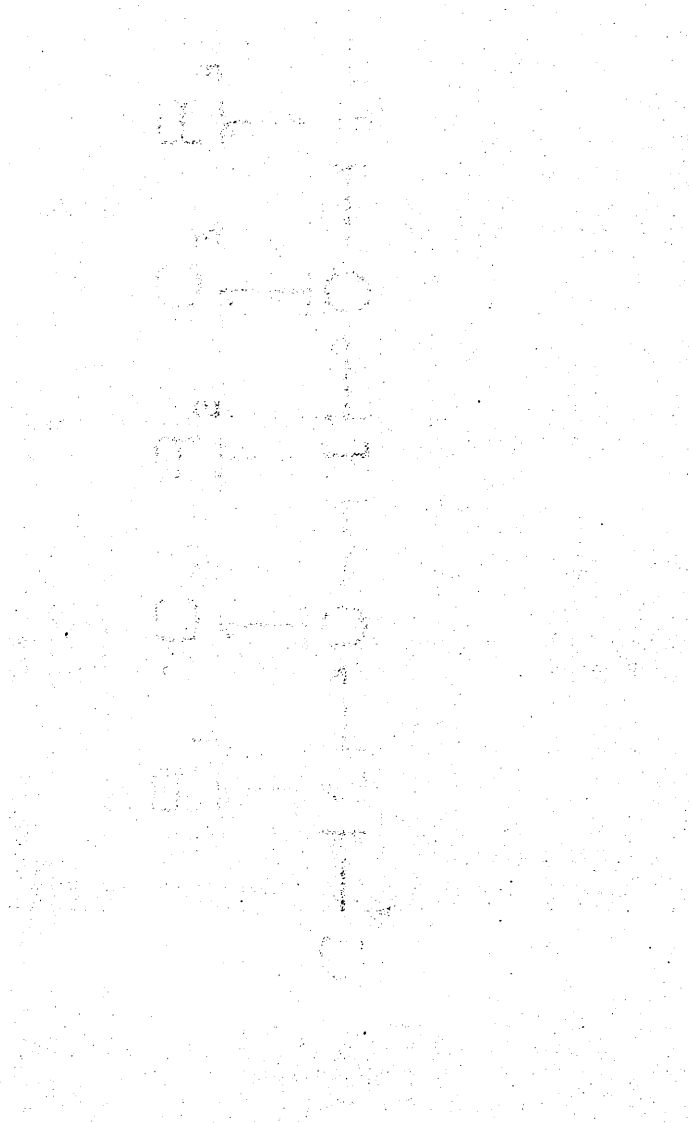

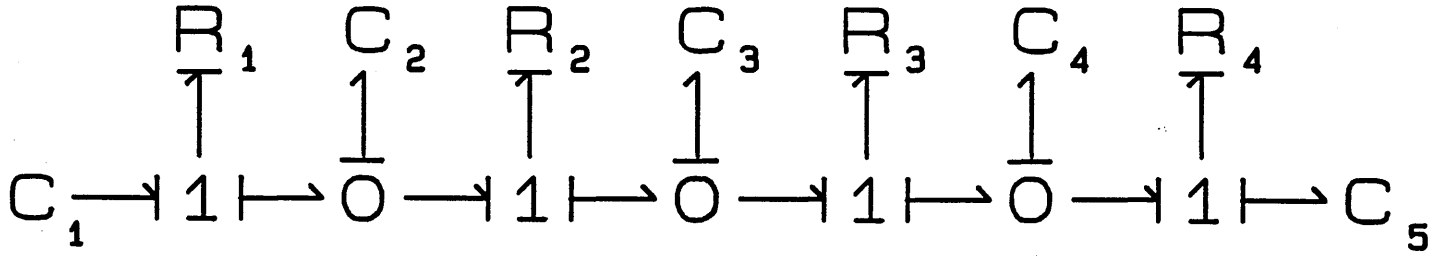
R1
C2
R2
C3
R3
C4
R4
C1
1
0
1
0
1
0
1
C5

FIGURE 1.5.

Arbitrary labelling of power bonds around a central capacitor (C_3) of a linear bond graph model (eg. fig(1.4)), used for deriving general state-space equation.

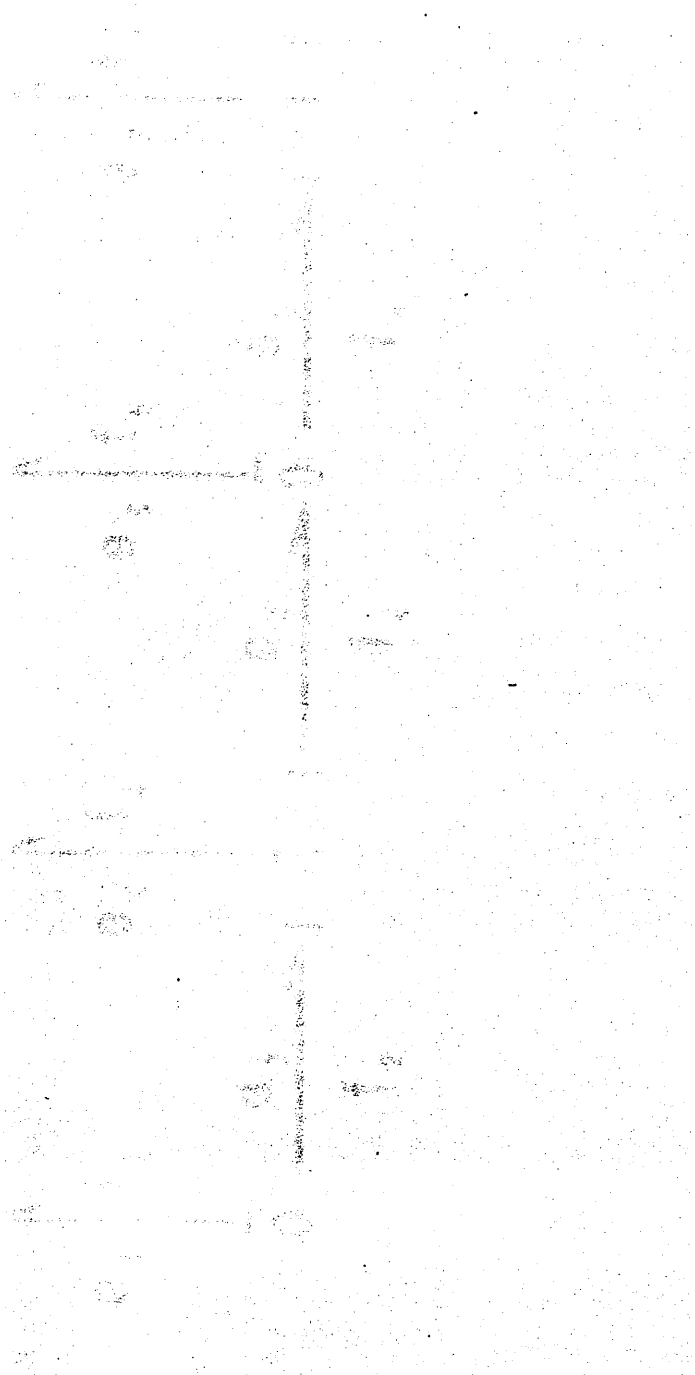

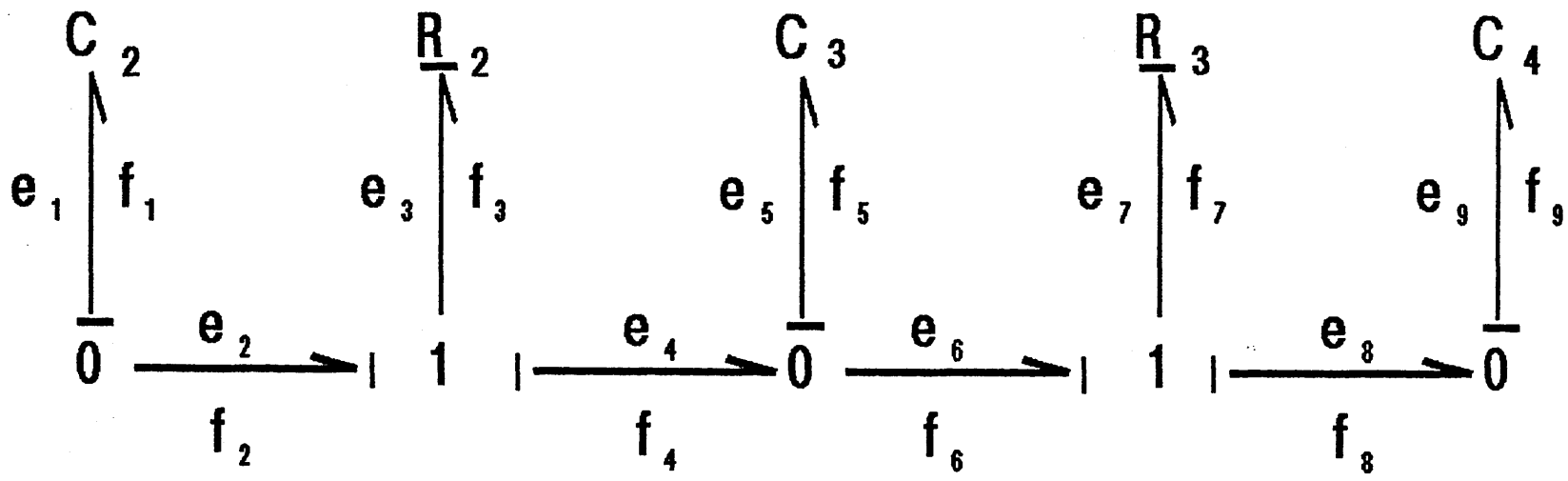
C 2
R 2
C 3
R 3
C 4
e 1
f 1
e 3
f 3
e 5
f 5
e 7
f 7
e 9
f 9
0
e 2
1
e 4
0
e 6
1
e 8
0
f 2
f 4
f 6
f 8

REFERENCES FOR CHAPTER ONE

[1] A. Katchalsky and P.F. Curran, Non-Equlibrium Thermodynamics in Biophysics. Harvard University Press, Cambridge, MA. (1965).

[2]. R. Clausius. Poggendorffs Ann. Physik. **125**, (1865) 390.

[3]. Lord Rayleigh (J. W. Strutt), Proc. Math. Soc. (London) **4**, (1873), 357.

[4]. L. Onsager. Phys. Rev. **37**, (1931) 2265.

[5]. D.Karnopp and R.Rosenberg, System Dynamics: A Unified Approach, Wiley-Interscience, New York (1975).

[6]. G.Oster, A.Perelson and A.Katchalsky, Nature, **234**, (1971) 393.

[7]. H.Paynter. Analysis and Design of Engineering Systems, MIT, Cambridge, MA, (1961).

[8]. R.Paterson. Network thermodynamics, Chapter 1 in Membranes Structure and Function, E. E. Bittar (Ed.), J.Wiley and Sons, New York (1980).

[9]. R.Paterson and Lutfullah in, Ion Exchange Technology, D.Naden and M.Streat (Eds.). Ellis Horwood, Chichester, England (1982).

[10]. R.Paterson and Lutfullah. J. Membrane Sci. **23**, (1985) 59.

CHAPTER TWO

ONE DIMENSIONAL DIFFUSION PROBLEMS WITH INFINITE BATH CONDITIONS

2.1 INTRODUCTION

The simplest implementations of network thermodynamics applied to diffusion phenomena is the simulation of one dimensional problems with infinite bath conditions. These results have been obtained and published previously [1], [2]. In this work three examples have been chosen to validate the new method of integration described in Section 1.3.8. In each of these the network thermodynamic result obtained using the exponential function eqn(1.44) are compared to the available analytical solutions for these systems. In addition the theory presented in this chapter for planar, spherical and cylindrical diffusion modelling is built upon in later chapters, being incorporated into the ion exchange (non linear) diffusion bead models in Chapter 3, to swelling hydrogels in Chapter 4 and to the limited cylinder model and other 2D systems in Chapter 5.

Analytical solutions exist for each of the problems discussed in this section and the results obtained from the mathematical theory are compared to the computer simulations. As the mathematical techniques examine the diffusion system as a continuum one might not expect the network thermodynamic approach to give identical results without considering a near infinite number of lumps. In practise however, as will be shown below, the computer models yield very precise predictions for linear models with between 10 - 30 volume elements. In fact by increasing beyond this degree of reticulation one approaches limitations of accuracy imposed by the computer hardware.

Much of the theory and techniques presented in this

chapter will be referred to and applied in the discussions of more complex systems later in the text. The formulations for resistance and capacitance values derived below for several diffusional geometries remain similar in form for a variety of diffusional phenomena. Ion exchange problems discussed in Chapter Three for example are developed from the spherical model. In addition the swelling diffusion problems in Chapter Four are described as modifications to the simple planar example given below. Similarly the simulation of a limited cylinder relies on theory discussed in this section for the diffusion from an infinite rod.

The basis for all quantitative simulation using the bond graph and resultant state-space equations to describe the system dynamics, is the recognition and formulation of the resistive and capacitative processes in terms of measurable parameters.

2.2 FICKIAN DIFFUSION MODEL.

Steady state diffusion is described by Fick's first Law, eqn(2.1), [3].

$$J = - D\frac{d\bar{c}}{dx} \qquad (2.1)$$

J is the flux density, D the diffusion coefficient and $\bar{c}$ concentration. The axis of diffusion x may be either planar, cylindrical or spherical (for the latter two x is normally replaced by r to emphasise radial symmetry). It was stated in Chapter 1, (Section 1.2.3), that the single phenomenological equation (eqn(1.11)) was identical in form to Fick's Law, and so therefore it would be desirable to relate the resistance coefficient R, to the experimentally

measurable Diffusion coefficient, D.

In chemical diffusion the flow in eqn(1.11) is that of matter with the charge q being simply the number of moles, n, of chemical species, that is to say the diffusant, eqn(2.2):

$$f = \frac{dq}{dt} = \frac{dn}{dt} \tag{2.2}$$

For a true thermodynamic description the effort should be defined as chemical potential μ, as appears in the dissipation function, eqn(1.4) [4]. In this work however we choose to define the effort as concentration, this allows us to develop the convenient Fickian formulation as desired, [2]. It should be noted that as a consequence the dimensions of the effort and flow products are no longer of power and that the treatment must therefore be regarded as pseudo-thermodynamic. (Strict thermodynamic implementations for simulating chemical diffusion have been developed and shown to produce identical results as to the methods presented here [5].) There is the likely possibility that steps in concentration across phase boundaries may have to be considered. To facilitate this the external solution is chosen as a single reference phase, concentrations are modified for expression as moles per volume of this solution using the distribution coefficient, α, eqn(2.3).

$$\alpha = \frac{\bar{c}}{c} \tag{2.3}$$

$\bar{c}$ is the concentration within the diffusing medium and c is the hypothetical concentration in moles per unit volume of reference solution. Effort, e, is then defined by eqn(2.4).

$$e = c = \frac{\bar{c}}{\alpha} \tag{2.4}$$

This method proves most useful for handling ion selectivities in ion exchange processes (Chapter 3), although the exchanger phase was chosen as the reference in that analysis.

2.3 Planar diffusion.

The general methods are illustrated by a derivation of R and C values for Fickian models in planar conditions, [1], [2].

We wish to examine the consequences of effort defined as concentration for the constitutive equations of the resistor and capacitor for planar diffusion.

The effort input to the bond graph resistor, eqn(1.11) is the difference between two adjacent efforts, eqn(1.18). Since we have defined effort as concentration, (eqn(2.4)), this is equivalent to a concentration step across the Fickian resistor and we may write the constitutive equation as eqn(2.5).

$$f = R^{-1}(-\Delta c) \tag{2.5}$$

For planar diffusion the integration of Fick's Law to consider this step in concentration is trivial and leads to eqn(2.6).

$$J = -D\left(\frac{\Delta \bar{c}}{\Delta x}\right) \tag{2.6}$$

Δx is the distance between lump centres, (Section 1.3.5). Since the flux is defined as a flow per unit area A, we may write equivalently:

$$f = D\,A\left(\frac{-\Delta\bar{c}}{\Delta x}\right) \tag{2.7}$$

Substituting for the hypothetical concentration using eqn(2.4) gives eqn(2.8).

$$f = \frac{D\,A\,\alpha\,(-\Delta c)}{x} \tag{2.8}$$

Comparison with eqn(2.5) reveals the resistance coefficient to be given by eqn(2.9).

$$R = \frac{\Delta x}{D\,A\,\alpha} \tag{2.9}$$

Substituting concentration for effort in the integral constitutive equation for the bond graph capacitor gives eqn(2.10).

$$c = C^{-1}\,q \tag{2.10}$$

The charge q, equivalent to the number of moles of chemical species, n, may be related to the concentration by the lump volume v, eqn(2.11).

$$q \equiv n = \bar{c}\;v = c\,\alpha\,v \tag{2.11}$$

Substituting in eqn(2.10) shows the capacitance to be simply the volume of the lump scaled by the distribution coefficient, eqn(2.12).

$$C = \alpha\,v \tag{2.12}$$

Since the capacity is dependant on the volume of a bond graph lump and not the particular geometry, eqn(2.12) gives the capacitance for all bond graph models discussed in this thesis. The resistance however is found by integration over a plane and this must be reformulated for spherical and cylindrical models.

2.3.1 Release from the faces of a plane sheet into an infinite volume.

The new systems discussed in this thesis which have one dimensional planar symmetry are the swelling/diffusion hydrogels, Chapter 4. In this simple example of pure Fickian diffusion we here chose the parameters typical of caffeine release from a fully swollen tea leaf since it will be used later for comparison with the more complex model in which swelling and diffusion occur simultaneously, Chapter 4.

The simulation considers release from the faces of a planar leaf only into an infinite volume. This is not a severe limitation as the leaf membrane is so thin that diffusion from the edges will be negligable by comparison. Edge effects are considered explicitly in Chapter 7. The bond graph required to model this system is the C-C linear model illustrated in fig(1.4). The leaf itself is modelled by the R-C chain while the terminal capacitors (C_1 and C_5 for a three lump bond graph as shown in the example fig(1.4)), account for the capacitance of the contacting solution. Due to the symmetry of this system, only half the system need be modelled, the diffusion process is identical for each half of the leaf and there is no net diffusional transfer between the two halves.

The tea leaf example (Chapter 4) has a swollen thickness of, **l**, 1.008×10^{-2}cm area A, 0.16 cm^2, and diffusion coefficient for Caffeine $5.0 \times 10^{-7} cm^2 s^{-1}$. Since infinite bath conditions are considered the distribution coefficient, α, may be ignored from the R and C equations

above, eqns(2.9), (2.12). To assign values for the resistances and capacitances one must consider the degree of reticulation desired, since this will necessarily affect the magnitudes of both. The reticulation number, n, is the number of equal volume lumps used to represent the half membrane (leaf).

The distance between adjacent lump centres x, is the total leaf thickness divided by twice the number of lumps, n, chosen in the model, eqn(2.13).

$$\Delta x = \frac{1}{2n} \tag{2.13}$$

The resistances of the bond graph may then be calculated from eqn(2.9), with the exception of R_1 which has half this value.

The volume of each lump, v, is simply the total volume of the leaf V divided by double the number of lumps, eqn(2.14).

$$v = \frac{V}{2n} = \frac{1}{2}\frac{A}{n} \tag{2.14}$$

The volumes for the terminal capacitors were $1000cm^3$ for this simulation, which is effectively infinite.

Therefore the values of the R and C coefficients may be determined from the leaf's thickness, area, diffusion coefficient, which are all measurable parameters.

One can see that the assignments for the set of state-space equations (eqns(1.33) to (1.35)) require only the additional information of the respective charge values, q. These are easily determined for this system in which there is considered to be an initially uniform concentration of

caffeine in the leaf membrane. This requires that all volume elements contain the same amount of material, which is given by the total initial loading, q_o, divided by double the number of lumps, n, in the model, eqn(2.15).

$$q = \frac{q_o}{2n} \tag{2.15}$$

The initial charge of caffeine in the leaf, was 1.6×10^{-5}mmol, which corresponds to an initial concentration of .01M (expressed in moles caffeine/litre of swollen leaf). The collecting volume was considered to be initially free of caffeine and therefore the charge on capacitor C_1 was zero.

With these values of q and the diffusion coefficient the R and C terms may be calculated, eqns(2.9) and (2.12) allowing integration of the state-space equations as described in Section 1.3.8. Normally these parameters are fed to a general computer program, which calculates the R, C and q values for an n lump model, and proceeds to integrate the state-space equations. One further consideration to be made is that of the step time interval, H (eqn(1.44), over which each state-space equation is individually integrated, to obtain an updated charge value. For the simulated release of Caffeine from the tea leaf the integration step time of 0.5s was found to be adequately small, for even a thirty lump model.

As the state-space equations are integrated to yield new q values repeatedly as the simulated time proceeds, the charge in C_1 is of particular interest since this is the quantity of caffeine released into the water (infinite

bath). Fig(2.1) shows the computed kinetics of release for one, three and thirty lumped models, by plotting the calculated collection of material in C_1, as a fraction of the initial leaf loading, q_o. It can be seen (and verified in table(2.1)), that the results using a thirty lump model are in excellent agreement with the analytical solution for this release, eqn(2.16), [3].

$$\frac{q}{q_o} = 1 - \sum_{k=0}^{\infty} \frac{8}{(2k+1)^2\pi^2} \exp\left\{ \frac{D(2k+1)^2\pi^2 t}{l^2} \right\} \qquad (2.16)$$

Where q is the quantity of diffusant (caffeine) in the collecting bath, equivalent to q_1 in the bond graph model at time t.

Less than 0.5% disparity is observed.

This validates the network thermodynamic approach and provides a firm basis for discussing more complex systems. The availability of the analytical solution is due to the restrictions of infinite bath and uniform loading. Conditions other than these may be included in the bond graph model with little modification. Initial non-uniform dispersions may be considered by setting different q values in each volume element of the model. Similarly by merely altering the size of the capacitance C_1, finite bath conditions may be simulated. Non-uniform dispersions will be discussed for two dimensional diffusion in Chapter 5 whilst finite bath sizes are considered in detail for ion exchange systems in the following chapter.

The simulations of diffusion in one dimension from three dimensional objects of other geometries, specifically

spherical and cylindrical diffusion are identical, except in the geometry of reticulation and subsequent calculation of the resistances.

2.4 SPHERICAL DIFFUSION

For spherical diffusion the integration of Fick's Law to consider a radial step in concentration is not as trivial as for the planar case, but does not present any particular difficulties.

Rewriting Fick's Law to emphasise the radial geometry.

$$f = D\,A\left(\frac{-d\bar{c}}{dr}\right) \tag{2.17}$$

At each radial position r, the area A is given by the equation for the surface area of a sphere, eqn(2.18).

$$A = 4\pi r^2 \tag{2.18}$$

Substituting in the equation for flow, eqn(2.19)

$$f = \frac{D4\pi r^2(-d\bar{c})}{dr} \tag{2.19}$$

Integrating this equation over the radial distance from r_j to r_{j+1} yields the relationship between flow and the step in concentration, eqn(2.20).

$$f = \frac{D4\pi .\ (-\Delta\bar{c})}{\left(\frac{1}{r_j} - \frac{1}{r_{j+1}}\right)} \tag{2.20}$$

This is analogous to eqn(2.7). Substituting for the hypothetical concentration c, using eqn(2.4) and comparing as before with the constitutive equation for the bond graph resistor, eqn(1.11), gives the resistance of a spherical

resistor as, eqn(2.21).

$$R_j = \frac{\left(\frac{1}{r_j} - \frac{1}{r_{j+1}} \right)}{4\pi D\alpha} \qquad j=1,\ 2,\ \ldots n \tag{2.21}$$

The capacitances of the bond graph are again given by the volume of the element, v and where appropriate scaled by the distribution coefficient, α, eqn(2.12).

2.4.1 Release from a spherical bead into an infinite bath.

The C-C bond graph may be used to model diffusion from a spherical bead, which is a one dimensional diffusion problem also. In this instance the entire system is modelled by the bond graph as opposed to only half for the plane sheet described above. The reticulation of a spherical bead is accomplished by dividing into a number of, again equal volume lumps, that is, a central core surrounded by a number of progressively thinner shells, rather like an onion. This coring is illustrated in fig(2.2) in which the solid circles show the radial distances of the lump edges. The dotted circles mark the radial positions from the sphere centre which divide each lump into two equal volumes, (the volume centre). The radial distances between lump centres as observed do not remain constant, but decrease towards the outer surface of the sphere.

We consider an n lump model to consist of n volume elements making up the sphere with C_1 as in fig(1.4)

accounting for the capacitance of the core and the other terminal capacitor C_{n+1} the capacitance of the collecting volume. In this way fig(2.2) depicts the coring for a 4-lump model, with the sphere divided into four equal volumes. The volume enclosed up to the radius of the volume centre of the j^{th} lump, v_r is given by eqn(2.22).

$$v_r = (j - \tfrac{1}{2})\, v \qquad (2.22)$$

Where v is again the unique volume of the bond graph lump and may be found from the total volume of the sphere V, eqn(2.23).

$$v = \frac{V}{n} = \frac{4\pi r_o^3}{3\,n} \qquad (2.23)$$

r_o is the radius of the spherical bead. v_r may likewise be found from the equation for the volume of a sphere, leading to eqn(2.24).

$$v_r = \frac{4}{3}\pi r_j^3 \qquad (2.24)$$

Therefore the radius r_j may be related to the total radius of the bead, r_o and the number of lumps, n, by combining eqns(2.22) to (2.24).

$$r_j = \left(\frac{j - \frac{1}{2}}{n} \right)^{\frac{1}{3}} r_o \qquad j=1,\ 2,\ \ldots n \qquad (2.25)$$

This facilitates computation of the spherical resistances in eqn(2.21). Note that eqn(2.25) is valid from j=1 to n only. As R_n is calculated for the resistance to flow between the outer lumps volume centre and the surface

of the sphere r_{n+1} in eqn(2.21) is therefore equal to r_o the sphere radius.

The capacitance is found on substitution of the lump volume v in eqn(2.12) using eqn(2.23), giving eqn(2.26).

$$C = \frac{\alpha 4\pi r_o^3}{3\ n} \tag{2.26}$$

The resistances and capacitances for a spherical model may therefore be calculated from the bead's radius, the diffusion and distribution coefficients, all measurable parameters, and the number of lumps used.

The ion exchange bead examples of the next chapter have radius, r_o, 0.1cm and the diffusion coefficient of the pre-loaded ion D, is $1.0x10^{-6}cm^2s^{-1}$. These parameters have been chosen for this simple test system, and used for comparison in the more complex examples of Chapter 3. Again we model release from an initially uniform distribution in the bead into an infinite bath at zero concentration. Each of the charges on the bead capacitors, q, is given by eqn(2.27).

$$q = \frac{q_o}{n} \tag{2.27}$$

Where q_o is the total amount (moles) of diffusant in the bead and n the number of lumps in the model. A step time for integration of the state-space equations, H, of .0125s was used. Once more we can compare results obtained using two, four and thirty lump models, against the analytical solution for spherical diffusion, eqn(2.28) [3].

$$\frac{q}{q_o} = 1 - \sum_{n=1}^{\infty} \frac{1}{n^2} \exp\left(- n^2 \pi^2 \frac{D\,t}{r_o^2} \right) \qquad (2.28)$$

This gives the total diffusant released, q as a fraction of the initial loading, q_o, at time t, and may be compared to eqn(2.16) for the plane sheet.

Excellent agreement is achieved for the thirty lump model, once more the results are within 0.6% of the analytical solution. This is shown in fig(2.2) where the simulated kinetics for the three models are plotted. The data may also be examined in detail in table(2.2). This serves as a verification of the network thermodynamic formulation for spherical diffusion, and also provides an example of isotopic ion exchange in a spherical bead for comparison with ion exchange processes discussed in the next chapter.

2.5 CYLINDRICAL DIFFUSION.

Commonly drug delivery devices are of near cylindrical geometry due to the ease of implant and for oral use. It is therefore useful that a cylindrical diffusion model be developed also. In this section the existing formulations for radial diffusion from an infinite cylinder, [1] will be analysed and tested using the new methods for integration. In the later chapters on two dimensional diffusion this theory will be incorporated into the limited cylinder model, which approximates a pill shape. The development of a cylindrical model is similar to that for spherical flow. With diffusion being radial here also, we can substitute in

eqn(2.17) the area of flow using the equation for the surface area of a cylinder, eqn(2.29).

$$A = 2 \pi r l \tag{2.29}$$

Where l is the length of cylinder considered.

Thus the flow is given by substitution of this into eqn(2.17).

$$f = D2\pi rl \left(\frac{-d\bar{c}}{dr} \right) \tag{2.30}$$

Integrating over the radius from r_j to r_{j+1} gives the flow as a function of the concentration step between these two radii, eqn(2.31).

$$f = \frac{D\ 2\ \pi\ l}{\ln\left(\frac{r_{j+1}}{r_j} \right)} \ (-\Delta\bar{c}) \tag{2.31}$$

Substituting $\Delta\bar{c}$ for the hypothetical concentration, c, eqn(2.4) and comparing with the constitutive equation for the bond graph resistor, gives the resistance as eqn(2.32).

$$R_j = \frac{\ln\left(\frac{r_{j+1}}{r_j} \right)}{2\ \pi\ D\ \alpha\ l} \qquad j=1,\ 2,\ \ldots n \tag{2.32}$$

The capacitance of a lump as for all models is given by the lump volume, v, scaled by the distribution coefficient, α eqn(2.12).

2.5.1 **Diffusion from an infinite rod into an infinite volume.**

Infinite cylinder implies that the diffusion is occurring radially only with no net diffusion normal to the radius. Diffusion from the face of the cylinder has to be considered for finite dimensions, which is a two dimensional diffusion problem. This will be discussed in Chapter 5.

The n lump model cylinder model was reticulated into n equal volumes as for a sphere. Similarly to the sphere model, the radial distances between adjacent lump centres do not remain constant but decrease towards the outer surface. The system may be conceived as a core cylinder surrounded by progressively thinner cylindrical shells. Each lump has a capacitative and resistive function and together the system may be described by the C-C linear bond graph, of which a four lump example is shown in fig(1.4). C_1 for this system accounts for the capacitance of the core of the cylinder and C_{n+1} the capacitance of the external solution, if there is one. The volume enclosed by the radius up to the volume centre of the j^{th} lump is given by the equation for the volume of a cylinder radius, r_j, eqn(2.33).

$$v_r = \pi r_j^2 \, 1 \qquad (2.33)$$

This may be related however to the volume of a single lump using eqn(2.22) and since there are n equal volumes in the model, eqn(2.34) may be written.

$$v = \frac{\pi r_o^2 l}{n} \qquad (2.34)$$

Substituting eqns(2.33) and (2.34) into eqn(2.22) again yields an equation for the radius to the volume centre of the j^{th} lump, r_j, eqn(2.35).

$$r_j = \left(\frac{j - \frac{1}{2}}{n} \right)^{\frac{1}{2}} r_o \qquad j=1, 2, \ldots n \qquad (2.35)$$

This then allows the calculation of the resistance values using eqn(2.32). This equation is valid from j=1, the radii to the volume centre of the core to j=n, the volume centre of the outer shell. The resistance R_n is calculated over the radius from the volume centre of the outer lump to the surface of the cylinder, thus r_{n+1} in eqn(2.32) equals r_o the cylinder radius.

The volume of a lump v is given by the total volume of the cylinder divided by the degree of reticulation. Therefore the capacitance is defined by eqn(2.36), using eqns(2.12) and (2.34).

$$C = \alpha v = \frac{\alpha \pi r_o^2 l^2}{n} \qquad (2.36)$$

Thus the capacitances and resistances of the bond graph may be calculated from the cylinder length and radius and the diffusion and distribution coefficients, all accessible quantities.

This test case considers diffusion from a cylinder

section of length, l, .2cm, since this is the length of the limited cylinder example that will be discussed in Section 5.4.2. The diffusion coefficient, D, was $1.0x10^{-7}cm^2sec^{-1}$ and the solution reservoir taken as $1000cm^3$, effectively infinite, so that once more the distribution coefficient can be ignored. To simulate diffusion from initial uniform loading in the cylinder, the lump q values are given by eqn(2.27). The initial charge in the collecting volume is zero. By examining the evolution of charge in this volume the kinetics of release can be simulated as in previous examples.

The step time used for integration was 0.25s. This was found to be adequately small even for a thirty lump model. In a similar manner to the sphere and plane sheet examples the collecting charge is plotted in fig(2.3) for two, four and thirty lump models and are compared to the analytical solution for radial diffusion from a cylinder with surface concentration zero, eqn(2.37), [3].

$$\frac{q}{q_o} = 1 - \sum_{k=1}^{\infty} \frac{4}{\beta_k^2} \exp\left\{ \frac{-D\,\beta_k^2\,t}{r_o^2} \right\} \qquad (2.37)$$

Where β_k coefficients are the roots of eqn(2.38), in which $J_0()$ is the Bessel function.

$$J_0(\beta_k) = 0 \qquad (2.38)$$

As for the other geometries considered in this series, the thirty lump model reproduces the mathematical solution to Fick's law to high accuracy (0.4%). The data for fig(2.4) may be inspected in table(2.3).

2.6 CONCLUSIONS

The new methods of integration (Section 1.3.8) were shown to give identical results to that using Runge-Kutta integration, [5], conferring great advantages in computational speed. This was not of particular importance for these test systems but was invaluable to the study of computationally intensive simulations such as the non-linear and multi-dimensional models developed in later chapters.

In the course of testing these integration methods we have covered the majority of principles that are common to all simulation work subsequently presented. These include choice of reticulation, setting up and integration of the state-space equations and choice of step time. In addition the formulations for resistance and capacitance functions remain similar for the more complex examples which are dealt with in the following chapters.

FIGURE 2.1.

Diffusion from a planar membrane: Comparison of network thermodynamic simulation with the analytical solution for Fickian diffusion from planar membrane. Results obtained using 1-, 3- and 30- lump bond graph models are compared, curves 1, 2, and 3 respectively, analytical solution represented by points, eqn(2.16), [3]. Parameters used for system of Caffeine release from swollen tea leaf, area A, $0.159cm^2$, thickness l, 0.01008cm and diffusion coefficient of Caffeine D, $5.0x10^{-7}cm^2s^{-1}$. Ordinate represents amount of Caffeine released into infinite bath as fraction of initial loading. Abscissa is simulated time in seconds. Using thirty lumps with step time H, $3.75x10^{-4}s$ produces result within 0.5% agreement of analytical solution. (See table(2.1)).

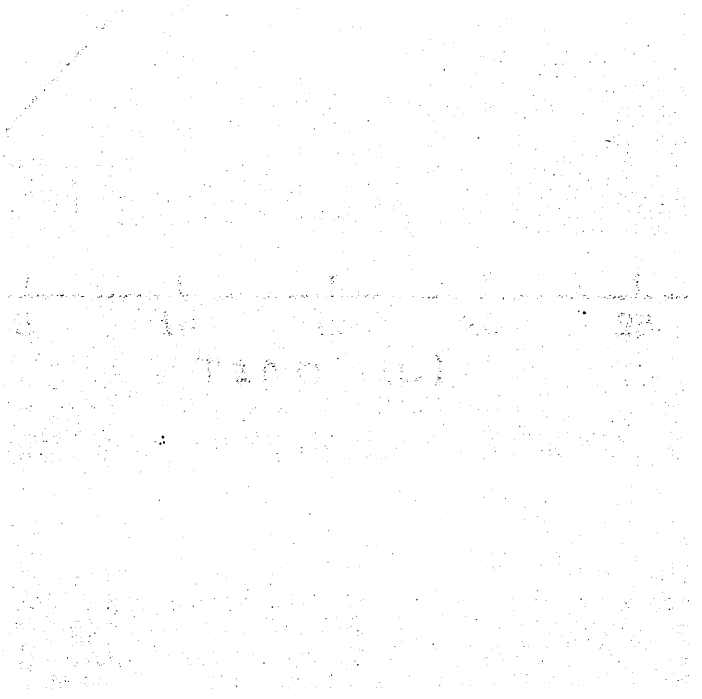

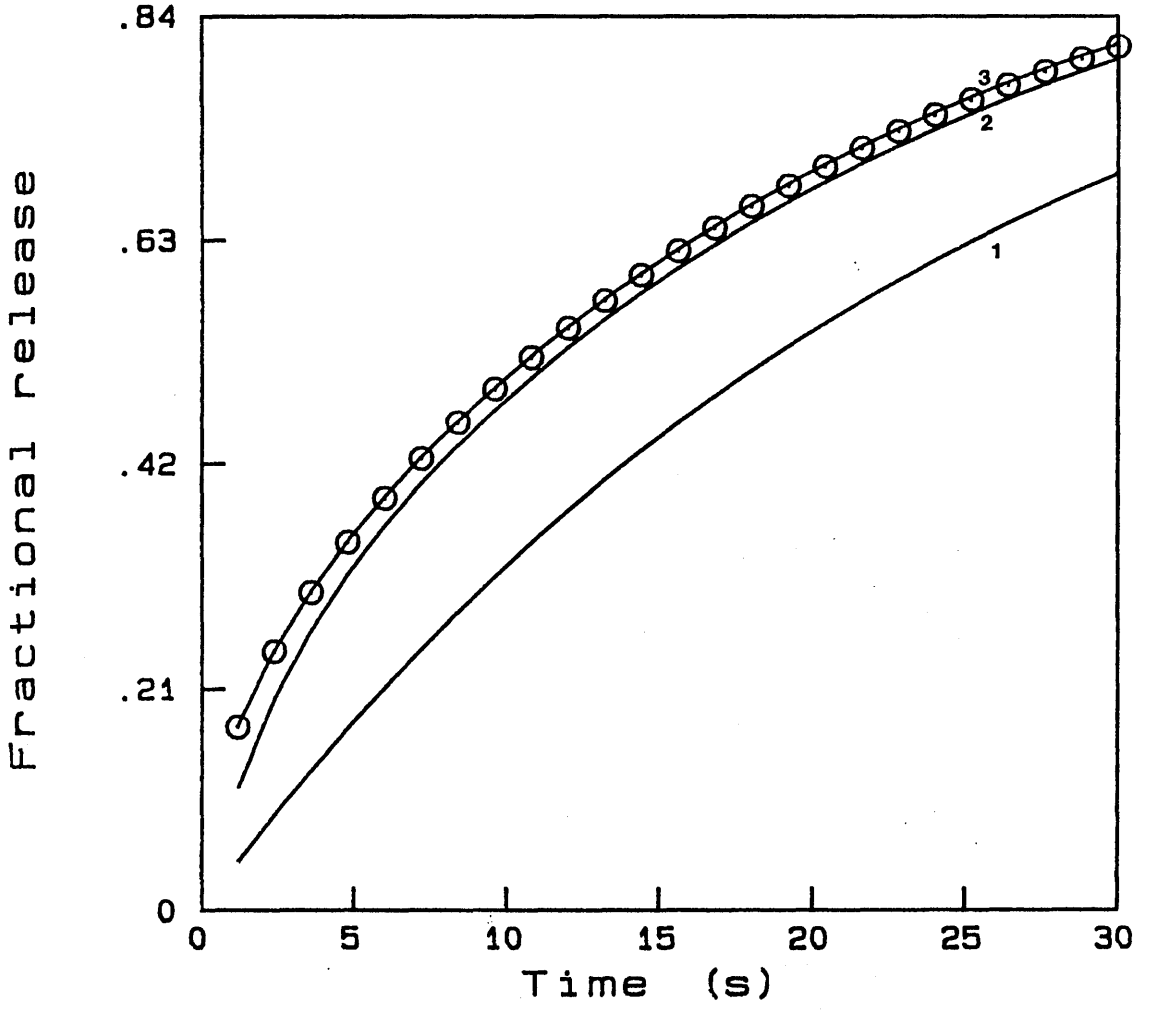
Planar model
Fractional release
.84
.63
.42
.21
0
0
5
10
15
20
25
30
Time (s)
1
2
3

FIGURE 2.2.

Hypothetical coring of spherical model into n equal volumes. Solid lines show radial distances of lump edges. Dotted lines show radial distance of lump centre, dividing each lump volume into two equal halves.

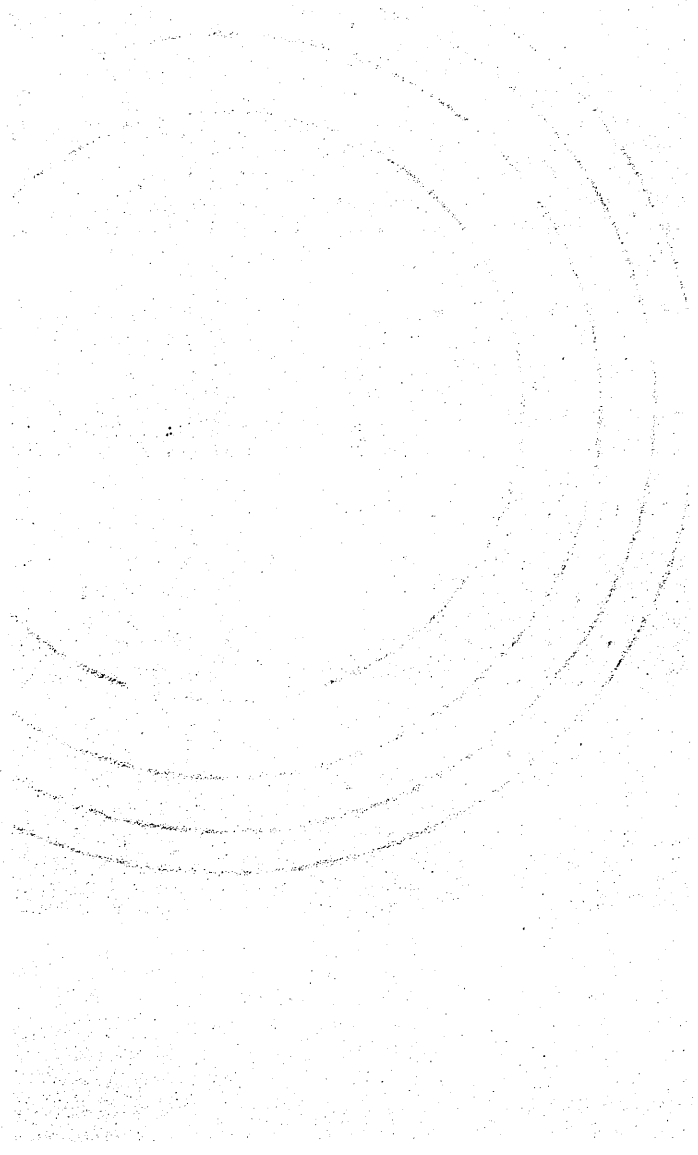

4 LUMP MODEL

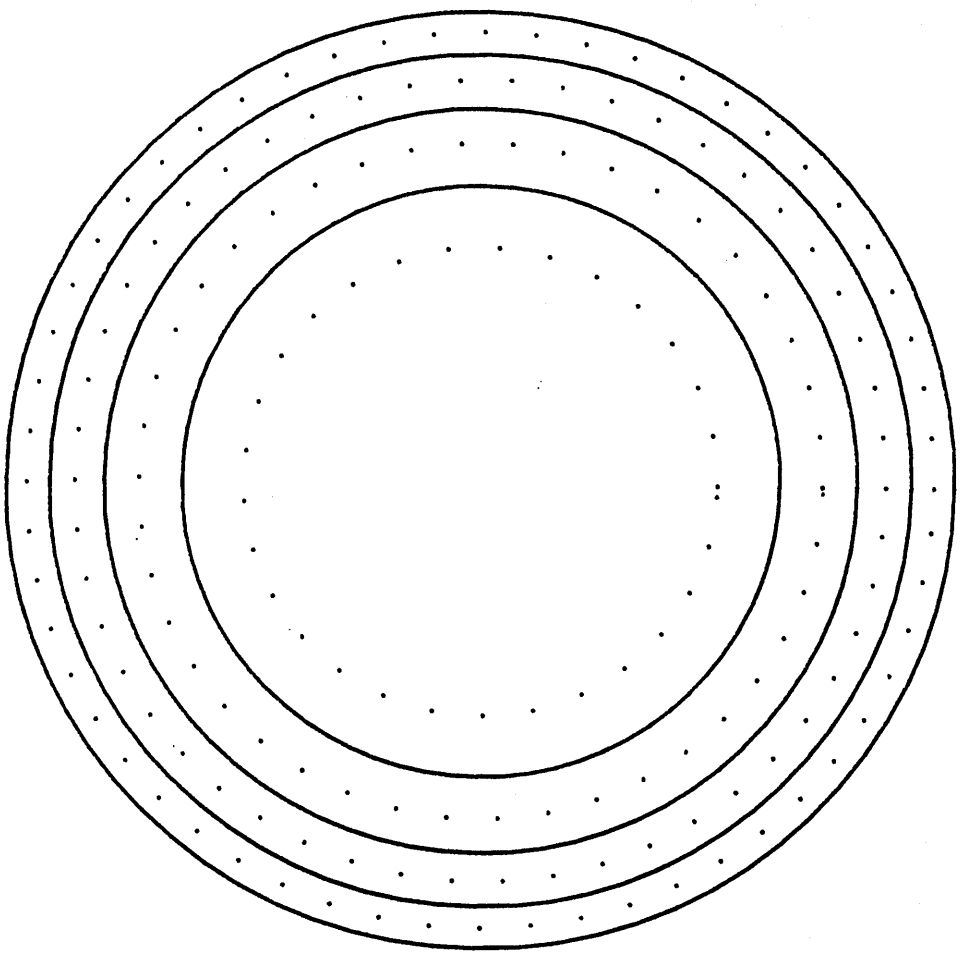

FIGURE 2.3.

Comparison of network thermodynamic simulation with the analytical solution for diffusion from a sphere into an (effectively) infinite volume. Results obtained using 2-, 4- and 30- lump bond graph models are compared, curves 1, 2, and 3 respectively, analytical solution represented by points, [3], eqn(2.29). Parameters used, bead radius r_o, 0.1cm, diffusion coefficient D, $1.0 \times 10^{-6} cm^2 s^{-1}$ and bath volume $1{,}000 cm^3$. The ordinate represents amount of diffusant released into infinite bath as fraction of initial loading. Abscissa is time in seconds. Using thirty lumps with step time H, $1.25 \times 10^{-2} s$ produces result within 0.6% agreement of analytical solution.

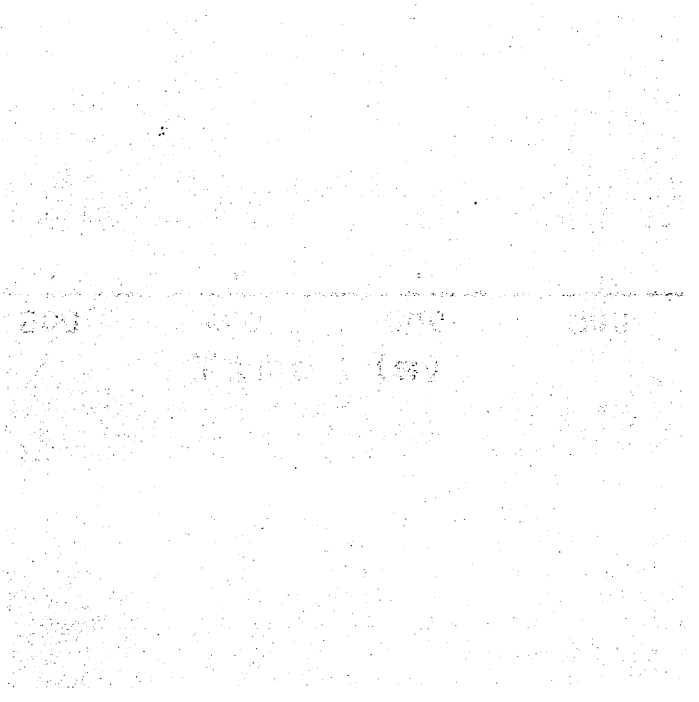

Spherical model

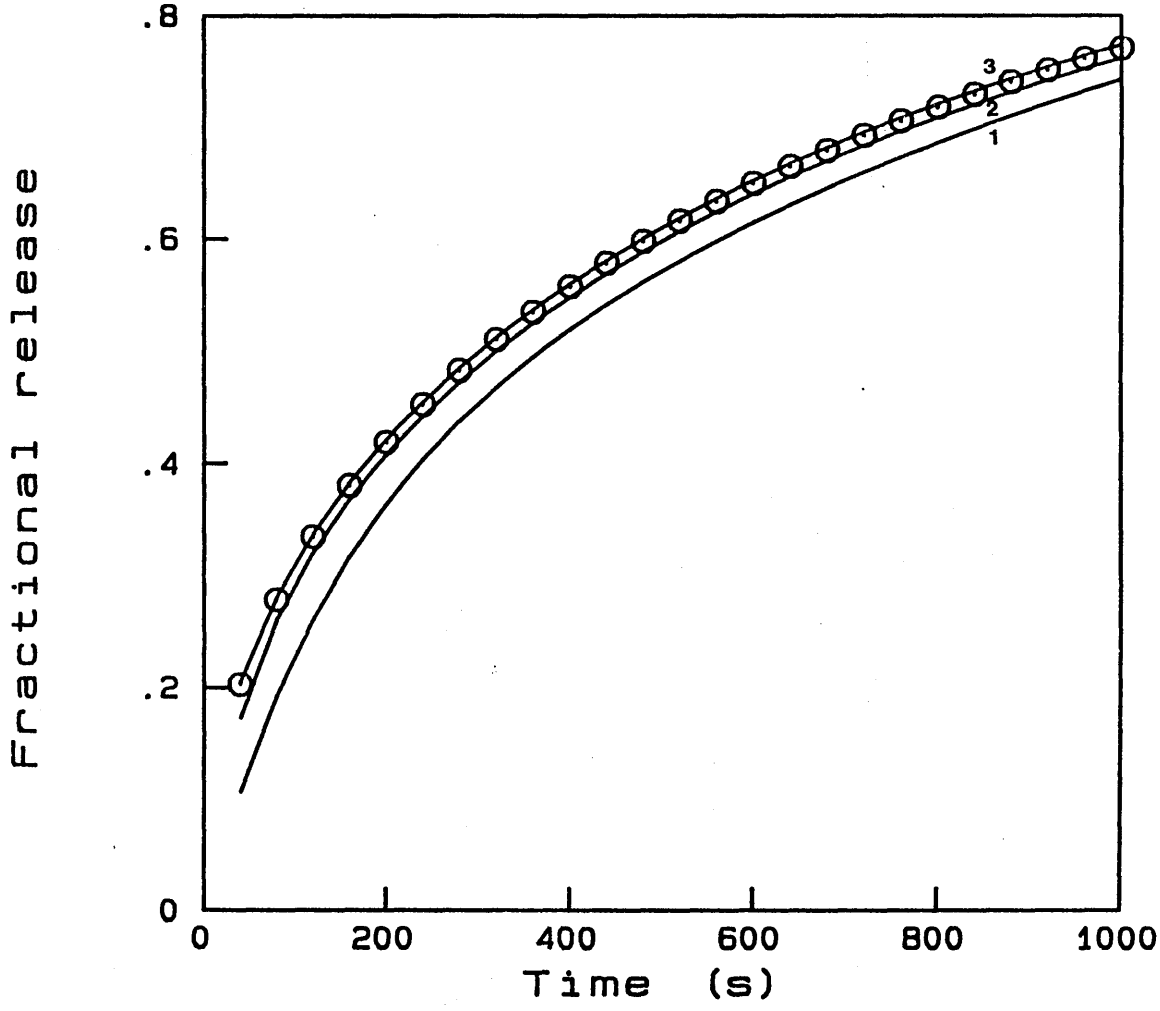

FIGURE 2.4.

Comparison of network thermodynamic simulation with the analytical solution for diffusion from a section of infinite rod into an infinite volume. Results obtained using 2-, 4- and 30- lump bond graph models are compared, curves 1, 2, and 3 respectively, analytical solution represented by points, [3], eqn(2.38). Parameters used, cylinder radius r_o, 0.1cm, section length l, 0.2cm, diffusion coefficient D, $1.0 \times 10^{-7} cm^2 s^{-1}$ and bath volume $1000 cm^3$. Ordinate represents amount of diffusant released into infinite bath as fraction of initial loading in section. Abscissa is simulated time in seconds. Using thirty lumps with step time H, 0.25s produces result within 0.4% agreement of analytical solution.

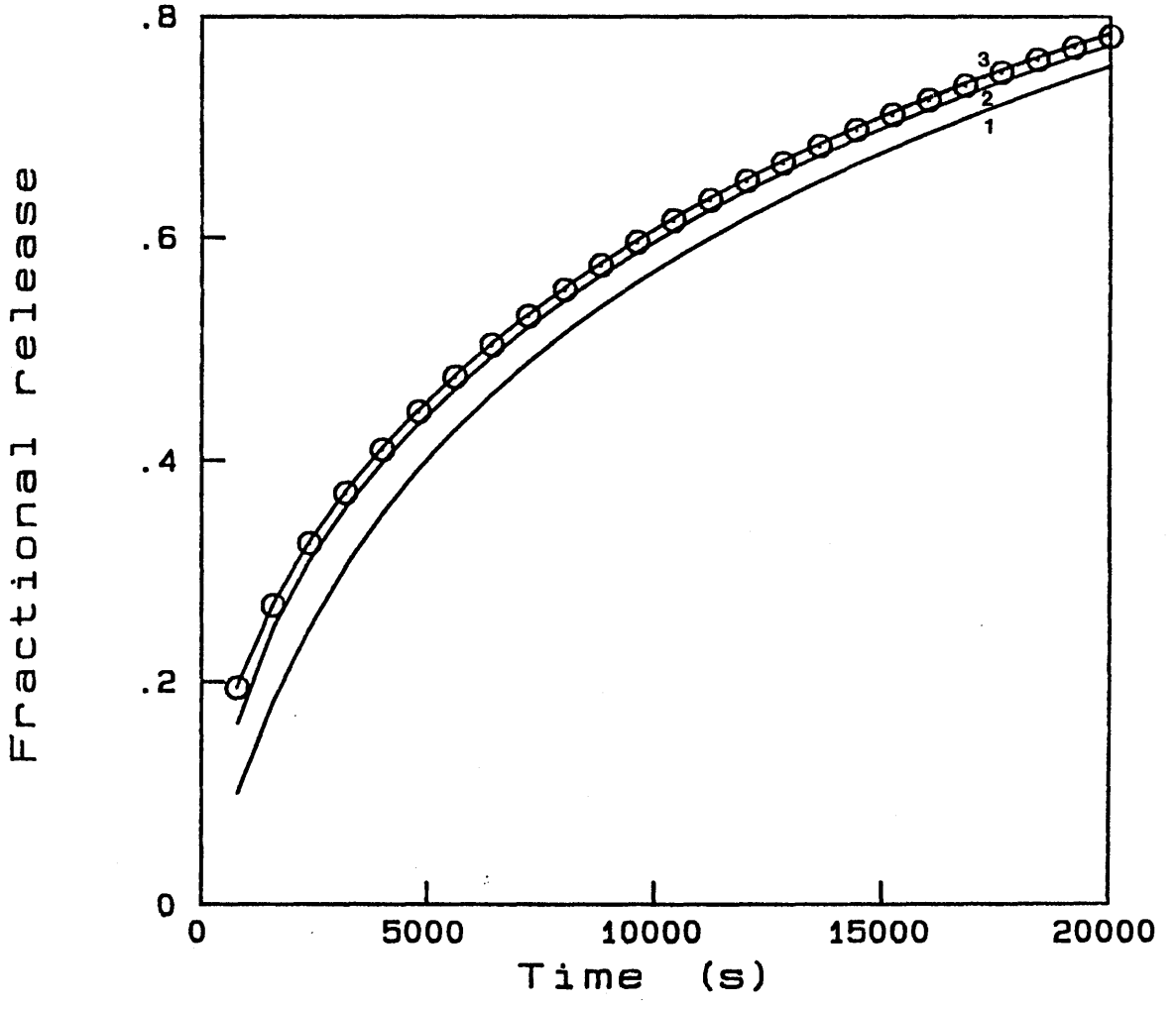
Cylindrical model
Fractional release
.8
.6
.4
.2
0
0
5000
10000
15000
20000
Time (s)
3
2
1

TABLE 2.1

Simulation of of fractional release (q/q_o) from faces of planar membrane into an infinite volume. Results produced using three degrees of reticulation compared to the analytical solution for an infinite bath in second column, eqn(2.16), [3]. Thickness of membrane, l, .01008cm, area A, 0.159cm^2, diffusion coefficient of caffeine D, $5.0x10^{-7}cm^2s^{-1}$

		Bond graph simulations		
Time(s)	Analtcl	30 lump	3 lump	1 lump
1.2	0.173	0.174	0.117	0.046
2.4	0.245	0.246	0.200	0.090
3.6	0.300	0.301	0.264	0.132
4.8	0.347	0.348	0.317	0.172
6.0	0.388	0.389	0.362	0.210
7.2	0.425	0.426	0.402	0.247
8.4	0.459	0.460	0.438	0.282
9.6	0.490	0.492	0.470	0.315
10.8	0.520	0.521	0.501	0.346
12.0	0.547	0.549	0.529	0.377
13.2	0.573	0.575	0.556	0.405
14.4	0.597	0.599	0.581	0.433
15.6	0.620	0.622	0.604	0.459
16.8	0.642	0.644	0.626	0.484
18.0	0.662	0.664	0.647	0.508
19.2	0.681	0.684	0.667	0.530
20.4	0.699	0.702	0.685	0.552
21.6	0.716	0.719	0.703	0.573
22.8	0.732	0.735	0.719	0.592
24.0	0.747	0.750	0.735	0.611
25.2	0.762	0.765	0.749	0.629
26.4	0.775	0.778	0.763	0.646
27.6	0.788	0.791	0.776	0.663
28.8	0.800	0.803	0.789	0.678
30.0	0.811	0.815	0.800	0.693

TABLE 2.2

Table of fractional release q/q_o, from a sphere into infinite bath, see fig(2.3). Results produced using three degrees of reticulation compared to the analytical solution for an infinite bath, [3], eqn(2.29) in second column. Radius r_o, 0.1cm and diffusion coefficient D, $1.0x10^{-6}cm^2s^{-1}$.

		Bond graph simulations		
Time(s)	Analtcl	30 lump	4 lump	2lump
40	0.202	0.203	0.172	0.106
80	0.279	0.280	0.260	0.191
120	0.335	0.336	0.320	0.260
160	0.380	0.382	0.367	0.316
200	0.419	0.421	0.407	0.363
240	0.452	0.454	0.442	0.403
280	0.482	0.485	0.472	0.437
320	0.510	0.512	0.500	0.468
360	0.534	0.537	0.525	0.495
400	0.557	0.559	0.548	0.519
440	0.578	0.581	0.569	0.541
480	0.598	0.600	0.588	0.561
520	0.616	0.619	0.607	0.580
560	0.633	0.636	0.624	0.598
600	0.649	0.652	0.640	0.614
640	0.664	0.667	0.655	0.630
680	0.679	0.682	0.670	0.645
720	0.692	0.695	0.683	0.659
760	0.705	0.708	0.696	0.673
800	0.717	0.720	0.708	0.686
840	0.729	0.732	0.720	0.698
880	0.740	0.743	0.731	0.710
920	0.751	0.754	0.742	0.721
960	0.761	0.764	0.752	0.732
1000	0.770	0.774	0.762	0.742

TABLE 2.3

Simulation of diffusion from section of infinite rod, fig(2.4). Data are fractional release, q/q_o from cylinder, section length, 0.2cm, radius 0.1cm, diffusion coefficient D, $1.0x10^{-7}cm^2s^{-1}$ and bath volume $1000cm^3$. Results using three degrees of reticulation compared to analytical solution for an infinite bath, [3], eqn(2.38) in second column.

Bond graph simulations

Time(s)	Analtcl	30 lump	4 lump	2 lump
800	0.194	0.194	0.162	0.100
1600	0.269	0.270	0.249	0.181
2400	0.325	0.326	0.309	0.248
3200	0.370	0.372	0.357	0.304
4000	0.410	0.411	0.398	0.351
4800	0.444	0.446	0.433	0.392
5600	0.475	0.477	0.465	0.428
6400	0.503	0.505	0.493	0.460
7200	0.529	0.531	0.520	0.488
8000	0.553	0.555	0.544	0.514
8800	0.575	0.577	0.566	0.538
9600	0.596	0.598	0.587	0.560
10400	0.615	0.618	0.607	0.581
11200	0.634	0.636	0.625	0.600
12000	0.651	0.654	0.643	0.618
12800	0.667	0.670	0.659	0.635
13600	0.683	0.686	0.675	0.651
14400	0.698	0.700	0.689	0.667
15200	0.712	0.714	0.703	0.681
16000	0.725	0.728	0.717	0.695
16800	0.737	0.740	0.729	0.708
17600	0.749	0.752	0.741	0.721
18400	0.761	0.764	0.753	0.733
19200	0.772	0.775	0.764	0.745
20000	0.782	0.785	0.774	0.756

REFERENCES FOR CHAPTER TWO

[1]. R.Paterson and Lutfullah in, Ion Exchange Technology, D.Naden and M.Streat (Eds.). Ellis Horwood, Chichester, England (1982).

[2]. R.Paterson and Lutfullah. J. Membrane Sci. **23**, (1985) 59.

[3]. J.Crank. The Mathematics of Diffusion, Clarendon Press, Oxford, England (1959).

[4]. R.Paterson. Network thermodynamics, Chapter 1 in Membranes Structure and Function, E. E. Bittar (Ed.), J.Wiley and Sons, New York (1980).

[5]. P.Doran. Ph.D. Thesis, Glasgow University, Scotland, (1977).

CHAPTER THREE

NON-LINEAR ONE DIMENSIONAL DIFFUSION WITH SPECIFIC EXAMPLES IN ION EXCHANGE KINETICS.

3.1 INTRODUCTION

In the introduction to this thesis it was stated that coupling phenomena would not be discussed explicitly. Although ion exchange theory must include electro-diffusional coupling between ions, we will simplify by examining bi-ionic exchange only. In so doing we require only one 'mutual' diffusion coefficient common to both ions. The problem becomes one of treating systems with non-linear, concentration-dependant diffusion coefficients, [1]. This serves as an excellent example of non-linear resistivity since the relationship for the variation of the diffusion coefficient is given explicitly using Nernst-Planck theory and not by an **ad hoc** expression. Only for the trivial case of isotopic exchange (ions of equal charge and diffusion coefficient), which results in a time independant diffusion coefficient, can the kinetics of ion exchange be solved analytically.

It is convenient that this latter problem has been solved previously by numerical techniques, specifically by Helfferich and Plesset [2]. They performed numerical integrations to simulate the kinetics of exchange between monovalent ions in a spherical bead with infinite bath conditions. With, as we shall see, successful reproduction of the Helfferich and Plesset system by network modelling, we may proceed to much more complex issues previously unsolved, specifically those of the effects of finite collecting volumes and varying selectivities, both of which are important practical and theoretical considerations.

In this chapter the theories for the formulations of

diffusion coefficient and selectivity are discussed and how these are input to the bond graph model for spherical and planar diffusion, (discussed in Chapter 2). The methods outlined in the previous chapter for computer simulation based on the linear C-C model, fig(1.4), are identical except with the consideration that the appropriate bond graph parameters are updated repeatedly throughout the calculations.

3.2 BI-IONIC ION EXCHANGE. AN EXAMPLE OF NON-LINEAR FICKIAN DIFFUSION.

Consider the exchange process between two counter ions, **a** and **b**. In the absence of coion, the stoicheometry is given by eqn(3.1).

$$\nu_a \mathbf{a}^{z_a}_{resin} + \nu_b \mathbf{b}^{z_b}_{solution} \longrightarrow \nu_b \mathbf{b}^{z_b}_{resin} + \nu_a \mathbf{a}^{z_a}_{solution} \qquad (3.1)$$

ν_a and ν_b are the stoicheometric coefficients and z_a, z_b the signed valencies of the ions. The requirement of electroneutrality may be stated by eqn(3.2).

$$\nu_a z_a + \nu_b z_b = 0 \qquad (3.2)$$

In all cases (except for the trivial example of exchange between two ions with equal valency and mobility) there will be diffusion potentials set up during exchange. The flux densities of either of the exchanging ions may be approximated by the Nernst-Planck equation, eqn(3.3).

$$J_i = -D_i \left[\frac{d\bar{c}_i}{dx} + z_i \bar{c}_i \frac{F}{RT} \frac{d\psi}{dx} \right] \qquad (3.3)$$

The labelled ion i may represent either of the

exchanging ions **a** or **b** throughout this discussion. x is the axis of diffusion. (Both linear and radial diffusion will be considered). ψ is the electrical potential. Barred concentrations are those within the exchanger phase. The system is subject to certain restrictions however which simplify the problem. Due to electroneutrality in the resin phase the concentrations of the two exchanging counterions may be related, eqn(3.4).

$$z_a\bar{c}_a + z_b\bar{c}_b = c_f = \text{constant} \qquad (3.4)$$

Where c_f is the concentration of fixed ionic groups within the ion exchanger. There is an additional condition of zero electric current at all locations within the exchanger phase, eqn (3.5).

$$z_aJ_a + z_bJ_b = 0 \qquad (3.5)$$

From eqns(3.3), (3.4) and (3.5), electric potential terms may be eliminated and the ionic fluxes J_a and J_b may be represented in Fickian form, eqns (3.6), (3.7).

$$J_a = D_a^* \left(\frac{-d\bar{c}_a}{dx} \right) \qquad (3.6)$$

$$J_b = D_b^* \left(\frac{-d\bar{c}_b}{dx} \right) \qquad (3.7)$$

Where the coefficients D^*_a, D^*_b are equal and define a common or mutual diffusion coefficient D_{ab}.

$$D_a^* = D_b^* = D_{ab} = \left[\frac{D_a D_b \left(z_a^2 \bar{c}_a + z_b^2 \bar{c}_b \right)}{D_a z_a^2 \bar{c}_a + D_b z_b^2 \bar{c}_b} \right] \qquad (3.8)$$

The mutual diffusion coefficient, D_{ab} is a function of the concentrations of both counterions in the phase and so it's value will vary from point to point in the exchanger. Since network thermodynamics assumes local equilibrium in each volume element the mutual diffusion coefficient will vary from bond graph lump to lump.

Note that either of eqns(3.6) or (3.7) is equivalent to Fick's law (eqn(2.1)) with a variable diffusion coefficient, consequently we can, without further modification, use the theory of Chapter 2 to obtain the R and C values of a Fickian model, but now with a variable rather than a constant D value. Diffusion in a planar membrane separating two solutions and ion exchange by a spherical bead in contact with an external solution will be considered. It is an indication of the power of the network method that a single bond graph may be applied (with appropriate formulations for the R and C coefficients) to solve each, (see Sections 2.3 and 2.4). A major advantage of bond graph theory is its economy in formulating problems.

3.3 ION SELECTIVITY.

To define the R and C coefficients of the C-C bond graph for bi-ionic exchange modelling one must choose which of the ions is to determine the (unique) effort in the

system. This is an arbitrary choice since the concentrations of each ion may always be found from the other using eqn(3.4). Once this choice has been made a Fickian formulation is considered: A direct analogy with the examples in Chapter 2. The governing diffusion coefficient and therefore the resistances however are time dependant.

One difference in the approach here though is that by defining a unique effort the previous choice of the external solution as the reference phase is not used for the ion exchange model. Instead the exchanger phase is chosen since the ionic composition in this phase is restricted by the principle of co-ion exclusion and the requirement of electroneutrality in the phase. As a result, efforts within the exchanger phase may be defined as the corresponding concentrations directly. The bond graph resistances and capacitances, (with the exception of the capacitance of the external solution), may be calculated without using the selectivity relationships. By this method planar and radial resistances are given by eqns(3.9) and (3.10) respectively.

$$R = \frac{\Delta x}{D_{ab} A} \tag{3.9}$$

$$R = \frac{\left(\frac{1}{r_j} - \frac{1}{r_{j+1}} \right)}{4\pi D_{ab}} \tag{3.10}$$

Eqn(3.10) gives the resistance between any two radii,

r_j and r_{j+1}, the radii for which diffusion is calculated between in this model is discussed explicitly below.

Capacitance is now simply the exchanger lump volume, eqn(3.11)

$$C = v \tag{3.11}$$

The concentration of the reference ion in the external solution, $\bar{c}_i$ must be related to a hypothetical equilbrium concentration c_i. In this work ion b is chosen as the reference ion. Thus the hypothetical concentration, c_b may always be found using the distribution coefficient, α defined by eqn(3.12), (compare with eqn(2.3)).

$$\alpha = \frac{\bar{c}_b}{c_b} \tag{3.12}$$

A common system of effort is therefore maintained. As a consequence the external solution capacitance is simply its volume, v_e, divided by the distribution coefficient, eqn(3.13). (Compare with the equations for capacitance using the external solution as the reference phase, eqn(2.12).)

$$C = \frac{v_e}{\alpha} \tag{3.13}$$

This distribution coefficient is not constant but varies with the relative concentrations of both ions across the phase boundary. The equilibrium position of a bi-ionic exchange system may be described by the molar selectivity coefficient, defined by eqn(3.14), [1].

$$K'^{a}_{b} = \frac{\bar{c}_a^{|z_b|} \; c_b^{|z_a|}}{c_a^{|z_b|} \; \bar{c}_b^{|z_a|}} \qquad (3.14)$$

For the exchange of mono-valent ions, which will form the bulk of this discussion, eqn(3.14) may be solved for α rather simply, eqn(3.15).

$$\alpha = \frac{c_f}{K'^{a}_{b} \, c_a + c_b} \qquad (3.15)$$

This gives the equilibrium position for mono-valent ions as a function of the concentrations in the external solution.

The more complex example of uni-divalent exchange will be considered in Section 3.5.3.

A further complication, although one which may be easily incorporated into the network model, is that of a variable K'^{a}_{b} value. This situation is not uncommon in ion exchange systems and as such should be considered. It also demonstrates very clearly the severe non-linear nature of these ion exchange diffusion problems. One theory for variable selectivity which has found much success, especially for zeolite exchangers, is Kielland's semi-empirical equation, eqn(3.16), [3]. Barrer has since derived this equation from theory [4]. It has been chosen here for the purposes of illustration only since the empirical constant, w may be changed to give a suitably variable isotherm. Any theoretical or experimental

expression for K'^{a}_{b} as a function of loading may be used in these models.

$$\ln K'^{a}_{b} = \ln {}^{N}\kappa^{a}_{b} + w\left(\bar{N}_a^{\,2} - \bar{N}_b^{\,2} \right) + \ln \frac{\gamma_a}{\gamma_b} \qquad (3.16)$$

This formulation of Kielland's equation is valid for univalent exchange only and so a discussion of variable selectivity is limited to these. $\bar{N}_a$, $\bar{N}_b$ are the mole fractions of the ions in the exchanger, assuming exclusion of co-ion. (These must be approximated using the average concentrations of each ion in the outermost lump.) ${}^{N}\kappa^{a}_{b}$ is the rational thermodynamic equilibrium constant and γ_a, γ_b are the activity coefficients of the respective ions. We simplify our use of the equation considerably by considering the examples in which the quantities:

$$\ln {}^{N}\kappa^{a}_{b} \quad \text{and} \quad \ln \frac{\gamma_a}{\gamma_b}$$

are both zero. Fig(3.1) shows the isotherm produced under these conditions with w = 2.

3.4 EVALUATION OF R AND C COEFFICIENTS.

As the resistors R_2 to R_n in an n lump planar model are required to account for the resistance between two adjacent lump centres there is an added complication that these volumes will have different local D_{ab} values. As a consequence, the total resistance must be found as the sum of the resistances from each lump centre to the adjacent lump edge, (since they are in series). For planar diffusion this is given by eqn(3.17).

$$R_j = \frac{1}{n\,A}\left(\frac{1}{D^j_{ab}} + \frac{1}{D^{j+1}_{ab}}\right) \qquad j=2,\ 3,\ ..n \qquad (3.17)$$

Where D^j_{ab} is the local diffusion coefficient in the j^{th} volume element. For the planar model volumes 1 and n+2 correspond to well stirred aqueous solution volumes, with no resistive component. Therefore the resistances R_1 and R_{n+1} may be calculated without further complication.

In the sphere model however, volume 1 is the bead core with diffusion coefficient D^1_{ab}. Therefore by similar argument the radial diffusion resistances R_1 to R_{n-1} must also be found as a sum, eqn(3.18), derived from eqn(2.21).

$$R_j = \frac{\left(\frac{1}{r_j} - \frac{1}{r^e_j}\right)}{4\pi D^j_{ab}} + \frac{\left(\frac{1}{r^e_j} - \frac{1}{r_{j+1}}\right)}{4\pi D^{j+1}_{ab}} \qquad j=1,\ 2,\ ..n-1 \qquad (3.18)$$

Where r^e_j is the radial distance from the centre of the sphere to the outer edge of lump j, defined by eqn(3.19). Derived in an analogous way to that for eqn(2.25), (which defined the radii of the lump centres in a spherical model).

$$r^e_j = \left(\frac{j}{n}\right)^{1/3} r_o \qquad j=1,\ 2,\ ...n \qquad (3.19)$$

R_n may be calculated as usual for the resistance from the volume centre of the outer lump to the sphere surface

using D^n_{ab}, the sum of eqn(3.18) reduces to one term. (When j=n, $r^e_j = r_{j+1} = r_o$).

As the time dependent parameters, D_{ab} and α appear in the expressions for bond graph resistance and capacitance, respectively, it is necessary to update the R and C values throughout the simulation. This can only be done between integration steps (over which the R and C coefficients are regarded as pseudo-constants (Section 1.3.8)). The step time is reduced so that the inherent error in this assumption is reduced below the precision desired. It is to be noted that time is treated similarly to space in network thermodynamics. Space is reticulated into a finite number of volume elements or lumps which are small enough to model a continuum. Time likewise is broken into finite steps for integration. This temporal reticulation is fine enough to allow continuously changing non-linear processes to be simulated. In short the system dynamics are performed in much the same way as cartoon movies are animated.

Obviously non-linear processes require increased calculation. The varying nature of the bond graph parameters impose further reductions in the step time and this also leads to greater computational effort, nevertheless these simulations are relatively undemanding of computation time, and are within the capabilities of a modern desktop micro computer.

3.5 APPLICATIONS TO A NUMBER OF BOUNDARY CONDITIONS.

The flexibility of the bond graph model will be illustrated in this section by progressively introducing additional non-linear components as more and more complex

problems are addressed.

For ease of interpretation certain features of all the examples given below will remain common throughout. Changes in these and ancillary parameters will be made only to introduce some new effect. The exchanger materials are considered to have unit molarity (moles/litre of resin) of fixed charge and at time zero to be entirely in the ion **a** form. External solutions in the spherical bead models are also considered to contain pure solutions of a salt of ion **b** only. (For the ion exchange membrane example directly below there is a second contacting solution containing a salt of ion **a** only). In all cases coion exclusion is assumed complete.

3.5.1 Ion exchange diffusion through a membrane.

This section describes the simulation of an ion exchange membrane, from an initial condition of zero loading of ion **b** throughout the membrane, through to the steady state in which the ionic flows are constant. This state is achieved when the effort across the membrane is held constant. This is equivalent to considering infinite bath conditions at both faces. On the left hand side of the membrane is a pure solution of a salt of ion **b**, on the right an equivalent solution of a salt of ion **a**. In common with the ion exchange bead examples below the exchanger is initially in the **a** form. In principle any initial condition could be considered.

The modelling of a planar membrane dividing two solutions has been described above using the C-C linear bond graph. The methods for setting up this model are

identical, cf. those of Section 2.3.1, except that the formulations of R and C for a bi-ionic exchange system must be substituted in the state-space equations. In addition, the entire system is modelled, so that the membrane is conceptually divided into n and not 2n volume elements. (As described in Chapter 1.)

Test input data for this example has been obtained from Helfferich and Ocker, [5], who predicted the steady-state profiles for this system using **ad hoc** numerical techniques. The membrane was a sodium/hydrogen exchanger initially in the hydrogen form (our ion **a**). The left hand, (effectively infinite solution), contains 1M sodium chloride, $NaCl_{(aq)}$. The right hand solution is a 1M hydrochloric acid, $HCl_{(aq)}$. The chloride ions are entirely excluded from the membrane phase and it is the concentration of Na^+ ion that is chosen as the unique effort. The charges on the capacitors in the bond graph were set according to the initial amount of sodium in each volume element of the model, and the simulation followed the flow of Na^+. (As a consequence C_1 only, the capacitor of the left hand solution was charged at time zero.)

The membrane had area, A, $2.5cm^2$ and thickness, l, 0.1cm. The self diffusion coefficients of Na^+ and H^+, D_b and D_a were respectively, 2.44 and $4.0x10^{-6}cm^2sec^{-1}$ and the external solution volumes were effectively infinite at $1000cm^3$. For simplicity, and to standaridse with the examples to follow, the exchange membrane was assigned unit molarity of fixed charge. The R and C values in the state-space equations were updated after each step time of 0.5s.

For this example we were interested mainly in the

evolution of concentration profiles during the exchange process. As the concentration of ion b (or Na^+) was chosen as the effort for this model concentrations of sodium were obtained directly from the charge in each volume element (lump). By plotting these simulated concentrations at the position of the lump centre and joining these points, concentration profile were constructed. For a thirty lump model, as used here, the profiles appear quite smooth, fig(3.2). Not only can this technique predict the steady-state profile in agreement with Helfferich and Ocker, but also the evolution to this steady state condition.

The ability to construct concentration profiles in this manner is invaluable in the study and understanding of dynamic systems. By plotting the average concentration in each lump at it s volume centre, a true representation of the simulated data is produced. It is possible to interpolate or curve fit the data to build a picture of the concentration distribution over the entire system, but usually this is not necessary, as noted above. The method can be extended to the construction of two dimensional concentration profiles, illustrated in Chapters 5 and 6. In the next section a slightly different approach is used for presenting concentration profiles in a sphere, in which radial distances between lump centres are not equal.

3.5.2 Ion exchange between a spherical bead and an infinite bath.

An equivalent ion exchange problem except with spherical symmetry is the exchange of mono-valent ions between a bead and an infinite volume bath. As an example,

a bead of radius, r_o, 0.1cm is considered with the self diffusion coefficient of ion **a**, D_a, being $1.0 \times 10^{-6} cm^2 s^{-1}$. Clearly the kinetics of this system also depend on the self diffusion coefficient D_b. To study the effects of different D_a and D_b values, D_a is kept constant for all spherical bead examples in this chapter, and the value of D_b is changed as necessary. For brevity only the ratio D_a/D_b is quoted.

For this initial infinite bath example, three such ratios were chosen. No matching experimental data was sought but Helfferich and Plesset have previously examined the kinetics of exchange for these infinite bath conditions using again an **ad hoc** numerical approach. These results were reproduced using a bond graph model of the system as a means of testing these new bond graph methods. This approach also serves to validate the use of the bond graph for solving non-linear diffusion problems in general.

The ratios of D_a/D_b examined were 5 and 10, compared to the isotopic case in which D_a/D_b is 1 and the exchange kinetics are given by the analytical solution for isotopic diffusion, eqn(2.28).

Of special interest here is the total uptake of ion **b** into the bead, which is equivalent (for mono-valent ions) to the amount of ion **a** released into the bath. This may be found either by summing the charges in the bead capacitors, (C_1 to C_n in an n lump model), or alternatively by plotting the disappearance of charge in the capacitor representing the external solution, C_{n+1}. (n is 30 in these models).

The resultant simulations are presented in fig(3.3),

together with the data from Helfferich and Plesset (circles around points), [5]. The total amount of ion b in the bead has been plotted as a fraction of the fixed charge against a dimensionless time parameter, τ, eqn(3.20).

$$\tau = \frac{D_a t}{r_o^2} \tag{3.20}$$

The broken curve is the analytical solution for the isotopic exchange calculated from eqn(2.28), the test computer simulation of which has been discussed in Section 2.4. The network thermodynamic simulations reproduce the kinetic release data to within 0.1%, as is clearly illustrated in fig(3.3). Curve 1 is the exchange rate for D_a/D_b equal 10, which results in the slowest kinetics. Curve 2, for D_a/D_b equal 5, lies between the uptake curve of the latter and the isotopic exchange simulation.

Similarly to the planar membrane example in Section 3.5.1, concentration profiles may be constructed by plotting the concentration of ion b in each lump at the volume centre. For these profiles the ordinate is fractional exchange, c_b/c_f, (since c_f was chosen as 1M here, this is in fact the absolute concentration of ion b), the abscissa is fractional radius, r/r_o. (On this scale position 0 is the centre and 1 the outer surface of the bead). Unfortunately, since the volume elements in the sphere model become progressively thicker towards the centre, (as described in Chapter 2), the profiles would not appear uniformly smooth unless the number of lumps used was

very large, far in excess of the requirement for quantitative accuracy. In this study the profiles are illustrated by drawing a horizontal bar corresponding to each lump at a level corresponding to the average concentration in that volume. In addition, a vertical notch has been drawn on each bar to indicate the radial position of the volume centre of each lump.

The evolution of concentration profiles in beads with D_a/D_b ratios of 5 and 10 are shown in figs(3.4) and (3.5). These correspond to the exchange kinetics of fig(3.3), curves 2 and 1 respectively. (Note that for these models there are 30 bead local volumes in total and therefore 30 horizontal bars for each profile shown.)

3.5.3 Ion exchange between a spherical bead and limited volume with constant selectivity.

A more complex system is the ion exchange process between a resin bead and a limited bath. This problem involves variable distribution and selectivity considerations. In the examples considered in this section the external bath was taken equal in volume to the bead, with the initial concentration of ion b in this volume, 1M, ensuring that the exchange process would not proceed to near completion. The radius of the bead remained at 0.1cm, which was considered to be initially entirely in the a form with fixed charge also 1M. This convention was not chosen for simplicity, because any external volume may be used with equal felicity, but rather to make the interpretation of the simulations easier and to highlight the intrinsic effects of selectivity without complication.

Initially isotopic exchange was examined. In this, the simplest possible case, diffusion coefficients $D_a=D_b$ and the selectivity coefficient K'^{a}_{b}, eqn(3.14) taken is unity. By choosing the general set of bead and concentration parameters, defined in the previous paragraph, it is clear that the equilibrium position will be one where concentrations in the bead and solution are equal. The upper curve, curve 1 in fig(3.6), shows the exchange kinetics for this example, plotting, (as for fig(3.4)), the uptake of ion b as a fraction of the total fixed charge. Since final equilibrium positions were of particular interest, the simulations were carried on longer than the examples of the previous section. As expected the fractional exchange approached 0.5 as $t \rightarrow \infty$.

Secondly, an identical system was considered except that the diffusion coefficient ratio D_a/D_b was 10 with D_b much the slower ion. The kinetics, in fig(3.6) as curve 2, are observed to be much slower as expected.

We may examine the effects of introducing a much slower ion by examining the penetration profiles of ion b into the sphere. Fig(3.7), ($D_a/D_b=1$) and fig(3.8), ($D_a/D_b=10$) may be compared, giving for each model the evolution of the concentration levels of ion b across the bead. Both are presented through to equilibrium but the half times for these exchange processes $t_{1/2}$ were approximately 5min ($\tau=0.03$) for isotopic exchange compared to 30min ($\tau=.18$) for $D_a/D_b=10$.

Further study of this system allowed the effects of differing selectivities to be examined. Taking the slower exchange kinetics, (with $D_a/D_b=10$), the selectivity (K'^{a}_{b})

was changed to 0.5 (b selected) in the first instance, and then to 2.0 (a selected). We would expect the resultant equilibrium positions to lie on either side of the non-selective example (K'^{a}_{b}=1). Fig(3.9) shows the simulated exchange rates. Curve 1 is the exchange for K'^{a}_{b} unity, as curve 2 in fig(3.6) but plotted through to equilibrium, (achieved at around τ, 2.7). Curves 2 and 3 show exchange kinetics for K'^{a}_{b} equal 0.5 and 2.0 respectively. As expected they lie equally above and below (respectively) the non-selective model (K'^{a}_{b}=1). This is an excellent illustration of the effects of selectivity in general. Note from fig(3.9) that each simulation reaches equilibrium at the same time. Selectivity factors dictate the final equilibrium position only, and not the time taken to achieve it.

The concentration profiles for the selectivity examples of 0.5 and 2.0 have also been presented for comparison in figs(3.10) and (3.11), showing evolution of the exchange process in the bead to equilibrium when the concentration of b in the bead is uniform and time invariant.

3.5.4 Ion exchange processes with variable selectivity.

As discussed in the initial sections of the chapter, the issue of selectivity may be further complicated by having a variable selectivity coefficient K'^{a}_{b}. To work through an example of this behaviour the limited bath conditions used above were altered to include the effects of varying K'^{a}_{b} using Kielland's equation, eqn(3.16), to dictate the selectivity pattern. The system that was examined in this Section is one of the standard spherical

bead, radius 0.1cm, initially entirely in the **a** form with 1M fixed charge, immersed in an efficiently stirred collecting volume equal to only one quarter of the bead's volume: severe limited bath conditions. The concentration of the salt of ion **b** in this solution however was 2M in the model (compared to 1M in all the above examples). That was as before equal total concentrations of (univalent) ions **a** and **b** in both phases. The self diffusion coefficient ratio, D_a/D_b was again taken as 10. This example is about the most complex mono-valent bi-ionic exchange problem which could be envisaged. The isotherm produced by setting the empirical constant **w** in Kielland's equation to 2, shown in fig(3.1), was used to define a concentration variable selectivity coefficient between exchanger and the (well-stirred) limited bath.

The simulated kinetics of exchange are shown by the upper curve, curve 2 in fig(3.12), again the fractional exchange is plotted against τ, eqn(3.20). This shows a rapid uptake of ion **b** into the exchanger. It was of interest to examine the exact nature of the varying selectivity for this simulation. This has been illustrated in fig(3.13) by plotting the natural logarithm of K'^{a}_{b} against τ. An initial sharp selectivity inversion is observed in the first minute of exchange in which the selectivity coefficient K'^{a}_{b}, dropped from 7.4, (**a** selected, when little or no ion **b** is present), to 0.2, (**b** selected). The K'^{a}_{b} value then gradually increased, reversing approximately 15 minutes later (τ=0.1), and continued up to the equilibrium position at which K'^{a}_{b}

equalled 2.6 (a selected). (This position is not shown on fig(3.13), which follows the selectivity up to τ = .4 only.)

For comparison of the exchange kinetics a second simulation was considered with identical system parameters except constant selectivity equal 2.6, so that the same equibrium position was to be expected. The kinetics of this exchange were observed to be somewhat slower than that for variable K'^{a}_{b}. Perhaps the most interesting result of this section is the observation that variable selectivity affects the speed of ion b uptake into the sphere. This does not suggest however that the times taken to achieve equilibrium are different.

Examination of the evolving concentration profiles for constant selectivity (K'^{a}_{b}=2.6), fig(3.14) and variable selectivity, fig(3.15) gives explanation of the disparity between uptake rates. In the variable selectivity model the concentrations of ion b are comparatively high at the surface of the exchanger (approximated by the average charge in the bead's outer lump). The effect of this in Kielland's equation is to render the exchanger even more selective for ion b and this does not reverse until the fractional concentration in the bead at the surface drops below 0.5. This is observed to occur at least 15mins after time zero up to which point ion b is rapidly taken up into the outer areas of the bead. Note that the diffusional gradients within the exchanger in this model are still great, even after the time at which little ion exchange is observed between the bead and external solution. (The fourth profile is taken at $D_a t/r_o^2$ equal to .15, well on to

the linear part of the curve in fig(3.13)).

These particular results must be regarded as unique to this example. Clearly other relationships for selectivity variation will lead to different kinetics. What is illustrated however is that the particular effects are impossible to predict without computer simulation and that network thermodynamics is a superb tool for probing complex system dynamics in this way.

3.5.3 Uni-Divalent ion exchange.

All the previous examples in this chapter have considered the exchange of mono-valent ions. This avoids the requirements for handling valencies in the expressions for mutual diffusion coefficient, eqn(3.8), and more especially in dealing with selectivity. There is no particular reason why ions of other valencies cannot be considered and in this section an exchange process with ion **a** divalent and ion **b** univalent was simulated to illustrate this.

For this uni-divalent exchange we return to constant selectivity, K'^{a}_{b} equal 0.5 (**b** selected) and define the limited bath equal in volume to the bead as previously. The bead radius, as in all previous examples, was 0.1cm, the self diffusion coefficient ratio D_a/D_b was again 10. The fixed charge concentration was 1M, but note that the initial concentration of ion **a** in the bead is now 0.5M since it is a doubly charged species. The simulation of the exchange process is presented by means of successive concentration profiles of ion **b**, fig(3.16). These are plotted as previously with fractional concentration versus

fractional radius. These results may be compared to the analogous mon-valent exchange process described in Section 3.5.3. The purpose of this example however is mainly to illustrate the applicability of the model to all bi-ionic exchange processes. (The computer program for uni-divalent exchange simulation is given as an example in Section A.1 of the Appendix).

3.6 CONCLUSIONS.

The topic of ion exchange kinetics is an important one which has stimulated much discussion and research. Here we have presented it as an example of non linear diffusion and discussed the methods by which we can simulate these processes under the framework of network thermodynamics and the bond graph model. The complexities of the ion exchange systems are evident, especially for variable selectivity, (and in fact this chapter is the only one of this thesis in which the issues of selectivity are treated in depth). It is noteworthy that the basic (isotopic) bond graph needs no modification and no extensions of theory are required. It is only necessary to update resistances and capacitances of the model, to accomodate changing diffusion and distribution coefficients as they vary during the ion exchange process: The basic bond graph model has remained identical throughout. Clearly network thermodynamics is an extremely flexible technique.

FIGURE 3.1.

Example isotherm produced using Kielland's semi-empirical equation, eqn(3.16), with empirical constant w, equal 2. Molar fraction of ion b in exchanger, $\bar{x}_b$ plotted against molar fraction of ion b in solution, x_b.

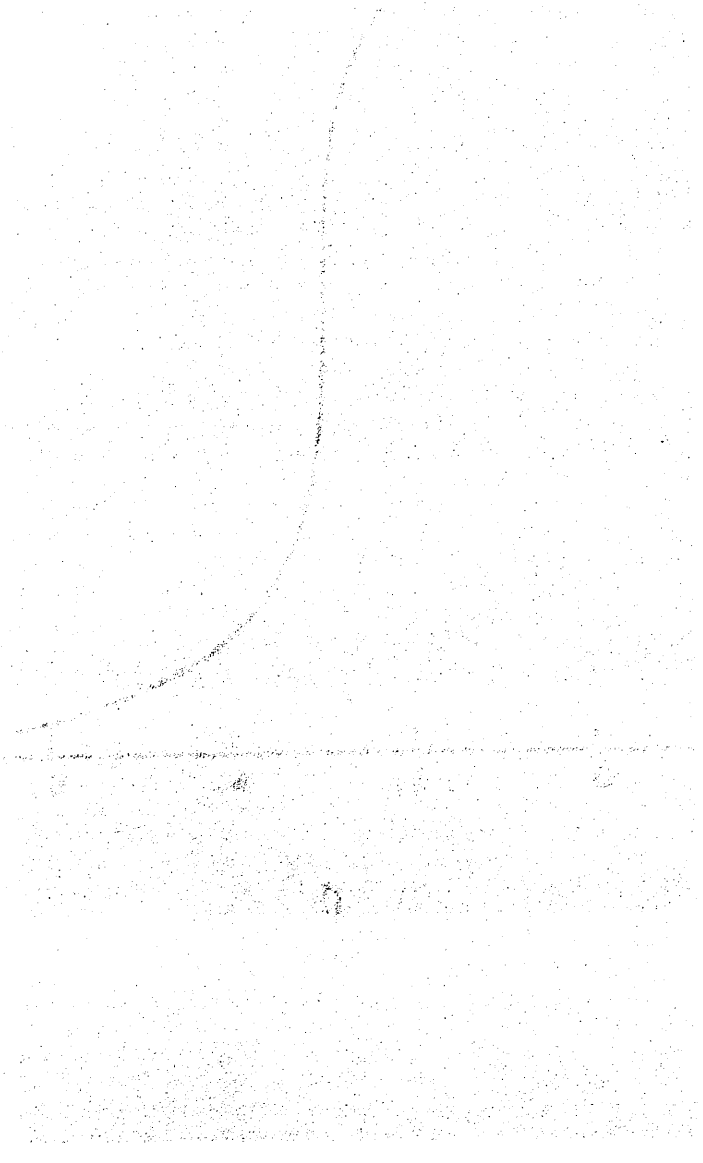

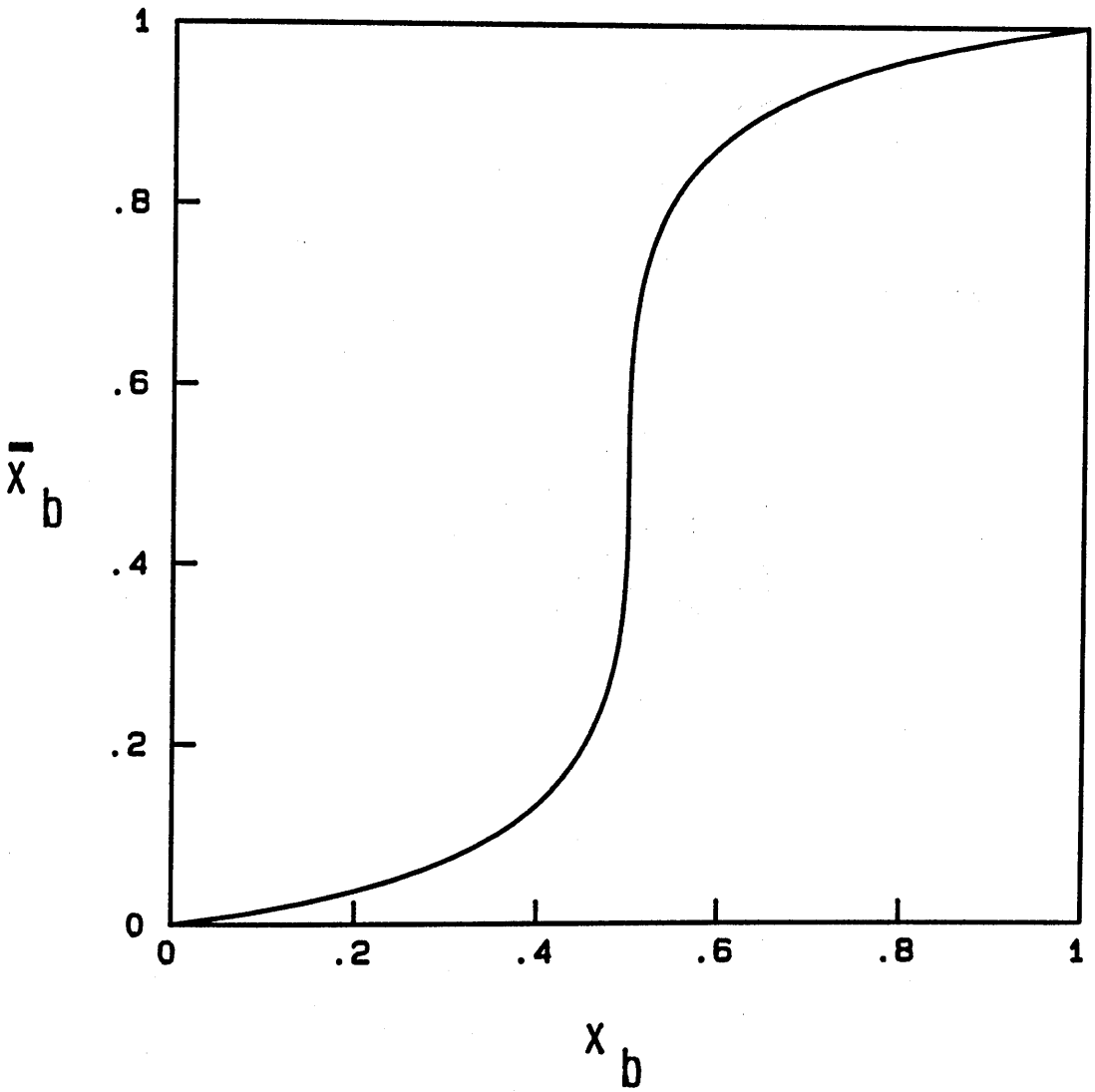
1
.8
.6
.4
.2
0
0
.2
.4
.6
.8
1
$\bar{x}_b$
x_b

FIGURE 3.2.

Sodium ion concentration profiles within sodium/hydrogen ion exchange membrane. Membrane thickness, 0.1cm, area, $2.5cm^2$, initially in the H^+ form. Diffusion coefficient of H^+, D_a, $2.44x10^{-6}cm^2s^{-1}$; diffusion coefficient of Na^+, D_b, $4.0x10^{-6}cm^2s^{-1}$. Ordinate represents distance from sodium solution side expressed as fraction of total membrane thickness, so that 0 is face contacting solution of 0.1M $NaCl_{(aq)}$, and 1 is face contacting solution of $HCl_{(aq)}$, also 0.1 ABSCISSA sodium ion. Essentially infinite bath conditions on each side ($1000cm^3$ volume). Profiles shown at times, in seconds, 5 to 45 in steps of 5, then at 55, 75 and finally 110. Final profile coincides to steady state predicted by Helfferich and Ocker, [5].

NaCl / HCl

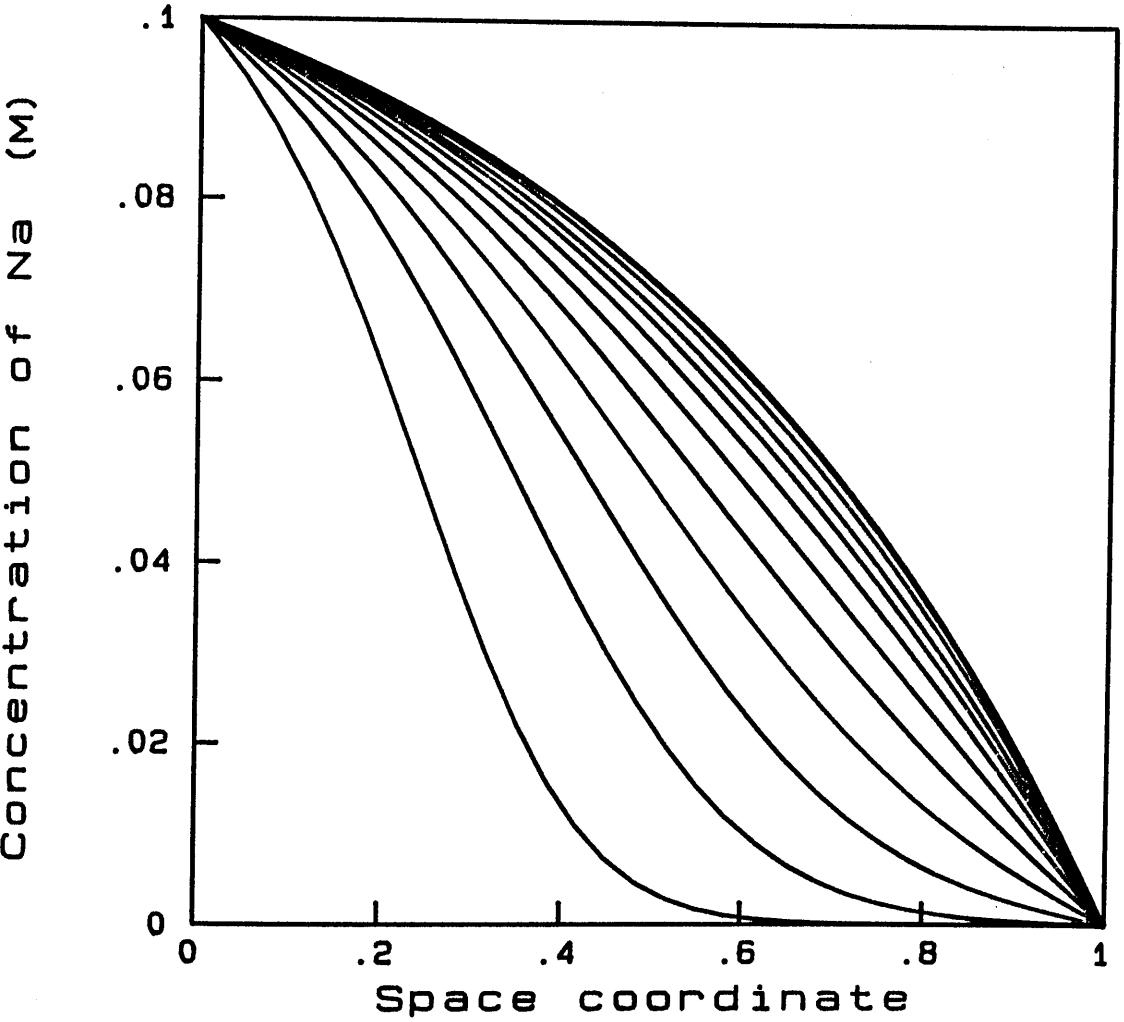

FIGURE 3.3.

Comparison of ion exchange kinetics for different self diffusion coefficient ratios. Bead radius, r_o, 0.1cm and essentially infinite bath ($1000cm^3$). Self diffusion coefficient of ion a, D_a, $1.0x10^{-6}cm^2s^{-1}$. Fractional exchange calculated from total concentration of ion b within bead as fraction of total fixed charge concentration, c_f (1M), against dimensionless time D_at/r_o^2. Initial concentration of ion b in external solution also 1M.

Curve 1 $D_a/D_b=10$

Curve 2 $D_a/D_b=5$

Curve 3 $D_a/D_b=1$

This latter (isotopic) exchange calculated from analytical solution for spherical diffusion with infinite bath conditions, eqn(2.28)).

Data for points imposed on curves 1 and 2 obtained from Helfferich and Plesset [2].

Figure 2

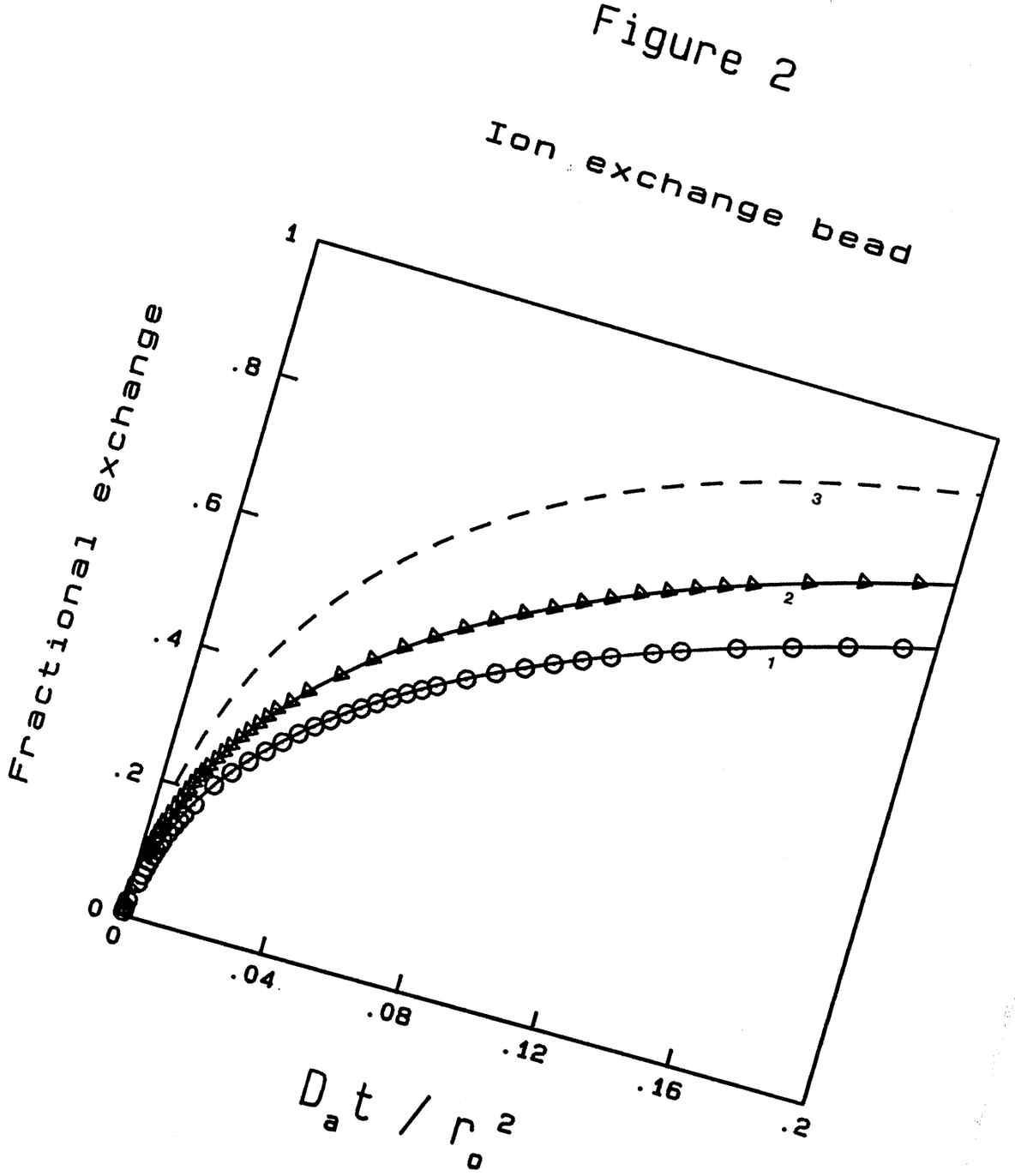
Ion exchange bead
Fractional exchange
1
.8
.6
.4
.2
0
0
.04
.08
.12
.16
.2
$D_a t / r_o^2$
1
2
3

FIGURE 3.4.

Concentration profiles of ion b within spherical bead for exchange between ions with self diffusion coefficients, D_a, $1.0 \times 10^{-6} cm^2 s^{-1}$ and D_b, $2.0 \times 10^{-7} cm^2 s^{-1}$; $D_a/D_b = 5$.

Essentially infinite bath conditions ($1{,}000 cm^3$) with concentration of ion b, 1M. Concentration plotted as fraction of fixed ionic charge in bead (1M). Horizontal line spans radial thickness of each lump of which there are thirty. Vertical notch gives position of lump centre. Profiles shown at dimensionless times ($D_a t/r_o^2$), 0.01, 0.03, 0.05, 0.07, 0.01, 0.15, and 0.2.

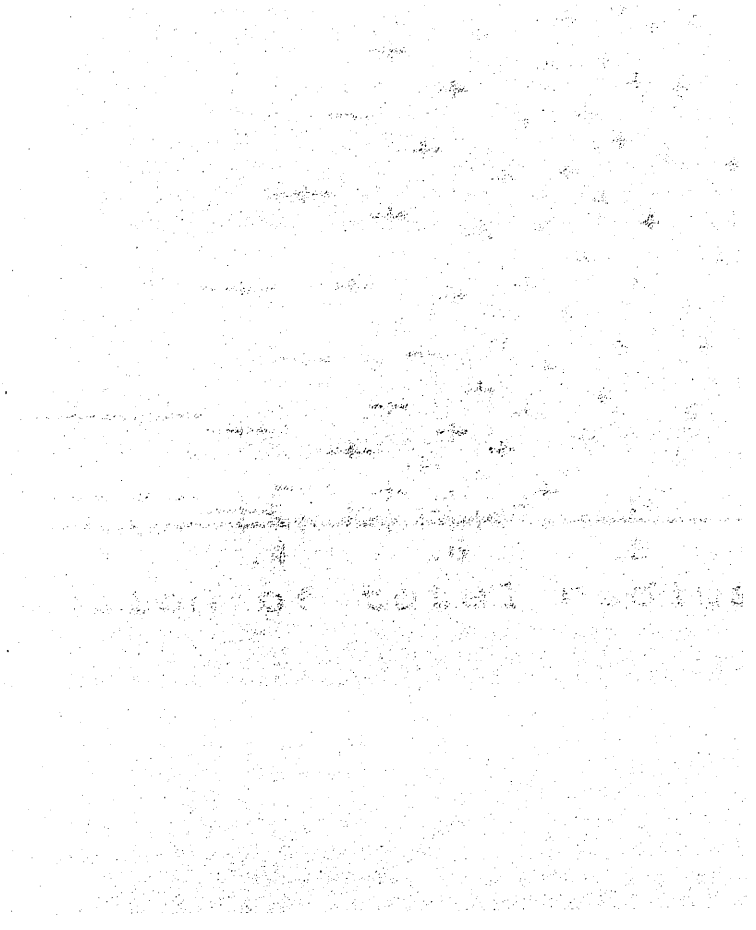

D ratio = 5

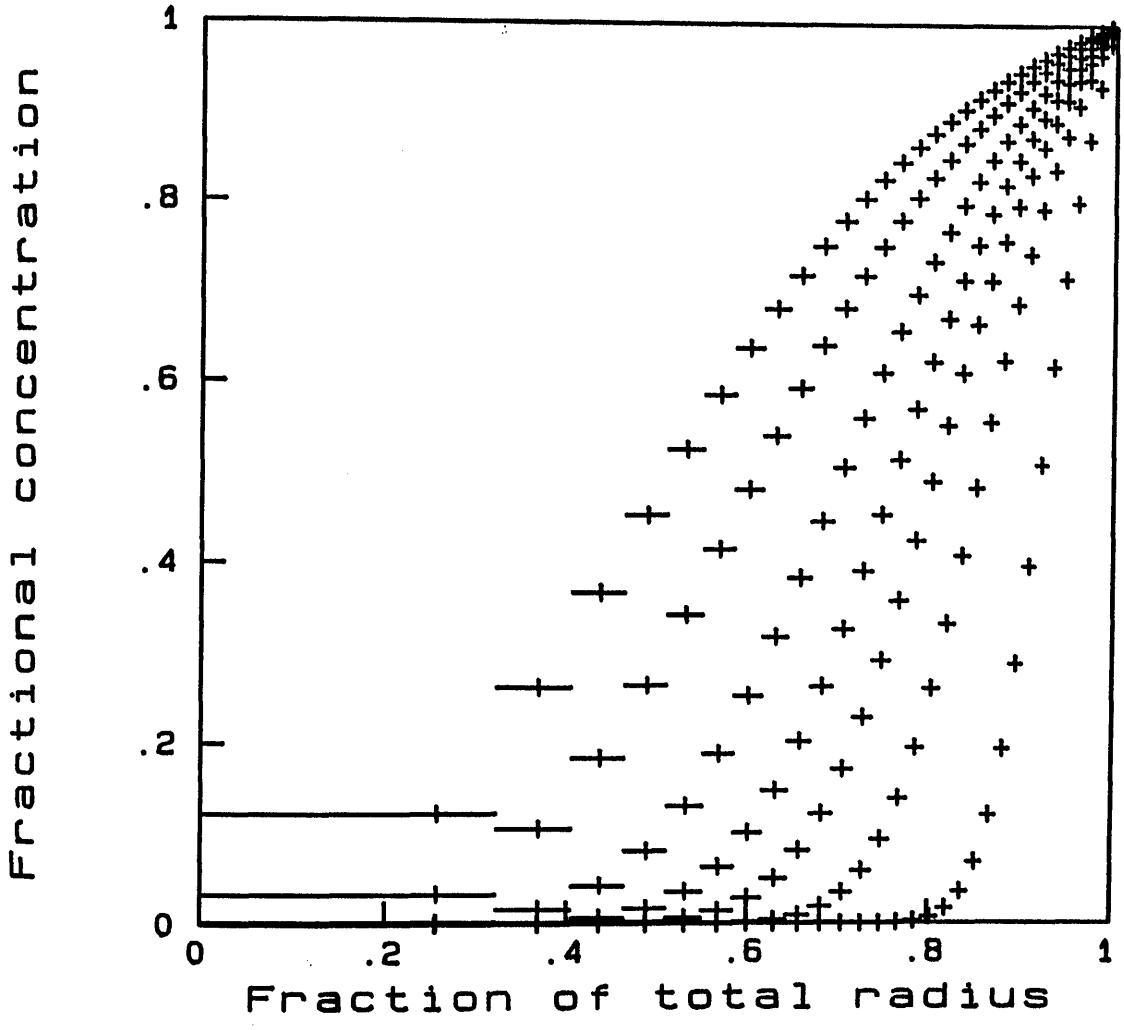
Fractional concentration
1
.8
.6
.4
.2
0
0
.2
.4
.6
.8
1
Fraction of total radius

FIGURE 3.5.

Concentration profiles of ion **b** within spherical bead for exchange between ions with diffusion coefficients, D_a, $1.0 \times 10^{-6} cm^2 s^{-1}$ and D_b, $1.0 \times 10^{-7} cm^2 s^{-1}$.

Essentially infinite bath conditions ($1000 cm^3$) with concentration of ion **b**, 1M. Ion **b** loading of bead plotted as fractional exchange at each location in bead. Horizontal lines span radial thicknesses of each of the thirty lumps. A vertical notch marks the position of the lump centres. Profiles shown at dimensionless times ($D_a t / r_o^2$), 0.01, 0.03, 0.05, 0.07, 0.01, 0.15, and 0.2.

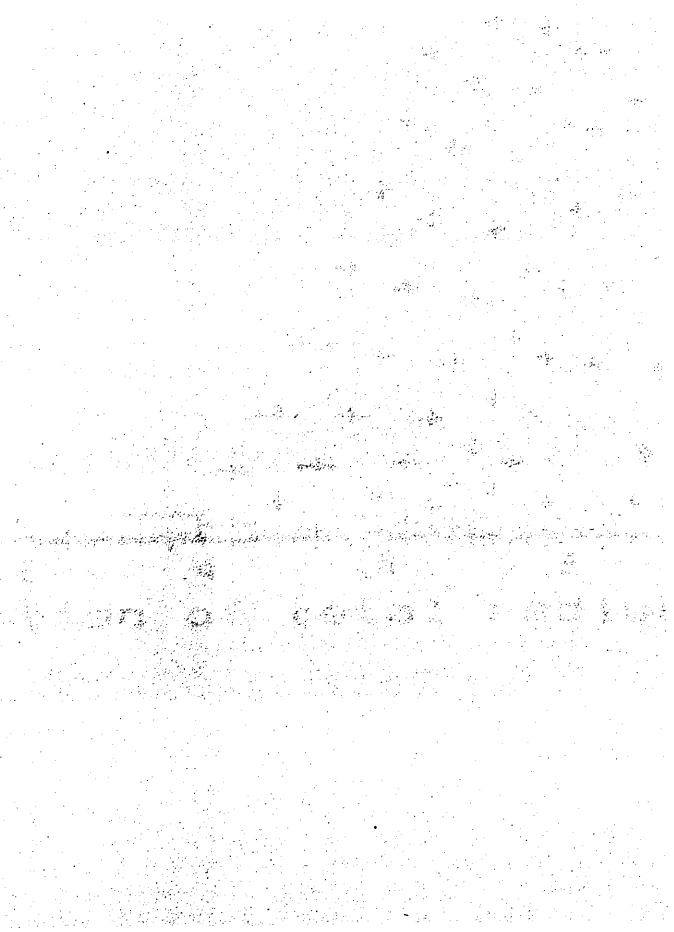

D ratio = 10

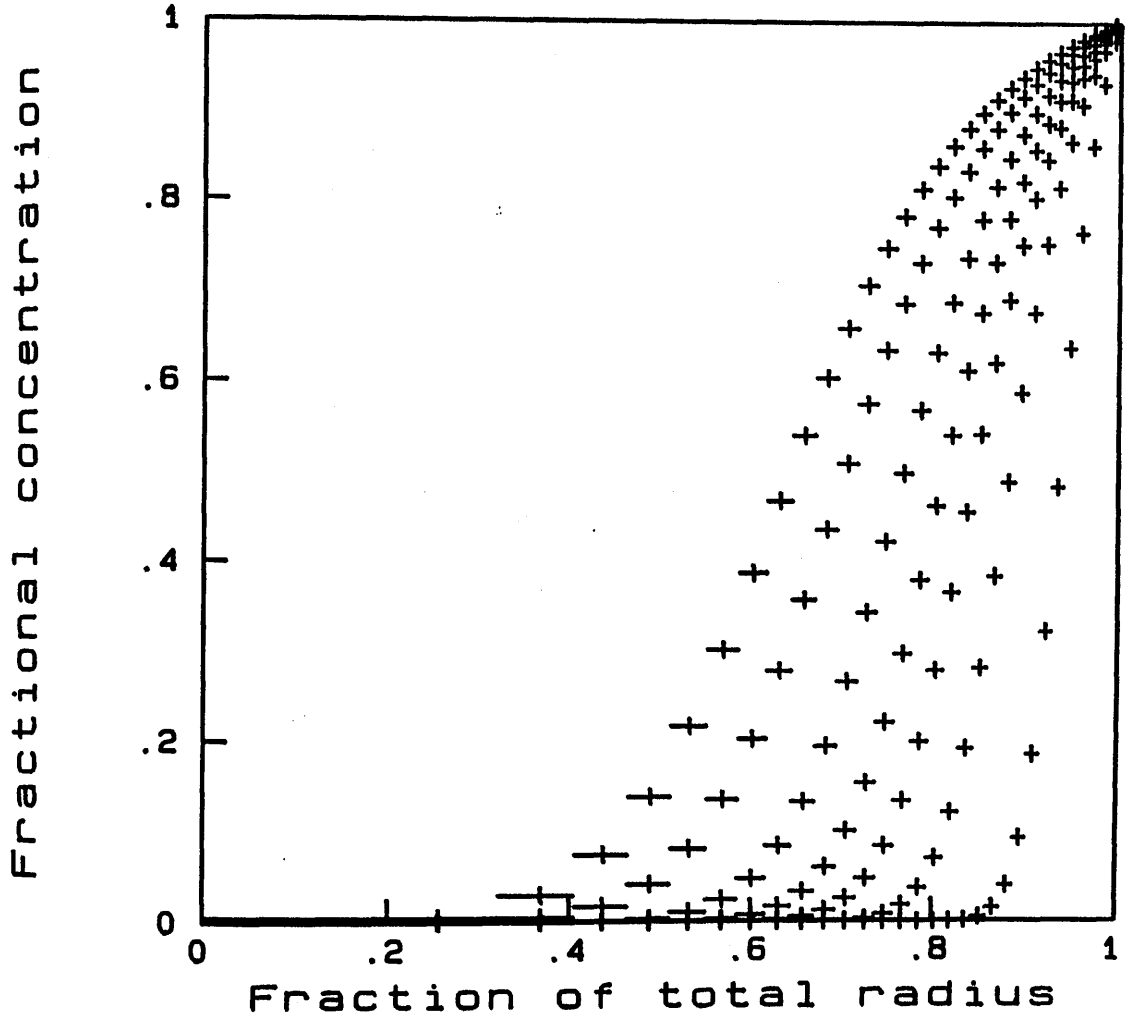
Fractional concentration
1
.8
.6
.4
.2
0
0
.2
.4
.6
.8
1
Fraction of total radius

FIGURE 3.6.

Ion exchange kinetics for different D_a/D_b ratios under limited bath conditions. Bead radius, r_o, 0.1cm, external solution volume equals bead volume, approximately $0.0042cm^3$.

Molar selectivity coefficient, K'^{a}_{b} unity.

Fractional exchange calculated from total concentration of ion **b** within bead as fraction of total fixed charge concentration, c_f (1M), plotted against dimensionless time parameter τ, $D_a t/r_o^2$. Initial concentration of ion **b** in external solution also 1M.

Curve 1. $D_a/D_b=1$.

Curve 2. $D_a/D_b=10$

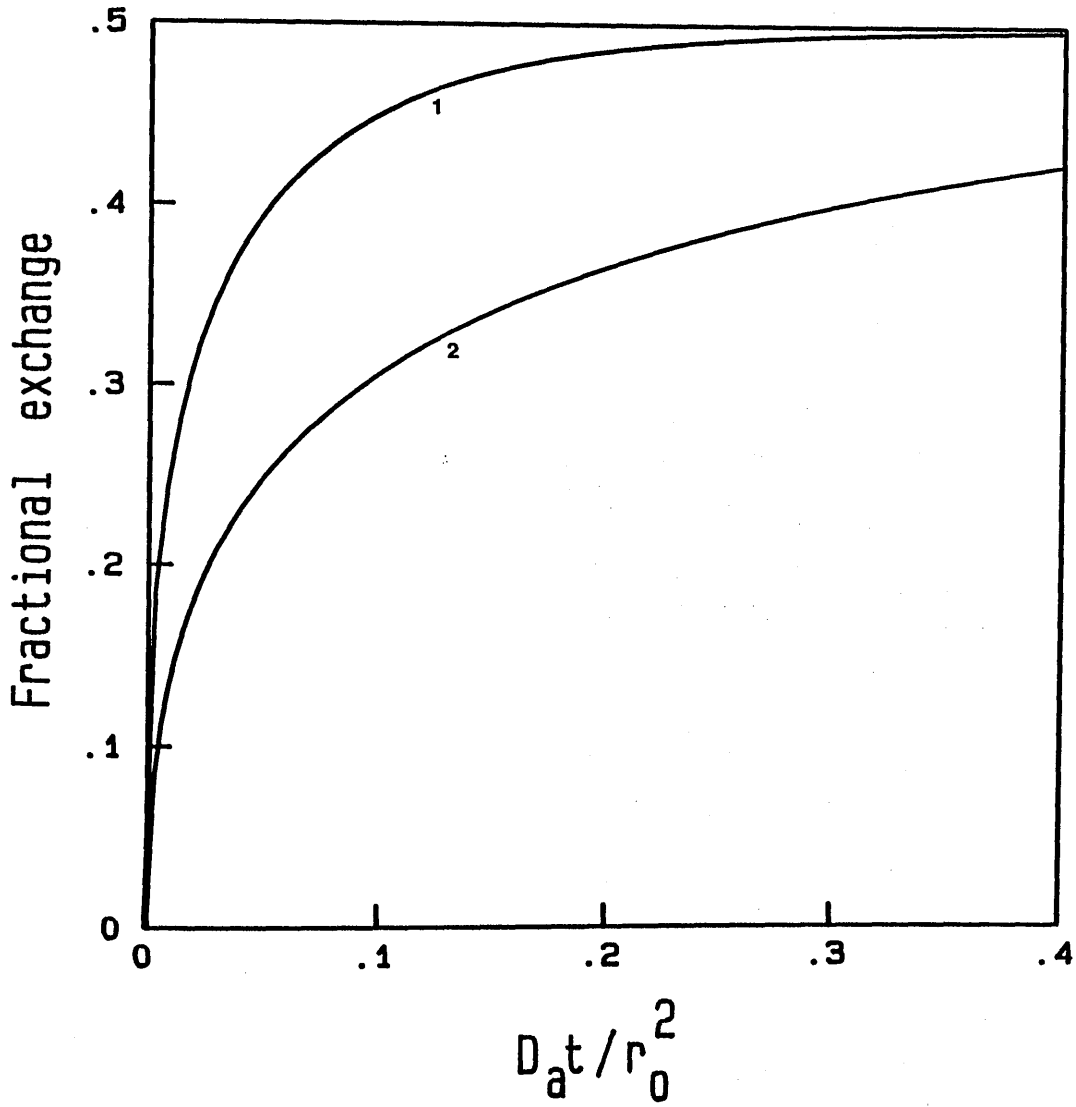
.5
.4
.3
.2
.1
0
0
.1
.2
.3
.4
1
2
Fractional exchange
$D_a t / r_0^2$

FIGURE 3.7.

Concentration profiles of ion b within spherical bead for exchange between ions with diffusion coefficients, D_a and D_b, $1.0 \times 10^{-6} cm^2 s^{-1}$.

Molar selectivity coefficient, K'^{a}_{b} unity.

Radius of bead r_o, 0.1cm. Volume of external solution equals volume of bead, approximately $.0042 cm^3$, in which initial concentration of ion b, 1M, which is equal to concentration of fixed ionic charge in exchanger, c_f. Concentration plotted as fraction of c_f. Horizontal lines span radial thicknesses of each of the thirty lumps. A vertical notch marks the position of the lump centres. Profiles shown at dimensionless times ($D_a t/r_o^2$), .02, .04, .06, .08, .1, .12, .14, .16, .2, .24, .36.

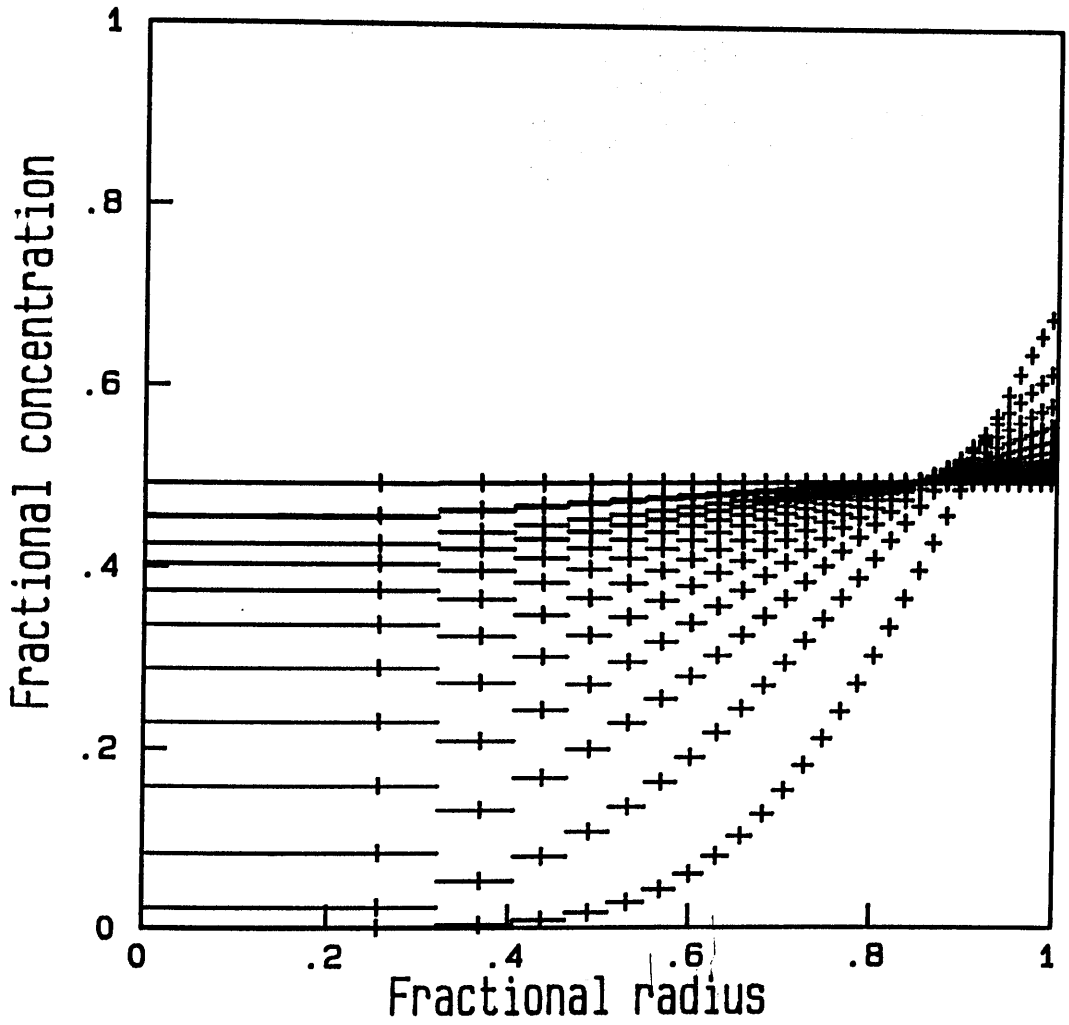
Fractional concentration
1
.8
.6
.4
.2
0
0
.2
.4
.6
.8
1
Fractional radius

FIGURE 3.8.

Concentration profiles of ion b within spherical bead for exchange between ions with diffusion coefficients, D_a, $1.0 \times 10^{-6} cm^2 s^{-1}$, D_b, $1.0 \times 10^{-7} cm^2 s^{-1}$.

Molar selectivity coefficient, K'^{a}_{b} unity.

Radius of bead r_o, 0.1cm. Volume of external solution equals volume of bead, approximately $.0042 cm^3$, in which initial concentration of ion b, 1M, which is equal to concentration of fixed ionic charge in exchanger, c_f. Concentration plotted as fraction of $\bar{c}_f$. Horizontal lines span radial thicknesses of each of the thirty lumps. A vertical notch gives positions of lump centres. Profiles shown at dimensionless times ($D_a t/r_o^2$), .01, .07, .17, .27, .4, .6, .8, 1.0, 1.5, 2.7.

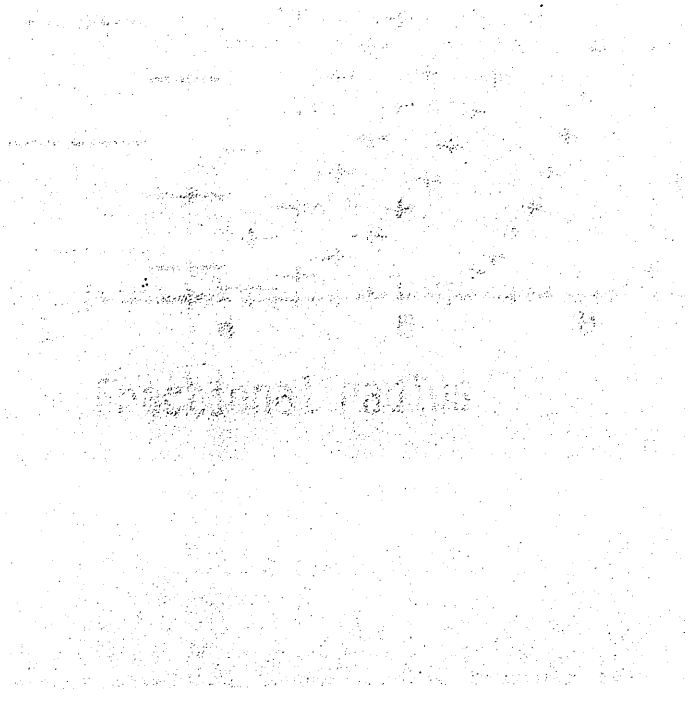

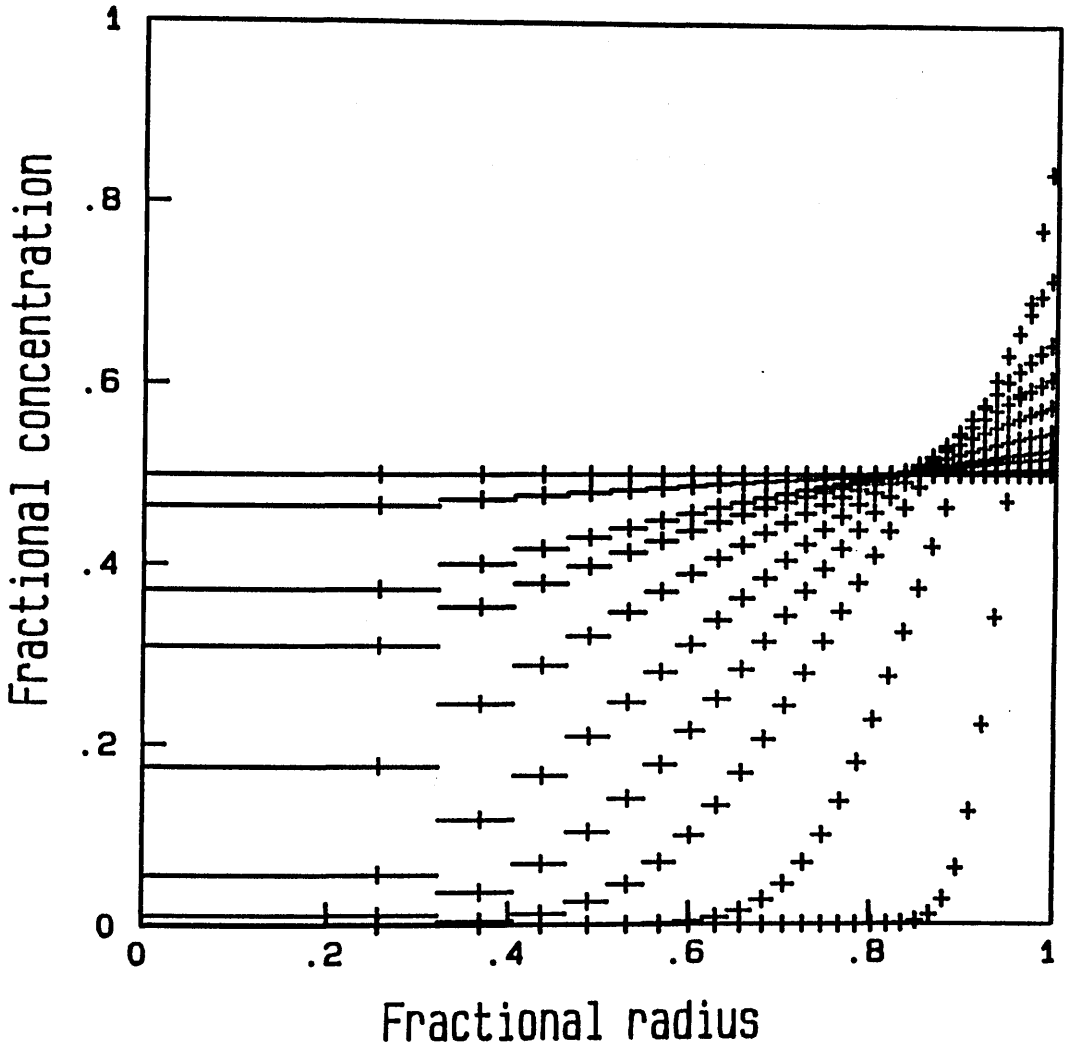
Fractional concentration
1
.8
.6
.4
.2
0
0
.2
.4
.6
.8
1
Fractional radius

FIGURE 3.9.

Ion exchange kinetics with limited bath conditions, for different selectivities. Bead radius, r_o, 0.1cm, external solution volume equals bead volume, approximately .0042cm^3. Fractional exchange of ion **b** within bead plotted against dimensionless time, $D_a t/r_o^2$. Initial concentration of ion **b** in external solution also 1M.

Diffusion coefficients D_a, $1.0 \times 10^{-6} cm^2 s^{-1}$,

D_b, $1.0 \times 10^{-7} cm^2 s^{-1}$.

Curve 1. $K'^{a}_{b}=1.0$

Curve 2. $K'^{a}_{b}=0.5$.

Curve 3. $K'^{a}_{b}=$ ²

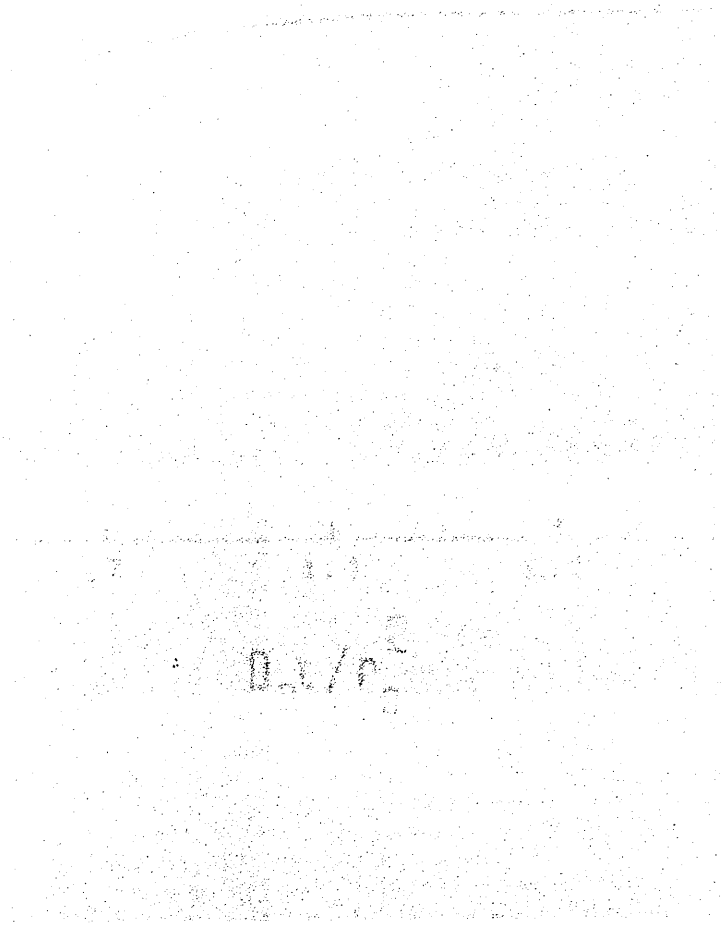

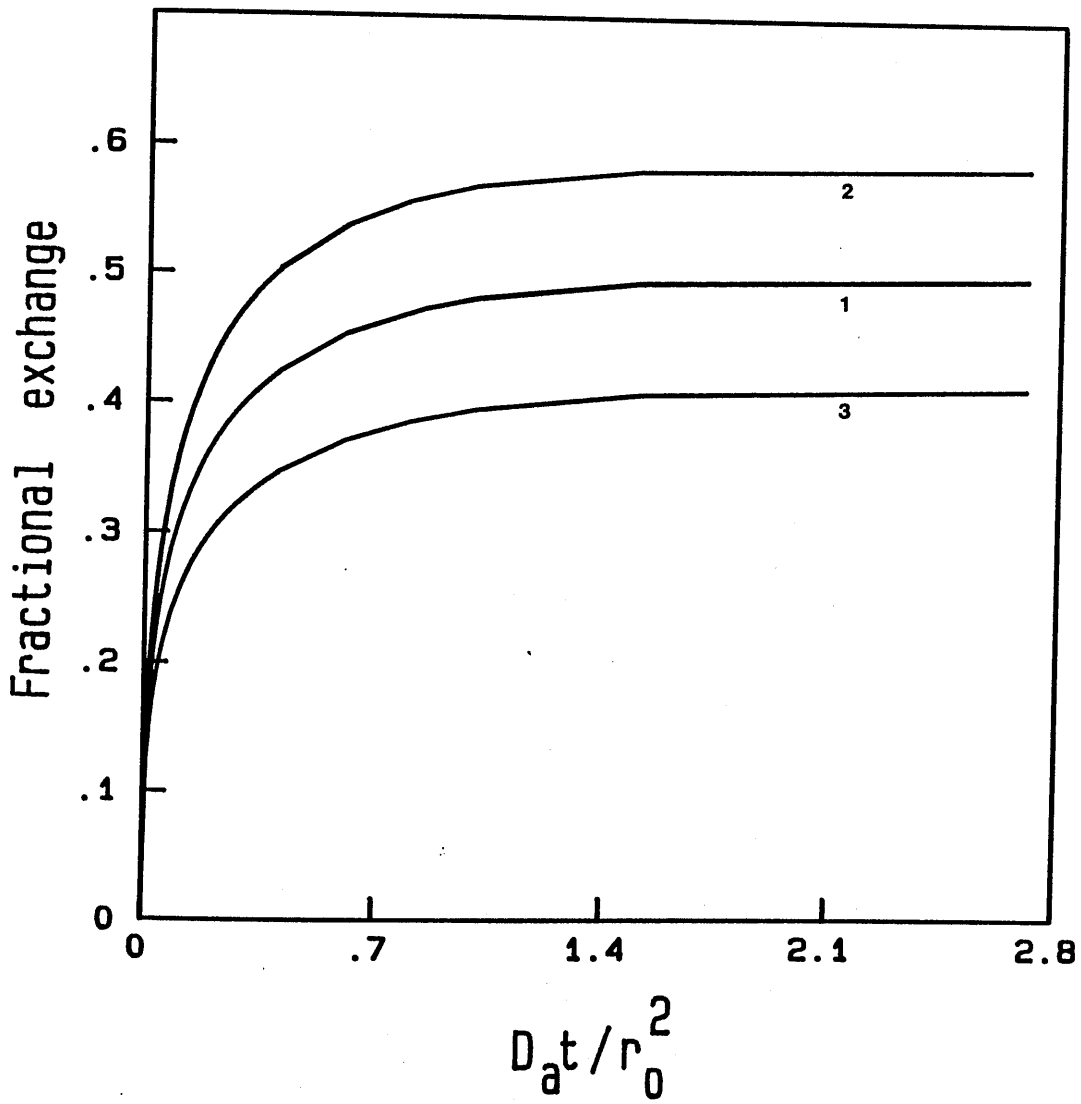
Fractional exchange
.6
.5
.4
.3
.2
.1
0
0
.7
1.4
2.1
2.8
2
1
3
$D_a t / r_0^2$

FIGURE 3.10.

Concentration profiles of ion b within spherical bead for exchange between ions with diffusion coefficients, D_a, $1.0 \times 10^{-6} cm^2 s^{-1}$, D_b, $1.0 \times 10^{-7} cm^2 s^{-1}$, ($D_a/D_b = 10$).

Molar selectivity coefficient, K'^{a}_{b} equal to 0.5.

Radius of bead r_o, 0.1cm. Volume of external solution equals volume of bead, approximately $.0042 cm^3$, in which initial concentration of ion b, 1M, which is equal to concentration of fixed ionic charge in exchanger, c_f. Concentration plotted as fraction of c_f. Horizontal lines span radial thicknesses of each of the thirty lumps. A vertical notch marks the positions of the lump centres. Profiles shown at dimensionless times ($D_a t/r_o^2$), .1, .7, .17, .27, .4, .6, .8, 1.0, 1.5, 2.7.

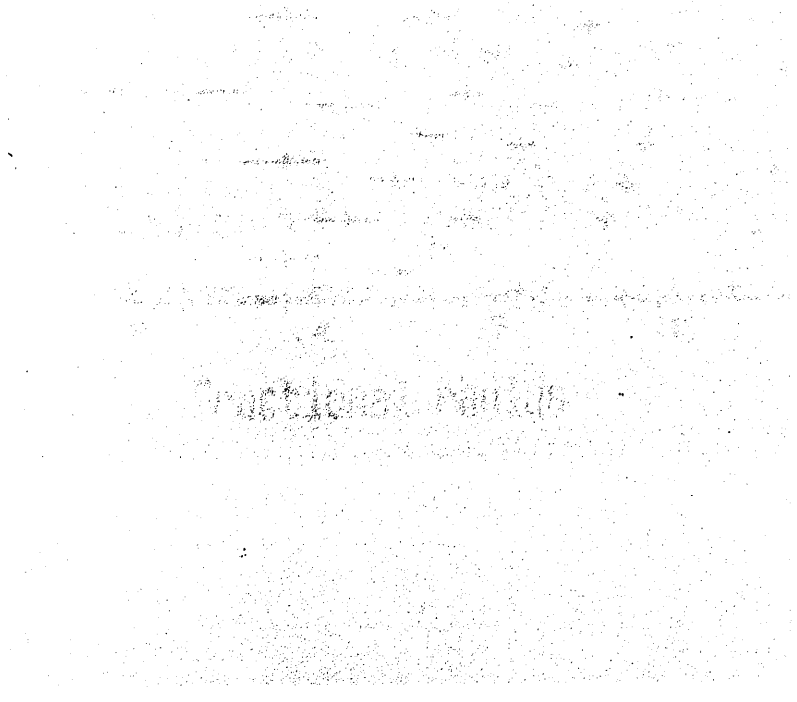

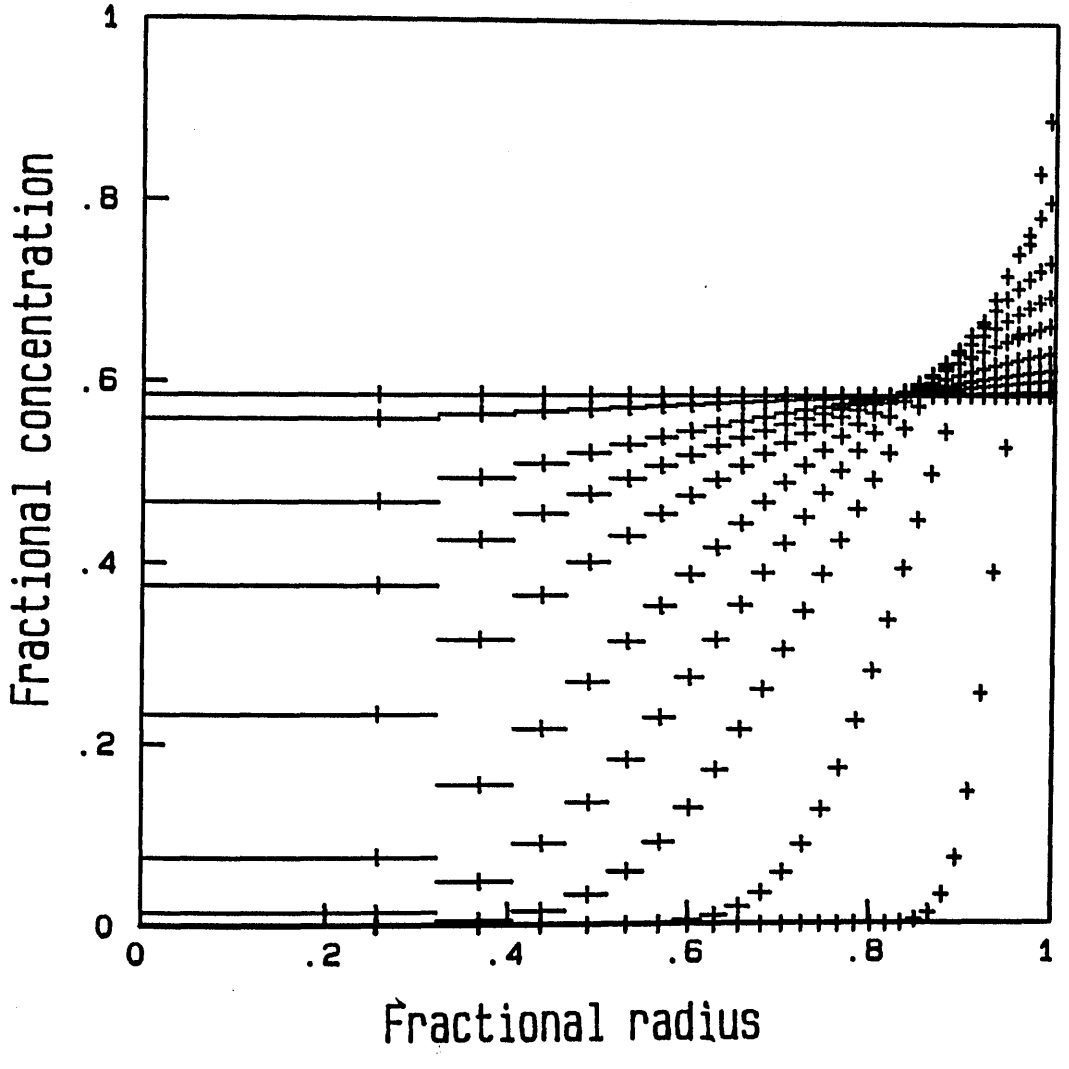
Fractional concentration
1
.8
.6
.4
.2
0
0
.2
.4
.6
.8
1
Fractional radius

FIGURE 3.11.

Concentration profiles of ion b within spherical bead for exchange between ions with diffusion coefficients, D_a, $1.0 \times 10^{-6} cm^2 s^{-1}$, D_b, $1.0 \times 10^{-7} cm^2 s^{-1}$. ($D_a/D_b = 10$).

Molar selectivity coefficient, K'^{a}_{b} equal to 2.0.

Radius of bead r_o, 0.1cm. Volume of external solution equals volume of bead, approximately $.0042 cm^3$, in which initial concentration of ion b, 1M, which is equal to concentration of fixed ionic charge in exchanger, c_f. Concentration plotted as fraction of c_f. Horizontal lines span radial thicknesses of each of the thirty lumps. Vertical notches give positions of the lump centres. Profiles shown at dimensionless times ($D_a t/r_o^2$), .1, .7, .17, .27, .4, .6, .8, 1.0, 1.5, 2.7.

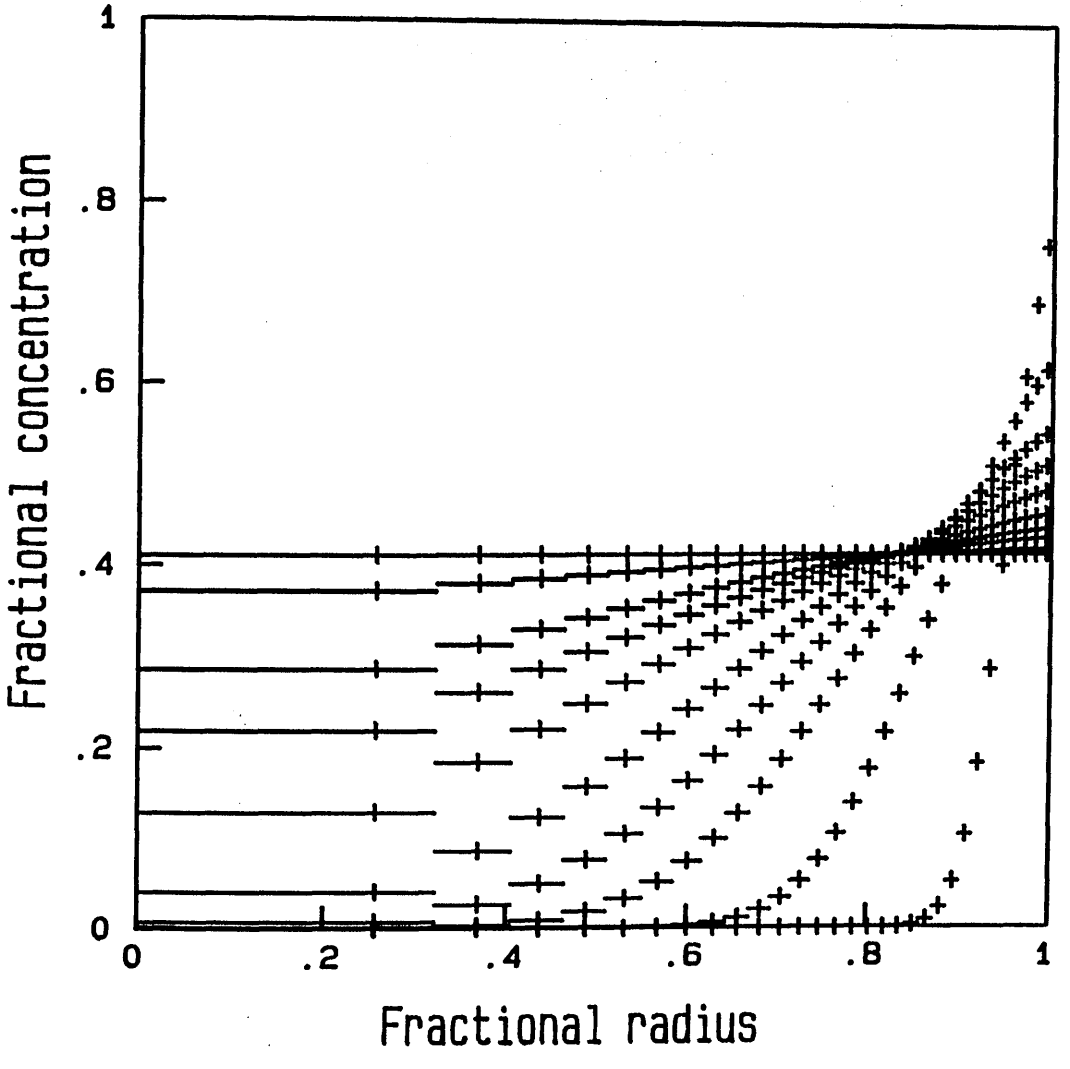
Fractional concentration
1
.8
.6
.4
.2
0
0
.2
.4
.6
.8
1
Fractional radius

FIGURE 3.12.

Comparison of ion exchange kinetics with limited bath conditions, for variable and constant selectivity. Bead radius, r_o, 0.1cm, external solution volume quarter bead volume, approximately $2.094 \times 10^{-3} cm^3$. Fractional exchange calculated from total concentration of ion b within bead as fraction of total fixed charge concentration, c_f (1M), plotted against dimensionless time parameter τ, $D_a t/r_o^2$. Initial concentration of ion b in external solution, 2M, (double fixed ionic charge concentration within exchanger). Diffusion coefficient ratio $D_a/D_b=10$.

Curve 1. Exchange simulated for variable selectivity defined by isotherm produced using Kielland's semi-empirical equation, eqn(3.16) with w equal 2.0, fig(3.1). Final equilibrium selectivity coefficient, K'^a_b, 2.6.

Curve 2, simulated exchange for constant K'^a_b, 2.6.

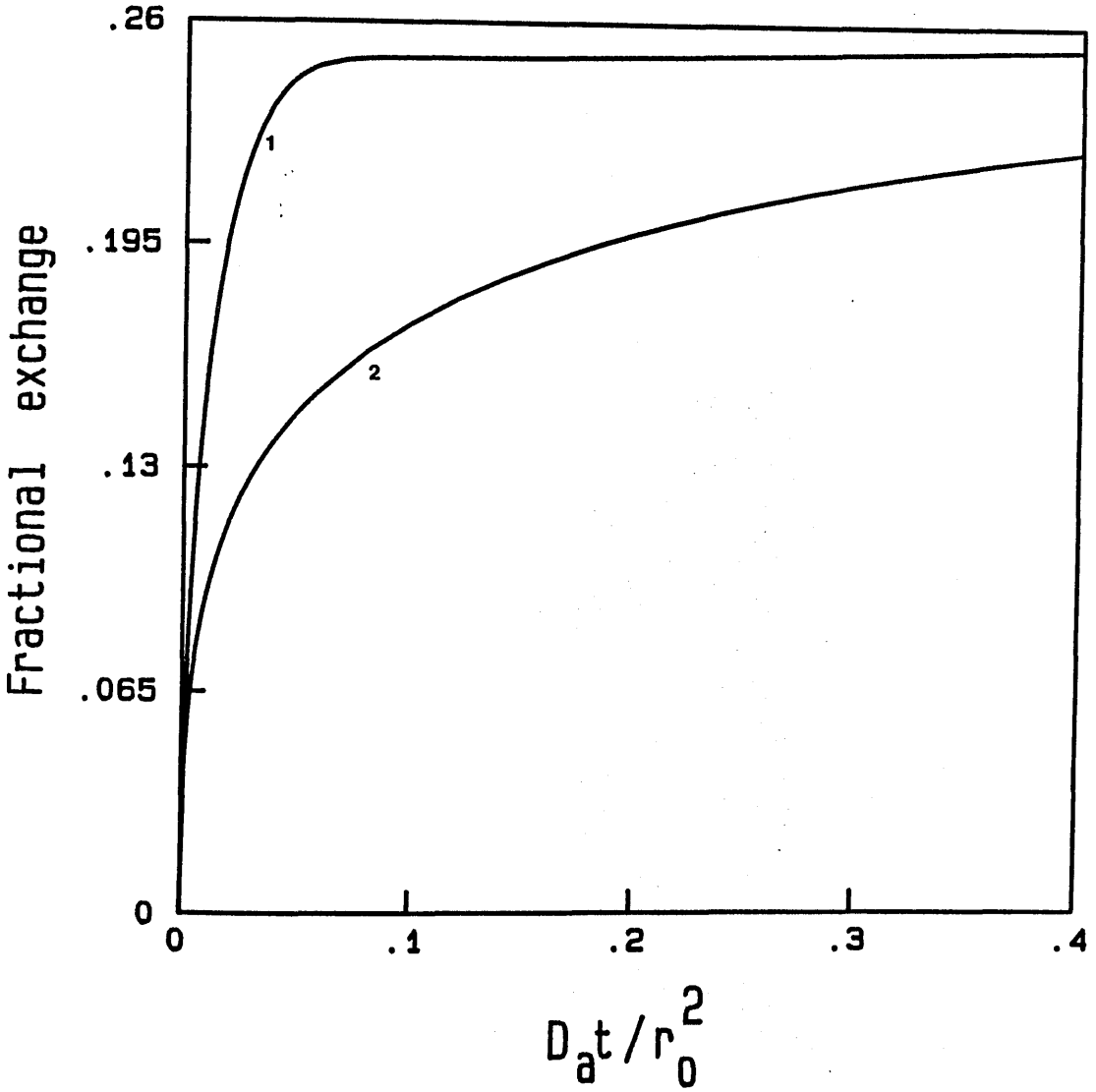
.26
.195
.13
.065
0
Fractional exchange
1
2
0
.1
.2
.3
.4
$D_a t / r_0^2$

FIGURE 3.13.

Actual variation of selectivity at surface of ion exchange bead during simulated exchange process with selectivity defined by isotherm produced using Kielland's semi-empirical equation, eqn(3.16) with w equal 2.0, fig(3.1). Natural logarithm of molar selectivity coefficient K'^{a}_{b} plotted against dimensionless time parameter, τ, $D_a t/r_o^2$.

Input system parameters for simulation were, bead radius, r_o, 0.1cm, external solution volume of quarter bead's volume, approximately $2.094 \times 10^{-3} cm^3$. Total fixed charge concentration, c_f, 1M. Initial concentration of ion b in external solution double c_f, 2M. Diffusion coefficients, D_a, $1.0 \times 10^{-6} cm^2 s^{-1}$, D_b, $1.0 \times 10^{-7} cm^2 s^{-1}$.

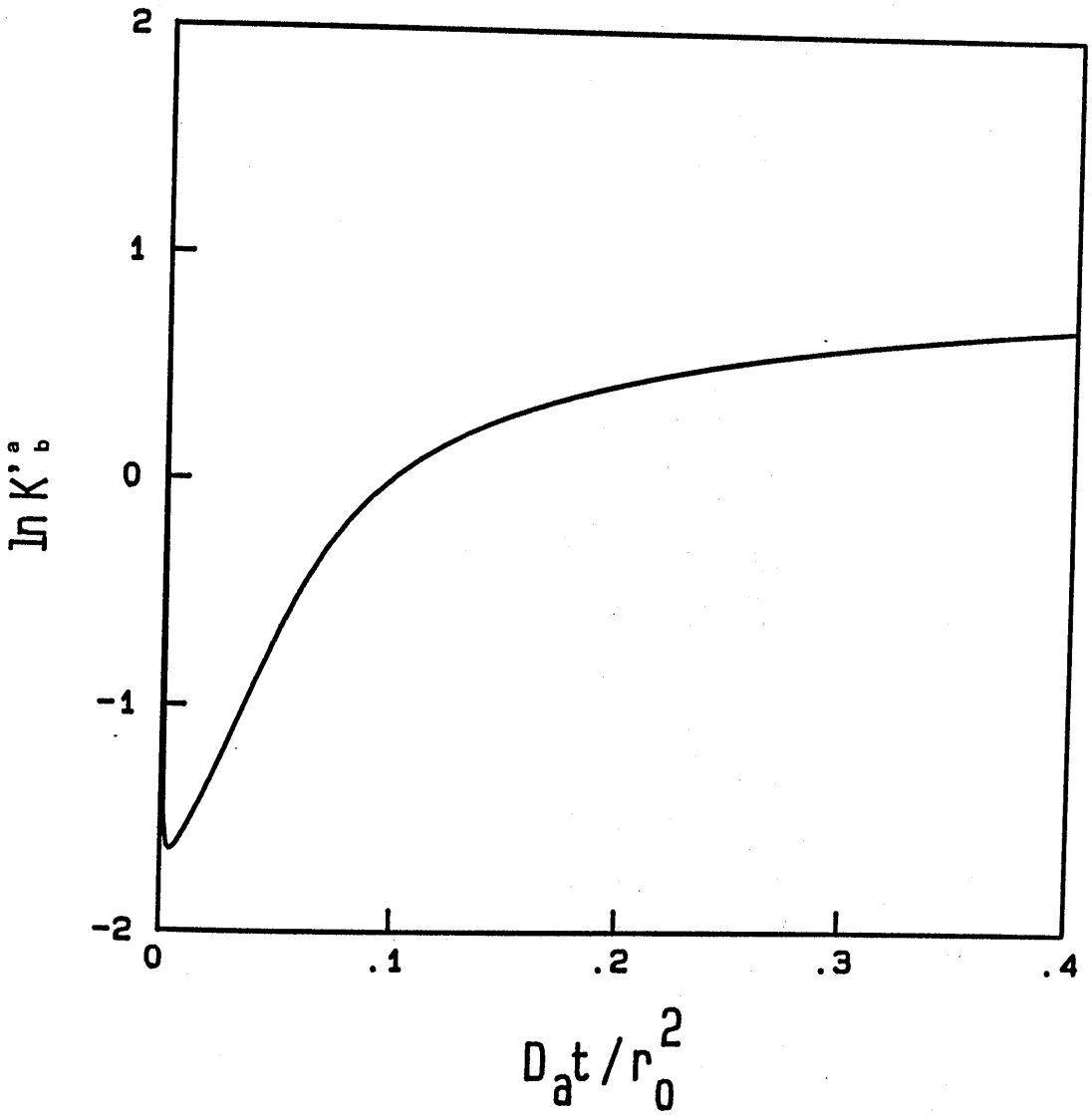
2
1
0
-1
-2
0
.1
.2
.3
.4
$\ln K'^{a}_{b}$
$D_a t / r_0^2$

FIGURE 3.14.

Concentration profiles of ion **b** within spherical bead for ion exchange between ions with self diffusion coefficients, D_a, $1.0 \times 10^{-6} cm^2 s^{-1}$, D_b, $1.0 \times 10^{-7} cm^2 s^{-1}$.

Volume of external solution equal to quarter of bead volume, (radius, r_o, 0.1cm), approximately $2.094 \times 10^{-3} cm^3$, in which initial concentration of ion **b**, 2M. Concentration of fixed ionic charge within exchanger, c_f, 1M.

Molar selectivity coefficient, K'^{a}_{b} equal 2.6. Concentration plotted as fraction of c_f. Horizontal line spans radial thickness of each lump of which there are thirty, with vertical notch giving position of lump centre. Profiles shown at dimensionless times ($D_a t/r_o^2$), .02, .04, .08, .16, .26, .4, .6, .8, 1.0, 1.5, 2.4.

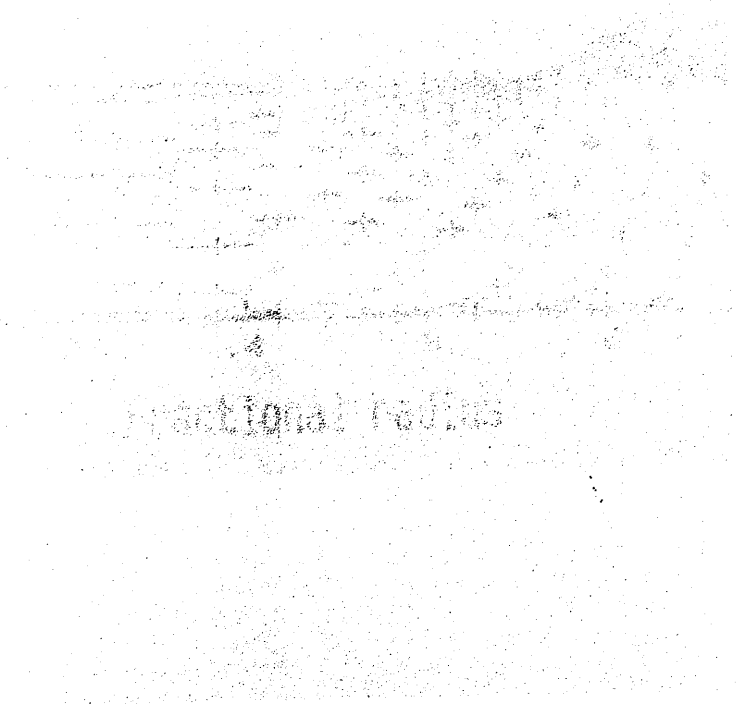

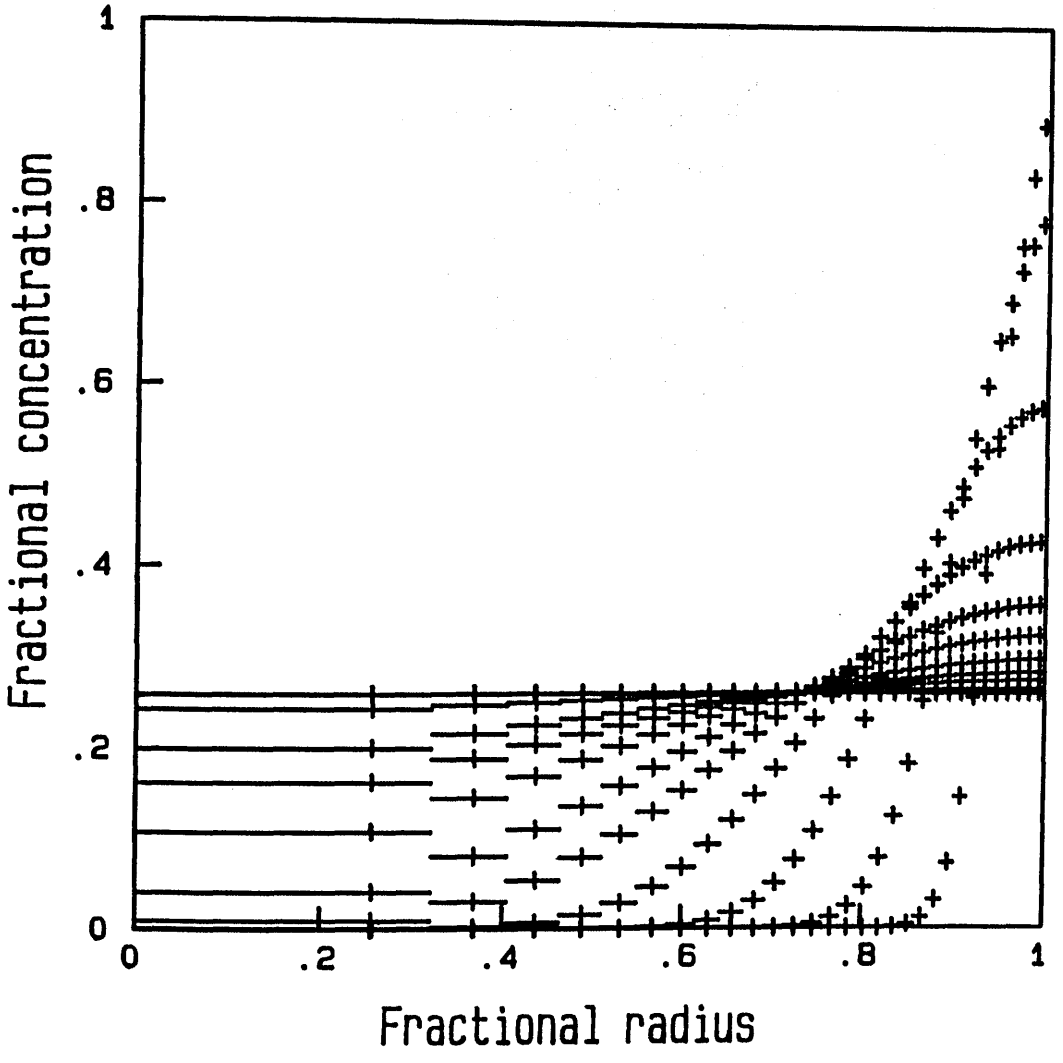
Fractional concentration
1
.8
.6
.4
.2
0
0
.2
.4
.6
.8
1
Fractional radius

FIGURE 3.15.

Concentration profiles of ion b within spherical bead for variable selectivity ion exchange.

Self diffusion coefficients, D_a, $1.0 \times 10^{-6} cm^2 s^{-1}$, D_b, $1.0 \times 10^{-7} cm^2 s^{-1}$.

Variable selectivity defined by isotherm produced using Kielland's semi-empirical equation, eqn(3.16) with w equal 2.0, fig(3.1).

Volume of external solution equal to quarter of bead volume, (radius, r_o, 0.1cm), approximately $2.094 \times 10^{-3} cm^3$, in which initial concentration of ion b, 2M. Concentration of fixed ionic charge within exchanger, c_f, 1M.

Concentration plotted as fraction of c_f. Horizontal line spans radial thickness of each lump of which there are thirty, with vertical notch giving position of lump centre. Profiles shown at dimensionless times ($D_a t/r_o^2$), .01, .03, .07, .15, .27, .4, .6, .8, 1.0, 1.5, 2.4.

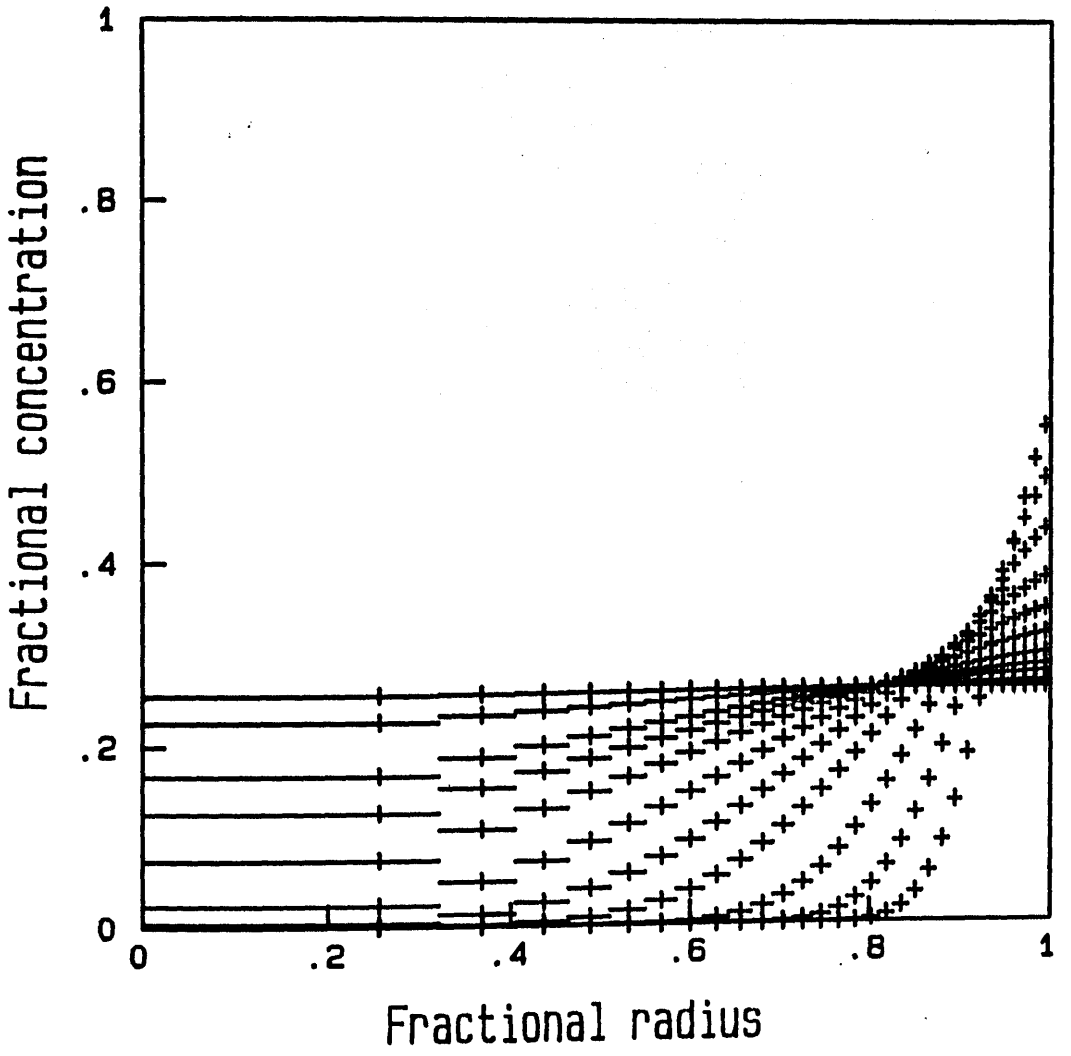
Fractional concentration
1
.8
.6
.4
.2
0
0
.2
.4
.6
.8
1
Fractional radius

FIGURE 3.16.

Concentration profiles of ion b within spherical bead for Uni-Divalent ion exchange. Ion a, initially the only ion present in exchanger is divalent.

Self diffusion coefficients, D_a, $1.0\times10^{-6}cm^2s^{-1}$, D_b, $1.0\times10^{-7}cm^2s^{-1}$.

Molar selectivity coefficient, K'^{a}_{b} equal 0.5.

Radius of bead r_o, 0.1cm. Volume of external solution equals volume of bead, approximately $4.1888\times10^{-3}cm^3$, in which initial concentration of ion b, 1M, which is equal to concentration of fixed ionic charge in exchanger, c_f. Concentration plotted as fraction of c_f. Horizontal line spans radial thickness of each lump of which there are thirty, with vertical notch giving position of lump centre. Profiles shown at dimensionless times (D_at/r_o^2), .02, .06, .12, .22, .4, .6, .8, 1.0, 1.2, 1.6, 2.0, 3.0.

Final equilibrium value, $\bar{c}_b$=.558M, $\bar{c}_a$=.221, c_b=.442, c_a=.279.

Uni-Divalent Exchange

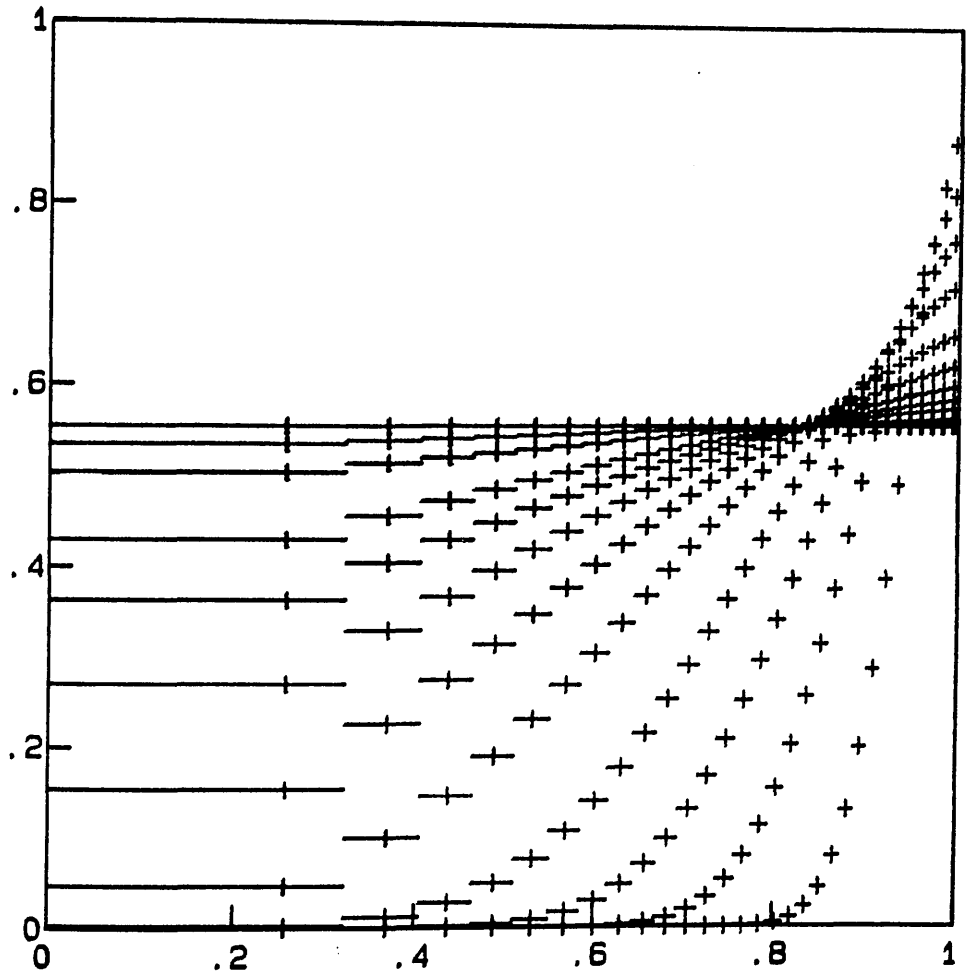

Fractional concentration

Fractional radius

REFERENCES FOR CHAPTER THREE

[1]. F.Helfferich, Ion Exchange, J. Wiley, New York (1962).

[2]. F.Helfferich and M.S.Plesset, J. Chem. Phys. **28** (1952) 418.

[3]. J. Kielland, J. Soc. Chem. Ind. (London), **54**, (1935) 232T.

[4] R.M Barrer and J.D. Falconer, Proc. Roy. Soc. (London), **A236**, (1956) 227.

[5]. F.Helfferich and H.D.Ocker, Z. Physik. Chemie, **10**, (1957) 213.

CHAPTER FOUR

NON-LINEAR ONE DIMENSIONAL DIFFUSION WITH MOVING BOUNDARIES, SWELLING DIFFUSION SYSTEMS.

4.1 INTRODUCTION

Novel drug release devices are being developed which may be used to deliver therapeutic doses at a constant optimal rate. One class of such devices which has proved particularly successful at meeting this objective is the swelling hydrogels, [1]. These hydrogels are typically polymerised polyethylene oxides, which swell reversibly when placed in water. The degree of swelling is dependent on the composition of the polymer but a 200% volume increase is possible. The swelling properties of these materials have been exploited by allowing the polymers to swell in a drug solution, which they absorb. On drying the drug is trapped immobile within the hydrogel matrix and when this device is implanted in a patient the process reverses, the polymer swells and the drug dissolves and diffuses out, but by careful control of these processes, near constant release of drug may be obtained over prolonged periods.

The combined process of swelling, drug dissolution and diffusion is perhaps the most complex of those employed by man-made free response systems. The balance of these simultaneous processes required to provide controlled release has, till now, been a matter of empiricism, inspiration and intuition on the part of the system designers. Although these creative elements must remain, it would be of exceptional value if it were possible to model such systems, to assist the design of new even more complex devices and to optimise existing ones. This leads us to a discussion of such diffusion systems in general, especially

those with moving boundary conditions, since the geometry of the device at each location is now time dependent. In this chapter the application of the bond graph model to such problems is developed.

Swelling-diffusion phenomena are not uncommon. A notable common or everyday example is the infusion of tea, in which caffeine is released from the swelling tea leaves.

It is not difficult to appreciate that progressively changing dimensions may be incorporated into a bond graph model in a similar fashion to that used in the previous chapter, where variable diffusion coefficients and selectivities were required for the ion exchange model. As with mathematical solutions to diffusion problems, network thermodynamics demands precise definition of system geometry, but this is required to be constant only over the step time interval of integration, H. The size of this step can be made sufficiently small to account for dimensional change over an arbitrarily large number of discrete steps.

Since the thermodynamic properties of a material must change in some way upon uptake and swelling in solvent, we would expect the diffusion coefficient of diffusants to vary also. In this way these systems are very similar to the ion exchange problems solved earlier (Chapter 3), since they may also be regarded as variable diffusion coefficient problems. In ion exchange the variation of the diffusion coefficient was defined explicitly by Nernst-Planck theory as a function of concentrations within the exchanger. The variation of D due to swelling will be dependent on many complex factors and will differ widely from one material to another. For most the precise relationships between

diffusion coefficient and degree of swelling are not predictable and must be measured directly, or as here sensibly guessed. One possibility is that the diffusion coefficient may be modified largely by tortuosity effects, as the polymer swells. In the swelling process the paths of diffusion become more plentiful and the overall resistance of the material to diffusional flow decreases. The polymer may interact with the diffusant by some other mechanism and changes in solvent levels may influence these also. For the purposes of the tea leaf model tortuosity effects were considered. In the later analysis of swelling hydrogels, independent experimental data has been used to obtain a numerical relationship between water content swelling and the diffusion coefficient of morphine in a specific gel.

For network modelling it is only necessary that the swelling be defined parametrically from separate experimental measurements. The aim of this chapter is not to unravel the mechanisms of swelling, rather the purpose is to illustrate the methods by which network thermodynamics may be used to simulate the complex diffusional processes from independent data, [2], [3], [4].

4.2 MODIFICATION OF DIFFUSION COEFFICIENT USING TORTUOSITY FACTORS.

As for ion exchange a local diffusion coefficient may be defined, D^j (cf D^j_{ab}, Section 3.4) for each volume element (lump) in the network model. As water enters a volume the characteristic diffusion coefficent for that lump will rise and the bond graph resistance drops. Assuming that this is due to the increasing of the

available paths for diffusion only, (tortuosity factors), it is possible to correlate resistance and swelling theoretically. There are many methods for predicting tortuosity factors, all must be considered approximate. In this example Prager's tortuosity formulation [5] has been used here, eqns(4.1),(4.2). θ is the tortuosity factor and D^* the intrinsic diffusion coefficient of the solute in a non-tortuous medium (v_w=1, θ=1).

$$D^j = D^* \theta \qquad (4.1)$$

Where

$$\theta = \frac{v_w (1 - v_w + v_w \ln v_w)}{2(1 - v_w + v_w \ln v_w) - 0.5 v_w (\ln v_w)^2} \qquad (4.2)$$

In which v_w is the volume fraction of water in volume element, j, eqn(4.3).

$$v_w = \frac{v - v_o}{v} \qquad (4.3)$$

In this expression v is the swollen volume of the element and v_o is it's original dry volume. Both the hydrogel and tea leaf examples were considered to swell to double their initial volume with a maximum equilibrium value of v_w, 0.5.

For the tea leaf example, in which these tortuosity corrections were used, the diffusion coefficient of the fully swollen material D_s was known, $5.0 \times 10^{-7} cm^2 s^{-1}$. Using D_s, a value for D^*, $1.217 \times 10^{-6} cm^2 s^{-1}$ was obtained from the tortuosity correction θ for a fully swollen leaf (v_w=0.5 in eqn(4.2)). D^* was then used to estimate the subsequent

diffusion coefficients in the partially swollen material by applying eqn(4.1). Although the choice of tortuosity expression is arbitrary this provides a viable self-consistent method of correction. The resultant relationship is shown in graphical form as a broken line in fig(4.1) in which D^j has been plotted against the fractional swelling, f_s, eqn(4.4).

$$f_s = \frac{v - v_o}{v_o} \qquad (4.4)$$

Since the systems considered in this chapter swell to twice their original volume, (v_w=0.5), f_s has a maximum value, f_m, of 1. On fig(4.1) for comparison, a straight line relationship between D^j and f_s has been plotted (solid curve), clearly Prager's approach predicts a near-linear increase in D^j with fractional swelling.

4.3 AD HOC KINETIC MODELS FOR SWELLING

The systems discussed in this chapter are considered to have planar geometry, and as such each can be described by the kinetics of release from the faces of a planar membrane, as discussed in Sections 2.3 and 3.5.1. This is not an unreasonable approximation for a tea leaf since it is thin enough so that diffusion from it's edges can be ignored. Even so, the kinetics of swelling are not entirely straightforward. Most experimental data provide only the total rate of solvent uptake by the membrane and do not provide information on the internal swelling profiles. For network models however the degree of swelling is required as a function of time and position in the swelling matrix.

In the absence of such detailed information, ad hoc kinetic models were examined which were comparable with the overall rates of water uptake observed. Computer simulations of drug release may then be made with the proviso that should more detailed swelling information become available it could be incorporated into these as desired without modification of the methods, described below.

4.3.1 Swelling by sharp water front.

Perhaps the simplest swelling model that can be envisaged is that of sharp solvent front penetration, with completely dry material directly adjacent to the fully swollen matrix. This is rather an extreme mechanism and perhaps unlikely for real systems, but it is an interesting limiting case for comparison with other approaches.

Due to the fact that the network model of a gel consists of a finite number of volume elements (lumps), the swelling profile is considered as a number of steps. A true representation of states is approached by using a sufficiently large number of lumps. The implementation of the sharp front mechanism is particularly simple and the degree of swelling at each time is represented by suitable numbers of fully swollen and unswollen lumps.

The water front is considered to advance at a rate K(cm/s) through a planar membrane, of initial thickness l_o(cm). n_s, defined by eqn(4.5), defines the integer number of lumps which, if fully swollen would approximate to the observed overall uptake of water of the whole membrane or leaf at time t.

$$n_s = \text{int}\left(\frac{2\,n\,K\,t}{l_o}\right) \qquad (4.5)$$

n is the number of lumps chosen to model the half thickness of the model slab. As defined above, n_s always underestimates the water content. To obtain a precise representation, the interfacial lump (between fully swollen outer layers and dry inner layers) is considered partially swollen. Its degree of swelling is estimated by eqn(4.6).

$$f_s = \left(\frac{2nKt}{l_o} - n_s\right) f_m \qquad (4.6)$$

This process is shown schematically in fig(4.2). Note that when the fractional part of eqn(4.5) is zero, the water front is on a lump edge.

4.3.2 Swelling with penetrating water front.

For this model the water front is also considered to move through the leaf at a linear rate K_p(cm s^{-1}). In this example however, the swelling profile is considered to penetrate linearly from fully swollen at the surface to zero swelling at the leading edge of the front, up to the time at which the two fronts advancing from opposite faces meet in the middle of the membrane. After that time the profile is assumed to remain linear with the fractional swelling, f_s, at the centre of the leaf thereafter increasing at a linear rate also, K_c(s^{-1}).

The swelling profile being linear, may be defined by two points. Since the outer surfaces of the membrane are fully swollen, (at f_m), the position of the solvent front fixes the profile throughout.

Up to the time at which the profiles meet t_c, the front advances through the membrane at rate K_p. The thickness of dry membrane remaining is given by eqn(4.7).

$$l_d = l_o - K_p t \qquad (4.7)$$

Note that when t equals t_c, l_d is zero; the water fronts have met in the middle. After time t_c, the second point which fixes the profile is the fractional swelling at the membrane centre, f^o_s, eqn(4.8).

$$f^o_s = K_c \left(t - t_c\right) f_m \qquad (4.8)$$

Once the profile has been fixed it is assigned in the network model. This is achieved by reading the fractional swelling at the lump edges from the linear profile and averaging to determine the mean volume increase for each lump. This also requires the resultant computer program to update the distance of all lump edges from the membrane centre as the simulation proceeds.

4.4 CALCULATION AND VARIATION OF R AND C COEFFICIENTS.

The bond graph capacitances and resistances must be updated in these simulations in an identical manner as to that for the ion exchange problems (Chapter 3). For the swelling diffusion examples, the changing geometries must also be considered in these calculations.

The consequences for the capacitance are straightforward, as the volume of an element increases, it's capacity for storing material increases. The original capacitance of a lump is given by eqn(4.9), which is simply a combination of the equations formulated previously for a

planar membrane, (eqns(2.12) and (2.14)).

$$C = \frac{\alpha V_o}{2n} \tag{4.9}$$

Where V_o is the original volume of the membrane, n is the number of lumps used in the reticulation of the half thickness, and α the distribution coefficient.

After swelling however the new capacitance is given by eqn(4.10).

$$C = \alpha v = \frac{\alpha (1 + f_s) V_o}{2n} \tag{4.10}$$

Where v is the updated volume of the element, obtained from the original volume, V_o, and the fractional swelling, f_s, eqn(4.4).

Resistances require more careful formulation since these are dependent on the increases of area, path length of diffusion, and on the diffusion coefficient itself which is also changing. All these parameters have unique values in each lump volume of the swelling membrane at each time during the swelling-diffusion process. We consider the polymer to swell isotropically. Therefore if a lump element with fractional swelling f_s has original dimensions, width, depth and thickness, w, d and l, the new volume is given by eqn(4.11), in which z is the factor of increase in each dimension.

$$z^3(wdl) = (1 + f_s) \left(\frac{V_o}{2n} \right) \tag{4.11}$$

Rearranging and cancelling for the dry volume gives z as a function of the fractional increase in volume or

swelling parameter, f_s (defined in eqn(4.4)), giving eqn(4.12).

$$z = \left(1 + f_s\right)^{1/3} \tag{4.12}$$

The average local area of volume element j, A_j and thickness l_j are given by eqns(4.13) and (4.14) respectively.

$$A_j = \left(1 + f_s\right)^{2/3} A_o \tag{4.13}$$

$$l_j = \left(1 + f_s\right)^{1/3} \frac{l_o}{2n} \tag{4.14}$$

Where l_o is the total membrane thickness when dry and A_o the original dry area, f_s is the fractional swelling in this particular volume.

Since the local diffusion coefficents in adjacent volume elements will differ, (as for the ion exchange examples of Chapter 3), the resistance between lump centres is the sum of the resistances from each lump centre to the adjoining edge, eqn(4.15).

$$R_j = \frac{l_j}{2D^j A_j} + \frac{l_{j+1}}{2D^{j+1} A_{j+1}} \qquad 2 \leq j \leq n \tag{4.15}$$

Resistors which are on the end of the R-C chain, have only one term. (Here we need consider R_1 only since R_{n+1} is

that directed towards the centre of the membrane, over which there is no concentration gradient and therefore zero flow.)

The local diffusion coefficients in each lump D^j may be found from whatever relationship is considered appropriate, the local volumes, areas and thicknesses are calculated from the fractional swellings in each volume, these will depend on the time and the kinetic model of swelling used. The complexities of thermodynamically modelling release from these systems is evident, it is the rigorous development of the bond graph model that allows the problem to be addressed so conveniently.

The updating of the parameters and R and C values that are dependent on them is accomplished in an identical manner as to that described for the ion exchange problems. Fundamentally there is no greater difficulty in simulating swelling diffusion phenomena except that a greater amount of computation is required.

4.5 CAFFEINE RELEASE FROM A SWELLING TEA LEAF.

The simulation of caffeine release from a tea leaf was chosen as an example of a swelling diffusion system as we had excellant data available for the system parameters [4]. For this test both water invasions by the sharp and penetrating front mechanisms described above were considered for comparison of the resultant release kinetics. Prager's equation for tortuosity prediction, eqn(4.2) was used to give the local diffusion coefficients in the swelling leaf for both of these examples.

The original thickness of the leaf considered was, l_o,

0.008cm and the dry area A_o, .1cm^2. The diffusion coefficient of caffeine in the fully swollen leaf was $5.0 \times 10^{-7} cm^2 s^{-1}$, this value can be read from the graphical presentation of Prager's formulation used here, fig(4.1).

The rate at which the water fronts advanced in the sharp front model, K in eqns(4.5) and (4.6), was $6.67 \times 10^{-5} cms^{-1}$. This means that the leaf was fully swollen at 60s. For the penetrating front example the rate of front advance, K_p in eqn(4.7), was double the rate for the sharp front model, $1.33 \times 10^{-4} cms^{-1}$, so that the fronts meet in the centre of the leaf at t_c of thirty seconds. After this time the rate at which the fractional swelling at the leaf centre increases, K_c in eqn(4.8) was $3.33 \times 10^{-2} s^{-1}$, this means that f^o_s reaches its maximum value, f_m, of unity thirty seconds after the fronts meet, a full sixty seconds only after time zero. The consequence for the rate of overall swelling using these two rates is shown in fig(4.3) in which the overall fractional swelling, f_s has been plotted against time. As expected, this rate is not far from linear.

For illustration purposes the resultant profiles of swelling using the penetrating front algorithm are presented in fig(4.4) at two second intervals for a thirty lump model. These swelling profiles and subsequent profiles of concentration within the leaf have been constructed by plotting the fractional swelling, f_s or concentration in each volume element at the position of the lump volume centre. The abscissa represents the distance from the centre of the membrane as a fraction of the fully swollen

membrane thickness. In this way the effects of increasing thickness are illustrated also. For these systems which swell to double their initial volume, f_m is 1, the final factor of increase in thickness, z in eqn(4.12) is $2^{1/3}$, which is approximately 1.26. The original thickness as a fraction of the final value is 0.8 and as a consequence the swollen dimensions are length, .01008cm and area .159cm^2. In this way the profiles are observed to span from zero to 0.8 at time zero and gradually extend to 1 as the swelling-diffusion proceeds. The swelling profiles resulting from the sharp front mechanism are easily envisaged and are not illustrated.

Using a thirty lump model and a step time of integration, H of $1.5x10^{-3}$s, the kinetics of caffeine release from this system were simulated. Infinite bath conditions were considered so that effects of selectivity, which have been illustrated in depth for ion exchange diffusion, could be ignored. For all examples in this chapter the initial charges on the capacitors, C_2 to C_{n+1} were assigned equal charges (q values) corresponding to uniform loading of diffusant, eqn(2.15). The charge on C_1 was zero indicating an initial absence of diffusant in the collecting volume. Initial boundary conditions for a planar membrane were discussed previously in Section 2.3.

For the simulation of release using the sharp front mechanism the concentration profiles follow the pattern of swelling, these are shown at 2s intervals in fig(4.5). Concentration profiles within the leaf, using a penetrating front model for swelling, are shown in fig(4.6), also at 2s intervals. It is the concentration gradients at the

surfaces of the membrane that are all important in determining the efflux from these systems. For the purposes of constant release kinetics this gradient should remain as constant as possible during the release process, indicating a quasi-steady state flow across the interface. It can be seen that for both swelling mechanisms the gradients towards the outer edge are close together and nearly constant as desired, figs(4.5) and (4.6).

This is reflected in the release kinetics which are presented in fig(4.7). The dashed line on this figure is the comparative release from a fully swollen membrane given the same initial loading and a constant diffusion coefficient equal to that of the fully swollen material, $5.0x10^{-7}cm^2s^{-1}$. This has been calculated from the analytical solution for diffusion from a planar membrane with infinite bath conditions, eqn(2.16). Curves 1 and 2 show the release of caffeine into the external bath versus time for the penetrating and sharp front swelling kinetics respectively. It can be seen that the effects of swelling do indeed lead to a slowing down of the release process and an approach to zero order kinetics: Constant release with time.

4.6 RELEASE OF MORPHINE FROM A SWELLING HYDROGEL.

The same thermodynamic model has been applied to the problem of drug delivery from a swelling hydrogel. Here only the penetrating front model for swelling has been tested, since the sharp front model, (Section 4.3.1) was considered quite unrealistic. Also tortuosity factors have not been used to predict diffusion coefficient. The

equilibrium swelling value for a hydrogel material depends on the conditions of synthesis, [3]. By measuring the release kinetics of morphine from fully swollen gels of different equilibrium swellings a straight line fit of diffusion coefficient versus water content has been obtained, eqn(4.16), [3]. It is assumed here that this relationship may also be applied to a hydrogel which is in the process of swelling.

$$D^j = (-1.86 + 6.5f_s) \times 10^{-6} cm^2 s^{-1} \qquad (4.16)$$
$$.3 \leq f_s \leq 1$$

This simulation considered the morphine release from a hydrogel slab which was initially free of water and which swelled to twice it's original volume, that is f_m is 1 here also, (as observed for some prepared gels, [3]). Reading from eqn(4.16), setting f_s equal to f_m, the maximum value for the diffusion coefficient is then $4.64 \times 10^{-6} cm^2 s^{-1}$. The original dimensions of the dry hydrogel slab were: thickness, l_o, .28cm and area A_o, $2.75cm^2$. In which the initial loading of morphine was 51.4mg or .18mmol, equal to a concentration of .23mmol per cm^3 of dry hydrogel. (Molecular weight of morphine $285.35 mgmol^{-1}$) Similarly to the above example (for a tea leaf) the factor of increase in each dimension is $2^{1/3}$, and so the fully swollen dimensions were; thickness, .3528cm and area, $4.365cm^2$. A thirty lump model was used once more to model the half thickness of the planar hydrogel membrane. A step time of, H, 0.5s was used.

The parameters for swelling using sharp front mechanism

were: K_p, (eqn(4.7)), $3.89 \times 10^{-5} cms^{-1}$. K_c (eqn(4.8)), $1.39 \times 10^{-4} s^{-1}$. Fig(4.3) showed the resultant total swelling for the tea leaf using the penetrating front mechanism. The kinetics of overall swelling for this hydrogel model are identical except for the time base. This can be converted by replacing the 60s maximum in fig(4.3) with 4 hours and rescaling the gratice marks to 40 minute intervals, (rather than 10s).

An equivalent approach has been used here to produce the concentration profiles, now presented at 8min intervals, fig(4.8). The same effect of bunching gradients directed out of the membrane is observed for this system. For comparison the release from a fully swollen device with equal drug has been calculated using the analytical solution for diffusion from the faces of a planar membrane, eqn(2.16), with the swollen dimensions of this system given above and the maximum diffusion coefficent, $4.64 \times 10^{-6} cm^2 s^{-1}$. Fig(4.9) compares the rates of morphine release by plotting the calculated absolute amount of morphine (mmol) in the collecting bath against time. The simulated diffusion from the swelling hydrogel membrane device is close to linear over a period of more than 3 hours and in marked contrast to free diffusion from the fully swollen material.

The rate of drug release is of fundamental importance in clinical applications. It has been calculated and shown in fig(4.10), where the simulated release rate of morphine in mgs^{-1} has been plotted against time in hours. This type of information from the simulation will allow clinicians to

decide dose levels. (The computer program for the simulation based on this hydrogel model is given in Section A.2 of the Appendix as an example.)

4.7 CONCLUSIONS

It is hoped that the network thermodynamic methods for simulating these systems described above will find early application in the design of novel drug release devices. It has been illustrated in this chapter, as for the ion exchange problems of Chapter 3 that the thermodynamic methods and bond graph techniques are extremely convenient for probing the dynamics of these systems. As in Chapter 3 (dealing with ion exchange) no modifications to the bond graph model have been made. The only requirement being a need to rescale R and C values as the diffusion proceeds. Although specific mechanisms of swelling have been chosen here for the purposes of example, other models and perhaps experimental data could be input to study their effects on release kinetics. Issues of limited collecting volume and variable selectivity which may be important considerations, especially **in vivo**, can be incorporated into the model with equal ease as illustrated for ion exchange. In addition the techniques for simulating swelling diffusion systems may be incorporated in the network thermodynamic methods for studying two and three dimensional diffusion, discussed below. No other numerical approach is as flexible or as robustly defined. The production of a Computer Aided Design system for drug delivery devices is a real possibility.

FIGURE 4.1.

Graphical presentation of Prager's tortuosity relationship with local diffusion coefficient D^j plotted as a function of f_s, the fractional swelling, eqn(4.4). Dashed line is prediction using Prager's tortuosity factor for tea leaf example, eqn(4.2). Solid line illustrates linear relationship for comparison.

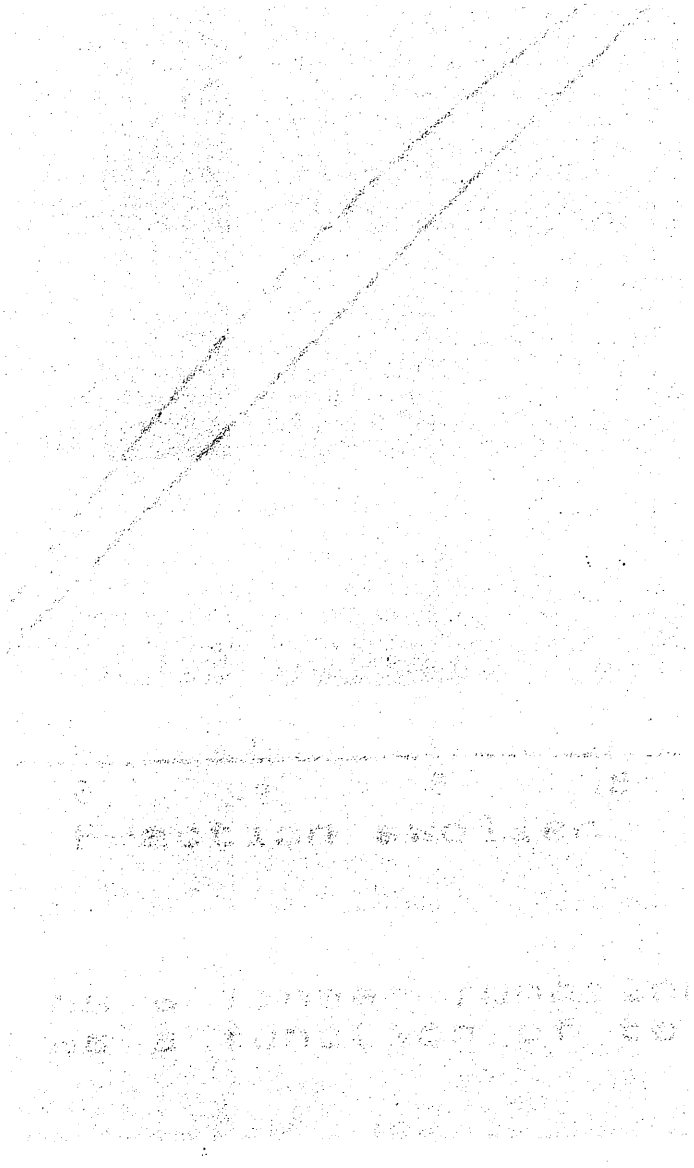

Expressions for D

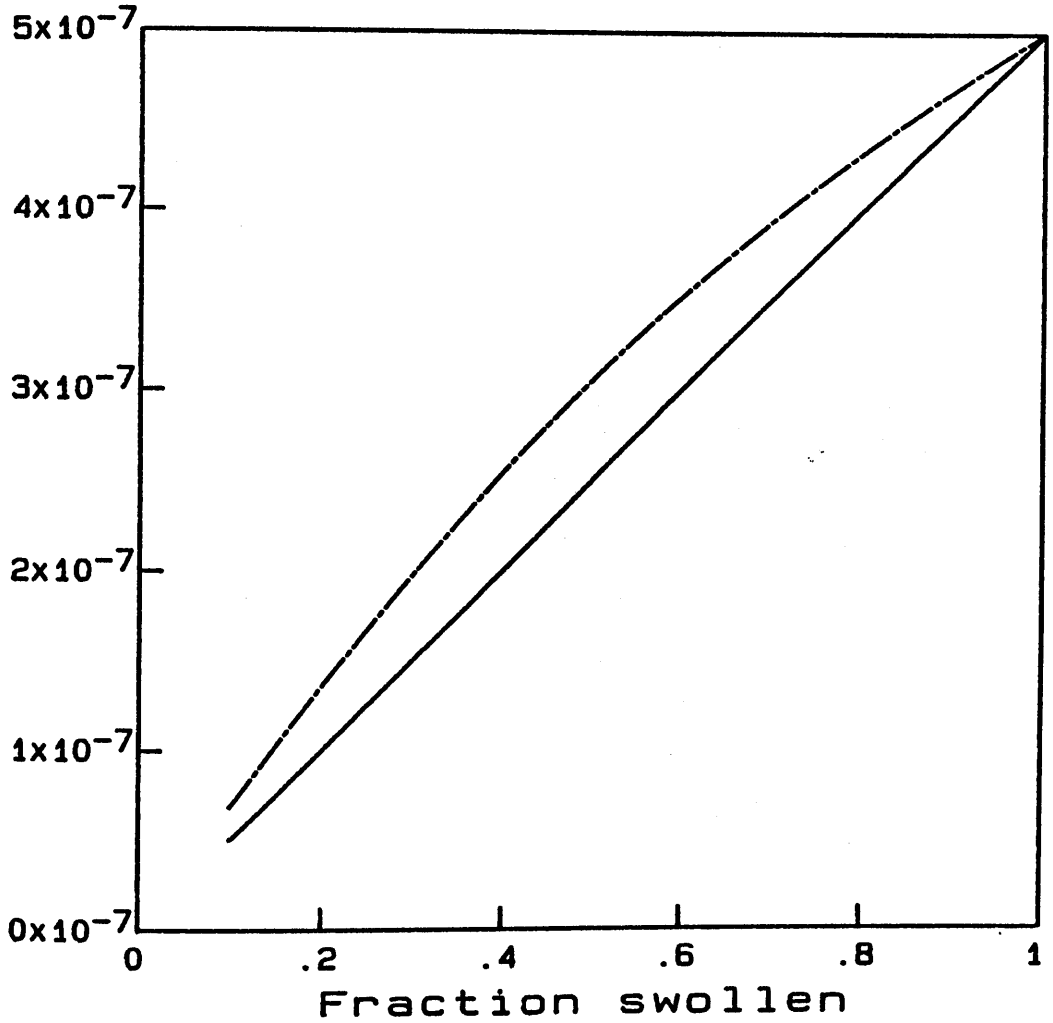

— D as a linear function
-- D as a function of tortuosity

FIGURE 4.2.

Schematic diagram showing how sharp front model is implemented in a network model. Shaded area shows areas of fractional swelling at time t.

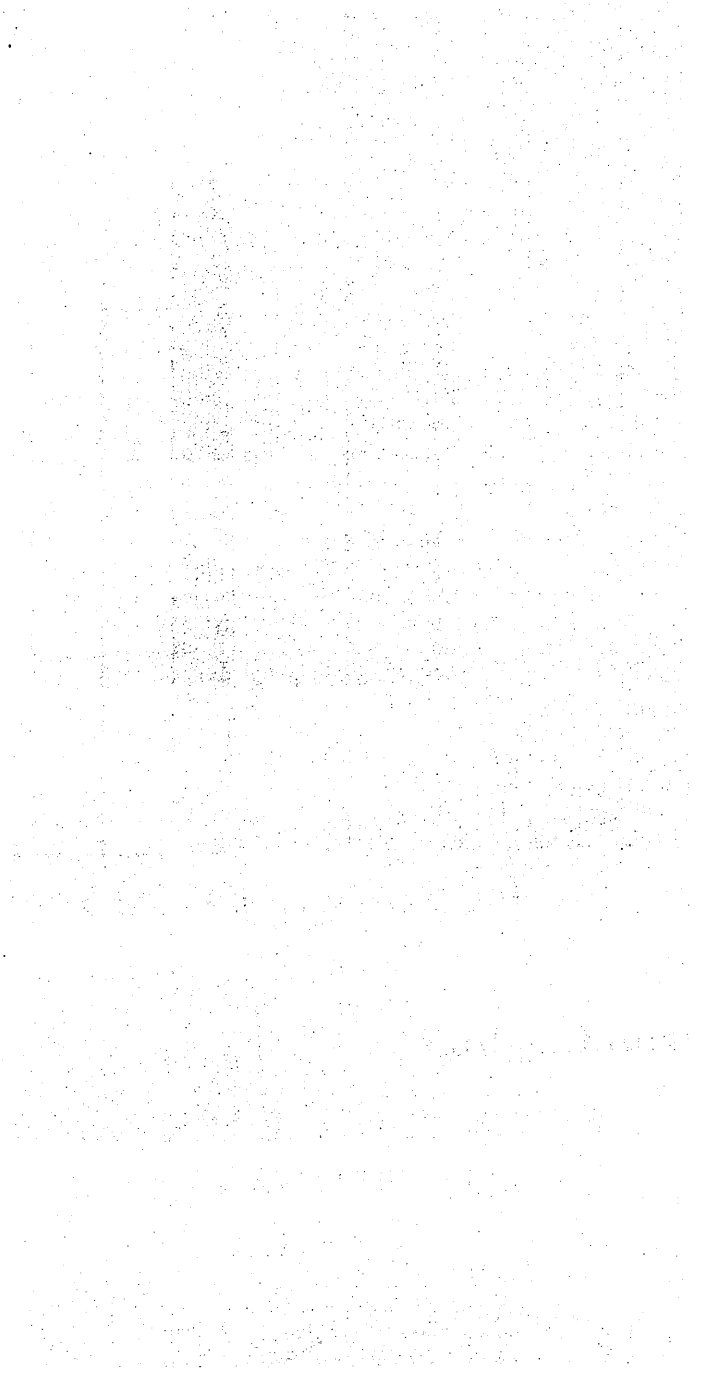

Implementation of Sharp front swelling

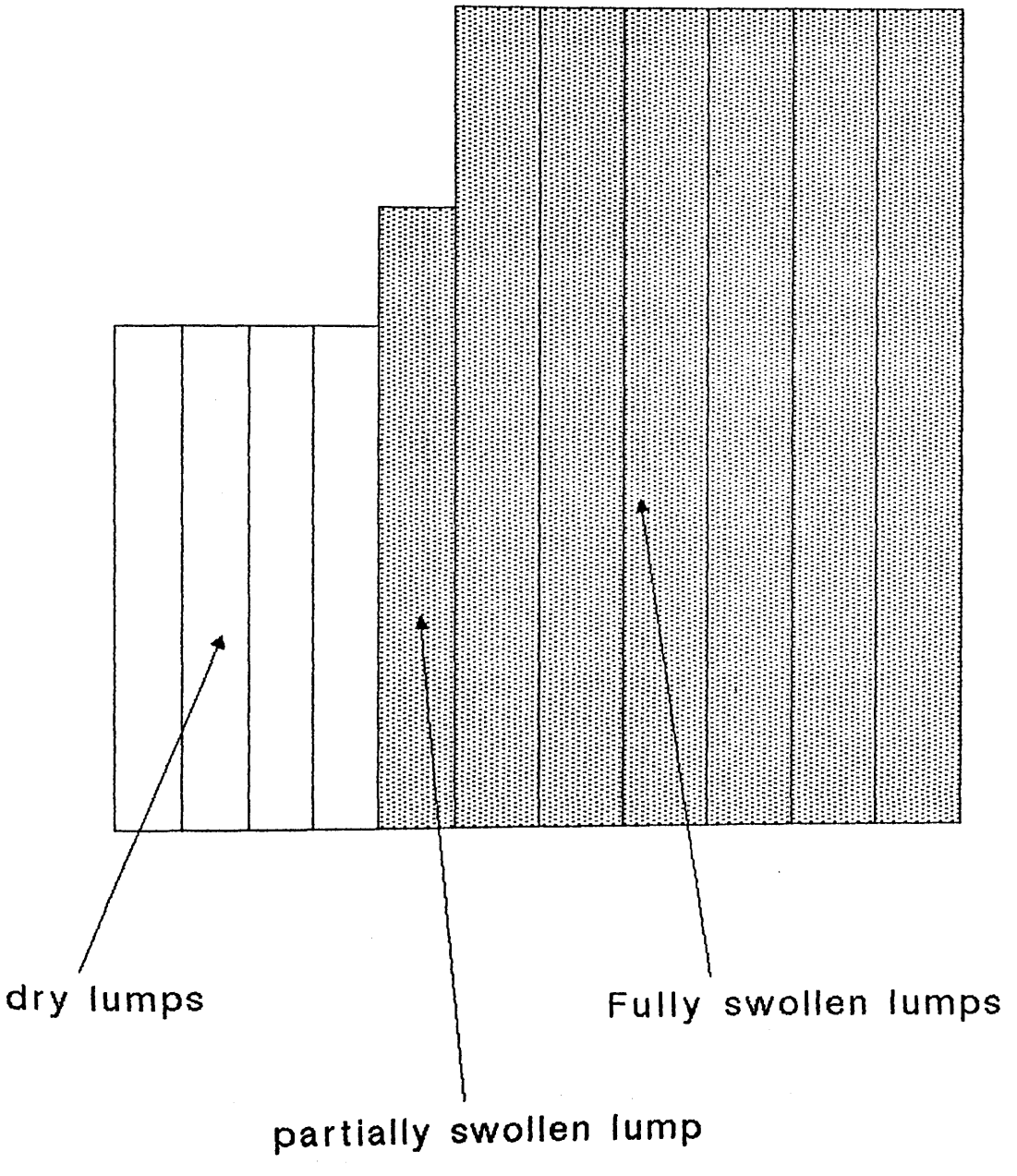

FIGURE 4.3.

Resultant overall water uptake and therefore fractional swelling using sharp front penetration model. Abscissa is time. This graph is for tea leaf parameters, however the total uptake for hydrogel model is identical except with shown gratice marks on abscissa at 40min intervals. For tea leaf $t_{1/2}$ (f_s=0.5, for system with f_m=1 as for these examples) is 30s, for hydrogel, 2 hours.

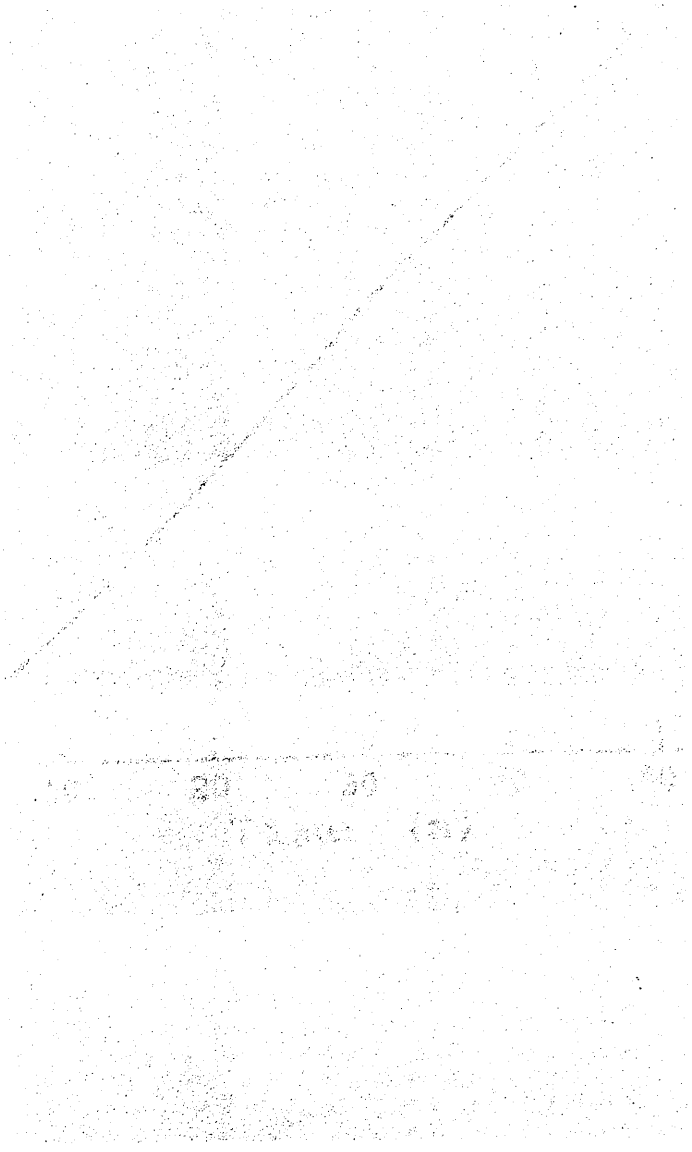

Total water uptake

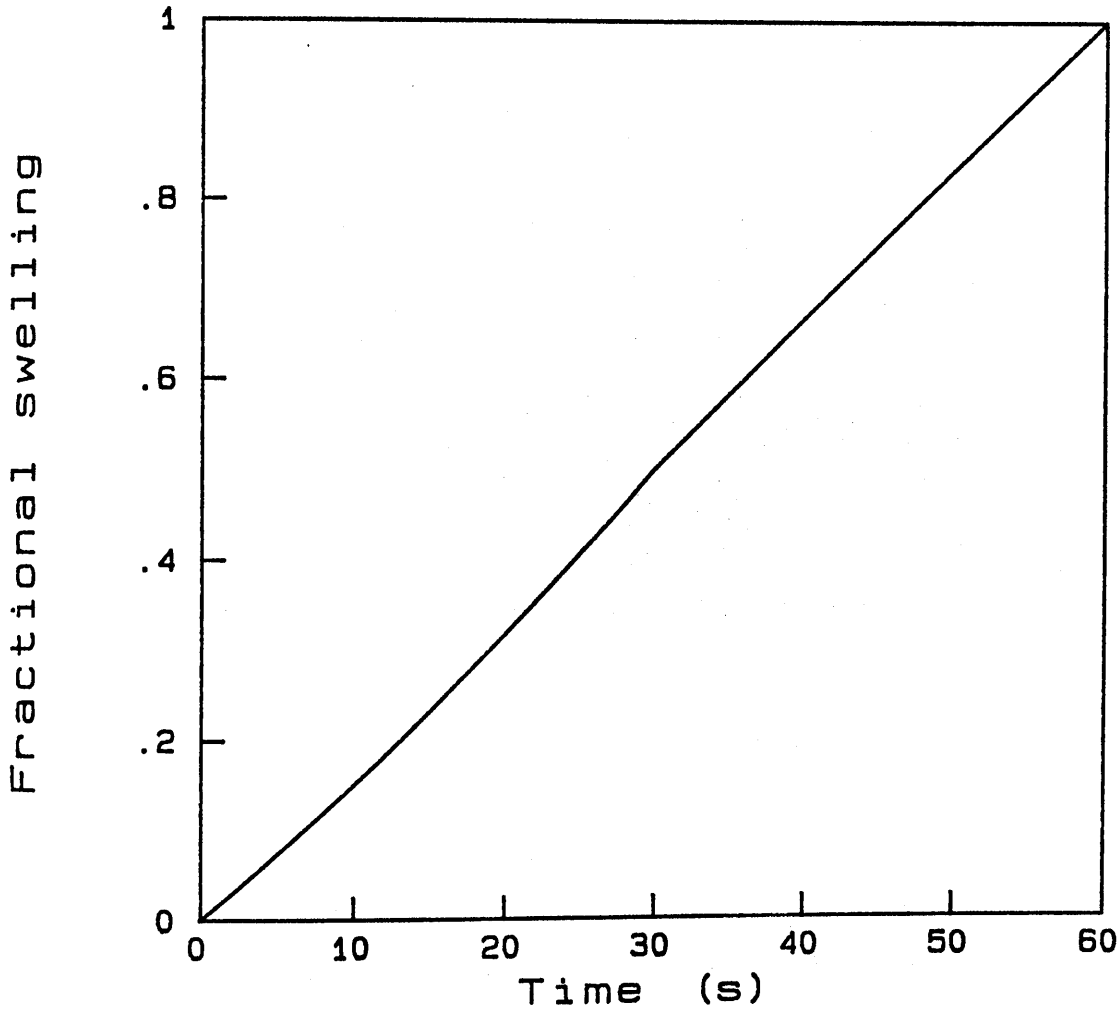

FIGURE 4.4.

Swelling profiles for penetrating front mechanism used for both tea leaf and hydrogel examples in thirty lump model. For tea leaf profiles these are at 2s intervals, for hydrogel example, 8min intervals. Constructed by plotting fractional swelling, f_s eqn(4.4), in each volume element at position of lump volume centre. Abscissa represents distance from centre of membrane calculated as fraction of fully swollen membrane thickness. For isotropic swelling profiles are observed to span from zero to approximately 0.8 finally extending to 1.

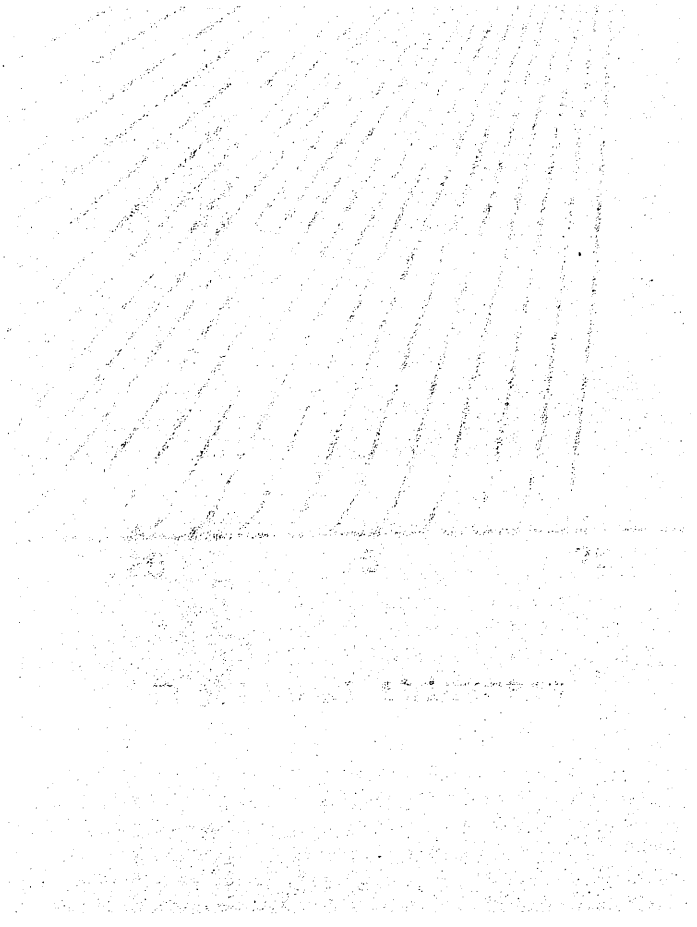

Swelling profile

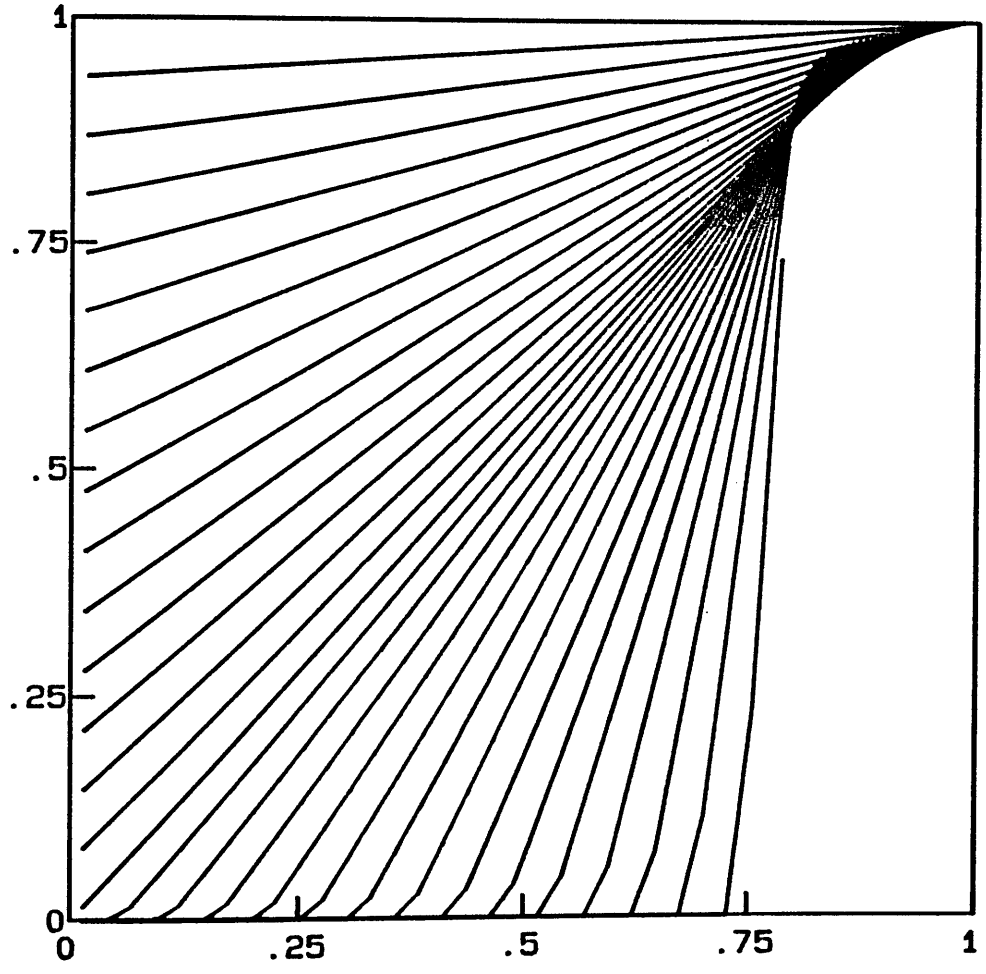

Fractional swelling

Fractional thickness

FIGURE 4.5.

Caffeine concentration profiles within leaf membrane using sharp front swelling mechanism. Profiles shown at 2s intervals by plotting concentration in each volume element of the thirty lump model at position of lump volume centre. Abscissa is distance from centre of membrane calculated as fraction of fully swollen membrane thickness. For isotropic swelling, profiles are observed to span from zero to approximately 0.8, actual thickness l_o, .008cm, finally extending to 1, full thickness, .01008cm. Ordinate is molar concentration, with initial loading .02mmol per cm^3 of leaf.

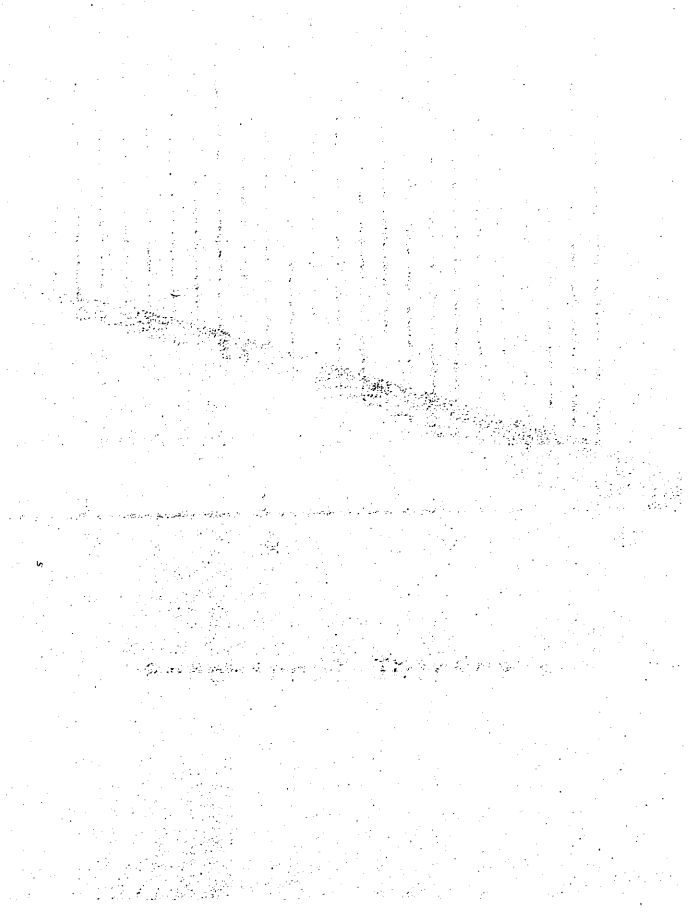

Release from Sharp Front

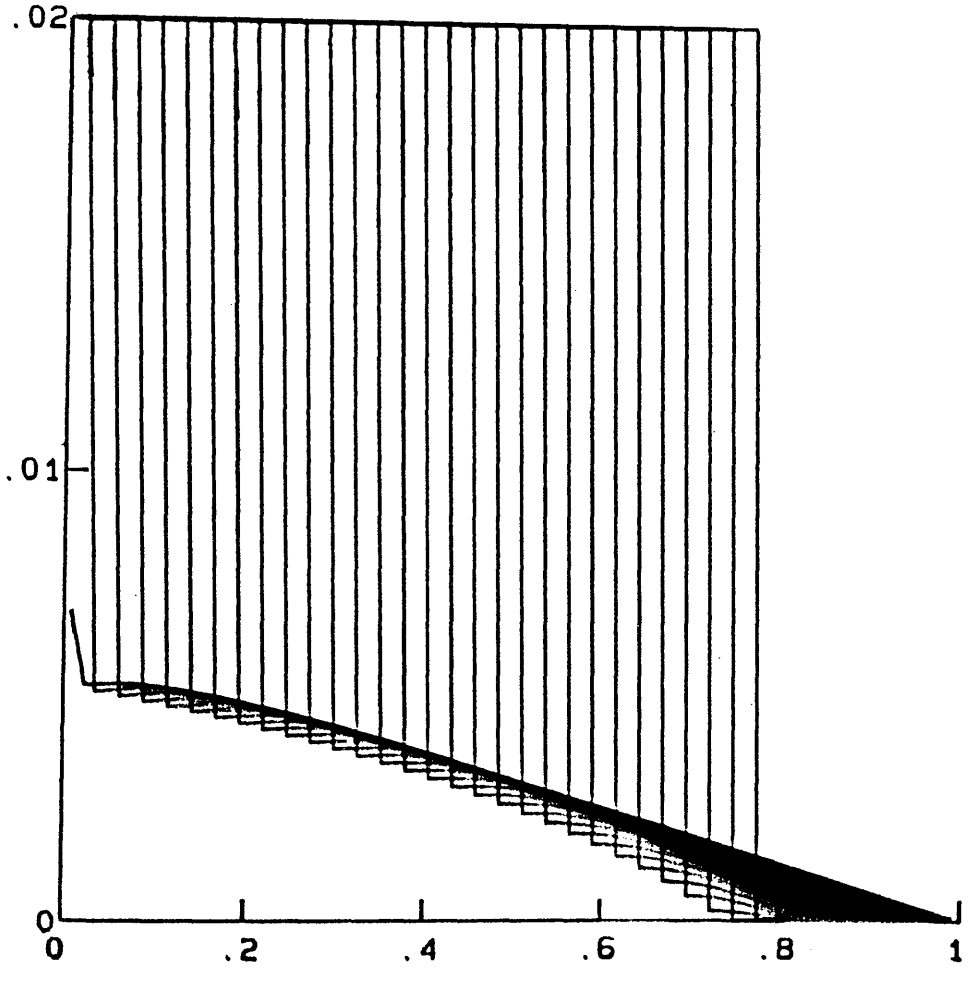

Fractional Thickness

FIGURE 4.6.

Caffeine concentration profiles within leaf membrane using penetrating front mechanism for swelling. Profiles constructed at 2s intervals by plotting concentration in each volume element of the thirty lump model at position of lump volume centre. Abscissa is distance from centre of membrane calculated as fraction of fully swollen membrane thickness. For isotropic swelling, profiles are observed to span from zero to approximately 0.8, actual thickness l_o, .008cm, finally extending to 1, full thickness, .01008cm. Ordinate is molar concentration. Initial loading, .02mmol per cm^3 of leaf.

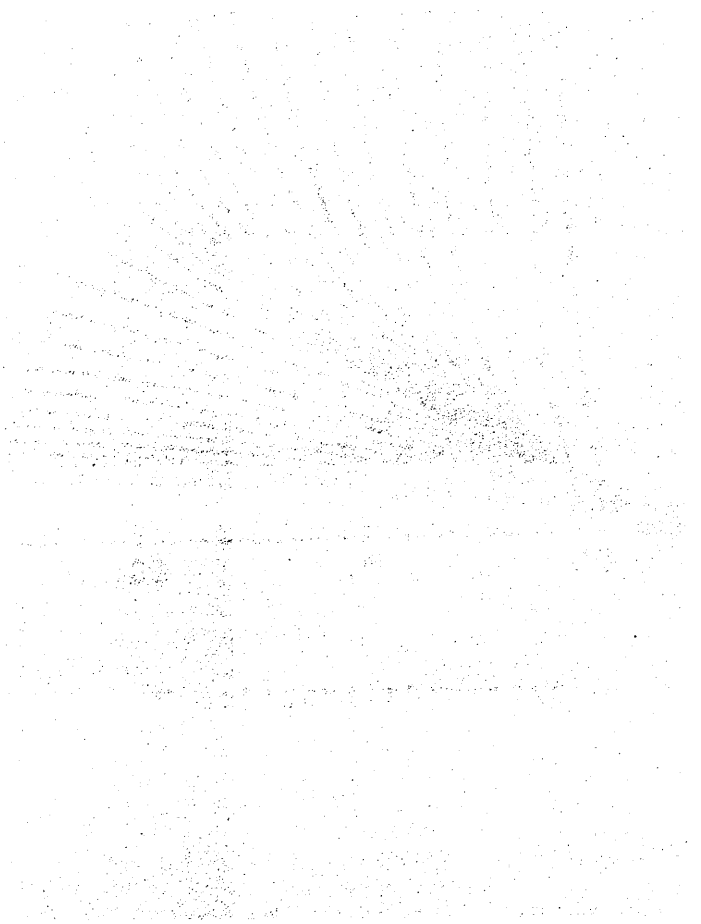

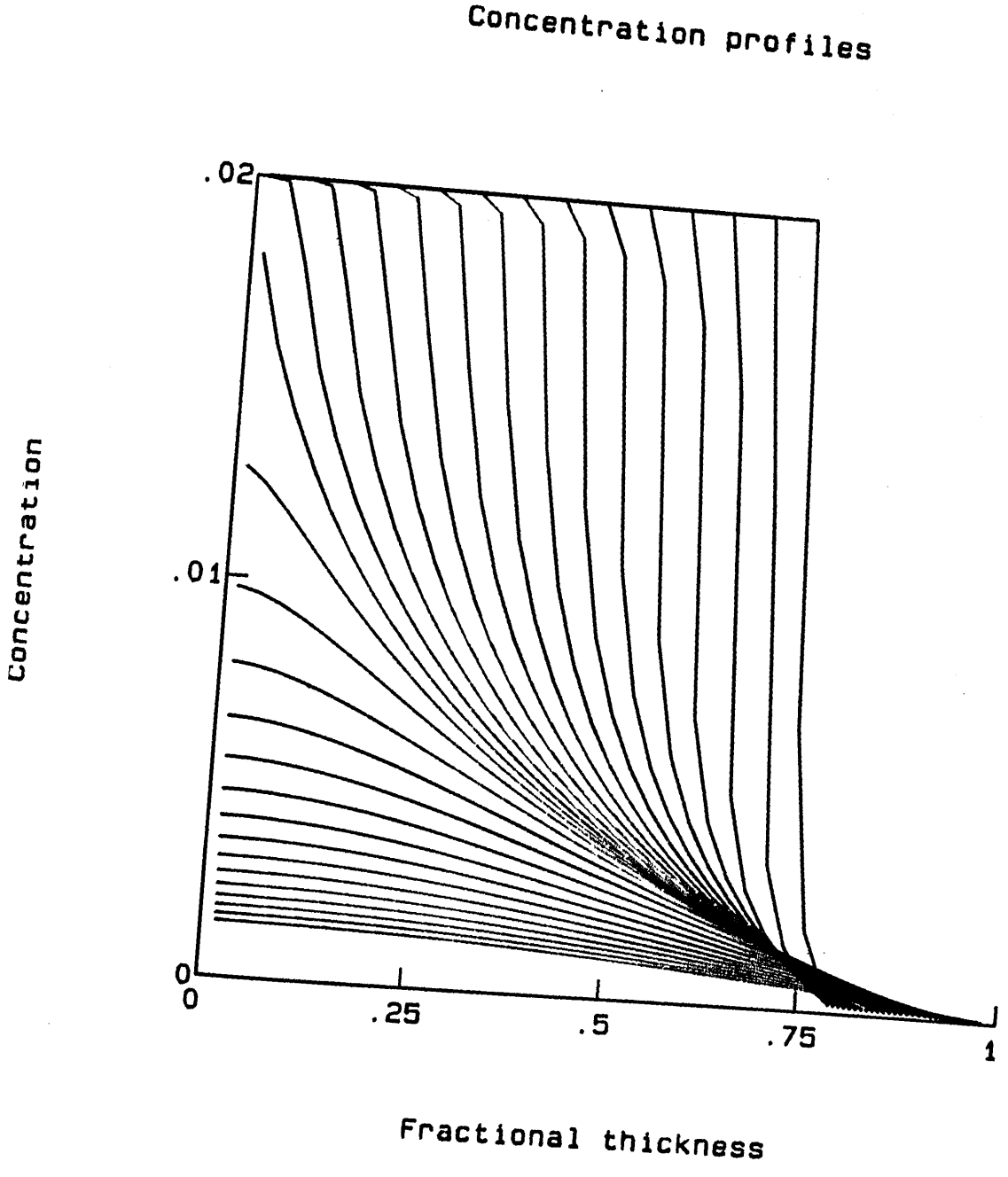
Concentration profiles
Concentration
.02
.01
0
0
.25
.5
.75
1
Fractional thickness

FIGURE 4.7.

Simulated caffeine release for sharp and penetrating front swelling mechanisms compared. Original dimensions of leaf membrane, thickness, .008cm, area, .1cm^2, swelling isotropically to double volume with length, .01008cm and area, .159cm^2. Initial loading of caffeine 1.6×10^{-5}mmol, corresponding to concentration of .02M in dry leaf. Thus amount of caffeine released into infinite bath in mmol is plotted against simulated time in seconds. Curve 1, simulated release for thirty lump penetrating front example, curve 2, diffusion from identical model using sharp front mechanism. Dashed curve calculated from analytical solution for release from fully swollen device at time zero with same initial loading (concentration .01mmol per cm^3 of swollen leaf).

Release from leaf

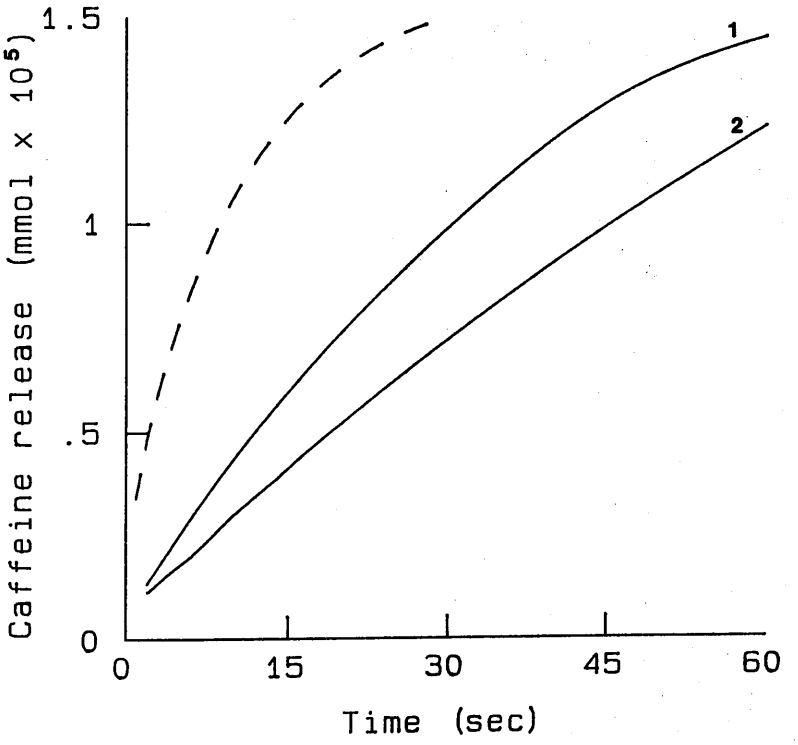

FIGURE 4.8.

Morphine concentration profiles within hydrogel slab using penetrating front mechanism for swelling. Profiles constructed at 8min intervals up to 4 hours by plotting concentration in each volume element of the thirty lump model at position of lump volume centre. Abscissa is distance from centre of membrane calculated as fraction of fully swollen slab thickness. For isotropic swelling, profiles span from zero to initially about 0.8, actual thickness l_o, .28cm, finally extending to 1, full thickness, .3528cm. Ordinate is molar concentration. Initial loading, 51.4mg in slab, that is .23mmol per cm^3 of dry hydrogel.

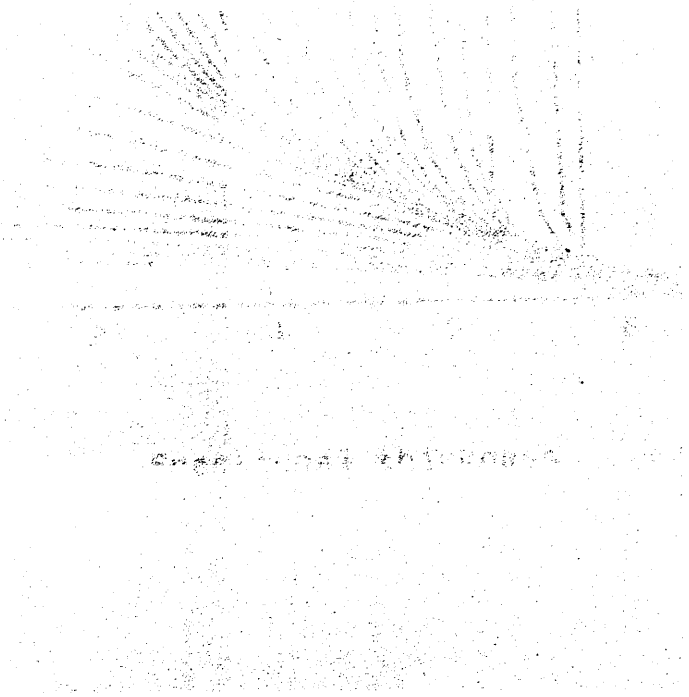

Swelling Hydrogel

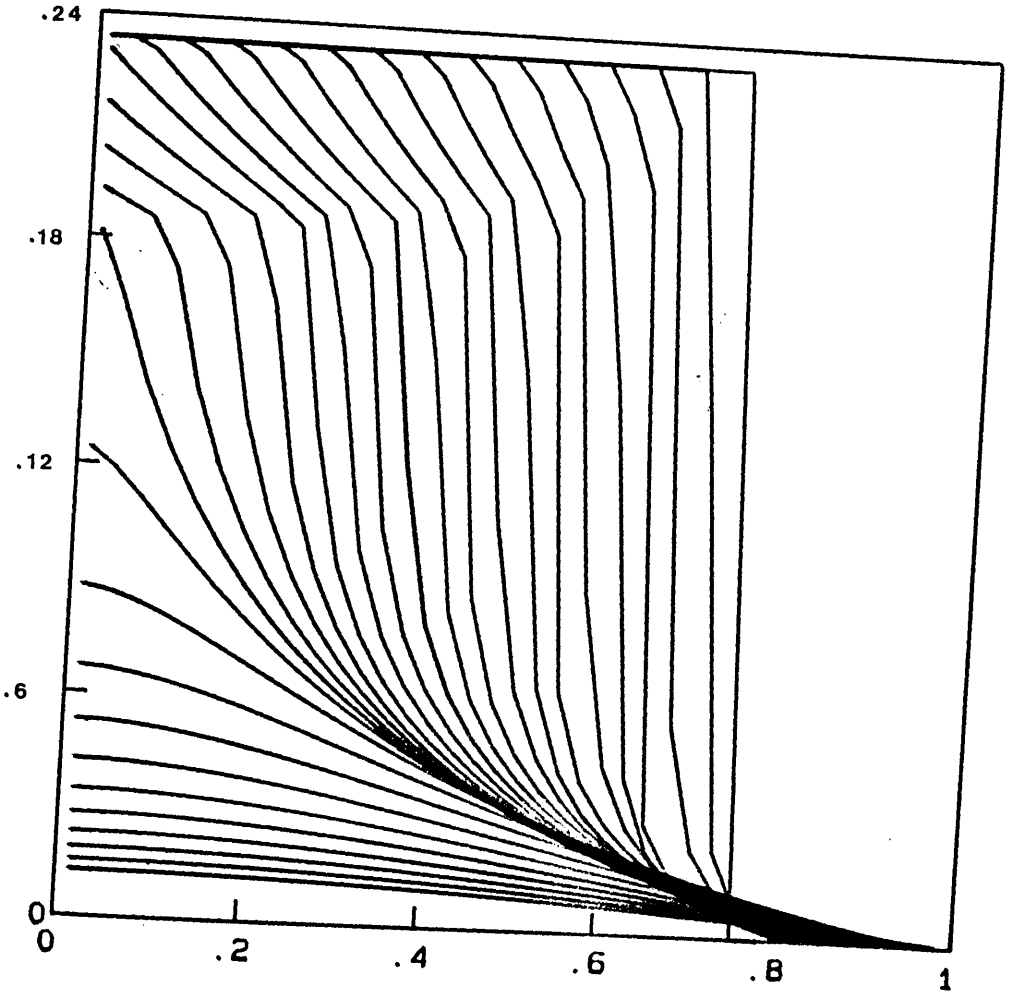

Concentration

Fractional thickness

FIGURE 4.9.

Simulated morphine release from hydrogel slab using penetrating front swelling mechanism, curve 1, compared to analytical solution for diffusion from faces of a fully swollen slab, curve 2. Original dimensions of hydrogel membrane, thickness, .28cm, area, 2.75cm^2, swelling isotropically to double volume with length, .3528cm and area, 4.365cm^2. Initial loading of morphine .18mmol, corresponding to concentration of .23M in dry slab (or .12M in fully swollen device). Thus amount of morphine released into infinite bath in mmol is plotted against simulated time in hours using thirty lump model.

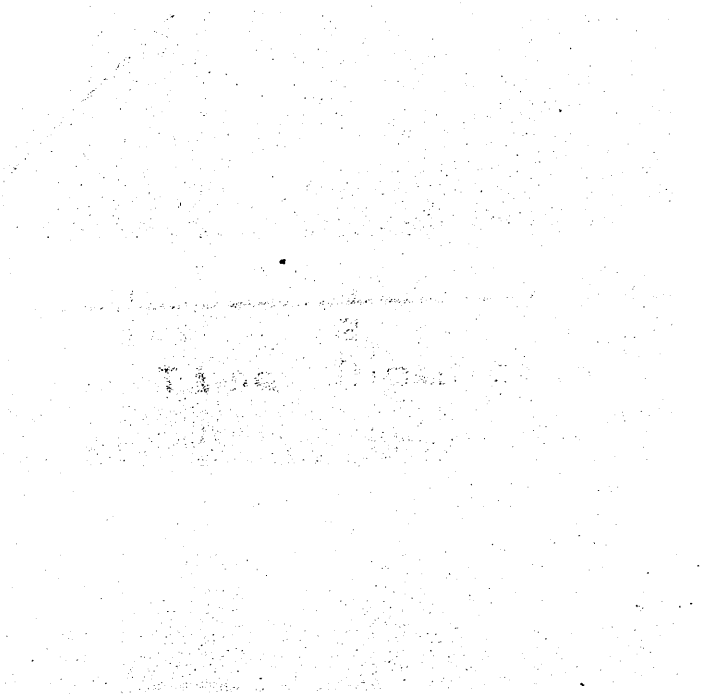

Swelling Hydrogel

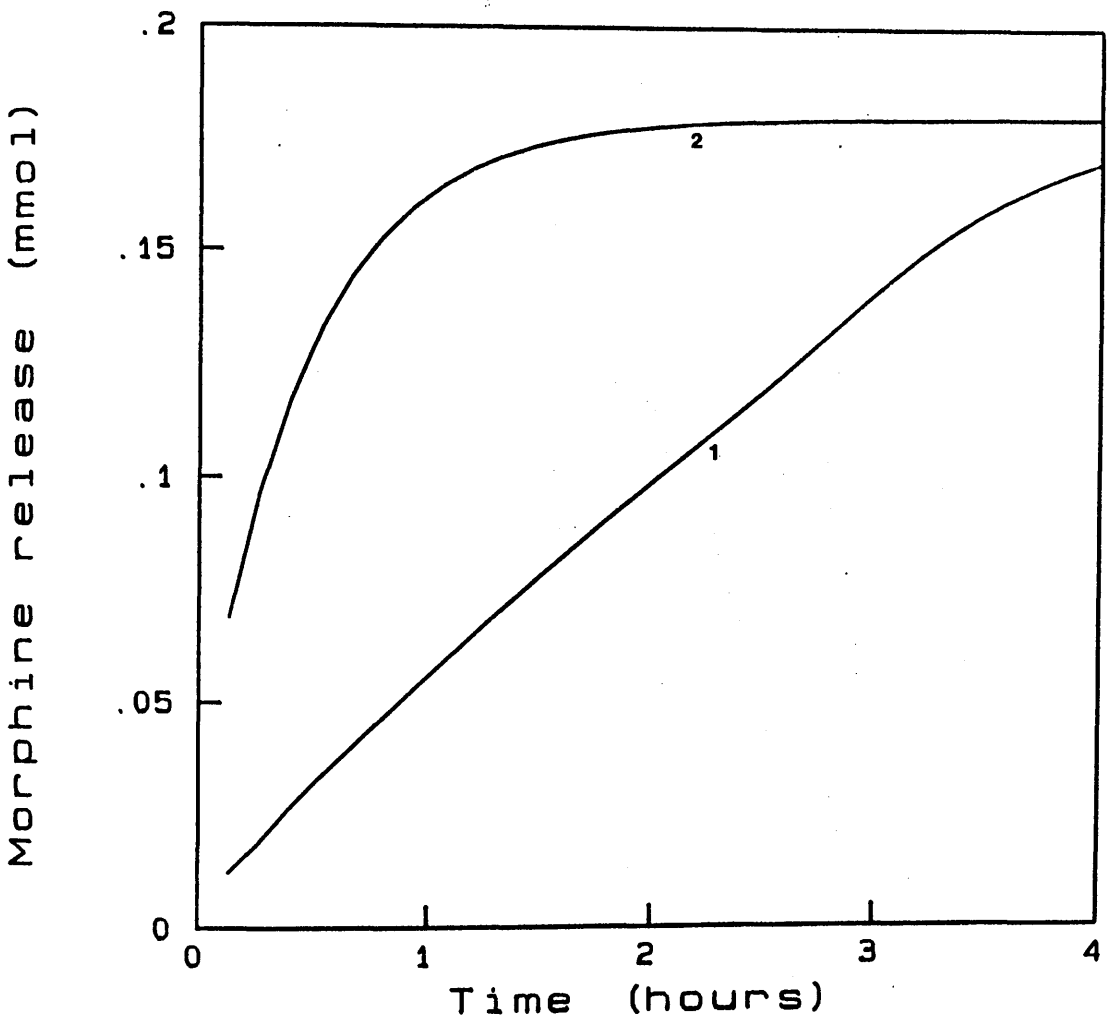

FIGURE 4.10.

Simulated rate of morphine release from hydrogel slab in mgs^{-1} plotted against time in hours. Penetrating front swelling mechanism, curve 1, compared to rate of release from fully swollen device, curve 2, (calculated using analytical solution for diffusion from faces of a fully swollen slab, eqn(2.16)). Original dimensions of hydrogel membrane, thickness, .28cm, area, $2.75cm^2$, swelling isotropically to double volume with length, .3528cm and area, $4.365cm^2$. Initial loading of morphine .18mmol, corresponding to concentration of .23M in dry slab (or .12M in fully swollen device).

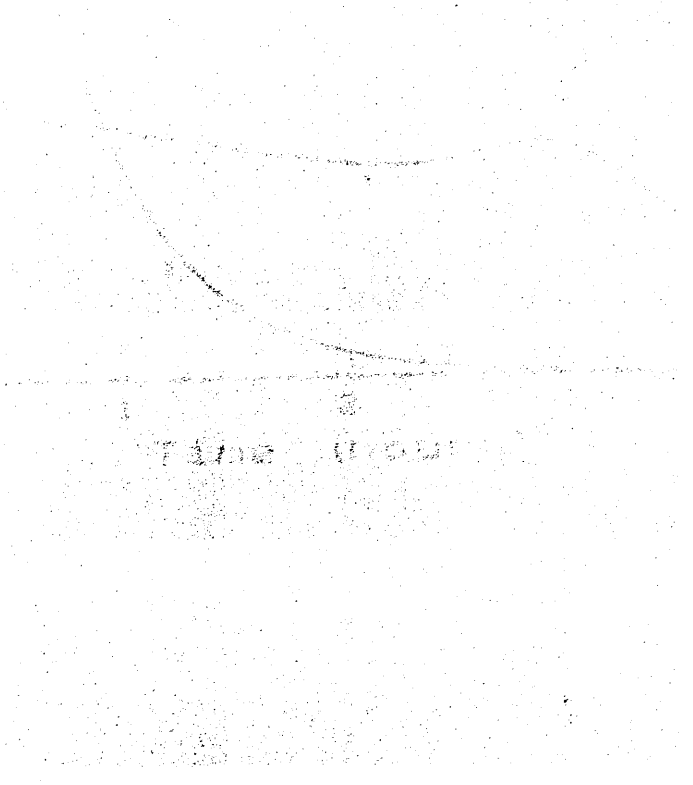

Morphine - Hydrogel

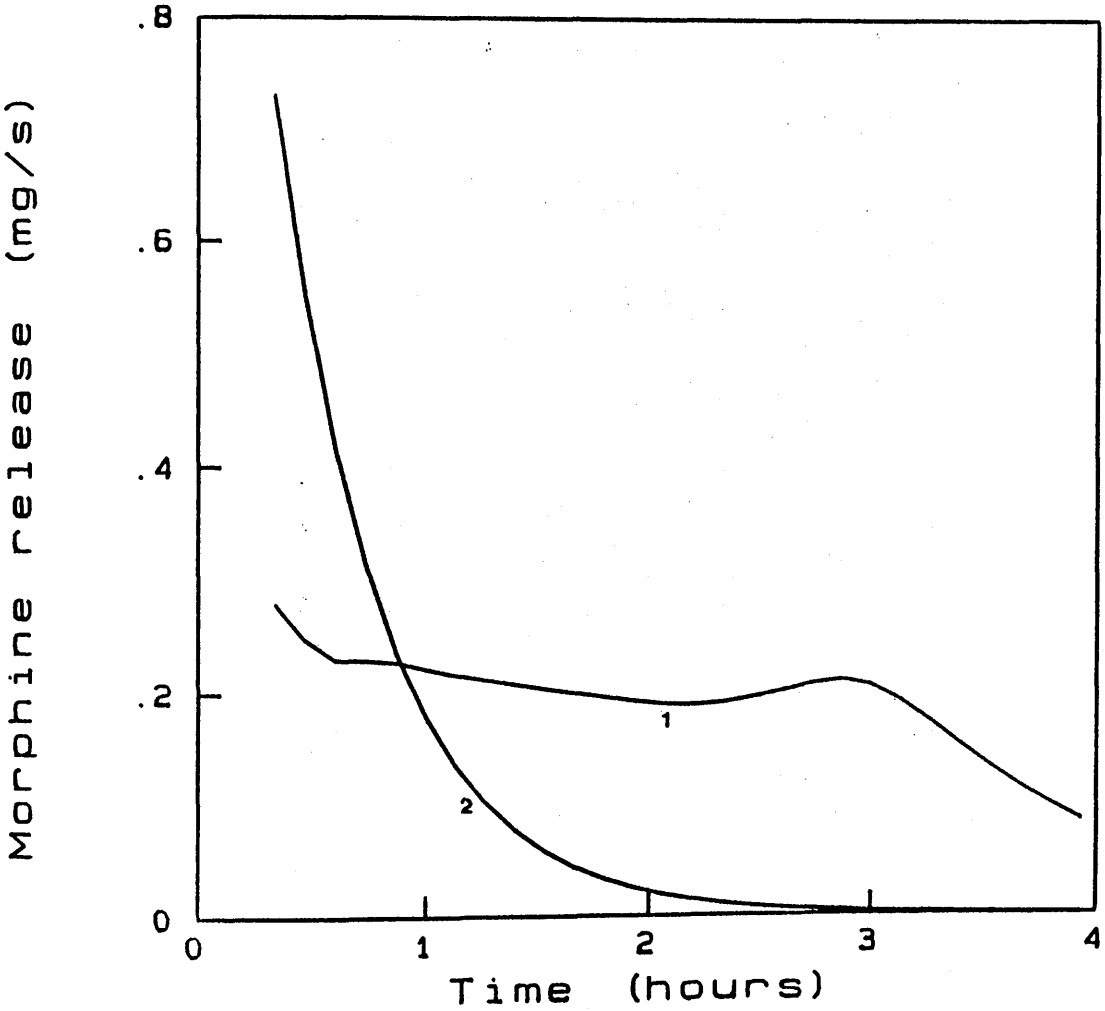

REFERENCES FOR CHAPTER FOUR

[1] N.B Graham and M.E. McNeill, Hydrogels for controlled drug delivery. Biomaterials, 5 (1984) 27-36.

[2] N.B Graham. University of Strathclyde. Glasgow. Private communication.

[3] M.E. McNeill. Ph.D. Thesis, University of Strathclyde, Glasgow, Scotland. (1987).

[4] M. Spiro. Imperial College London. Private communication.

[5] S. Prager. J. Chem. Phys. **33**, (1960) 122.

CHAPTER FIVE

DEVELOPMENT AND TESTING OF A BOND GRAPH FOR TWO DIMENSIONAL DIFFUSION.

5.1 INTRODUCTION

In Chapters 3 and 4 the applications of the C-C bond graph to non-linear diffusional problems of one dimensional symmetry were discussed. Many important systems may have less symmetrical geometries and diffusion in more than one dimension must be considered. In this chapter a bond graph model for two dimensional diffusion is developed, thus opening new possibilities for modelling diffusional phenomena. The ability to simulate two dimensional diffusion includes three dimensional geometries which have two dimensional diffusional symmetry. An obvious example is the release from the edges (only) of a plane sheet. The other interesting example given here is that of the diffusion from a limited cylinder, for which diffusional gradients normal to the radial plane can no longer be ignored. The limited cylinder may be particularly useful as approximating a pill shape, a favoured geometry for drug release devices.

All illustrative examples used here consider time invariant resistance and capacitance so that non-linearity and swelling are not discussed further. Instead the fundamental techniques required for simulating diffusion are presented and tested, with some more mathematically complex examples given in Chapter 6. Clearly however, the aspects of non-linearity described in Chapters 3 and 4 could be incorporated into the general framework for two and three dimensional diffusion, adopting the techniques used in the previous two chapters.

Complete mathematical solutions to diffusional problems

of a two dimensional nature are possible only for a limited number of very simple cases. To prove the validity of the network thermodynamic model developed here the initial applications were restricted to those for which such analytical solutions exist, and to which the network results might be compared quantitatively.

5.2 TWO DIMENSIONAL BOND GRAPH MODEL.

The design of a bond graph for the simulation of two dimensional diffusion was achieved using a similar philosophy to that used for 1D examples. No further thermodynamic theory is required. The power processing functions (R and C) are identical except that flow in a second dimension must be represented. Potentially the dissipative properties of a material under study may be different in each direction, therefore a distinction between two types of resistor are made (x and y, axial and radial). Since the extension of the diffusional problem into a second dimension is purely one of topology the modification to the theory is only in the layout and interconnection of the power processing elements already introduced for the simulation of chemical diffusion in earlier chapters.

5.2.1 Reticulation of systems in two dimensions.

For one dimensional diffusion the system is conceptually divided into n equal volume elements or lumps, Section 1.3.6. This division is performed along the axis of diffusion. The planar membrane is conceptually divided along it's length and the cylinder and sphere along their radii. A two dimensional model requires that the system be

reticulated along both axes of diffusion to produce a two dimensional array of volume elements. In each local equilibrium is assumed.

In this way an n_x X n_y model is a natural extension of an n lump model for one dimensional diffusion. x and y denote the diffusional directions with n_x being the degree of reticulation along the x axis, and n_y in the y-direction normal to x. There is no strict requirement for the resultant bond graph to be rectangular in shape as will be discussed below. For flow in a limited cylinder we adopt the convention that y is the radial axis of diffusion and x the axial. For plane sheet geometry both dimensions of flow are of course planar. Two dimensional simulation of diffusional flow with planar symmetry can consider only diffusion in the plane of the sheet and diffusion from the sheet edges. For diffusion from all faces of a sheet a bond graph model for three dimensional processes is required, (Chapter 7).

Reticulation of a plane produces a conceptual n_x X n_y array of lumps equal in volume and shape. For the limited cylinder model the radial division n_y is achieved by coring, (as for an infinite rod, Section 2.5). Axially the cored cylinder is divided into n_x equal slices along its length. This again produces a two dimensional array of equal volume elements except that these now have hollow cylindrical or cylindrical geometry (the volumes in the centre), fig(5.1) illustrates this reticulation diagramatically. The grid indicates the projection of the lump edges onto a plane, and the asterisks mark the

projected positions of the volume centres onto this plane also. Note that the volume centres are equally spaced along the planar axes of diffusion but, as described in Section 2.5, the radial distances between adjacent volumes in a cylinder model decrease progressively towards its outer surface.

5.2.2 Construction of bond graph.

As for the one dimensional model the resistance to flow between volume elements may be calculated over the distance between adjacent volume centres which share a common (lump) edge. The bond graph resistors lie on the edges of the lumps (grid lines in fig(5.1)). The lump capacitor which defines the (capacitative) ability of each volume element to store matter is placed at the lump volume centre, (shown as asterisks within grids on fig(5.1)).

Fig(5.2) shows a section of the constructed bond graph with the corresponding lump edge shown as a broken line, note that no attempt is made to show the true spacing of the capacitors and resistors in the model, this would be impractical. The true geometry of the modelled system is reflected in the resultant R and C values. The direction of power flow is arbitrary except that the conditions of power conservation must hold at the 0- and 1-junctions.

5.2.3 Labelling of R and C units and characteristic state-space equations.

To define a state-space equation, for a 2D system the capacitors and resistors of the bond graph must be labelled. Capacitors may be regarded as residing at the nodes of a grid and therefore each may be labelled by a

pair of x, y coordinates. These were assigned in these bond graphs by arbitrarily choosing the capacitor at the bottom left corner of the model as $C_{1,1}$. The resistors were classified into two types for the purpose of labelling and for subsequent calculation: R′, those lying on the edges parallel to the x direction and R′′, those lying on the edges parallel to the y axis, as is marked on fig(5.2). The x and y coordinate labels of the resistors are determined by their position relative to the grid defined by the capacitors.

R′ resistors are given the coordinates of the capacitors with the lowest y value to which they are adjacent. Similarly the R′′ units are given the x and y coordinates of the capacitors with the lowest x value to which they are adjacent. Fig(5.2) shows (perhaps more clearly) these assignments. This labelling scheme results in a concise state-space equation which easily translates into a computer program with a minimum of array storage.

The power bonds have been arbitrarily labelled from 1 to 17 on fig(5.2) for the purposes of deriving the characteristic state-space equation. The chosen numbering of the bonds illustrates that the two dimensional bond graph is equivalent to two R-C chains, at right angles, sharing a common capacitor $C_{x,y}$, (bond 5). The labelled portion of the chain parallel to the x axis with bonds numbered 1 to 9 is identical to the 1D bond graph of fig(1.5). So also is the chain parallel to the y axis, (bonds 10 to 17), but with a different numbering scheme.

The principle of common effort and power conservation

at the 0-junction connecting capacitor $C_{x,y}$ to the bond graph, allows the flow component of bond 5, f_5 to be related to the surrounding flows, eqn(5.1).

$$f_5 = \{f_4 - f_6\} + \{f_{13} - f_{14}\} \tag{5.1}$$

This is a similar first step as that taken to find the state-space equation for the 1D model, in fact we are not required to repeat such a detailed analysis of the bond graph. The flow difference between each brace of eqn(5.1) may may be expanded using the one dimensional state-space equation derived in Chapter 1, eqn(1.33), substituting for the appropriate labelling for each of the perpendicular R-C chains. By inspection the full state-space equation may be written, eqn(5.2).

$$\begin{aligned}\dot{q}_{x,y} = &-\left\{ \left(C^{-1}_{x,y}R''^{-1}_{x-1,y} + C^{-1}_{x,y}R''^{-1}_{x,y}\right)q_{x,y} \right.\\ &\left. + \left(\left(C^{-1}_{x-1,y}R''^{-1}_{x-1,y}\right)q_{x-1,y} + \left(C^{-1}_{x+1,y}R''^{-1}_{x,y}\right)q_{x+1,y}\right) \right\}\\ &-\left\{ \left(C^{-1}_{x,y}R'^{-1}_{x,y-1} + C^{-1}_{x,y}R'^{-1}_{x,y}\right)q_{x,y} \right.\\ &\left. + \left(\left(C^{-1}_{x,y-1}R'^{-1}_{x,y-1}\right)q_{x,y-1} + \left(C^{-1}_{x,y+1}R'^{-1}_{x,y}\right)q_{x,y+1}\right) \right\}\end{aligned} \tag{5.2}$$

The braces have been retained here for comparison with eqn(5.1).

This method of derivation is preferred since it allows the 'two dimensional' bond graph to be seen as a logical

extension of the one dimensional C-C model. As we might have expected the flows into a volume element are simply the sum of the net contributions in each direction. Note that the capacitive flow, $\dot{q}_{x,y}$ is a function of the capacitances (C), resistances (R) and charges (q) of it's nearest neighbours only. This greatly simplifies the techniques of simulation since each capacitor has a common state-space equation.

A two dimensional Universe is therefore represented by an N_x X N_y R-C plane of the type shown in fig(5.2). The thermodynamic system under study (equivalent to Clausius' World, Chater 1) may be defined by a closed edge of infinite resistors which isolate it allowing no exchanges of matter or energy with the rest of the Universe. This is a rather classical approach and we are in effect defining a closed system within the R-C plane. In this way all capacitors within the system have four surrounding neighbours. Up to three of these however may be beyond the 'diathermal' wall (on the outside of the infinite resistance edge), but the effect of an adjacent infinite resistor in eqn(5.2) is to render that term zero. The method therefore is self consistent with only C and q values within the thermodynamic system appearing in the set of state-space equations. The major advantage of this formulation is that the flow into each capacitor is given by a single equation (eqn(5.2)). Clearly any shape may be defined with no need for consideration of modified state-space equations for edge or corner positions in a bond graph. The result is an extremely modular approach to the computer simulation of the system dynamics.

Although eqn(5.2) may appear rather complex, it may be restated in the simplified form of eqn(1.36), with appropriate substitution for the two dimensional subscripts, eqn(5.3) except m_1 and m_2 have more terms.

$$\dot{q}_{x,y} = \frac{dq_{x,y}}{dt} = -m_1 q_{x,y} + m_2$$

$$m_1 = \left(C^{-1}_{x,y} R''^{-1}_{x-1,y} + C^{-1}_{x,y} R''^{-1}_{x,y}\right) + \left(C^{-1}_{x,y} R'^{-1}_{x,y-1} + C^{-1}_{x,y} R'^{-1}_{x,y}\right) \qquad (5.3)$$

$$m_2 = \left(C^{-1}_{x-1,y} R''^{-1}_{x-1,y}\right) q_{x-1,y} + \left(C^{-1}_{x+1,y} R''^{-1}_{x,y}\right) q_{x+1,y} + \left(C^{-1}_{x,y-1} R'^{-1}_{x,y-1}\right) q_{x,y-1} + \left(C^{-1}_{x,y+1} R'^{-1}_{x,y}\right) q_{x,y+1}$$

Regarding m_1 and m_2 as pseudo-constants (using the philosophy described in Chapter 1), allows the charge after time H, $q^H_{x,y}$ to be defined explicitly as an exponential function, eqn(5.4), as derived in Section 1.3.8.

$$q^H_{x,y} = \frac{m_2 - \exp(-Hm_1).(-m_1 q_{x,y} + m_2)}{m_1} \qquad (5.4)$$

At each step time H, eqn(5.4) may be applied to each capacitor of the bond graph in turn. It may be regarded as an integration operator which may be moved around the model until a completely updated two dimensional charge profile is obtained at time t+H. This cycle is repeated until the

simulation of the diffusion process is complete.

It is evident that, although the two dimensional bond graph is an extension of the one dimensional model the integration procedure remains essentially identical. With this highly modular approach the 2D bond graph is easily translated into an extremely efficient computer algorithm economical both in terms of memory usage and speed of numerical analysis.

5.3 SIMULATION OF DIFFUSION FROM THE EDGES OF A PLANE SHEET.

This two dimensional bond graph was initially applied to the problem of diffusion from the edges only of a plane sheet. The system was reticulated as described above and shown in fig(5.1). In this example the axes of diffusion are isotropic, as a result both types of resistor (R′ and R′′) may be formulated identically.

5.3.1 Bond graph model and R and C values.

Drawing complete sections of the two dimensional bond graph as in fig(5.2) is unnecessary for the purposes of illustrating the layout of the system. The R and C units projecting out of the plane in fig(5.2) need not be drawn since their presence in the bond graph may be implied by the 3-port 1- and 5-port 0-junctions respectively. Thus the representations of the resistive and capacitive functions in a reduced, pseudo-bond graph are as shown in fig(5.3). In this way the layout may be more easily presented on a page.

The release from the edges of a plane sheet may, due to the symmetry of the problem, be quantitatively analysed as

the diffusion from one of the four corners only. A 3x3 lump bond graph model of a corner is shown in fig(5.4). This is an isolated section of the N_x by N_y plane as described above but some further modifications to the representation in the pseudo-bond graph have been made for clarity. Firstly, 1-junctions connected to infinite resistances are not shown. Secondly 0-junctions with three adjacent infinite resistors are omitted and the capacitor element joined to it in the plane may be connected directly to the adjacent 1-junction with associated finite resistance. The representation of the bond graph model in fig(5.4) is favoured for emphasis of certain system features but the description of the system as an isolated piece of the R-C plane is preferred for the clear advantages of a universal treatment.

Since diffusion between volume elements of the collecting volume is not considered, each collecting capacitor is surrounded by three infinite resistances. These are shown explicitly in the pseudo-bond graph, (connected to the 1-junctions in fig(5.4)). For effectively infinite bath conditions the distribution of charge in these may be ignored. The effects of efficient stirring in a finite bath can be simulated by simply averaging the charges within the collecting capacitors after each integration.

Since the diffusion in both directions is isotropic and planar the assignment of an x and y direction is purely arbitrary. For the purposes of defining the R′ and R′′ coefficients the x axis is that parallel to the sheet′s

length and the y that parallel to the sheet's width. The sheet parameters required for modelling, as shown below, are length, l, width, w, depth, d, and diffusion and distribution coefficents, as usual D and α. Resistance to planar diffusion using a Fickian formulation was defined in Section 2.2, eqn(2.9), rewritten here as eqn(5.5).

$$R = \frac{\Delta x}{D\ A\ \alpha} \tag{5.5}$$

In which x is the path length of diffusion, (which may equally be replaced by y), D and α are the diffusion and distribution coefficients respectively and A is the area of flow.

For the resistors lying on the lump edges parallel to the y direction (R'', fig(5.2)) the resistance is that calculated for flow between adjacent volume centres in the x direction. Making the appropriate substitutions in eqn(5.5) leads to the definition of resistance as a function of the overall sheet dimensions and the imposed reticulation, eqn(5.6).

$$R''_{x,y} = \frac{2\ n_y\ l}{2\ n_x D\ w\ d\ \alpha} \tag{5.6}$$

In this equation n_x and n_y are the number of volume elements used to reticulate the length and width of the sheet corner. Therefore the area of flow is equal to the total planar area in the direction normal to the x axis, wd (width times depth), divided by the reticulation in this dimension, n_y. The path length between adjacent lumps is likewise equal to the total sheet length, l, divided by $2n_x$.

By similar argument R´ is given by eqn(5.7).

$$R'_{x,y} = \frac{2\, n_x\, w}{2\, n_y D\, l\, d\, \alpha} \qquad (5.7)$$

Resistors on the edges of the sheet, those adjacent to the terminal capacitors have half the resistances of those on edges between lumps.

As for any Fickian model, the capacitances are given by the lump volume, v scaled by the distribution coefficient, α. Thus we may restate eqn(2.12) here as eqn(5.8).

$$C_{x,y} = \alpha\, v \qquad (5.8)$$

Substituting values for the length, width and depth of each equal volume lump gives eqn(5.9).

$$C_{x,y} = \frac{\alpha\, l\, w\, d}{4 n_x n_y} \qquad (5.9)$$

5.3.2 Diffusion from initially uniform distribution in a square sheet into infinite bath.

The example of release from an initial uniform concentration in a square plane sheet from it´s edges into an infinite bath is the simplest two dimensional diffusion problem that may be considered. For such simple boundary and initial conditions the analytical solution for release is available as a product of the solutions to the one dimensional problem eqn(2.16), giving eqn(5.10) for a square of side 1, [1], [2].

$$\frac{q}{q_o} = 1 - \left(\sum_{k=0}^{\infty} \frac{8}{(2k+1)^2\pi^2} \exp\left(\frac{D(2k+1)^2\pi^2 t}{l^2} \right) \right)^2 \qquad (5.10)$$

Where q is here also the amount of diffusant released into the collecting bath at time t, as a fraction of the initial loading, q_o.

A bond graph model of a square sheet with length, width and depth 0.2cm and diffusion coefficient $2.0\text{x}10^{-7}\text{cm}^2\text{s}^{-1}$ was tested against this analytical solution by considering release from the edges into an infinite bath. The capacitance of the collecting volume were therefore taken as 1000cm^3 an arbitrary but effectively infinite value. For initial uniform conditions each lump of the model contains the same amount of material, defining $q_{x,y}$ at time zero. This is found from the initial total loading q_o, eqn(5.11).

$$q_{x,y} = \frac{q_o}{4\, n_x n_y} \qquad (5.11)$$

Where for a square $n_x = n_y$.

Three different degrees of reticulation were used 1x1, 3x3 and 30x30 lump models with a view to comparing the simulated release to that predicted by eqn(5.10). A step time of 0.1s was used. The integration cycle was repeated until approximately 0.6 fractional release was obtained. The total amount of diffusant in the collecting bath was found by summing the charges on the external capacitors (these are, as described above, the C units shown in

fig(5.4)). For a 30X30 lump model there are sixty of these capacitors and 960 capacitors in total, ($(n_x.n_y + n_x + n_y$, see fig(5.4).). The rapid integration procedures developed in the course of this research were invaluable for achieving the required precision in a reasonable computational time scale.

The results are shown graphically in fig(5.5), in which fractional release has been plotted against time in seconds. The solid curves labelled, 1, 2 and 3 are the simulated results for the 1X1, 3X3 and 30X30 lump models respectively. The imposed points are those obtained from the analytical solution and illustrate excellant agreement with the 30X30 lump model. This result may be inspected in table(5.1) where the data are tabulated for closer comparison. Less than 0.5% difference is shown between the analytical solution and the 30X30 lump bond graph model. This validates the network thermodynamic approach and the two dimensional bond graph model and opens the way for application to more complex systems.

To display concentration profiles in a 2D model we require a 3D representation of c,x,y at selected times. This was achieved by constructing a three dimensional projection, plotting the concentrations in each lump as height z, projected on the x,y plane at the position of the lump centre, (shown as asterisks on fig(5.1b)) and by joining up the points in both axes to form a grid. For greater than 20 lumps in each direction, x and y, the two dimensional concentration profiles can look rather smooth (see for example fig(6.10)). Once again this gives a true

representation of the data but the concentration at the edges of the lumps are not shown. Also, since the projected lump centres of the limited cylinder model do not define a regular grid there are some difficulties in illustrating this data on paper. For this reason it was necessary to curve-fit the data over two dimensions to obtain concentration data on a regular grid and by extrapolation, at the positions of the lump edges. Curve-fit algorithms however are not particularly well suited for sharp or 'jagged' profiles and in the discussion of the 'edge effect' in the next chapter planar analogues for the cylinder model have been used for illustration purposes. This is only a graphics problem though and there are commercially available software products for handling three dimensional data. For this plane sheet example, the concentration profile within the corner at 5000s has been first mirrored in both axes to obtain the concentration profile over the entire sheet and curve-fitted over the surface to show the condition of zero concentration at the sheet edges.

One method for illustration of three dimensional data is the isometric projection. Fig(5.6) shows the profile in this system at 5000s by this method. Concentration, as the z axis is plotted as a fraction of the initial loading, c/c_o. Therefore the maximum 'height' is 1. Another method used here is the contour map, fig(5.7). This is produced by drawing a series of 'iso-molar' lines (joining positions on grid of equal concentration) over a range of fractional concentration from 0 to 1. This method might not be as illustrative, but is in some cases more quantitatively

useful and indicates more clearly the directions of diffusional flows in the system (since these are normal to the iso-molar lines). In fig(5.7) the contours are plotted in 0.1 steps of fractional concentration, from zero (edge of the square) to 0.9 in the middle.

5.3.3 Irregular initial distributions of diffusant.

In bond graph modelling it is a trivial matter to deal with non-uniform initial distributions within the network. It is simply a matter of defining initial $q_{x,y}$ values. The importance of the bond graph's flexibility in this area is especially evident in the prediction of the subsequent behaviour of sharp or irregular initial distributions since these are problems for which mathematical analysis is not possible. This is potentially useful in drug release modelling since non-uniform initial distributions provide one means of controlling the release of bio-active materials from polymer devices discussed in Chapter 4. This will be examined in greater depth in the following chapter, Chapter 6.

It is useful to illustrate in this section the methods by which different initial dispersions of diffusant may be examined. For this purpose an example of diffusion within a plane sheet is considered from an initial condition of two highly concentrated spots. As a qualitative test completely arbitrary parameters were chosen and a relatively small bond graph model, 14X8 lumps was used to simulate the process. As this was a single phase problem there was no requirement for consideration of terminal capacitors or for distribution coefficient. The sheet dimensions were:

length, l, 1.4cm, width, w, 0.8cm. depth, d, 0.1cm and diffusion coefficient D, $2.8 \times 10^{-5} cm^2 sec^{-1}$. The initial concentration of the spots in the plane was .001M, fig(5.8a) shows the distribution of concentration at time zero by means of an isometric projection and since the data are presented 'raw', that is plotted at the lump centres with no smoothing or interpolation, this figure clearly shows the capacitors which contained an initial charge. Figs(5.8b) to (5.8e) present the simulated diffusion of material within this sheet as a series of concentration profiles at 20000 second intervals after time zero with fig(5.8f) giving the equilibrium position at t_∞. To emphasise the latter stages of diffusion the maximum concentration of diffusant at time 20000s, c_m (4.23×10^{-4}M) has been chosen as a maximum for figs(5.8b) to (5.8f) and concentration has been plotted as a fraction of this value (c/c_m). Therefore the original setting of .001M is 2.36 on this scale, fig(5.8a). Retaining this scale of fractional concentration the profiles from time 20000s to 80000s are shown as contour maps, figs(5.9a) to (5.9d). The contours are at fractional concentration steps (c/c_m) of 0.1 up to the maximum 1. In many ways the two methods of presenting these profiles complement each other.

The application of the bond graph model in this area will be examined in greater quantitative depth in Chapter 6.

5.4 SIMULATION OF DIFFUSION FROM A LIMITED CYLINDER.

A limited cylinder is a three dimensional object with two dimensional symmetry. Diffusion from a cylinder may

therefore be simulated using the two dimensional bond graph model with one axis of diffusion radial and the other planar, normal to the radial axis. The potential for application of this model may be greater than that for the plane sheet as the limited cylinder approximates a pill design.

The reticulation of the cylindrical system to produce a two dimensional array of lumps and the subsequent representation of these in the bond graph was described in Section 5.2. We now consider the layout of the bond graph required, within the N_x X N_y R-C plane and the formulation of the resistance and capacitance values.

5.4.1 Bond graph model and R and C values.

From symmetry only diffusion from one half of the cylinder's length need be quantitatively simulated. The bond required to model this system is an identical section of the R-C plane as to that for the plane sheet model, fig(5.4), all C units drawn are those of the collecting volume. The y direction on the page is the radial axis and the R' resistors, those lying on the lump edges parallel to the x axis, (fig (5.2)), account for Fickian resistance to radial diffusion. The R'' resistances are calculated for resistance to planar diffusion between adjacent lumps in the x direction.

The resistance to planar diffusion, eqn(5.5), may be defined for this model by substitution of the appropriate cylinder parameters, leading to eqn(5.12).

$$R''_{x,y} = \frac{n_y \, l}{2 \, n_x D \, \pi \, r_o^2 \, \alpha} \qquad (5.12)$$

In this expression the area of flow has been found from the area of the cylinder's section, normal to its radius (πr_o^2, where r_o is the cylinder radius), divided by the degree of reticulation along this axis (n_y). The path length of planar diffusion between adjacent lumps in the x direction is the cylinder length, l, divided by double the reticulation in this dimension, ($2n_x$ appears since only half of the cylinder's length need be modelled). This expression may be compared to that for the R'' resistances of the plane sheet model, eqn(5.6).

Radial diffusion was discussed in Section 2.5, the derived Fickian resistance may be rewritten here with appropriate consideration for two dimensional subscripts, eqn(5.13).

$$R''_{x,y} = \frac{\ln\left(\frac{r_{y+1}}{r_y}\right) n_x}{\pi \, D \, \alpha \, l} \qquad y=1, \, 2, \, \ldots n_y \qquad (5.13)$$

This is derived from eqn(2.32) substituting the length of cylinder section by the total cylinder length, l, divided by double the degree of reticulation in this axis ($2n_x$). r_y is the radial distance from the centre of the cylinder to the volume centre of lump x,y. These are found as before from eqn(2.35) with appropriate substitution of the subscripts, eqn(5.14).

$$r_y = \left(\frac{y - \frac{1}{2}}{n} \right)^{1/2} r_o \qquad (5.14)$$
$$y = 1, 2, \ldots n_y$$

Care must be taken, as for the one dimensional model in calculation of the resistance with $y = n_y$, these are on the edge of the outer cylinder lump in contact with the collecting bath and r_{y+1} is equal r_o in eqn(5.13).

The Fickian capacitance of a lump is given simply once more by its volume scaled by the distribution coefficient. The lump volume is found from the total volume of the cylinder divided by the degrees of reticulation in both directions. This leads to the formulation of the lump capacitance as eqn(5.15).

$$C_{x,y} = \frac{\alpha \pi r_o^2 l}{2 n_x n_y} \qquad (5.15)$$

5.4.2 Diffusion from initially uniform distribution into infinite volume.

The problem of release from an initially uniform concentration within a limited cylinder into an infinite bath allowed validation of this two dimensional bond graph model. The simple initial and boundary conditions of this system result in an analytical solution which is the product of the solutions of the corresponding one dimensional problem, [1], [2]. (As was release from the edges of a plane sheet). These are radial release from a cylinder section, eqn(2.37) (Section 2.5.1) and planar

release, normal to the radial axis, eqn(2.16). The resultant analytical solution is a rather lengthy expression.

$$\frac{q}{q_o} = 1 - \left\{ \left(\sum_{k=0}^{\infty} \frac{8}{(2k+1)^2\pi^2} \exp\left(\frac{D(2k+1)^2\pi^2 t}{l^2} \right) \right) \cdot \left(\sum_{k=1}^{\infty} \frac{4}{\beta_k^2} \exp\left(\frac{-D\,\beta_k^2\, t}{r_o^2} \right) \right) \right\} \qquad (5.16)$$

In which q/q_o is the fractional release at time t. l and r_o are the cylinder's length and radius respectively. β_k coefficients are the roots of the Bessel function eqn(2.38) as described in Section 2.5.1

The dimensions of the cylinder for this test system were: length, l, 0.2cm, radius, r_o, 0.1cm and diffusion coefficient $1.0\text{x}10^{-7}\text{cm}^2\text{s}^{-1}$. Similarly to the plane sheet example of Section 5.3.2 three degrees of reticulation have been tested, 1X1, 3X3 and 30X30 lump models. The simulations of the system dynamics, (after setting initial q values) were produced using a step time for integration of 0.1s. Fig(5.10) shows the simulated release into the infinite bath, found by summing the charges in the collecting capacitors at time t. The solid curves 1, 2, and 3 of fig(5.10), are the release kinetics simulated using the 1X1, 3X3 and 30X30 lump models respectively, the imposed points are the data for release predicted by

eqn(5.16). Excellant agreement was obtained between the analytical solution for release and that obtained by simulation using a 30X30 lump model. For more quantitative comparison these results are tabulated in table(5.2). Less than 0.5% difference was observed.

For comparison with the release from the edges of the plane sheet, the concentration profile within the limited cylinder model at time 5000s has been constructed. For this example also, the data obtained from simulation has been curve-fitted over the surface and presented as both an isometric projection, fig(5.11) and as a contour map, fig(5.12). As this profile was particularly smooth, performing the interpolation of the data in both directions was not difficult. To make the analogy with the plane sheet example complete the profile for the cylinder was mirrored over both axes.

The isometric projection of the smoothed data fig(5.11) is very similar to that for the plane sheet example, fig(5.6). The z axis or height has again been plotted as fractional concentration, c/c_o, with c_o the concentration in the sheet at time zero. The diffusional parameters of these two systems were chosen so that the release kinetics would be similar but on inspection of the concentration profiles within the sheet and cylinder, by means of the isometric projections, it is difficult to distinguish between the two. The contour map, fig(5.12), plotting the contours at the same levels of fractional concentration as for the plane sheet example in fig(5.7), (in steps of 0.1 up to 0.9), shows up the differences in diffusional

patterns rather more clearly. It is evident that there are advantages to both approaches for illustration. (The computer program for simulation of diffusion from a limited cylinder is included as an example in the Appendix, Section A.3.)

5.5 Conclusions.

This chapter has described the theoretical framework with which all two dimensional diffusion problems may be solved. The two dimensional bond graph has been developed as a logical extension to the highly successful one dimensional model and the examples provided have given validation of the techniques for simulating both diffusion in a plane and limited cylinder. This is an extremely important result as it shows that the two dimensional model may be exploited to the same extent as has been the one dimensional model, both in this thesis and previous work referenced in Chapter 2. In addition the logical development of this successfull model from the one dimensional bond graph suggests that a full three dimensional model may be developed which may then be used to model complex diffusional systems with total assymetry and geometric irregularity. This will be the topic of Chapter 7.

FIGURE 5.1.

Conceptual reticulation of systems to produce two dimensional array of volume elements or lumps.

a) Reticulation of limited cylinder to produce two dimensional array of equal volume lumps. Example 3X3 lump model with grid outlining positions of lump edges projected onto a plane. The asterisks mark the projected radial positions of the lump volume centres.

b) Plane sheet model, reticulated to give 3X3 array of equal volume lumps. The projected lump edges define a planar grid on which the positions of the lump volume centres have been marked by an asterisk.

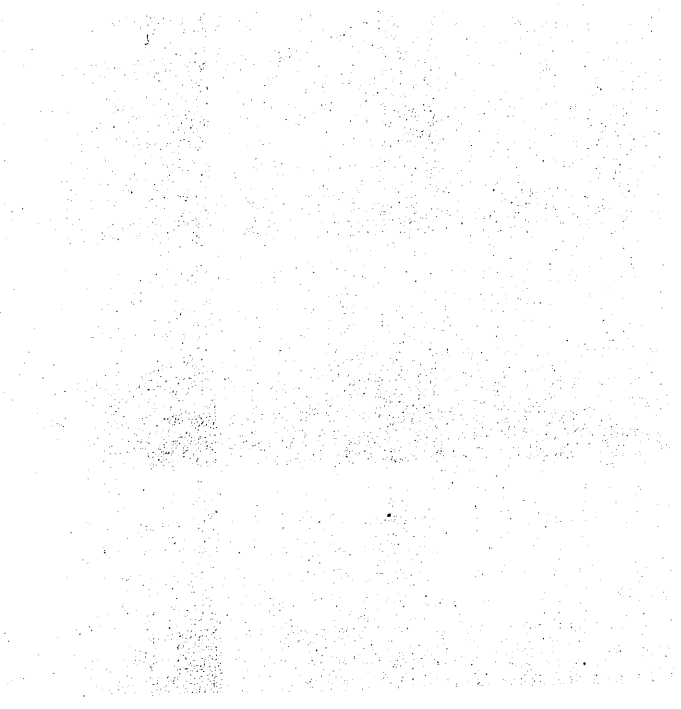

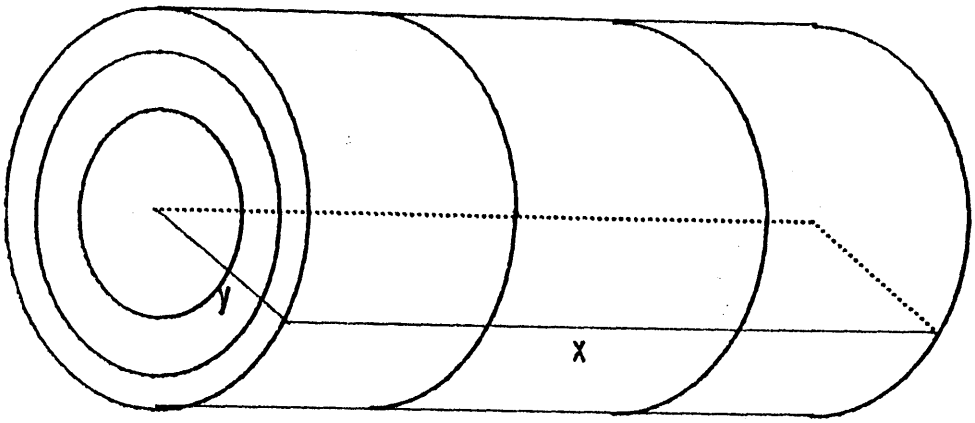

a)

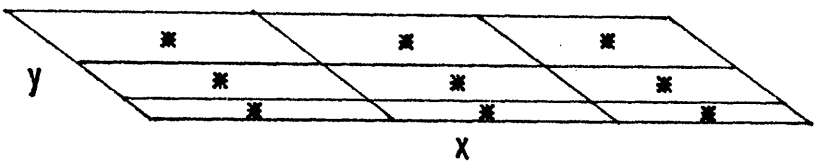

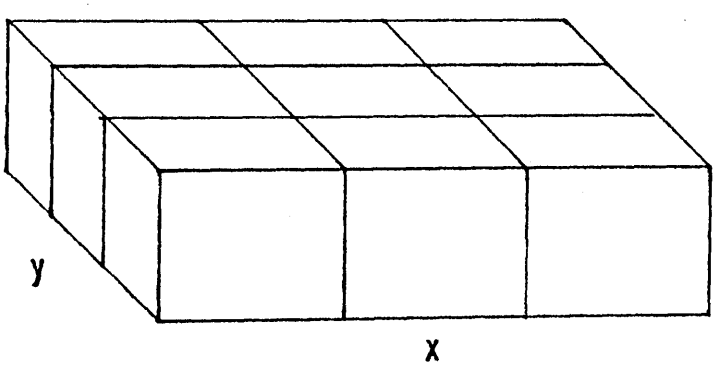

b)

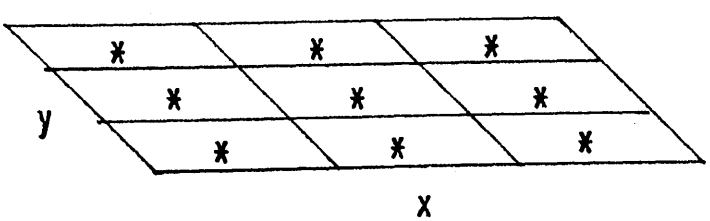

FIGURE 5.2.

Section of N_x X N_y R-C plane.

Full labelling of capacitors and resistors is shown and causality. Bonds are also arbitrarily numbered for formulation of characteristic state-space equation. Dashed rectangle outlines projected edge of lump, which may be correlated with centre lump edge in grids of fig(5.1).

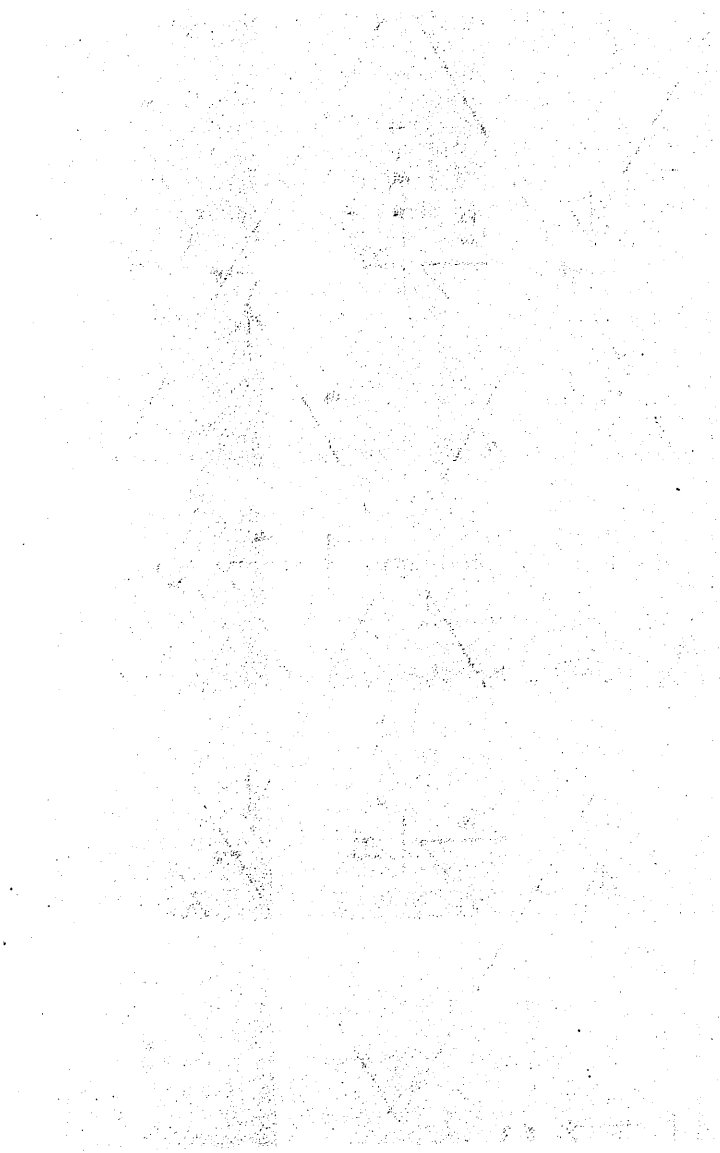

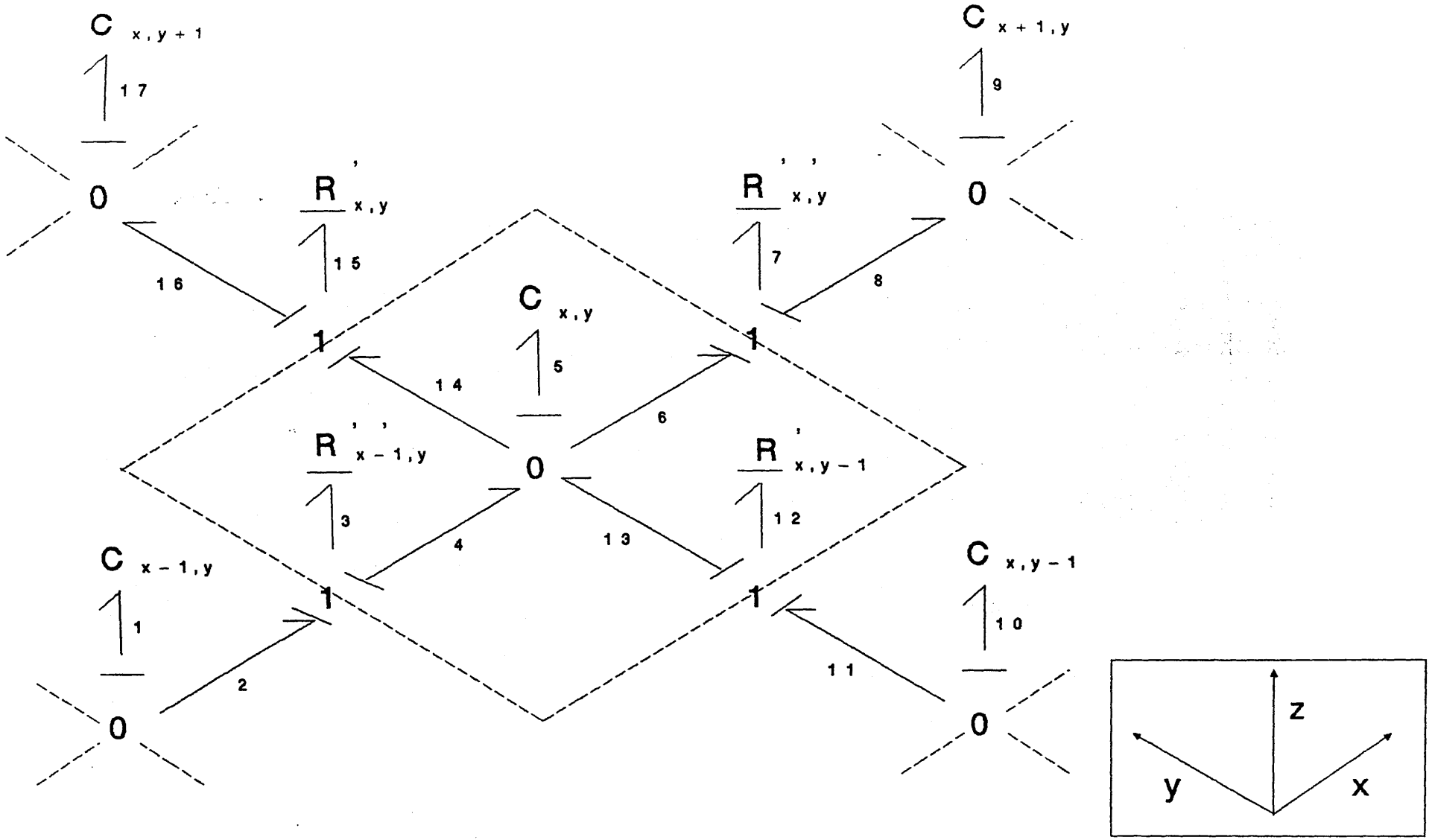
C x , y + 1
17
0
R' x , y
15
16
C x + 1 , y
9
R'' x , y
7
0
8
C x , y
5
1
14
6
1
R'' x − 1 , y
3
0
R' x , y − 1
12
4
13
C x − 1 , y
1
1
1
C x , y − 1
10
2
11
0
0
z
y
x

FIGURE 5.3.

Reduced forms of resistive and capacitive units in pseudo-bond graph representation of a section of the N_x X N_y R-C plane. Capacitors at 0-junctions and resistors at 1-junctions are not shown explicitly, rather their presence is implied by the junctions alone, as suggested in this figure.

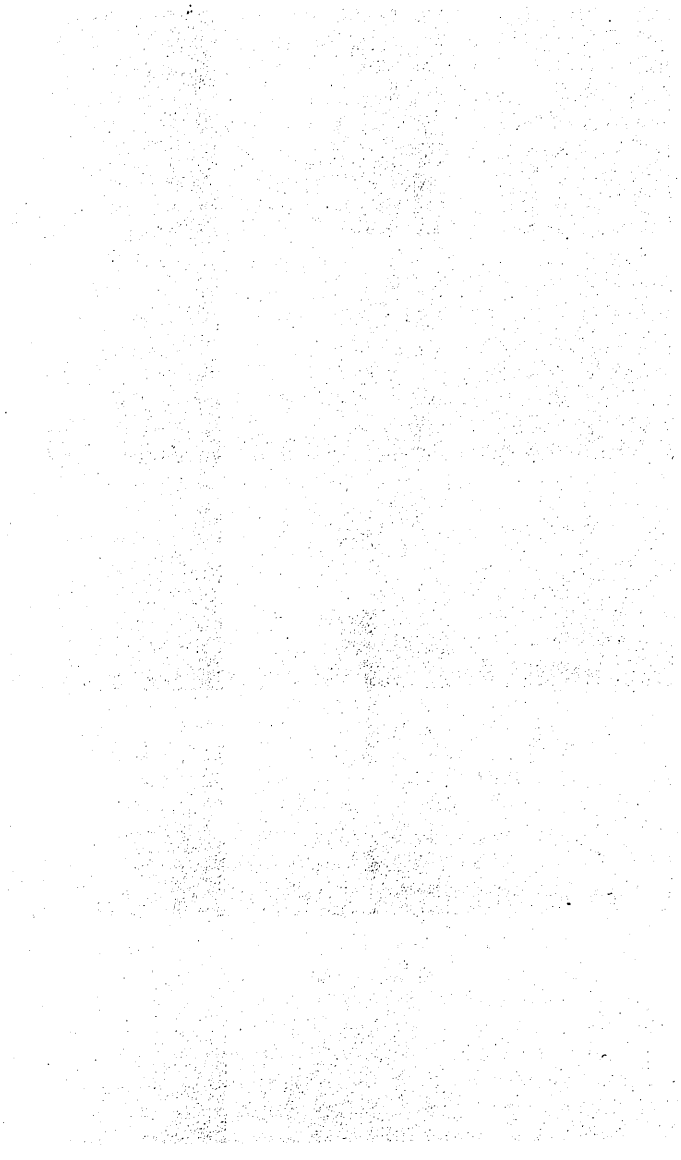

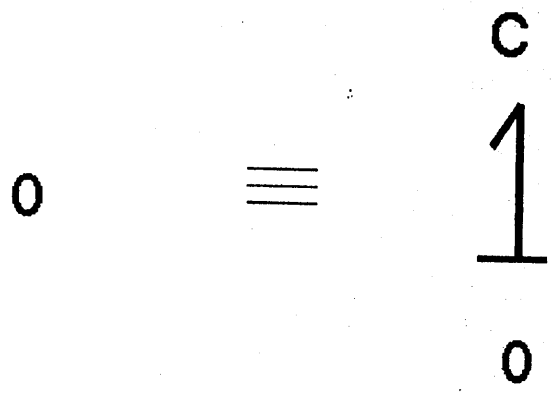
C
0
0

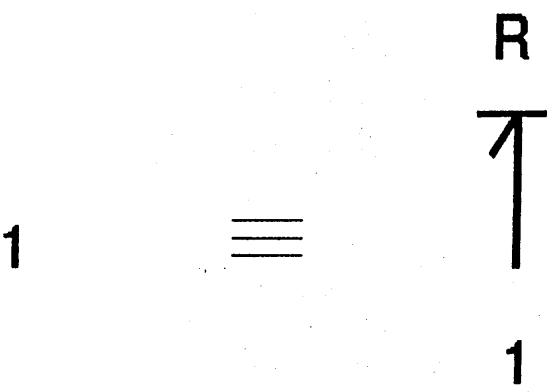
R
1
1

FIGURE 5.4.

Pseudo-bond graph for model of plane sheet corner. 3X3 lump model of sheet is shown with six terminal collecting capacitors. This is reduced representation of N_x X N_y R-C plane using the implied resistance and capacitance units as indicated in fig(5.3). In addition capacitors of collecting volume which are surrounded by three infinite resistances are shown connected directly to adjacent 1-junctions. (0-junctions with only two non-zero flows are mathematically redundant.)

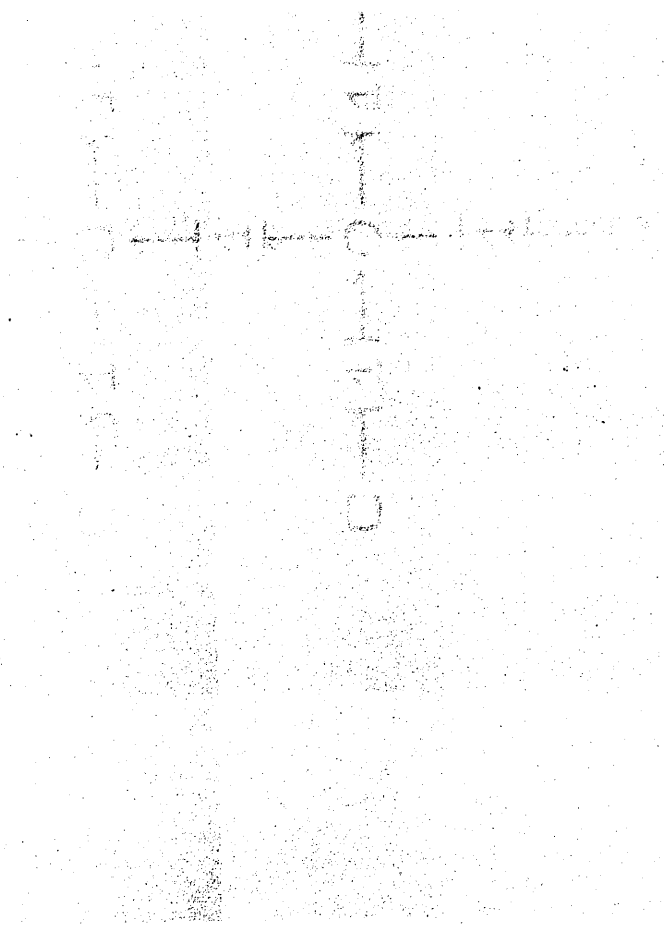

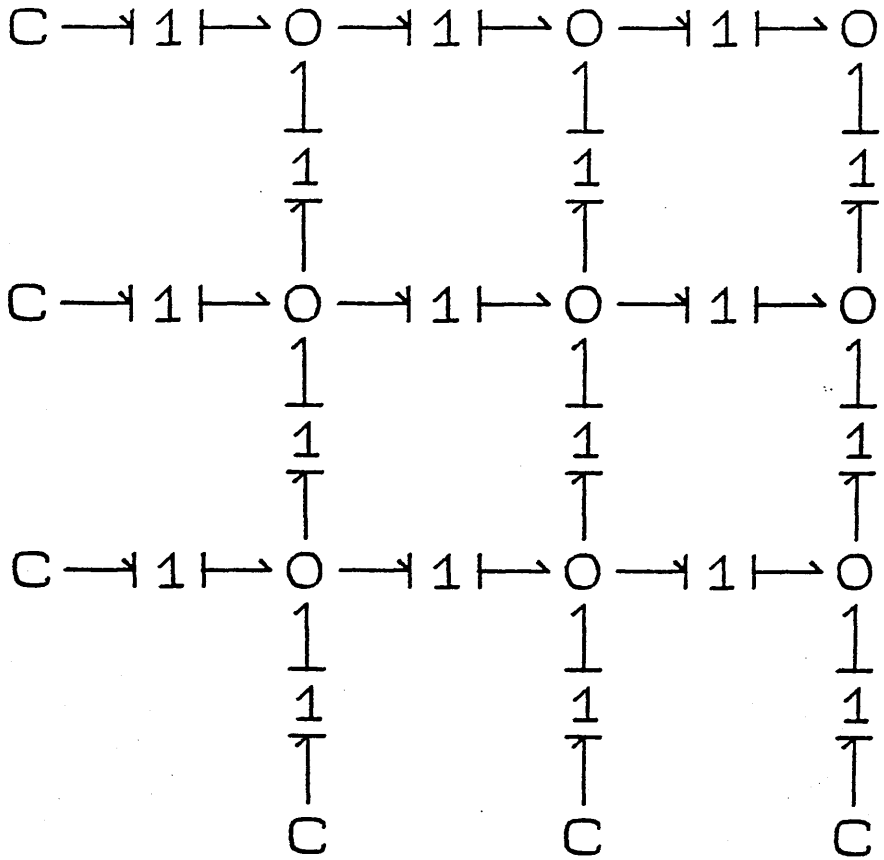
C
1
O
1
O
1
O
1
1
1
C
1
O
1
O
1
O
1
1
1
C
1
O
1
O
1
O
1
1
1
C
C
C

FIGURE 5.5.

Simulated efflux from edges of a square plane sheet. Fractional release, q/q_o, plotted versus time in seconds. Three degrees of reticulation of square corner are compared to the analytical solution for release with infinite bath conditions, eqn(5.10) [1], [2]. Square sheet parameters were: length of square side, l 0.2cm, depth, d 0.2cm and diffusion coefficient, D $2.0 \times 10^{-7} cm^2 s^{-1}$. A step time of H, 0.1s was used.

Curve 1, 1X1 lump model.

Curve 2, 3X3 lump model.

Curve 3, 30X30 lump model.

Points, analytical solution.

Less than 0.5% disparity is shown between 30X30 bond graph model and the mathematical prediction for release. Data presented in table(5.1).

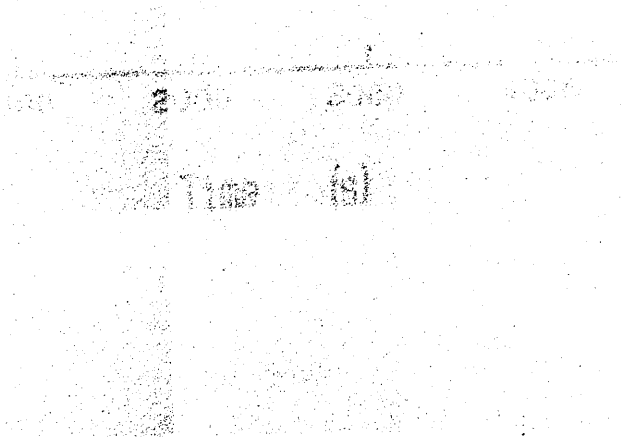

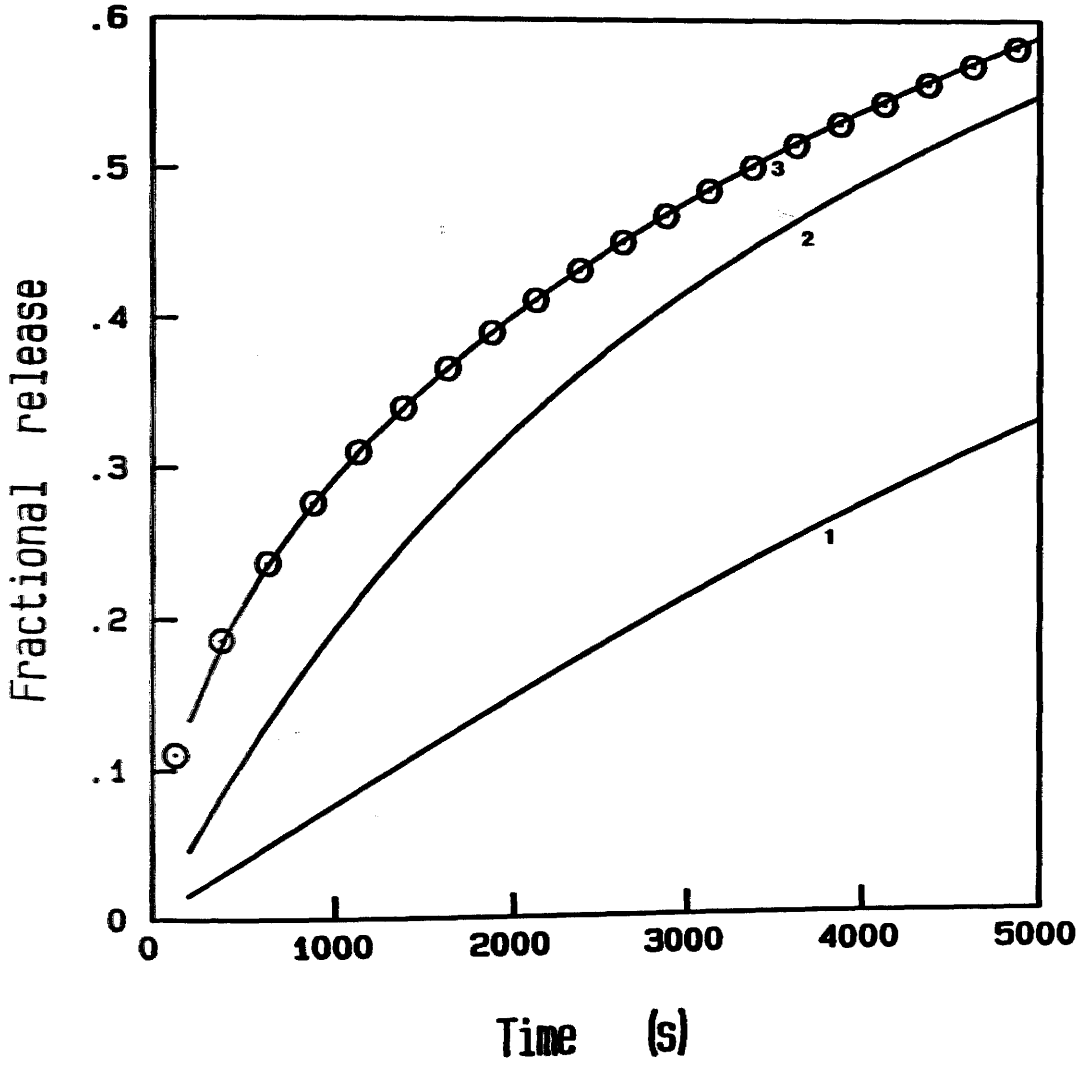
.6
.5
.4
.3
.2
.1
0
Fractional release
0
1000
2000
3000
4000
5000
Time (s)
1
2
3

FIGURE 5.6.

Isometric projection of smoothed concentration profile within square plane sheet at 5000s.

Complete profile constructed from simulation of release from sheet corner by symmetry. Fractional concentration, c/c_o (as height), obtained by two dimensional interpolation of average concentrations positioned at the lump volume centres within 30X30 lump model.

Parameters of square plane sheet were length of side and depth 0.2cm with diffusion coefficient $2.0 \times 10^{-7} cm^2 s^{-1}$.

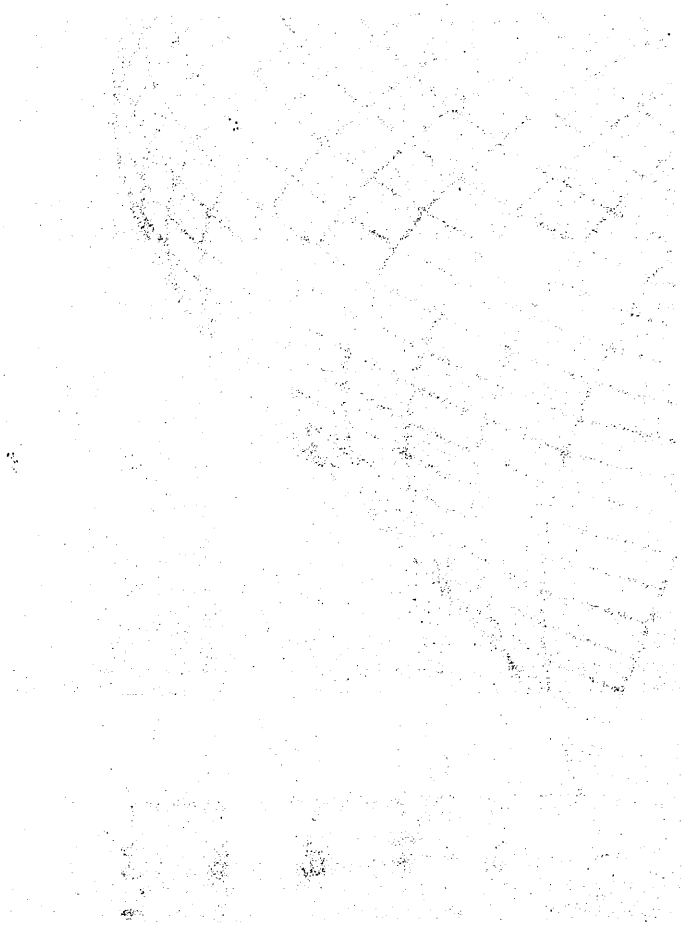

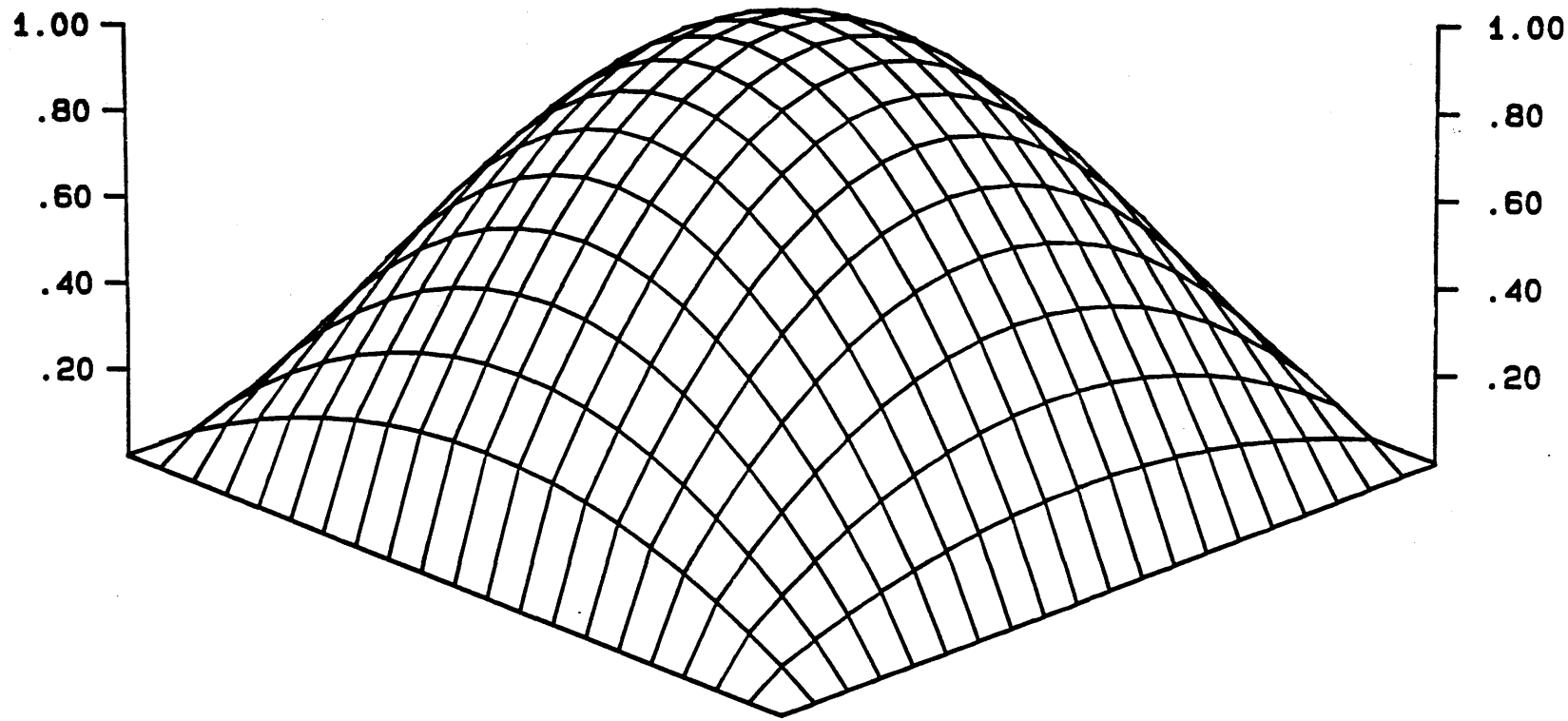
1.00
.80
.60
.40
.20
1.00
.80
.60
.40
.20

FIGURE 5.7.

Contour map representation of concentration profile within square plane sheet at 5000s.

Contours constructed on basis of fractional concentration data positioned at lump centres within a 30X30 lump model of the sheet. Contour lines drawn at 0.1 increments in fractional concentration (c/c_o) up to 0.9, with edge at zero.

Parameters of square plane sheet were length of side and depth 0.2cm with diffusion coefficient $2.0 \times 10^{-7} cm^2 s^{-1}$.

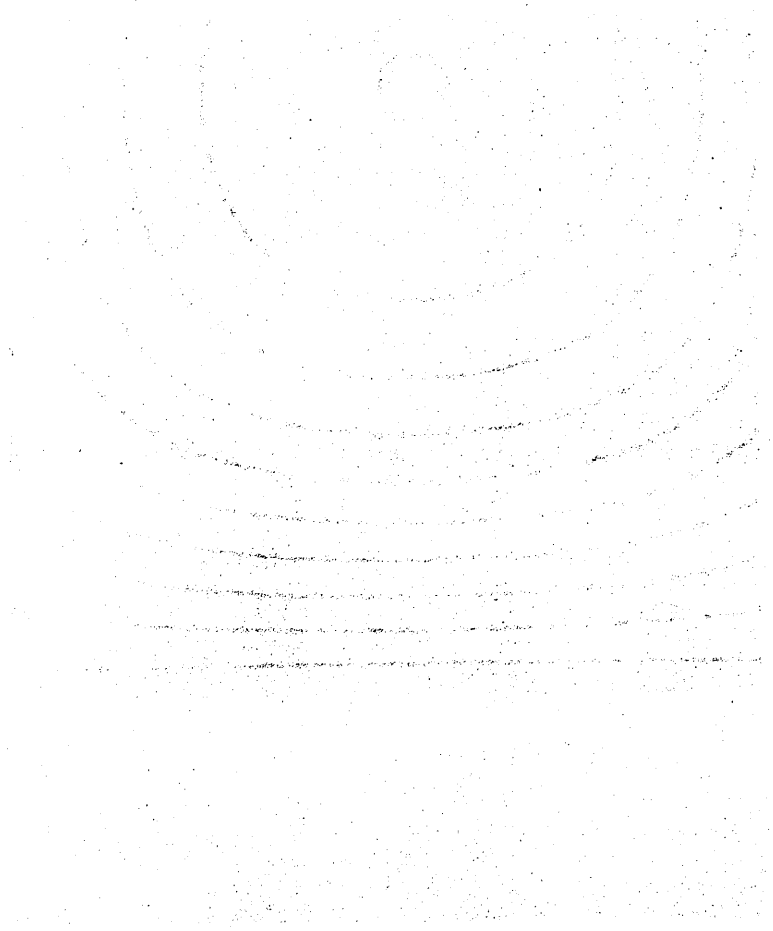

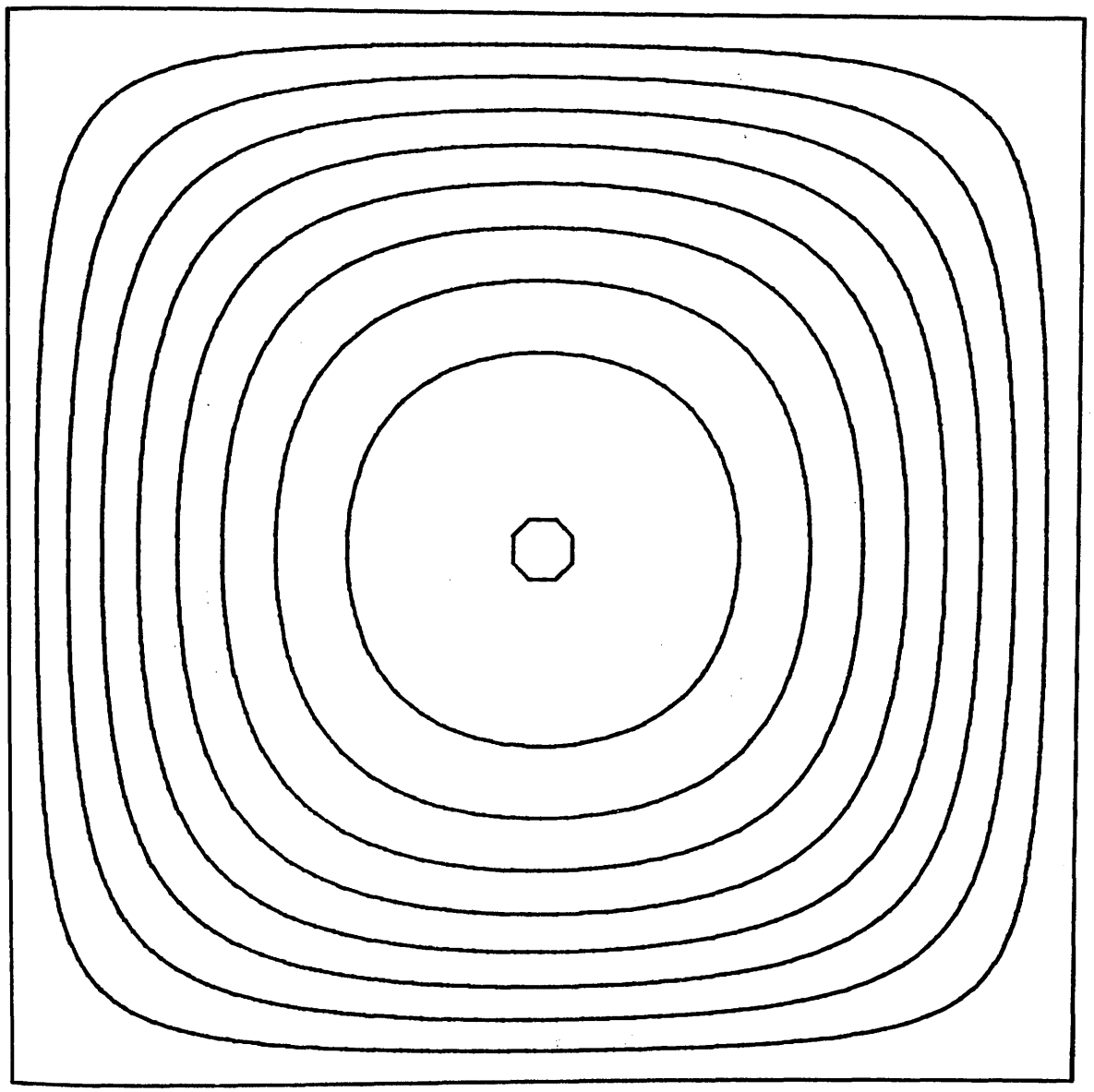

FIGURE 5.8.

Successive isometric projections of two dimensional concentration data within 14X8 lump plane sheet model.

Fractional concentration c/c_m (c_m, maximum concentration within sheet at time 20000 seconds), within each lump plotted as height, at positions of lump centres and joined to form grid. Parameters of sheet were: length, 1.4 cm, width, 0.8 cm, depth .1 cm with diffusion coefficient $2.8 \times 10^{-5} cm^2 s^{-1}$.

Figs(5.8a) to (5.8e), profiles showing initial condition and then evolution of system in 20000s intervals. Fig(5.8f), equilibrium position, t_∞.

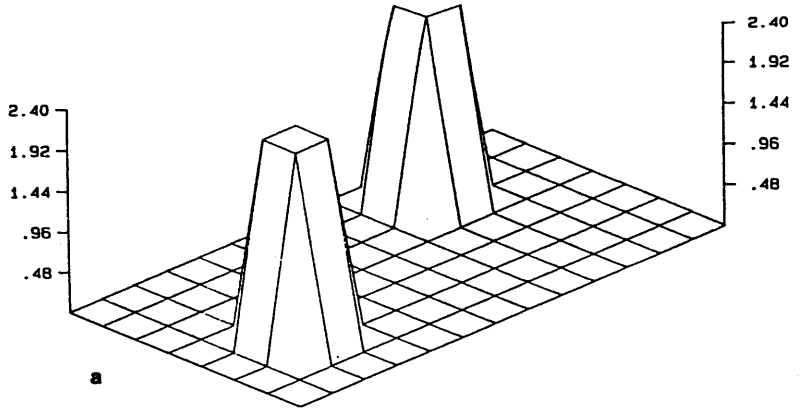
2.40
1.92
1.44
.96
.48
2.40
1.92
1.44
.96
.48
a

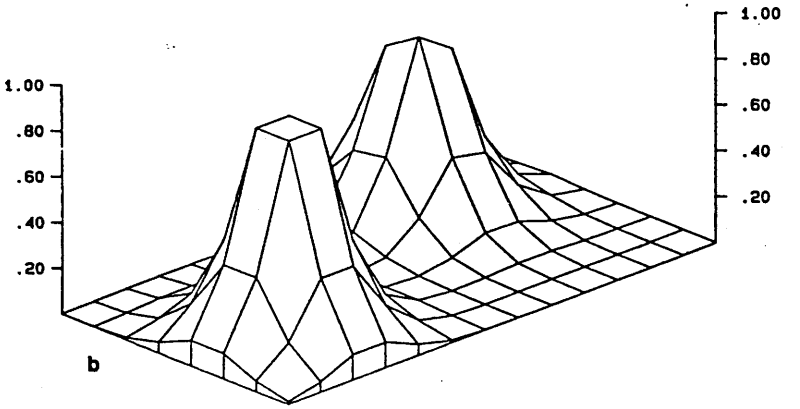
1.00
.80
.60
.40
.20
1.00
.80
.60
.40
.20
b

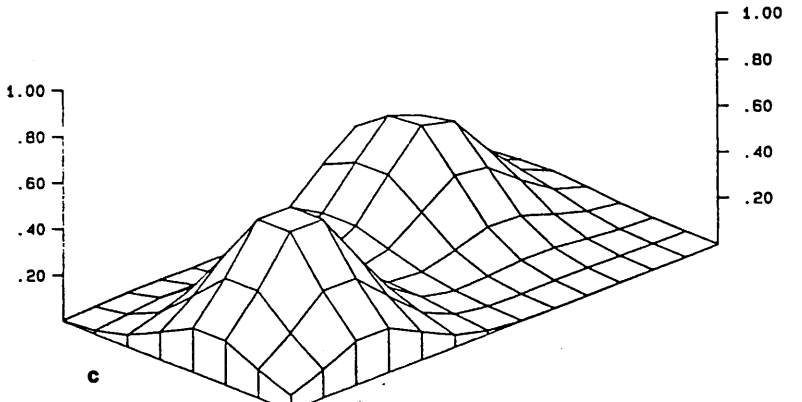
1.00
.80
.60
.40
.20
1.00
.80
.60
.40
.20
c

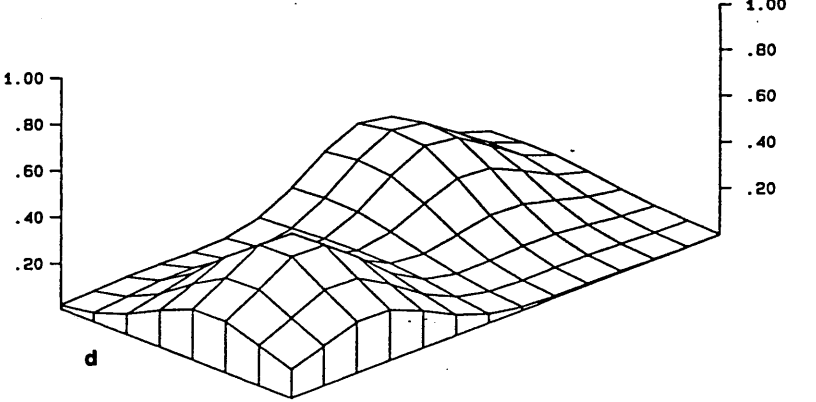
1.00
.80
.60
.40
.20
1.00
.80
.60
.40
.20
d

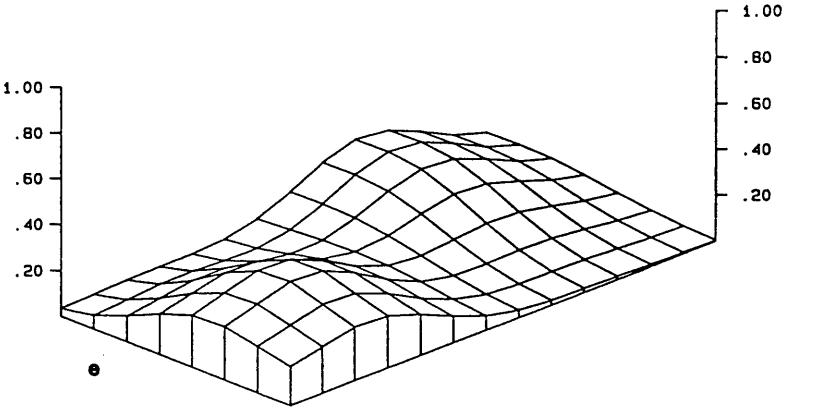
1.00
.80
.60
.40
.20
1.00
.80
.60
.40
.20
e

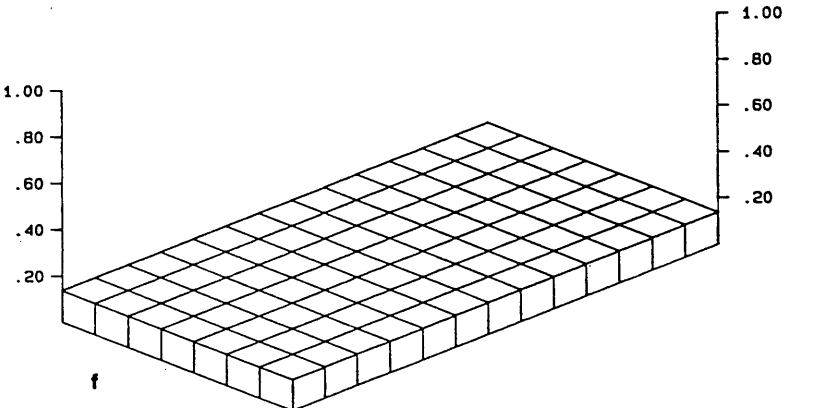
1.00
.80
.60
.40
.20
1.00
.80
.60
.40
.20
f

FIGURE 5.9.

Successive contour maps of concentration profiles within plane sheet.

Data are average fractional concentration (c/c_o) plotted at each volume centre of a 14X8 lump model. Contour lines are drawn in fig(5.9a) at fractional concentration levels of .067 and these levels are retained through to fig(5.9d). Contour maps shown at 20000s intervals corresponding to profiles shown in figs(5.8) to (5.8 e) and clearly illustrate also the flattening of the initial peaks or concentrated spots.

Parameters of sheet were: length, 1.4 cm, width, 0.8 cm, depth .1 cm and diffusion coefficient $2.8 \times 10^{-5} cm^2 s^{-1}$.

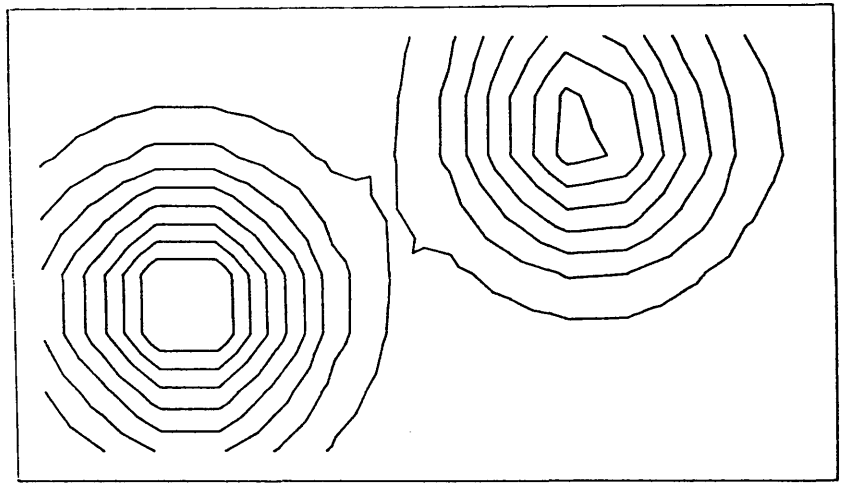

a

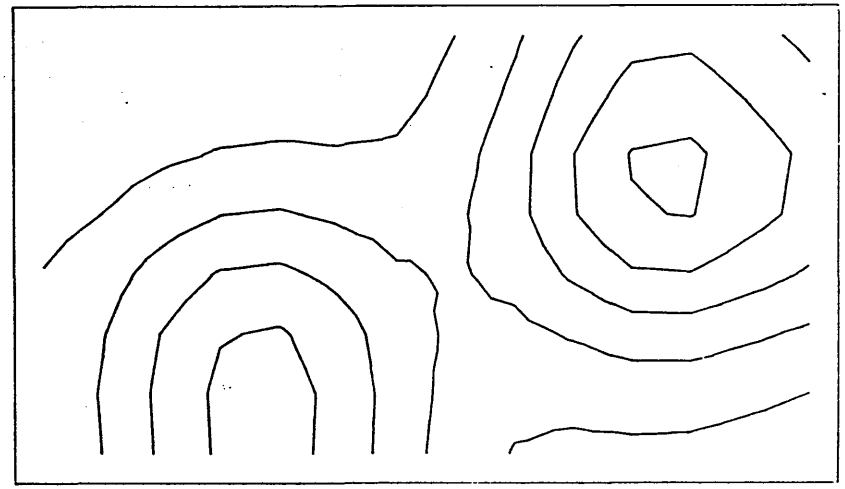

c

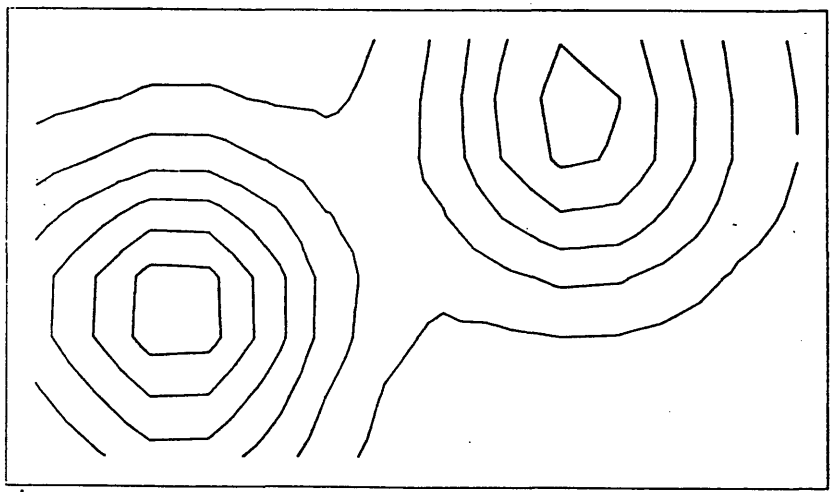

b

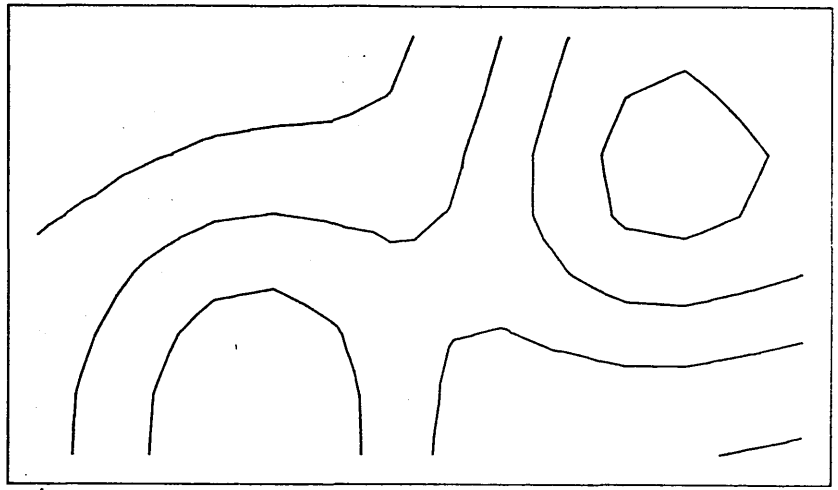

d

FIGURE 5.10.

Simulated efflux from a limited cylinder.

Fractional release, q/q_o, plotted versus time in seconds. Results obtained using three degrees of reticulation of half cylinder length are shown compared to the points calculated from analytical solution for release from this system into an infinite bath, eqn(5.16), [1], [2]. Cylinder parameters were length, 0.2cm, radius 0.1cm and diffusion coefficient $1.0x10^{-7}cm^2s^{-1}$. A step time of H, 0.1s was used to produce the bond graph simulations.

Curve 1, 1X1 lump model.

Curve 2, 3X3 lump model.

Curve 3, 30X30 lump model.

Points, analytical solution.

Less than 0.5% disparity is shown between 30X30 bond graph model and the mathematical prediction for release. Data presented in table(5.2).

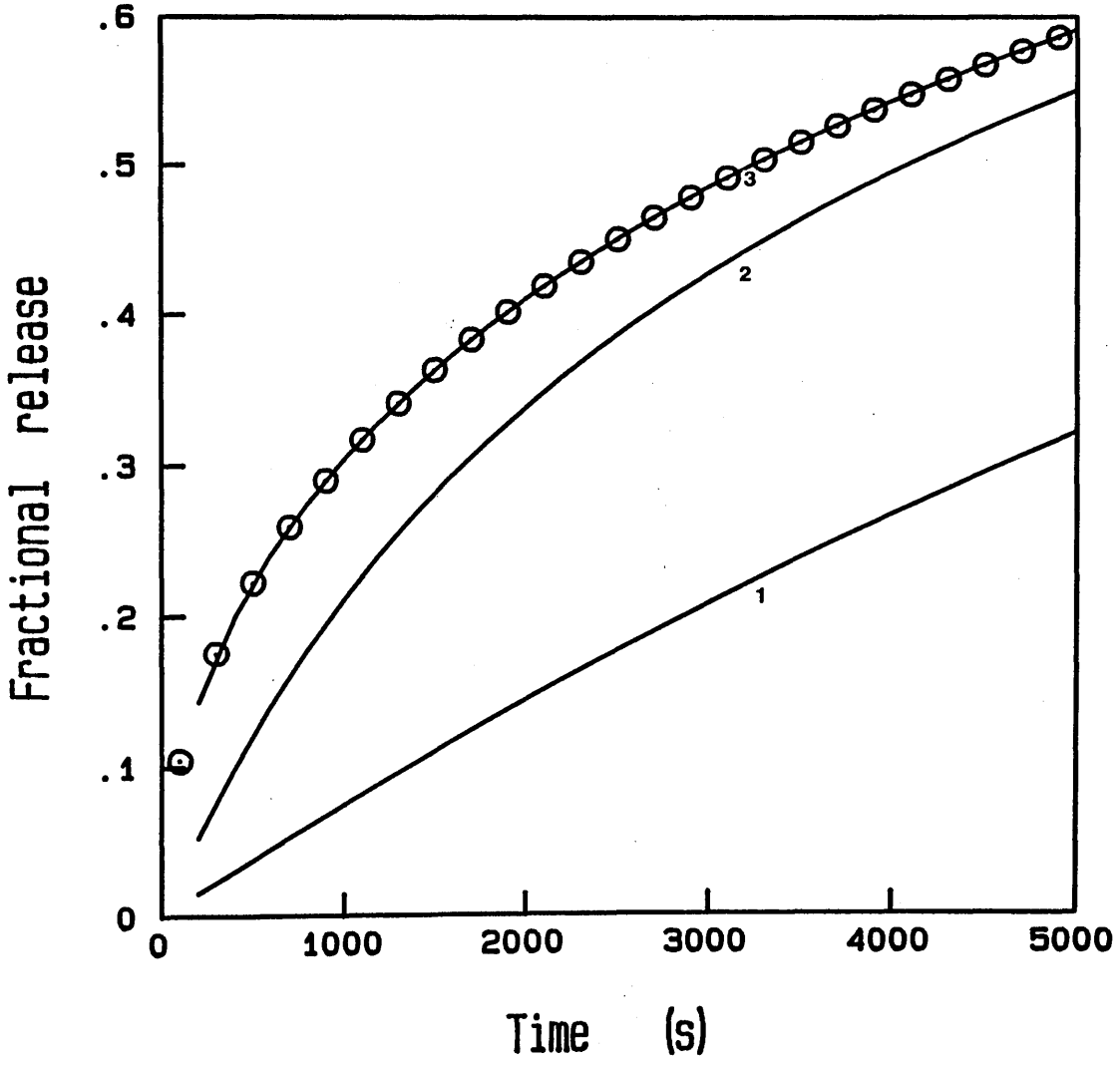
Fractional release
.6
.5
.4
.3
.2
.1
0
0
1000
2000
3000
4000
5000
Time (s)
1
2
3

FIGURE 5.11.

Isometric projection of smoothed concentration profile within limited cylinder model at 5000s.

Profile constructed from simulated fractional concentrations (c/c_o, height) in each lump positioned at the projected coordinates of the lump centres, (see fig(5.1a)). Data of 30X30 lump model was mirrored in both axes and interpolated to lie on regular grid.

Parameters of cylinder were length 0.2cm, radius 0.1cm and diffusion coefficient $1.0 \times 10^{-7} cm^2 s^{-1}$.

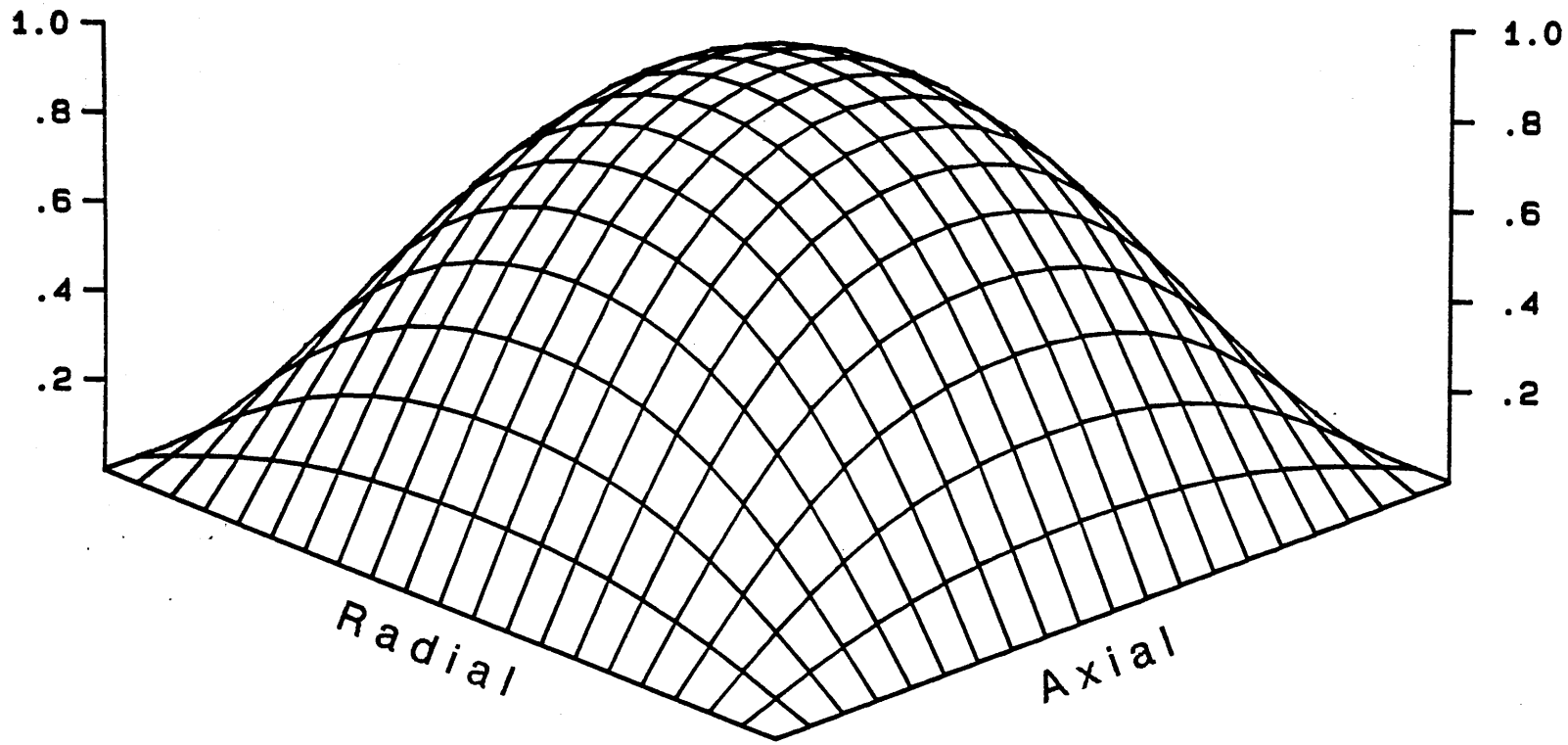
1.0
.8
.6
.4
.2
1.0
.8
.6
.4
.2
Radial
Axial

FIGURE 5.12.

Contour map representation of concentration profile within limited cylinder model at 5000s.

Contour lines drawn at fractional concentrations intervals (c/c_o) of 0.1 up to 0.9. Based on positioning of concentration data at lump centres (see fig(5.1a)) with 30X30 lump model.

Cylinder parameters were length 0.2 cm, radius 0.1 cm and diffusion coefficient $1.0 \times 10^{-7} cm^2 s^{-1}$.

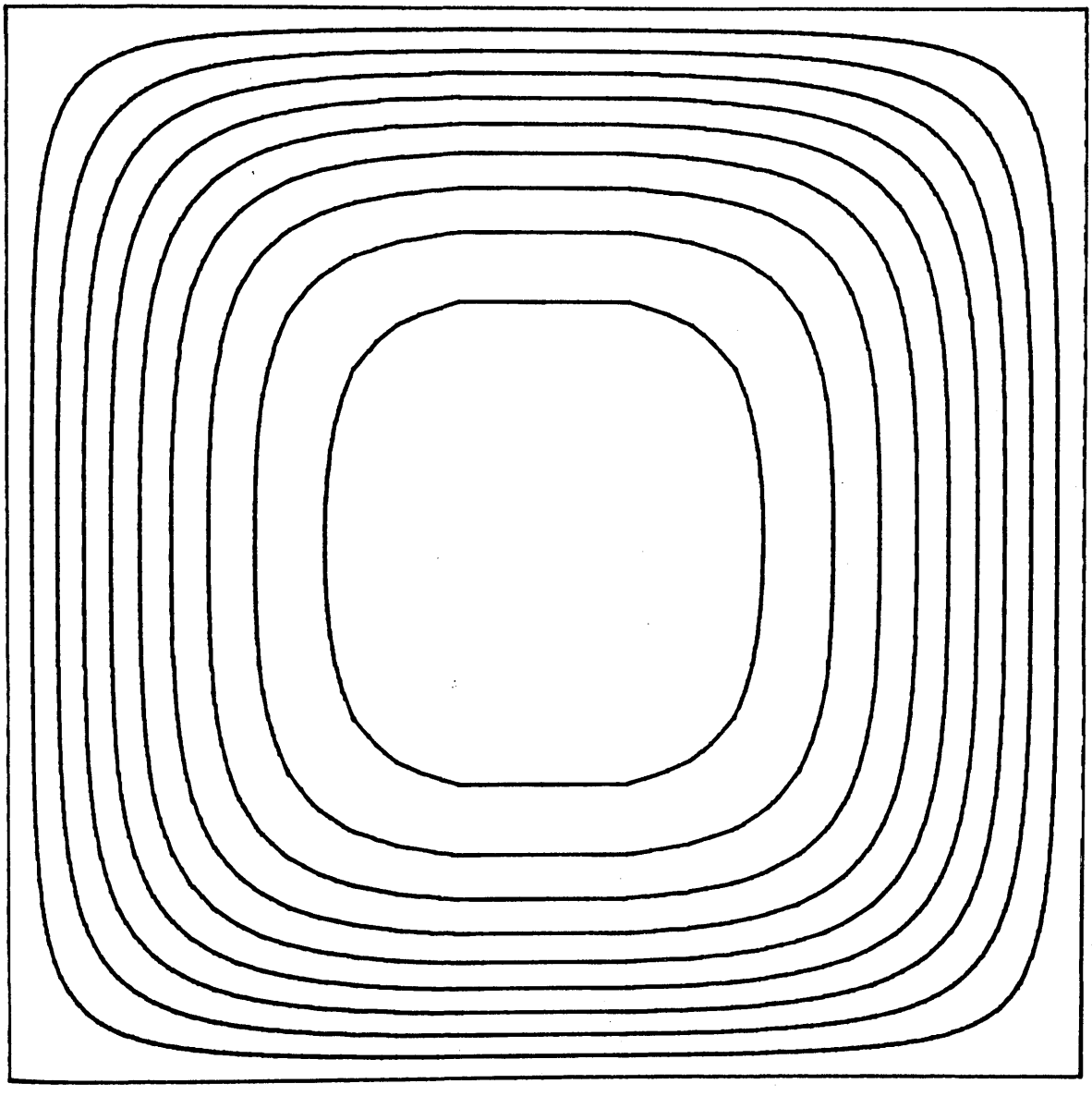
Radial
Axial

TABLE 5.1

Comparison of bond graph results for release from edges of square plane sheet with analytical solution, eqn(5.10), [1], [2]. (Data for fig(5.5).)

Fractional release (q/q_o) at time (s) is tabulated for 30X30 lump model of square corner. Sheet parameters were, length 0.2cm, depth, 0.2cm and diffusion coefficient, $2.0x10^{-7}cm^2s^{-1}$.

Time (s)	Analyical Solution	Computer Simulation
125	0.115	0.108
250	0.178	0.156
375	0.193	0.190
500	0.221	0.218
625	0.244	0.242
750	0.265	0.264
875	0.284	0.283
1000	0.302	0.300
1125	0.318	0.317
1250	0.333	0.332
1375	0.347	0.346
1500	0.360	0.359
1625	0.372	0.372
1750	0.384	0.384
1875	0.396	0.395
2000	0.406	0.406
2125	0.417	0.416
2250	0.427	0.426
2375	0.436	0.436
2500	0.445	0.445
2625	0.454	0.454
2750	0.463	0.463
2875	0.471	0.471
3000	0.479	0.479
3250	0.495	0.495
3500	0.509	0.509
3750	0.523	0.523
4000	0.536	0.536
4250	0.548	0.548
4500	0.560	0.560
5000	0.582	0.582

TABLE 5.2

Comparison of bond graph results for release from limited cylinder into infinite bath with analytical solution to this problem, eqn(5.16), [1], [2]. (Data for fig(5.10).)

Fractional release (q/q_o) at time (s) is tabulated for 30X30 lump model of half cylinder length. Cylinder parameters were, length 0.2cm, radius, 0.1cm and diffusion coefficient, $1.0x10^{-7}cm^2s^{-1}$.

Time(s)	Analytical	Simulation
200	0.144	0.142
400	0.200	0.199
600	0.241	0.241
800	0.275	0.275
1000	0.304	0.304
1200	0.330	0.329
1400	0.352	0.352
1600	0.373	0.373
1800	0.393	0.393
2000	0.410	0.411
2200	0.427	0.428
2400	0.443	0.443
2600	0.458	0.458
2800	0.472	0.472
3000	0.485	0.486
3200	0.498	0.498
3400	0.510	0.510
3600	0.521	0.522
3800	0.532	0.533
4000	0.543	0.544
4200	0.553	0.554
4400	0.563	0.564
4600	0.572	0.573
4800	0.582	0.582
5000	0.590	0.591

REFERENCES FOR CHAPTER FIVE

[1] H.S.Carslaw and J.C.Jaeger. Conduction of Heat in Solids. Clarendon Press, Oxford, England (1959).

[2] J.Crank, The Mathematics of Diffusion, Clarendon Press, Oxford, England (1959).

CHAPTER SIX

SIMULATION OF TWO DIMENSIONAL DIFFUSION WITH APPLICATIONS IN THE AREAS OF MEMBRANE SCIENCE AND DRUG DIFFUSION STUDIES.

6.1 INTRODUCTION

In Chapter 5 the basic theory for a 2D bond graph was developed and tested with simple problems. In this chapter we will explore its useful application in the areas of membrane science. Two examples in particular will be addressed, the first is the edge effect problem, which is a classic problem of membrane science. The second concerns once more the design of controlled release devices, and examines the effects (in two dimensions) of inhomogeneous initial distributions of diffusant within a polymer, in particular upon release rates. These examples are given to illustrate the power of these new modelling techniques. Many more could be identified. Despite a degree of symmetry in some of the problems chosen it must be stressed that all examples in this chapter are, in mathematical terms extremely complex even though non-linearity is not considered.

6.2 SIMULATION OF THE EDGE EFFECT IN MEMBRANE STUDIES.

The most common experiment in membrane characterisation is the measurement of the diffusion coefficient. From Fick's first law, eqn(2.1) it can be seen that one method for obtaining the diffusion coefficient, D, is to measure a steady state flux through a planar membrane of known dimensions. This can be very time consuming for membranes which cannot be cast thin, or for those which have high resistance to flow and the steady state is slow to develop. A quicker method is the 'time lag' experiment. This yields a value for the diffusion coefficient by calculation from the time lag, t_L, which is the extrapolated intersect of

the slope on achievement of the steady state and the x axis (time). From a mathematical analysis of Fick's law the diffusion coefficient, D is related to the time lag, t_L by eqn(6.1), [1].

$$D = \frac{l^2}{6\ t_L} \qquad (6.1)$$

Once more as elsewhere in this thesis, l is the thickness of the membrane. Recently a spray technique has been developed by Paterson and Doran, [2], for rapid measurment of D by analysing the membrane's response to forced oscillations of concentration.

All techniques however rely on the strict definition of membrane surface boundary conditions and assume a linear one dimensional diffusion. There is a very real experimental problem since the clamping of the membrane in the diffusion cell requires that part of the membrane surface is masked and so is not exposed to the source effort (the high concentration side at c_{se}) or the sink. Fig(6.1) shows this schematically. r_o is the total radius of the membrane disc and r_e is the radius of the 'exposed face'. Clearly there are diffusion patterns in these obscured membrane edges and it is their contribution to the overall flux that constitutes the edge effect. The normal approach is to ignore the clamped region and analyse the flow as a flux through the exposed area only. Depending on the system geometry this may or may not lead to significant error. Barrer, Barrie and Rogers, [3], have examined this problem analytically for steady state flow, and based their treatment on the study of an analogous system of steady

heat transference through rods by Jaeger and Beck some years earlier, [4].

These systems are in fact two dimensional diffusion problems with diffusional flows into the clamped edge region contributing to the overall observed flux through the membrane. The mathematics for predicting steady state flow through systems of this geometry, referenced above, are based on the boundary conditions of uniform flux at the exposed faces. Using the two dimensional bond graph it is possible to simulate the actual boundary conditions which approximate to constant concentrations at these membrane interfaces. The bond graph treatment not only predicts the steady state condition however, it also predicts the non-steady behaviour of these systems, and traces the evolution through to the steady state. This was therefore an excellent intermediate problem in that the mathematics are only partially known.

6.2.1 Bond graph model.

The bond graph required to model this cylindrical system is shown in fig(6.2). The C units shown explicitly are the capacitances of the external solutions. Only the planar edges, (along the y direction, see fig(5.4)), of the first three rows of lumps in this bond graph have flows directed from or into collecting capacitors. Therefore the cylinder core surrounded by two cylindrical shells define the exposed area, the outer two rows of lumps in this bond graph, model the clamped volume, this volume is surrounded by infinite resistances on three sides. Fig(6.2) may be considered to be a 3X3 lump cylindrical model with a 3X2

lump edge, or in general n_x X n_y lumps with n_c clamped edge lumps in the y direction. As equal volume lumps are used the ratio of n_y to n_c used to model a system defines the area of edge simulated. The R and C values are calculated for a limited cylinder with n_x by $(n_y + n_c)$ lumps, as described in Section 5.4.1. By calculating these values for a plane sheet geometry however a planar analogue may be studied. Electrical analogues of planar geometry were used by Barrer **et al** for experimental determination of the likely steady state concentration profiles within these systems. For ease of illustration we have simulated the analogous flow through a plane sheet with edge also, in which the radial parameters, r_o and r_e are replaced by w/2, where w is the entire width of the sheet and w_e, the width from the centre of the exposed face to the clamped edge. This is shown in fig(6.1) schematically and on fig(6.2) indicating the corresponding layout of the bond graph. It is noteworthy that the flexibility of the bond graph technique allows both examples to be treated using the same bond graph / algorithm.

6.2.2 Steady state results.

It was useful initially to simulate the behaviour of these systems in the steady state and compare the simulated flows in the bond graph model with those predicted by the mathematics of Barrer **et al** , [3]. The bond graph technique is again shown to be powerful since any initial concentration distribution may be defined and any boundary conditions may be set with equal ease. For this example we exploit both. Firstly the distribution of charge in the

volume elements or lumps of the model was set initially to what was guessed to be close to the steady state condition, this allowed rapid progression to simulation of the true steady state flow. To confirm these predictions the (same) steady state was approached from both sides, corresponding to rising and falling profiles in the membrane. Secondly the collecting capacitors were taken as effectively infinite with the charge in the right hand terminal capacitors of the bond graph corresponding to the source concentration/effort c_{se}, and the left hand side all at zero. Therefore a concentration gradient of c_{se}/l is maintained over the membrane. (In this discussion the effects of distribution coefficient are ignored for clarity but may easily be included). The simulations followed the response of the system until a steady state condition was achieved. This type of 'experiment' is of course impossible in the laboratory and is an excellent example of the powerful diagnostic capabilities of computer simulation.

The ratio of the steady state flux in this system, J, to the theoretical flux of the system allowing no flow through the edges, J_o is given by eqn(6.2), [3].

$$\frac{J}{J_o} = \frac{1}{\left(1 - \frac{16}{\pi^2} S \right)} \qquad (6.2)$$

In which S is the summation, eqn(6.3), over the odd values of i, (1, 3, 5...).

$$S = \sum_{i}^{\infty} \frac{\left[I_1(ir'_e)\right]}{i^2\left[I_1(ir'_o)\right]} \left(\left[I_1(ir'_o)\right]\left[K_1(ir'_e)\right] - \left[K_1(ir'_o)\right]\left[I_1(ir'_e)\right] \right) \tag{6.3}$$

r'_e and r'_o are the parameters, $\pi r_e/l$ and $\pi r_o/l$ respectively, $I_1()$ and $K_1()$ are the modified Bessel functions. It must be stressed however that this solution is obtained using boundary conditions of uniform flux at the exposed faces, which simplifies the mathematics, but does not correspond to the actual experimental conditions, [4]. Therefore we should not expect exact agreement between the results predicted from this equation and those obtained by experiment or by bond graph simulation which employs the true boundary conditions of constant concentrations at the faces.

Two parameters may be defined which classify these 'edge' systems: The length to exposed radius ratio, l/r_e and the quantity $(r_o - r_e)/r_e$, which gives the relative size of the edge portion. As equal volume lumps are chosen for the bond graph model, this latter function may be defined in terms of the number of lumps used in the y or radial direction, n_y and n_c. The outer radius of the lump x,y is given by eqn(6.4). This is derived in a similar fashion to eqn(2.35) in which the radial distances of the volume centres were defined for an infinite cylinder.

$$r_y^e = \left(\frac{y}{n_y + n_c} \right)^{1/2} r_o \qquad (6.4)$$

$$y=1,\ 2,\ \ldots(n_y + n_c)$$

Radial lumps are numbered from the core (y=1) to the outermost, $(y=n_y+n_c)$. The exposed radius r_e, is equivalent in the bond graph model to the the outer radius of the radial lump, r^e_y with $y=n_y$, (see fig(6.2)) and therefore the radius ratio $(r_o - r_e)/r_e$ may be defined by eqn(6.5).

$$\frac{r_o - r_e}{r_e} = \left(\frac{n_y + n_c}{n_y} \right)^{\frac{1}{2}} - 1 \qquad (6.5)$$

For these test examples several systems with different 1/a and $(r_o - r_e)/r_e$ ratios were simulated. The parameters chosen were rather extreme with the cylindrical length, 1, being greater than the exposed radius, r_e in all cases. These corresponded to examples given by Barrer **et al**, in which large edge effects were to be expected. The thickness and exposed radius of the cylinder are accomodated in the bond graph model in the calculation of the R and C values. The size of the edge simulated is dependant on the number of lumps used in the model, eqn(6.5).

We considered a membrane disc, thickness 1, radius, r_o, clamped such that the exposed membrane is a circular disc radius r_e at the centre. For modelling purposes it is convenient to examine the edge effect by simulating a series of conditions in which the central exposed membrane

area remains constant (r_e constant) and the total radius, r_o is increased progressively. This is equivalent to performing experiments with increasingly large membrane discs, but keeping the masking rings constant. In the bond graph model this is equivalent to adding progressively to n_c, the edge (obscured) lumps.

Although the steady state will be achieved from any initial conditions in the membrane, it was found practical (and economical in computer time) to 'guess' an initial condition which was not far from the true steady state and allow the simulation to evolve towards it. Accordingly at time zero, $q_{x,y}$ values were set for convenience. The steady state flows were obtained directly from the rates of flow into the external collecting capacitors.

For quantitative prediction of the steady state flow, 40X24 lump models were used (n_x X n_y) and 6 and 9 edge lumps were added (n_c) so that the ratio $(r_o-r_e)/r_e$ equalled, 0.118 and 0.486 respectively. The exposed radius, r_e was 2.604cm,in all simulations and the cylinder length, l, was changed between examples to examine the flow for l/r_e ratios of 2.56, 3.84 and 5.12. The diffusion coefficient of the membrane was $3.0x10^{-3}cm^2s^{-1}$ and the source effort or concentration, c_{se} was 1M. The results are shown in table(6.1). In this table we compare the steady state fluxes obtained from the bond graph simulation, J_e, to the analytical solution of Barrer, Barrie and Rogers [3], J of eqn(6.2) is tabulated as J'_e in table(6.1). To indicate the relative size of the edge effect the theoretical flux with no flow through the clamped edge is also tabulated, J_o. The observed difference between J_e and

J'_e may well be due to incorrect boundary conditions assumed for the mathematical analysis. Barrer et al were conscious of this intrinsic error but did not expect it to be significant. Clearly this error is dependant upon the parameters of the system under study and in extreme cases, with large edge effects much larger errors are expected, as is shown in table(6.1).

A clear advantage of using the bond graph model is that two dimensional concentration profiles may be constructed by directly inspecting the bond graph charge values, $q_{x,y}$. Barrer et al investigated the flows of current through a planar electrical analogue of the edge effect (using teledeltos paper) to illustrate the likely diffusional patterns within a membrane in the steady state. We also modelled a planar system to illustrate this. Fig(6.1) shows this system schematically. Diffusion through a sheet of width w is considered, with a total unclamped width in the centre, $2w_e$ exposed to the concentration source, (at c_{se}) or sink. As indicated in fig(6.2), (showing the bond graph model for this system), only diffusion through half the sheet need be modelled, as the flows through each half width, w/2, are identical.

In this simulation a 10X6 lump bond graph ($n_x X n_y$) with a 9 lump edge portion (n_c) was used to model the half sheet of total width, w, 2.6cm. Therefore the exposed half width, w_e was considered to be 0.52cm, ($n_y w/2(n_y+n_c)$). The thickness, 1, and depth, d of the sheet were 1cm and 1.04cm respectively, with a diffusion coefficient of $3.0x10^{-5} cm^2 s^{-1}$. The source concentration, c_{se} was 1M as for

the previous cylinder model.

The steady state concentration profile within this system was produced as described previously for a plane sheet, Section 5.3.3, and is shown in fig(6.3). Concentrations are given as a fraction of the source effort, c_{se}. (Note that as average concentrations within each lump are plotted the conditions at the edge of the sheet are not shown.) A contour map representation of this profile was also constructed, fig(6.4) which indicates clearly the diffusional flows (normal to the contours) into the edge portion which contribute to the overall flux. The contour lines for this map are drawn at 0.0625 levels in fractional concentration (c/c_{se}). (15 levels in the range 0.0625 to 0.9375).

6.2.3 Non-Steady state simulations.

The bond graph model is of course not restricted to steady state predictions. In the previous section the system was placed in an arbitrary state at time zero, to limit computational time. Under normal experimental conditions however the membrane is initially free of diffusant and a breakthrough period is observed; as discussed previously (Section 6.2), this is the basis of the time lag experiment. Results have been published previously for the bond graph simulation of this experiment without consideration of edge effects using a one dimensional model [5]. In this section we give an example simulation of the effect of a clamped edge on the measured time lag, t_L, using the bond graph model for 2D diffusion and illustrate the evolution of concentration profiles in

the two dimensions.

For this example the parameters of cylinder length, 6.67cm exposed radius, r_e, 2.604cm, and diffusion coefficient $3x10^{-3}cm^2s^{-1}$ were used. Six edge lumps, (n_c), were added to a 40x24 lump model (n_xXn_y), so that the $(r_o - r_e)/r_e$ ratio was 0.118, eqn(6.5). A source concentration, c_{se} of 1M was taken. (The simulated steady state flow is given in fig(6.1), row one.) For comparison the accumulation of material, q, at time t was calculated from the analytical solution to this problem, ignoring the clamped edge, eqn(6.6), [1]. This equation is valid only for zero diffusant in the membrane at time zero and a maintained zero concentration in the collecting volume.

$$\frac{q}{l\, c_{se}} = \frac{D\, t}{l^2} - \frac{1}{6} - \frac{2}{\pi^2} \sum_{i=1}^{\infty} \frac{(-1)^i}{i^2} \exp\left(\frac{-D\, i^2 \pi^2 t}{l^2} \right) \qquad (6.6)$$

Fig(6.5) shows the simulated diffusion through the membrane by plotting the total absolute amount of diffusant in the collecting volume with time, q, as a solid line. This value is found in the bond graph model by summing the charges on all the collecting capacitors (of which there are n_y). The dashed line is that calculated for this system ignoring flow through the edge, eqn(6.6). The system parameters chosen here for illustration lead to a large edge effect. Fig(6.5) shows clearly that the steady state flow is increased due to the contributing flows into the clamped region (to a degree given in table(6.1)). In addition the breakthrough period is extended. The

calculated time lag, t_L is increased from its true value by 130%. If the diffusion coefficient were to be calculated on the basis of this time lag from eqn(6.1), (assuming incorrectly negligable flow through the clamped edge region), a D_L value (L subscript used to indicate calculation from time lag) equal to $2.1x10^{-3}cm^2s^{-1}$ is obtained, an underestimate of 30% from the true D value. The diffusion coefficient calculated from the steady state flow D_s, (incorrectly taken as a flux through the exposed membrane area only, πr_e^2) is an overestimate of 23% in this example, (from the resultant flux tabulated in table(6.1)). Clearly this method of simulation could be used to routinely check experimental setup for likely edge effect error.

Not only can the output flow for such systems be predicted by simulation but also the evolution of the concentration profiles leading to the steady state may be obtained. In fig(6.3) a steady state concentration profile was illustrated for a planar membrane. Using this model once more, a series of concentration profiles were calculated for intermediate states in the evolution of this planar membrane from an initial condition of zero loading.

In this example the bond graph model of the half sheet used was as for that of fig(6.3), 10X6 (n_xXn_y) lumps with the number of edge lumps, n_c, equal 9. The entire width of the sheet, w, was 2.6cm, so that, from the ratio of n_c to n_y, the exposed half width considered, w_e was 0.52cm. The length, l and depth, d were 1cm and 1.04cm respectively with a diffusion coefficient equal $3.0x10^{-5}cm^2s^{-1}$. Concentration profiles at 1000s, 5000s and 10000s are shown

in figs(6.6a,c). Again no interpolation of the data was necessary and so the boundary conditions at the membrane faces are not shown. These illustrate the build up of material in the clamped edge as the diffusion proceeds.

6.3 NON UNIFORM DRUG DISTRIBUTIONS IN RELEASE DEVICES.

Another application of the two dimensional model is the study of non-uniform initial distributions of diffusant. It is useful to simulate the effects of a range of such conditions since they provide in principle a simple means of varying drug release rates. Although, in the examples given below, initial distributions were regular and symmetric this was not a limiting requirement, rather a matter of convenience. The bond graph method is not restricted in any way and quite irregular random initial conditions could be considered with equal ease to symmetrical or regular initial distributions. The examples given here were chosen for ease of interpretation and for illustration. Planar geometries only are considered. The techniques can easily be applied to the limited cylinder (pill) model or indeed extended to any three dimensional shape as developed in Chapter 7.

6.3.1 Release from plane sheet through edges with areas of zero concentration.

Diffusion from a square sheet through its edges was modelled previously, (Section 5.3.2) from a condition of uniform initial loading. The sheet parameters were as before (section 5.3.2) so that direct comparisons may be made: Sheet of side and depth 0.2cm with diffusion

coefficient, $2.0x10^{-7}cm^2s^{-1}$. For these simulations here a 25X25 lump bond graph model of the sheet corner was used. The model was 'run' as before except that certain areas in the corner were considered free of diffusant while the remainder were at uniform loading, c_o, 0.1M. The principle being that such voids would cause internal flows within the model and reduce the efflux of diffusant (drug) into the environment. Such effects might be desirable to control drug release and might help to create near constant rates.

The purpose was to examine the release rates from two complementary initial conditions within the plane sheet. Fig(6.7a) and fig(6.8a) show these initial concentration profiles within the sheet corner, using the linked capacitor representation as employed for the edge effect profiles in the previous section and described for the plane sheet example in Section 5.3.3. The profiles have been oriented so that the outer corner of the sheet, with two edges adjacent to the collecting volume, is nearest. As can be seen each initial condition is the exact reverse of the other. Fig(6.8a) shows isolated voids at zero concentration where previously there were peaks, fig(6.7a). Therefore the net addition of the concentrations in these two models at time zero would correspond to an initial uniform loading.

Figs(6.7b) to (6.7f) and likewise figs(6.8b) to (6.8f) show the evolution of the concentration distributions at 62.5s intervals after time zero up to 250s and then a further profile at 500s, to illustrate the final stages of release. Note that a consequence of the choice of initial distribution patterns is that the example shown in fig(6.8)

has greater overall loading of diffusant. This is reflected in the release kinetics.

The release kinetics for these two simulations are presented in fig(6.9). Fractional release (q/q_o) where q_o is the total amount of diffusant in a uniformly loaded sheet (at 0.1M) is plotted against time in seconds. Curve 1 is the simulated diffusion from the sheet with spots at 0.1M (fig(6.7)), curve 2 is the release from the sheet at 0.1M with isolated voids, (fig(6.8)), (larger amount of material in the system), and the upper solid curve, curve 3, is the release calculated from the analytical solution for uniform loading into an infinite bath, eqn(5.10). The addition of curves 1 and 2 equals the kinetics of release from the uniform release. This has been illustrated on fig(6.9) by plotting the sum of the data for curves 1 and 2 as points. The data for this figure is tabulated in table(6.2) for closer inspection of this self consistent result.

6.3.2 Release rates on re-distribution of drug below and above the solubility limit.

In the previous model we considered the effects of splitting a uniform sheet system into two complementary distributions, voids and peaks. In this section we adopt a different point of view. Now we consider a single membrane system (the planar membrane of previous examples), in which the initial loading is equal to that in the uniformly loaded sheet at 0.1M. The model contains 2500 lumps. Due to symmetry this may be treated as four 25X25 corner bond graphs. The total drug loading is placed in four, 12X12

lump spots, one in each corner, so that the concentration in each of these is 0.43M. Fig(6.10a) shows the original concentration profile in this system, oriented with the nearest lump, that adjacent to the square centre.

Many polymer devices contain drugs dispersed as crystals within the drug matrix. To illustrate the methods by which the dissolution and diffusion processes may be modelled, we now consider a system identical to that above, except with a dry loading 1.5 times the saturation concentration. This means in effect that crystals are present in the model. The previous initial concentration, 0.43M, was taken to be the saturation level, c_s, so that this example had 1.5 times the initial loading of the above and therefore also 1.5 times the amount of diffusant as in the uniformly loaded sheet at 0.1M, Section 5.3.2.

In the bond graph model a crystal' lump with loading above the solubility limit was considered to have a concentration at saturation level, c_s, with the remaining material, corresponding to the excess loading above this, in reserve (crystallised). Over the small step time for integration, H, the diffusional processes are treated as before. Between steps however the amount of material that has left the volume element or lump is replenished from the reserve and the capacitors remain at constant effort corresponding to a saturated concentration. Once the reserve has been used up the crystal has dissolved and diffusion proceeds as normal with concentrations (efforts) decreasing progressively. The error that is apparent in this technique is that the concentration at crystal edges

is allowed to dip below the saturation level at times when there is still crystallised diffusant present. This error is effectively eliminated by decreasing the step time.

Figs(6.10b) to (6.10e) give the decay of the concentration profiles for the initial example of loading at the saturation level. The fractional concentrations relative to the saturation level, c_s (0.43M), are shown at 125s intervals up to 500s. The equivalent set of profiles for the model with crystallised diffusant, figs(6.11a) to (6.11f) show the concentrations within the sheet (corner) at the times 250s to 1000s in steps of 250s, then at 2000s and finally the position at 5000s after zero. Now the corner has been oriented so that the closest lump, drawn at the bottom of the page is that with one edge only contacting the outer solution. These profiles appear rather different. The flat top on the profiles up to time 1000s indicates that a degree of crystallinity remains within that area. The concentration profiles after this time show a 'normal' decay as the diffusant is released from the edges of the sheet into the infinite bath.

Of greatest interest to the designers of drug release devices is the resultant effects of these distributions and crystallinity on the release behaviour. As previous we can obtain the simulated amount of diffusant released into the collecting bath by summing the charges in the appropriate solution capacitors of the model. Fig(6.12) compares the simulated efflux for the concentrated spot at saturation, curve 1, and as a crystal with loading 1.5 times above saturation, curve 2. Fractional release, q/q_o, has been plotted against time in seconds, where q_o is the total

loading in a sheet at uniform concentration 0.1M. Since the example of simulated release from crystallised diffusant considered an initial amount of material 1.5 times q_o, curve 2, if continued, would increase to 1.5 at time infinity. On this graph, for comparison the analytical solution of release from the uniformly loaded sheet, eqn(5.10), is included (broken line).

The non-uniform distribution of saturated spot or crystal show initial concave release profiles, with relatively constant release thereafter. The main advantage of crystal diffusion is that the saturated level is maintained at the dry locations for longer times and the total delivery can be increased, giving an extended time base for release. The examples of swelling diffusion gave more constant release than this simple inhomogeneous distribution but both mechanisms contribute to make the release profile flatter and more linear. When these functions are combined, as in hydrogels, very reliable systems are obtained, [6].

6.4 CONCLUSIONS.

The examples given in this section illustrate the methods by which the two dimensional bond graph, developed in Chapter 5, can be used to address a large variety of diffusion problems. In addition, the techniques for examining a system of a particular geometry, as illustrated by the edge effect problem, and for modelling crystallinity, can be extended to diffusion problems in three dimensions. The simulation of such systems is discussed in Chapter 7 in which a bond graph model for

three dimensional diffusion is developed.

FIGURE 6.1.

Illustration of the experimental set up for measurement of diffusion coefficients in membrane studies.

Section through cylindrical membrane shows radius of membrane faces exposed to external solutions, r_e and total radius of membrane r_o. Corresponding parameters for planar analogue model are also shown.

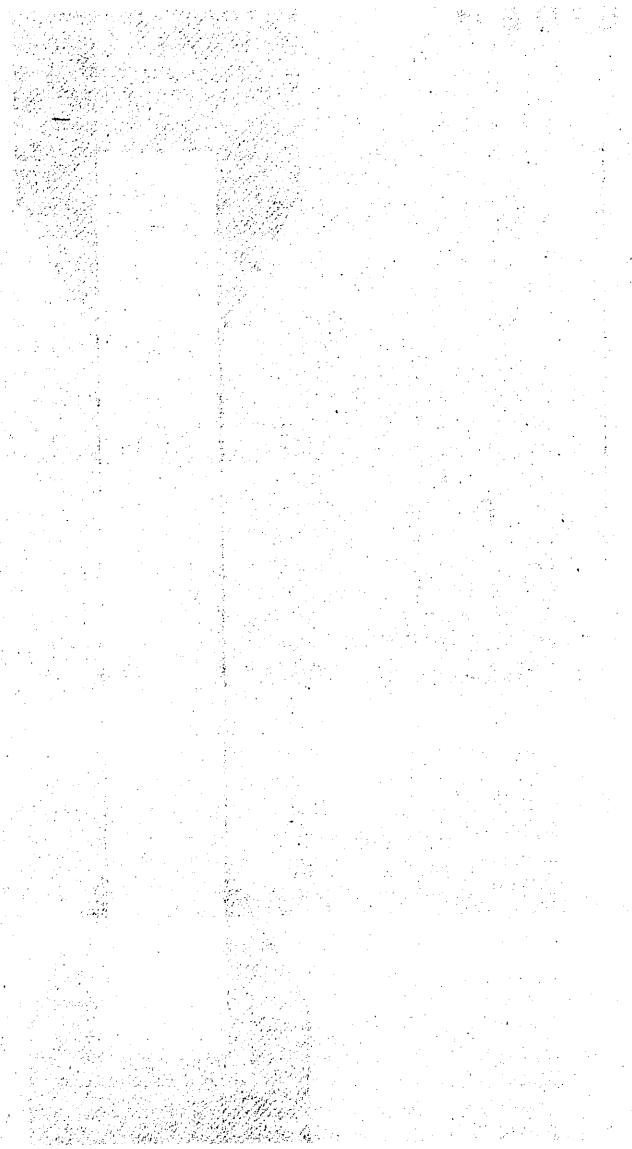

Edge Effect

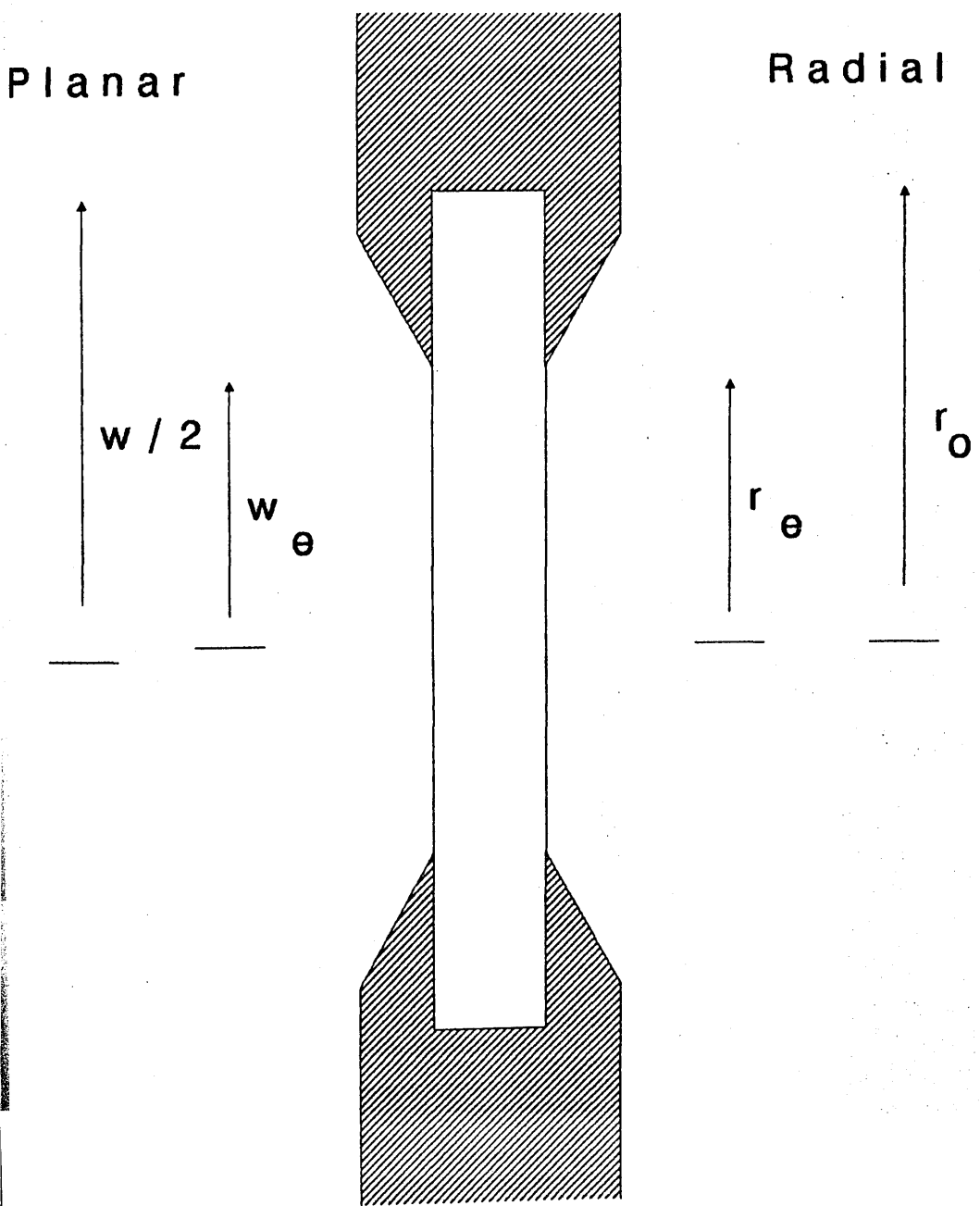

FIGURE 6.2.

Reduced representation of a bond graph for the simulation of edge effects in membrane studies. (See Section 5.3.1).

This representation may be regarded as a 3 X 3 lump model (n_x X n_y) with 2 rows of lumps modelling the clamped edge (n_c=2). The ratio n_c to n_y may be changed to accomodate different experimental conditions of clamped edge. Shown C units are collecting capacitors.

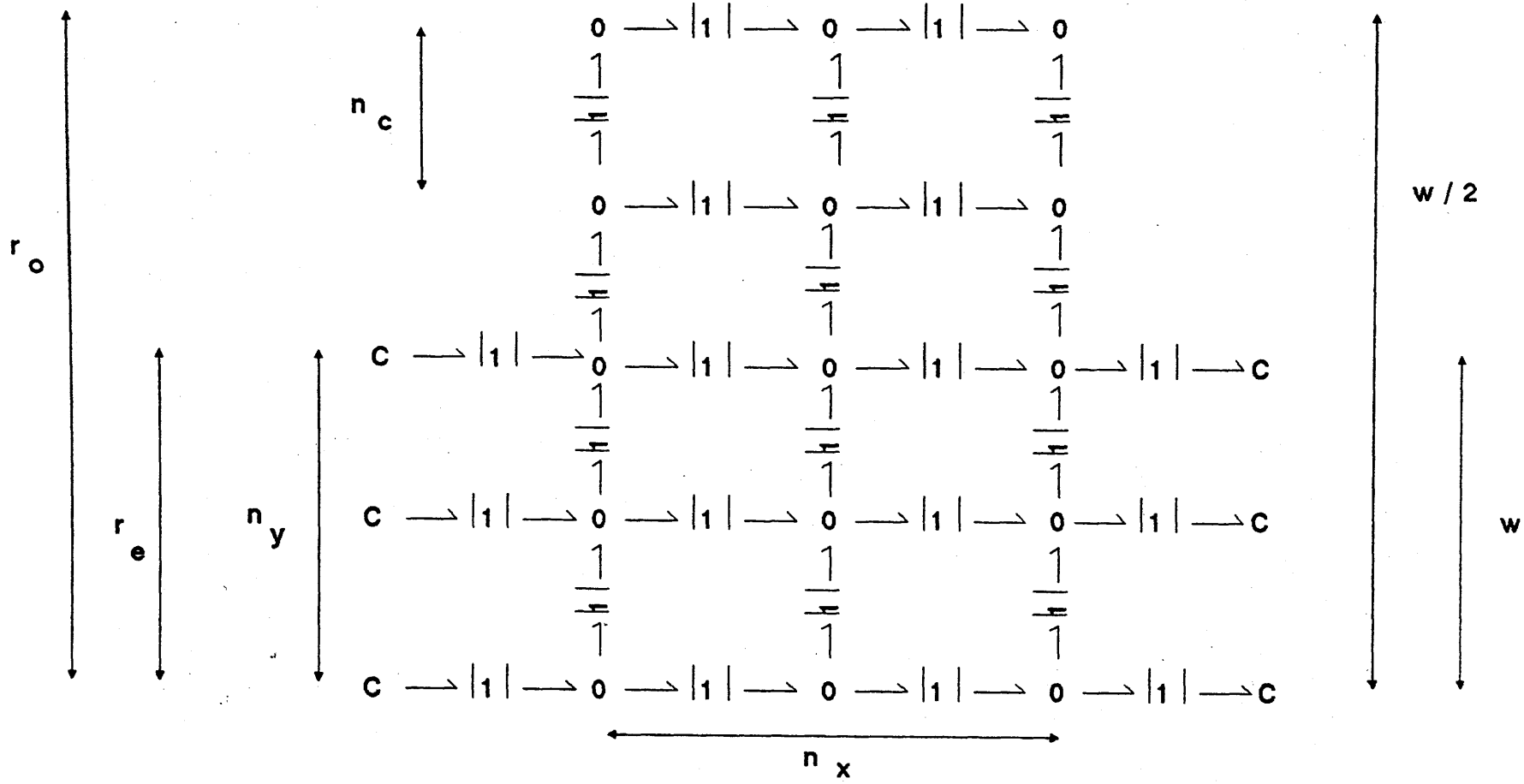
r o
r e
n y
n c
n x
w / 2
w
0
1
C

FIGURE 6.3.

Simulated steady state profile within planar analogue of edge effect shown as isometric projection.

The concentrations within a 10X15 lump model of the half sheet width have been mirrored over centre of sheet to give full profile. Exposed portion of sheet to external solutions is therefore 12 lumps wide (6 in model of half sheet), with 9 rows of lumps modelling the clamped region. Fractional concentration, c/c_{se} is plotted as height where c_{se} is the concentration of the right hand solution, the left is at zero. Sheet parameters were length, l, 1cm, total width, w, 2.6cm, depth, d, 1.04cm and diffusion coefficient, $3.0 \times 10^{-5} cm^2 s^{-1}$.

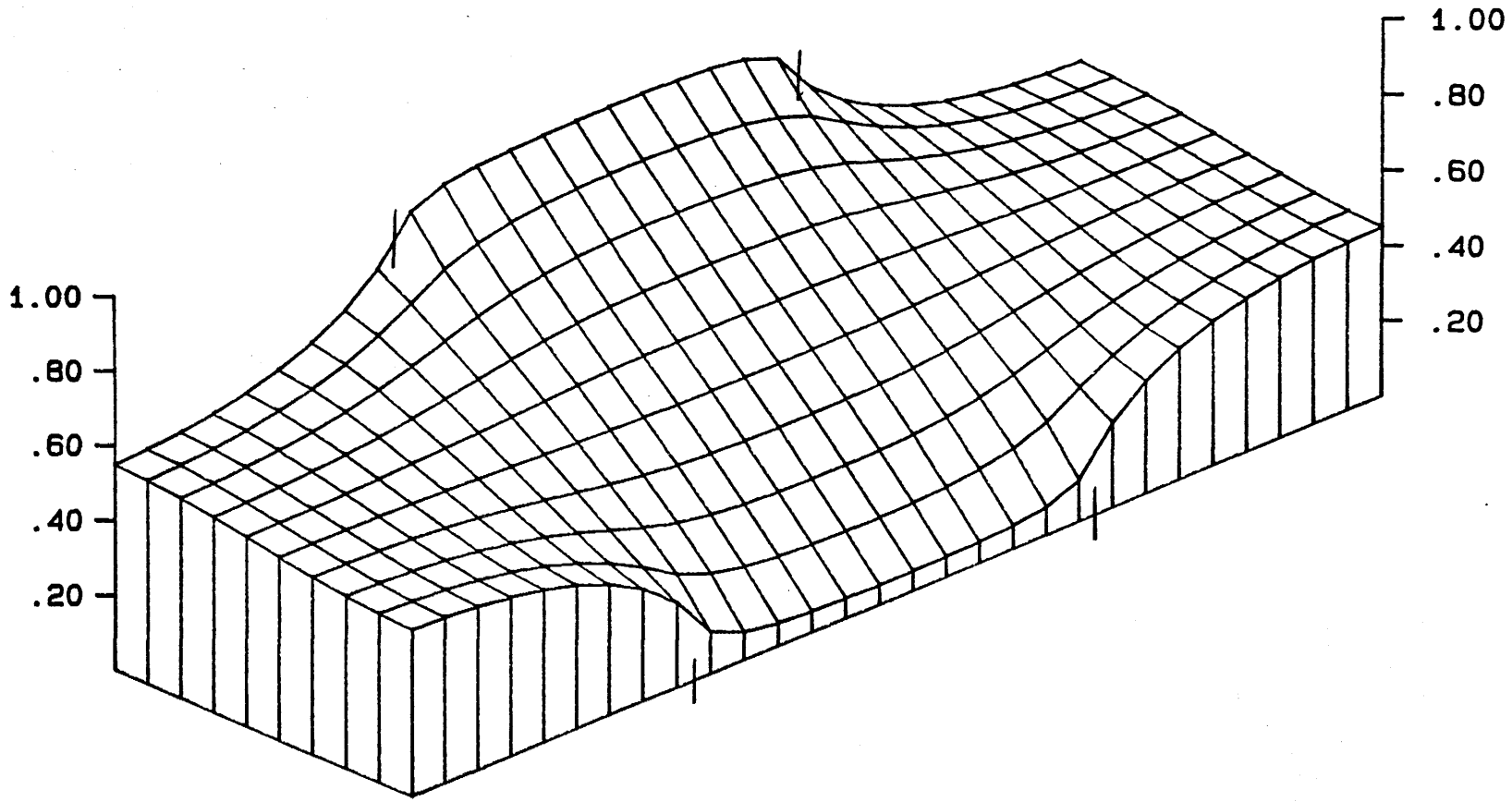
1.00
.80
.60
.40
.20
1.00
.80
.60
.40
.20

FIGURE 6.4.

Contour map representation of steady state concentration profile within planar analogue of edge effect.

The concentrations within a 10X15 lump model of the half sheet width have been mirrored over centre of sheet to give full profile. The portion of the model in contact with the external solutions is 12 lumps wide (6 in model of half sheet), clamped area is 9 lumps on each side. Contour lines are drawn at fractional concentration levels, c/c_{se}, of 0.0625. (Left hand side is high concentration end. Sheet parameters were length, l, 1cm, total width, w, 2.6cm, depth, d, 1.04cm and diffusion coefficient, $3.0 \times 10^{-5} cm^2 s^{-1}$.

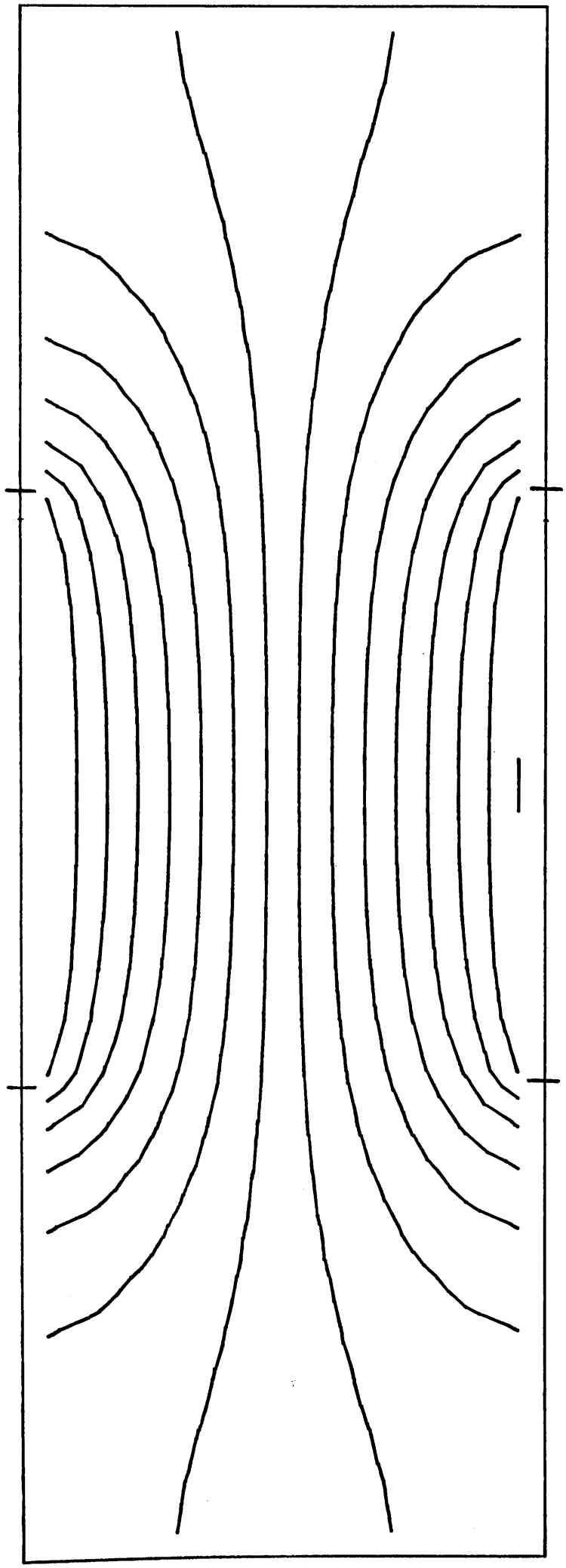

FIGURE 6.5.

Plot of total amount of diffusant collected in effectively infinite bath with concentration at zero.

Solid curve is edge effect simulation. 40x24 lump model of cylindrical system used with 6 lump edges: $(r_o - r_e)/r_e$ equals 0.118. Dashed line is analytical solution, eqn(6.6) for flow through system ignoring the edge portion, [1].

Source effort concentration c_{se}, 1M. Cylindrical membrane parameters were: exposed radius, r_e, 2.604cm, length, l, 6.67cm, and diffusion coefficient, $3.0 \times 10^{-3} cm^2 s^{-1}$.

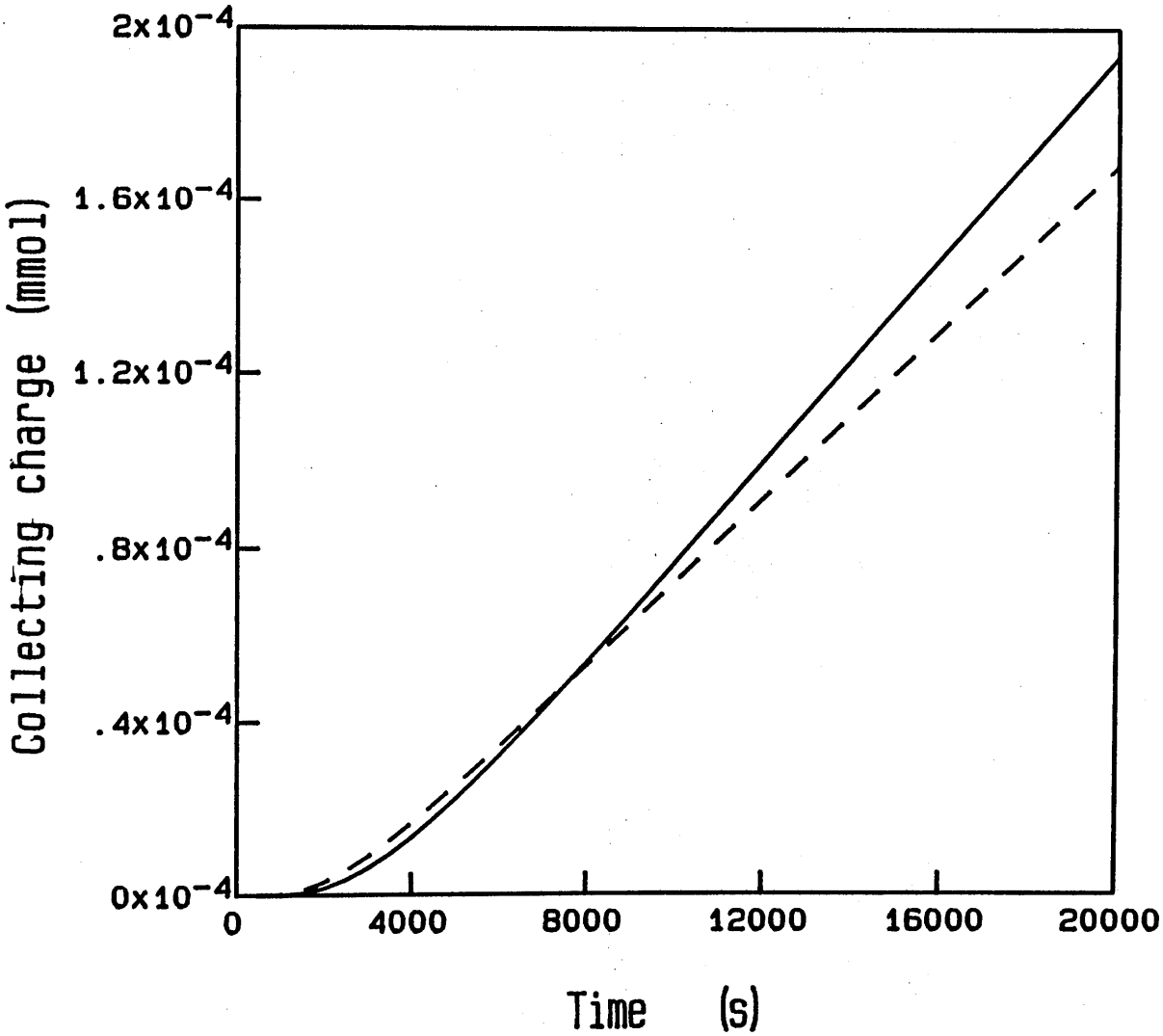
2x10⁻⁴
1.6x10⁻⁴
1.2x10⁻⁴
.8x10⁻⁴
.4x10⁻⁴
0x10⁻⁴
Collecting charge (mmol)
0
4000
8000
12000
16000
20000
Time (s)

FIGURE 6.6.

Illustration of approach to steady state in edge effect problem by means of successive concentration profiles within planar analogue.

The concentrations within a 10x15 lump model of the half sheet width have been mirrored over centre of sheet to give full profile, and are shown at 1000s, 5000s and 10000s after time zero, (a) to (c). Exposed portion of sheet to external solutions is 12 lumps wide with 9 rows of lumps modelling the clamped region. Fractional concentration, c/c_{se} is plotted as height where c_{se} is the concentration of the right hand solution, the left is at zero. Sheet parameters were length 1cm, total width, w, 2.6cm, depth 1.04cm and diffusion coefficient, $3.0 \times 10^{-5} cm^2 s^{-1}$. The steady state condition is shown in fig(6.3).

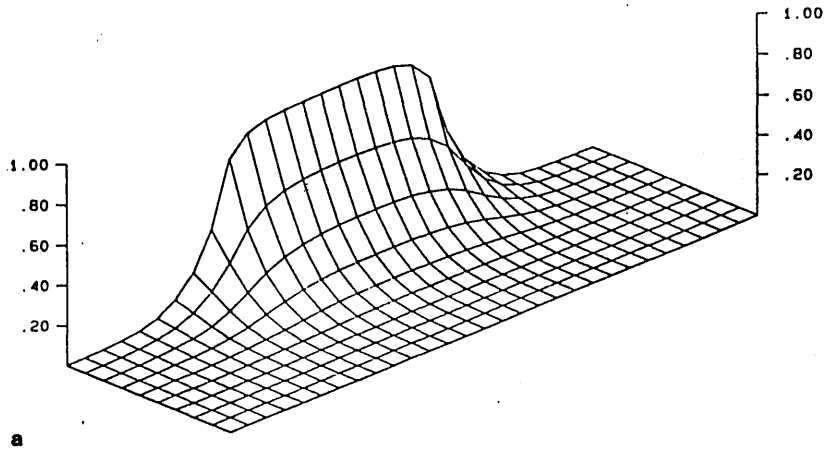
1.00
.80
.60
.40
.20
1.00
.80
.60
.40
.20

a

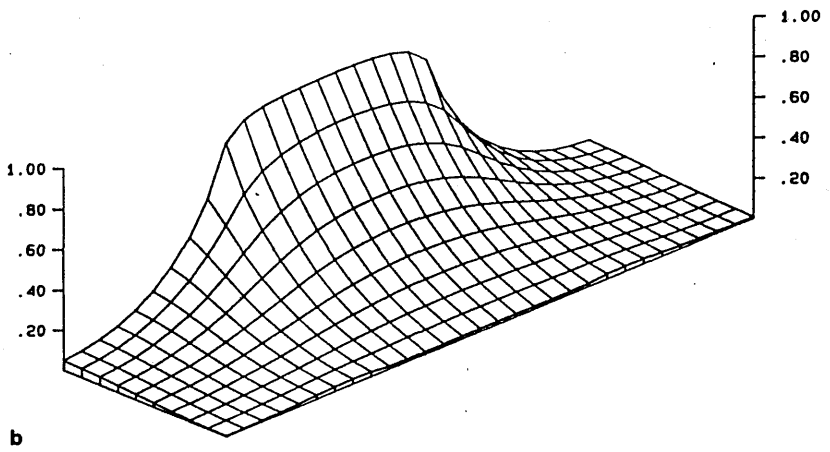
1.00
.80
.60
.40
.20
1.00
.80
.60
.40
.20

b

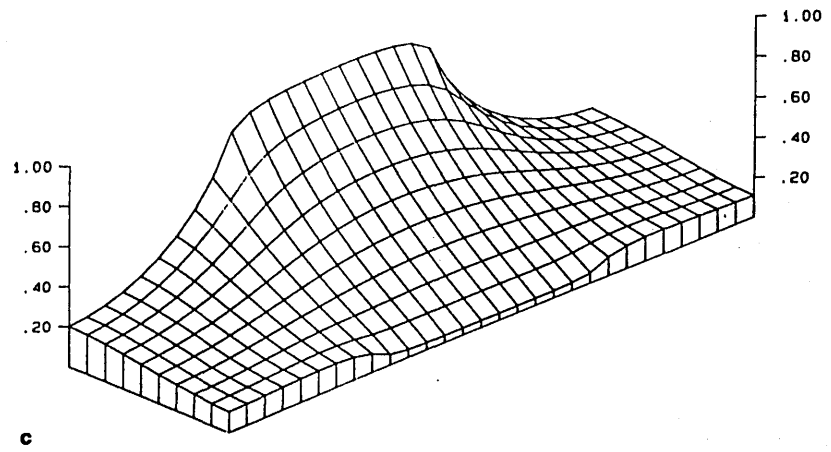
1.00
.80
.60
.40
.20
1.00
.80
.60
.40
.20

c

FIGURES 6.7 AND 6.8.

Succesive concentration profiles within planar square sheet corner during simulated release from edges into infinite bath.

Two simulations shown for identical system parameters with complementary initial distributions of material. Fig(6.7) is sheet mostly at zero with spots at 0.1M, fig(6.8) is opposite initial condition with sheet mostly at 0.1M and spots at zero.

Parameters of square sheet were sides, 0.2cm and depth also 0.2cm, with diffusion coefficient $2.0 \times 10^{-7} cm^2 s^{-1}$. Fractional concentration, c/c_o plotted as height, where c_o is initial maximum loading, 0.1M. Viewing corner from edges in contact with infinite bath.

Profiles are shown from initial condition (a), at 62.5s intervals up to 250s (b to e) then at 500s (f).

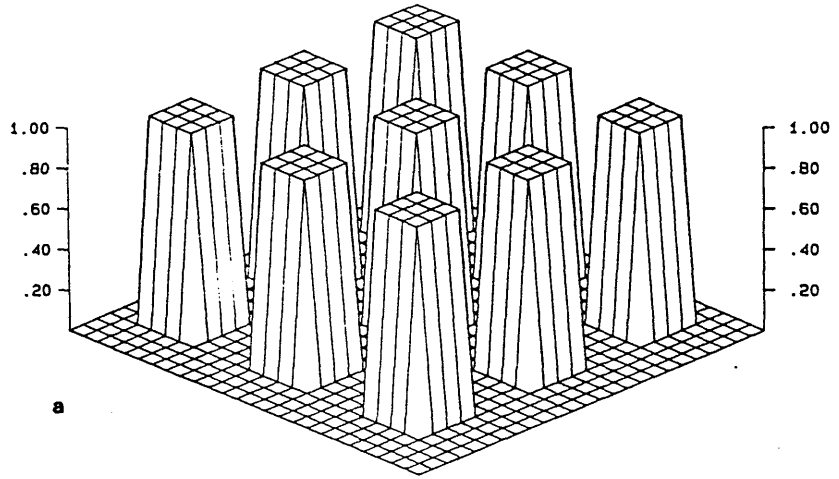
1.00
.80
.60
.40
.20
a

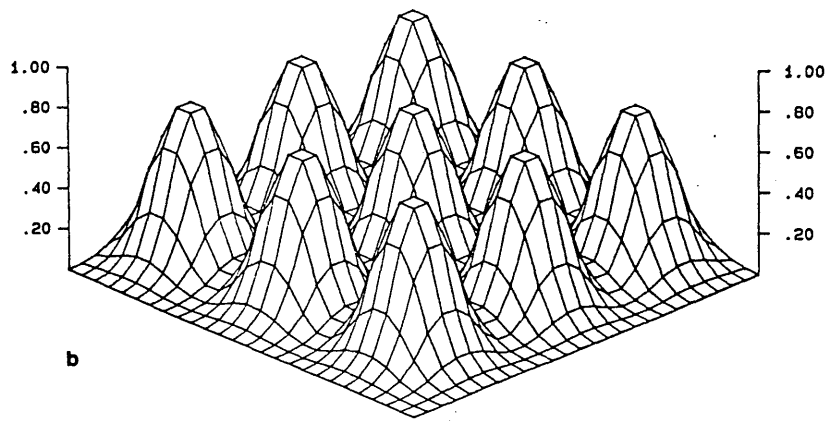
1.00
.80
.60
.40
.20
b

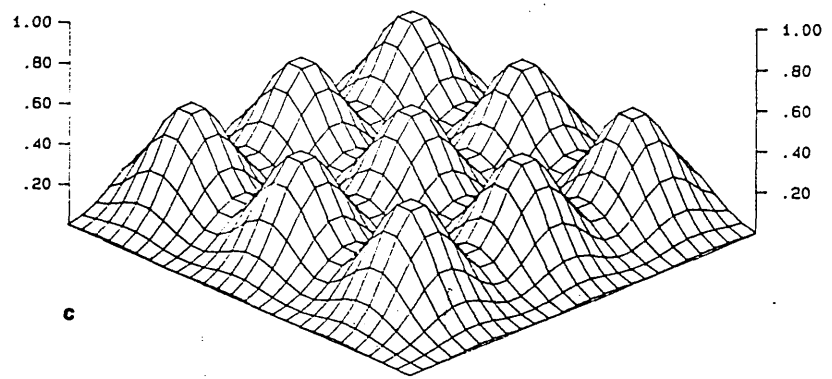
1.00
.80
.60
.40
.20
c

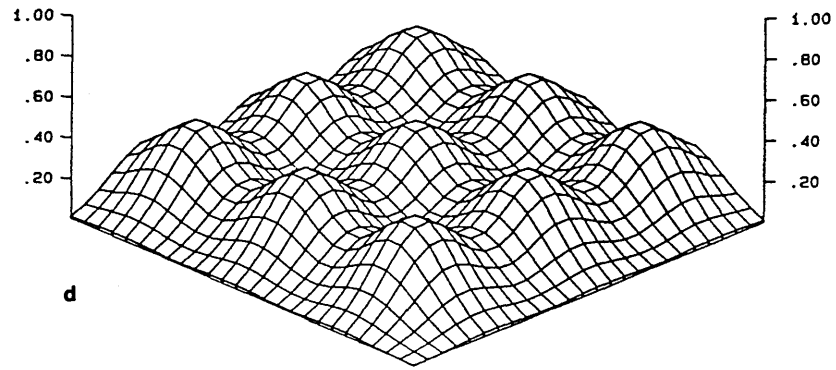
1.00
.80
.60
.40
.20
d

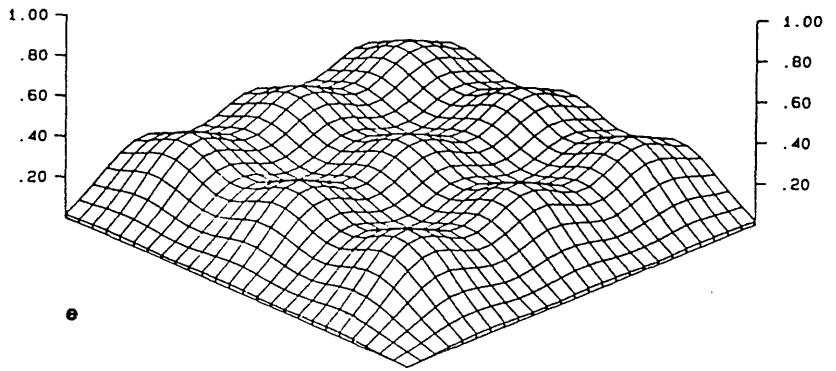
1.00
.80
.60
.40
.20
e

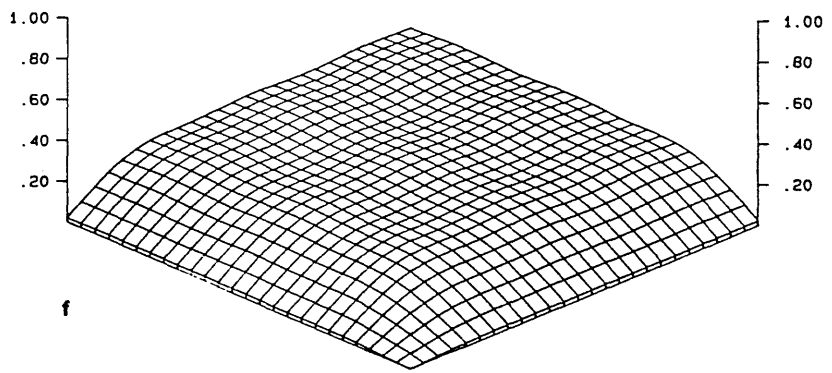
1.00
.80
.60
.40
.20
f

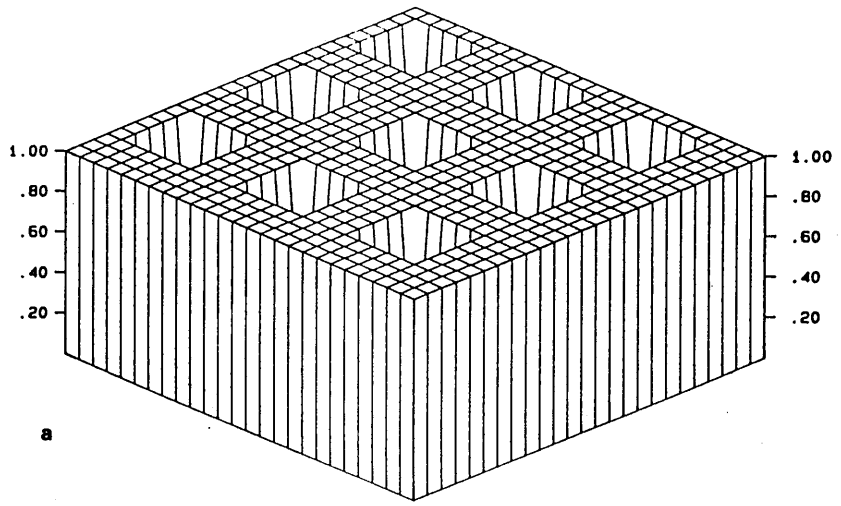
1.00
.80
.60
.40
.20
1.00
.80
.60
.40
.20

a

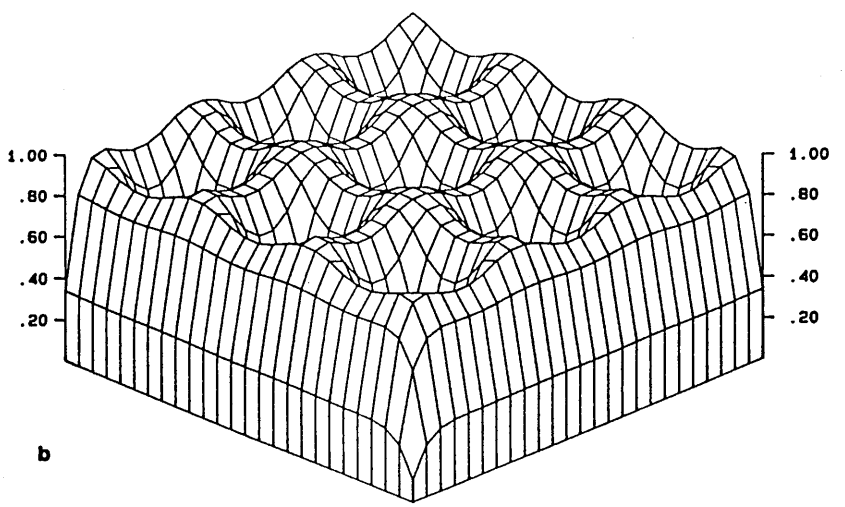
1.00
.80
.60
.40
.20
1.00
.80
.60
.40
.20

b

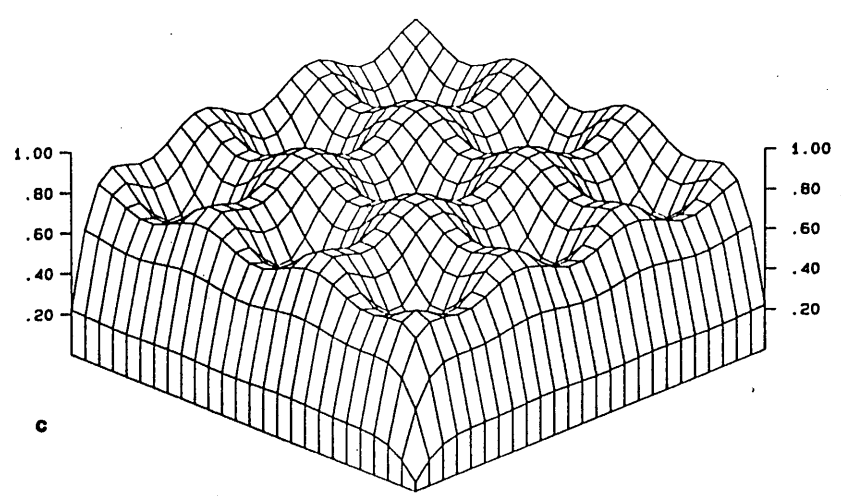
1.00
.80
.60
.40
.20
1.00
.80
.60
.40
.20

c

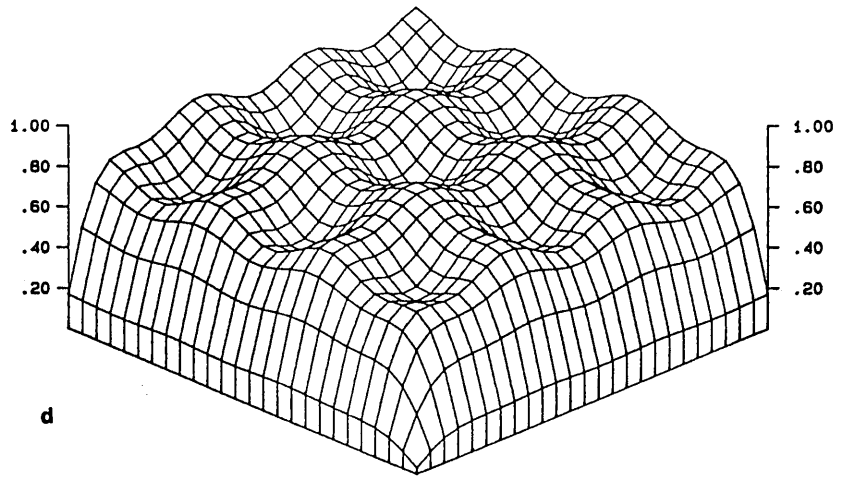
1.00
.80
.60
.40
.20
1.00
.80
.60
.40
.20

d

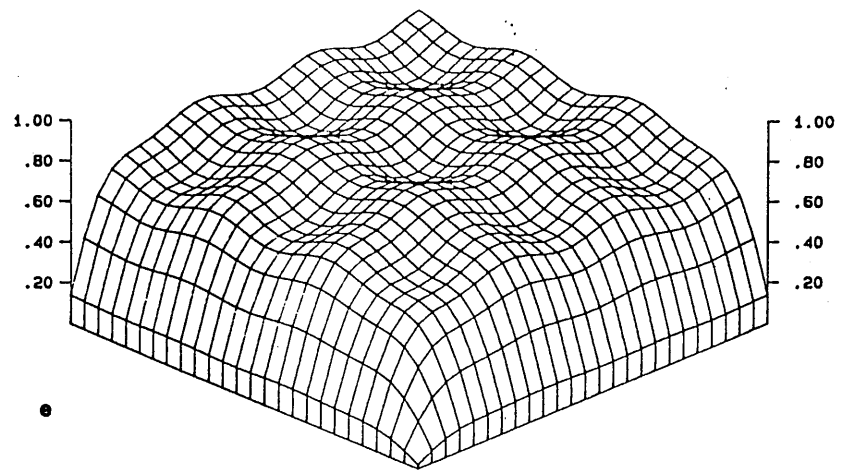
1.00
.80
.60
.40
.20
1.00
.80
.60
.40
.20

e

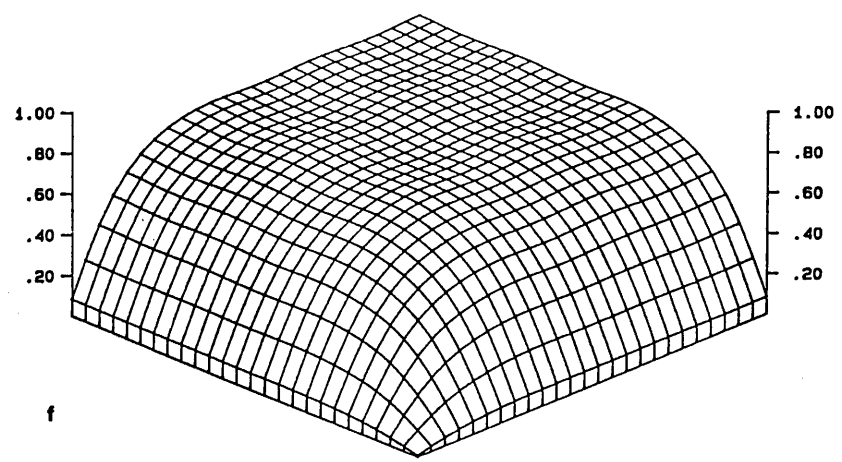
1.00
.80
.60
.40
.20
1.00
.80
.60
.40
.20

f

FIGURE 6.9.

Plot of release kinetics compared for three different distributions of material, maximum loading 0.1M in all.

Parameters of sheet modelled were side 0.2cm, depth 0.2cm and diffusion coefficient $2.0 \times 10^{-7} cm^2 s^{-1}$. Fractional release q/q_o, where q_o is amount of diffusant in uniformly loaded sheet at time zero, plotted against time in seconds.

Curve 1, release for sheet mostly at zero with spots at 0.1M. (figs(6.7)).

Curve 2, release for sheet mostly at 0.1M with spots at zero. (figs(6.8)).

Curve 3, analytical solution for release from square sheet uniformly at 0.1M into infinite bath, eqn(5.10).

Points, curves 1 and 2 added.

Non-Uniform Dispersions

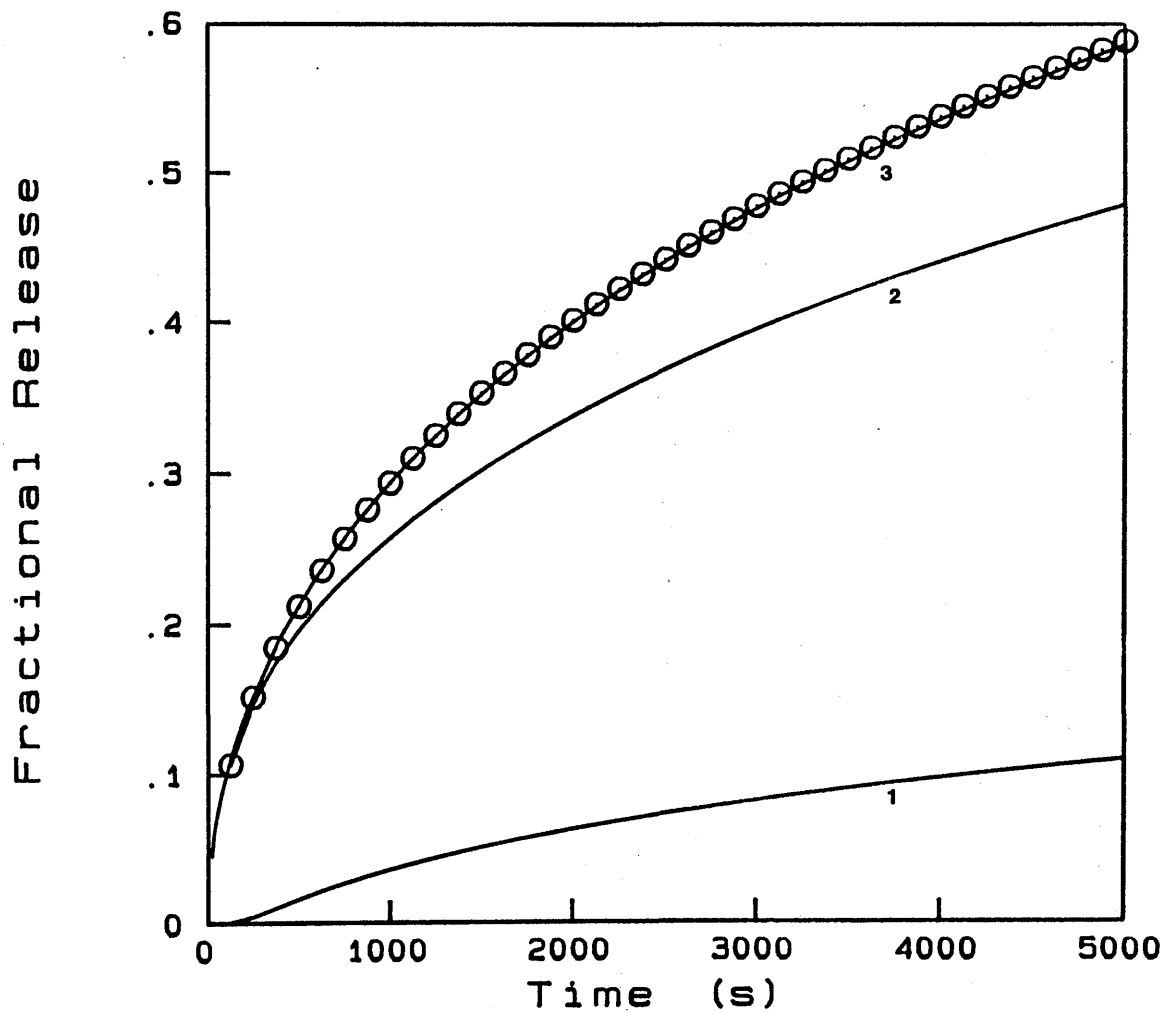

FIGURE 6.10.

Succesive concentration profiles within planar square sheet corner during simulated release from edges into infinite bath.

Initial distribution of material is one saturated spot, (12X12 lumps), 0.43M (c_s), in each corner, such that the total loading equalled q_o for sheet uniformly at 0.1M. Sheet parameters were of side, 0.2cm, depth 0.2cm and diffusion coefficient $2.0 \times 10^{-7} cm^2 s^{-1}$. Fractional concentrations c/c_s are plotted as height at the positions of the lump volume centres. Profiles are shown at 125s intervals up to 500s viewing from centre of sheet out to edges of corner contacting external solution.

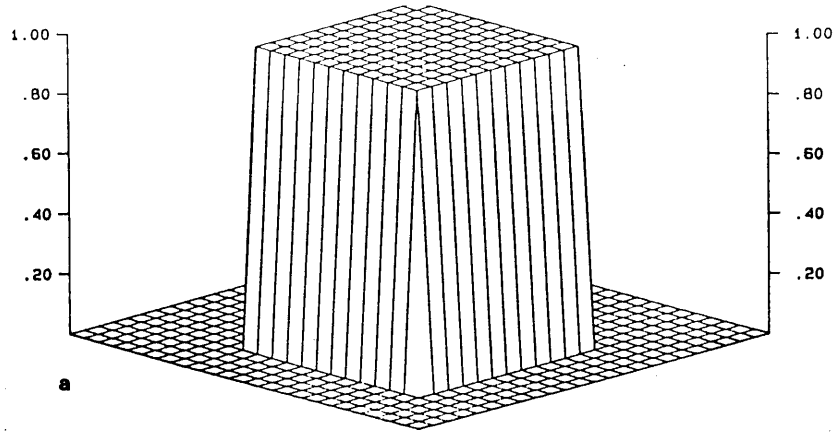
1.00
.80
.60
.40
.20
1.00
.80
.60
.40
.20

a

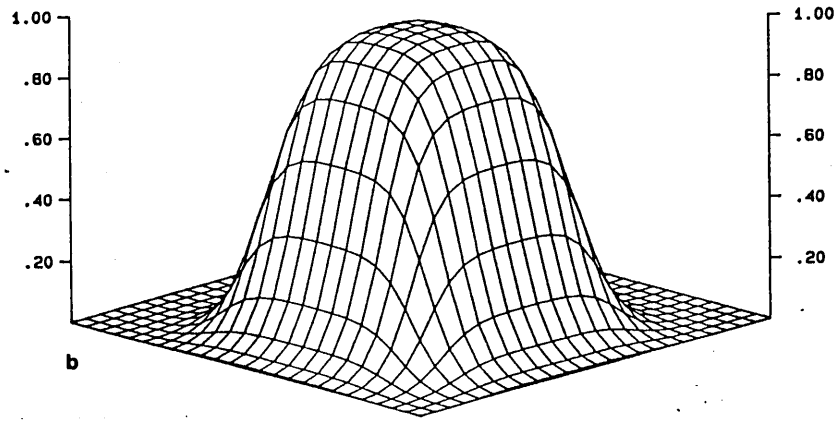
1.00
.80
.60
.40
.20
1.00
.80
.60
.40
.20

b

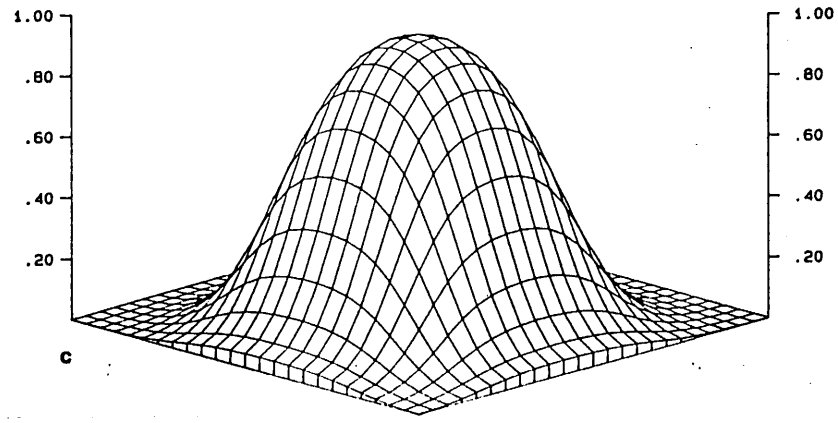
1.00
.80
.60
.40
.20
1.00
.80
.60
.40
.20

c

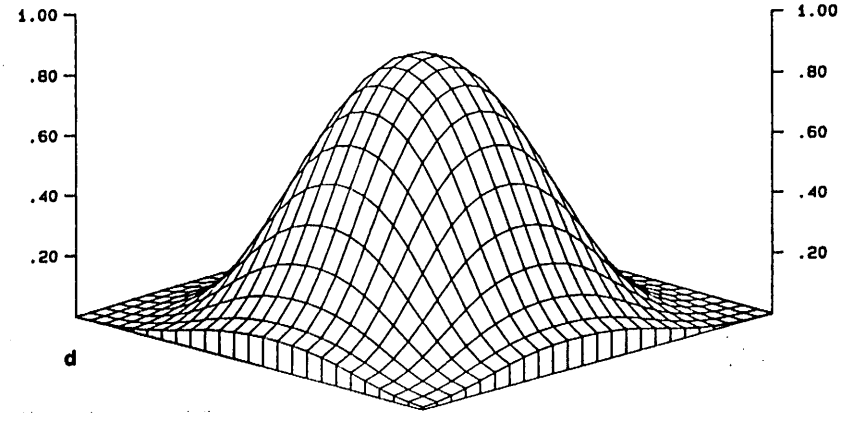
1.00
.80
.60
.40
.20
1.00
.80
.60
.40
.20

d

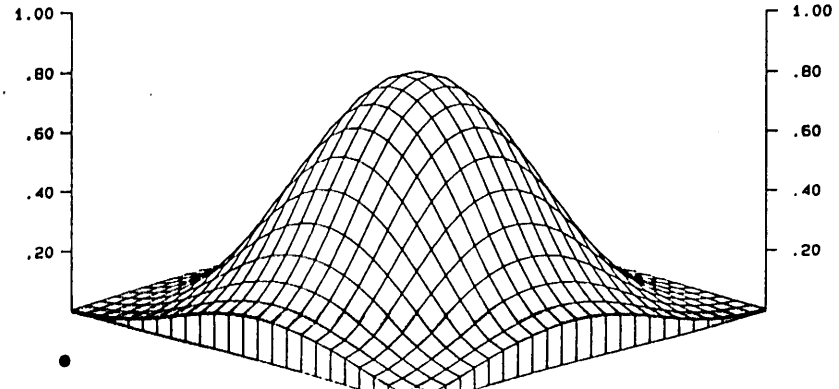
1.00
.80
.60
.40
.20
1.00
.80
.60
.40
.20

e

FIGURE 6.11.

Succesive concentration profiles within planar square sheet corner during simulated release from edges into infinite bath with initial loading above solubility limit.

Initial distribution of material is one spot at loading equal to 1.5 times saturation level, c_s (0.43M), such that the total initial loading equalled $1.5q_o$ for sheet uniformly at 0.1M. Sheet parameters were of side, 0.2cm, depth 0.2cm and diffusion coefficient $2.0 \times 10^{-7} cm^2 s^{-1}$. Fractional concentrations c/c_s are plotted as height at the positions of the lump volume centres. Profiles are shown at 250s intervals up to 1000s then at 2000s and finally at 5000s. Nearest lump is that with one edge only in contact with external solution.

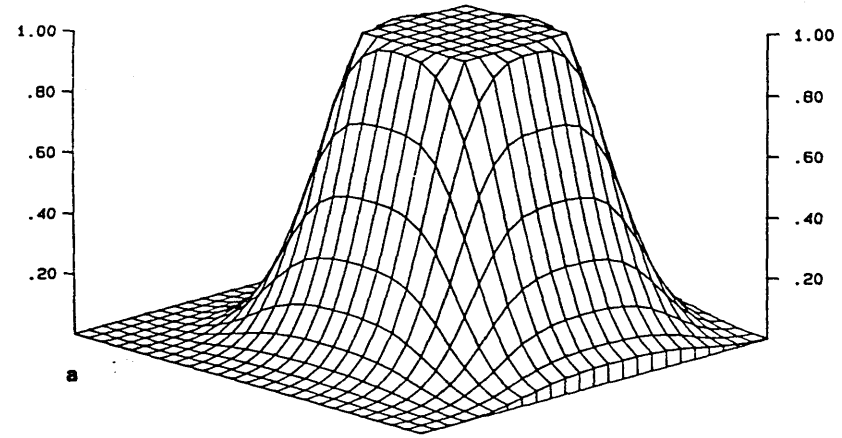
1.00
.80
.60
.40
.20
1.00
.80
.60
.40
.20
a

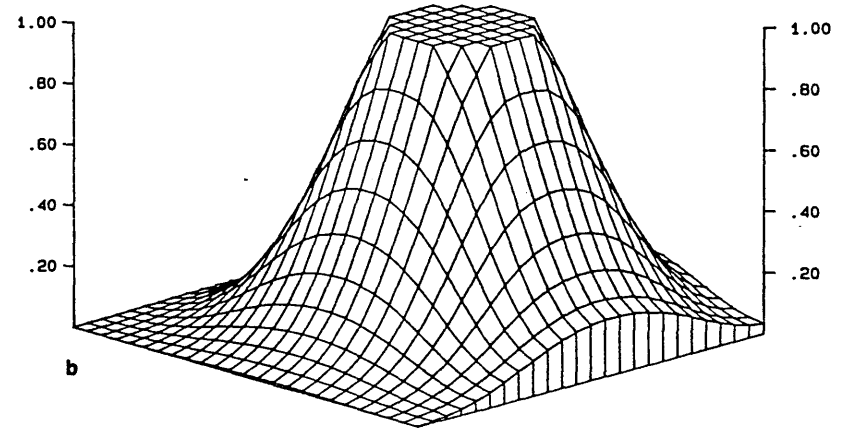
1.00
.80
.60
.40
.20
1.00
.80
.60
.40
.20
b

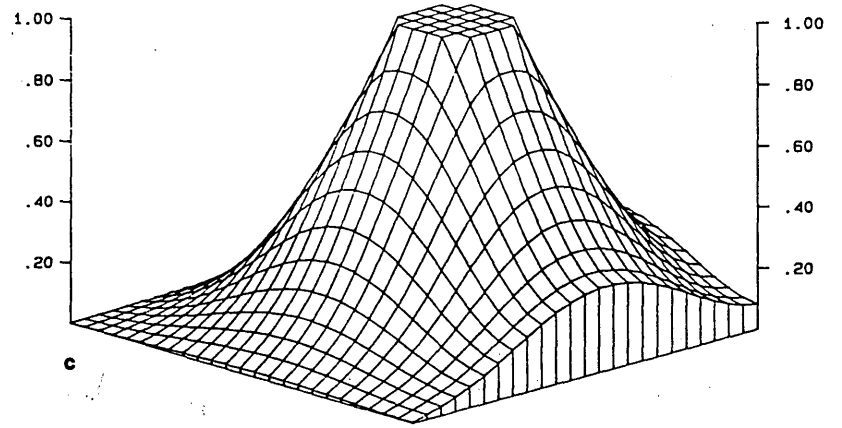
1.00
.80
.60
.40
.20
1.00
.80
.60
.40
.20
c

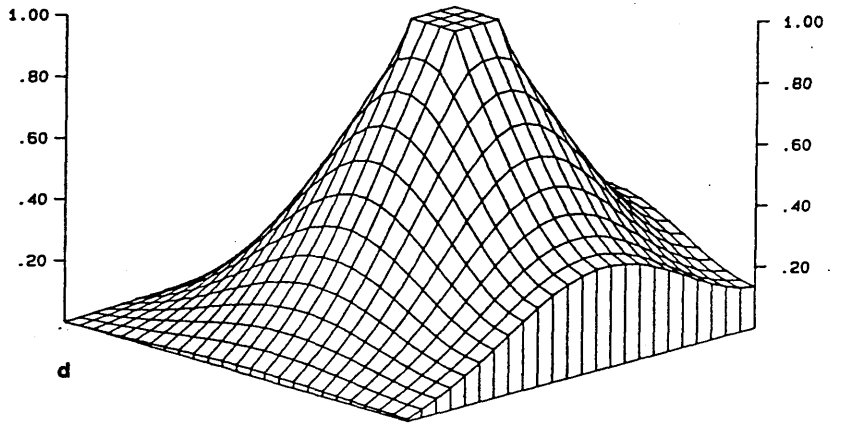
1.00
.80
.60
.40
.20
1.00
.80
.60
.40
.20
d

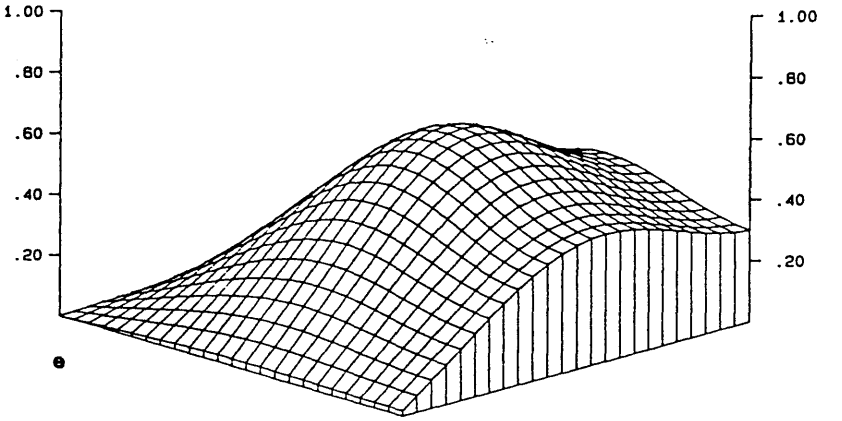
1.00
.80
.60
.40
.20
1.00
.80
.60
.40
.20
e

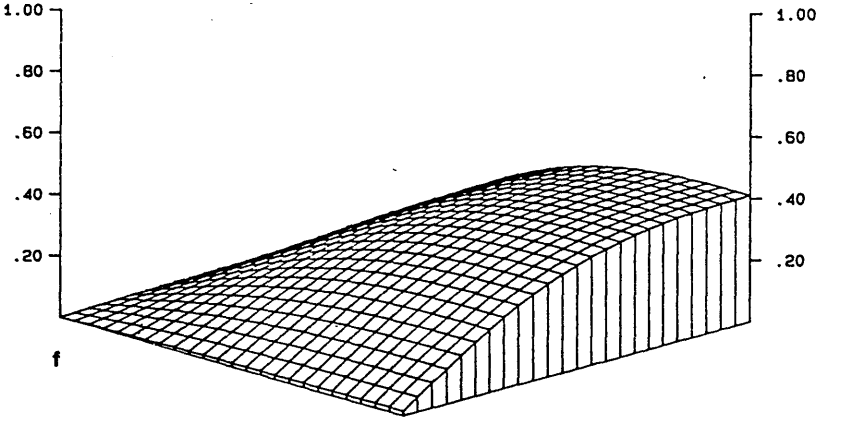
1.00
.80
.60
.40
.20
1.00
.80
.60
.40
.20
f

FIGURE 6.12.

Plot of release kinetics compared for three different distributions of material, and loading above solubility limit.

Parameters of sheet modelled were side 0.2cm, depth 0.2cm and diffusion coefficient $2.0 \times 10^{-7} cm^2 s^{-1}$. Fractional release from sheet edges q/q_o, where q_o is amount of diffusant in uniformly loaded sheet at 0.1M, plotted against time in seconds.

Curve 1, release for sheet with spot in each corner at 0.43M (saturation concentration).

Curve 2, release for sheet with spot in each corner at 1.5 times saturation loading, therefore with degree of crystallisation.

Curve 3 (broken), analytical solution for release from square sheet uniformly at 0.1M into infinite bath, eqn(5.10).

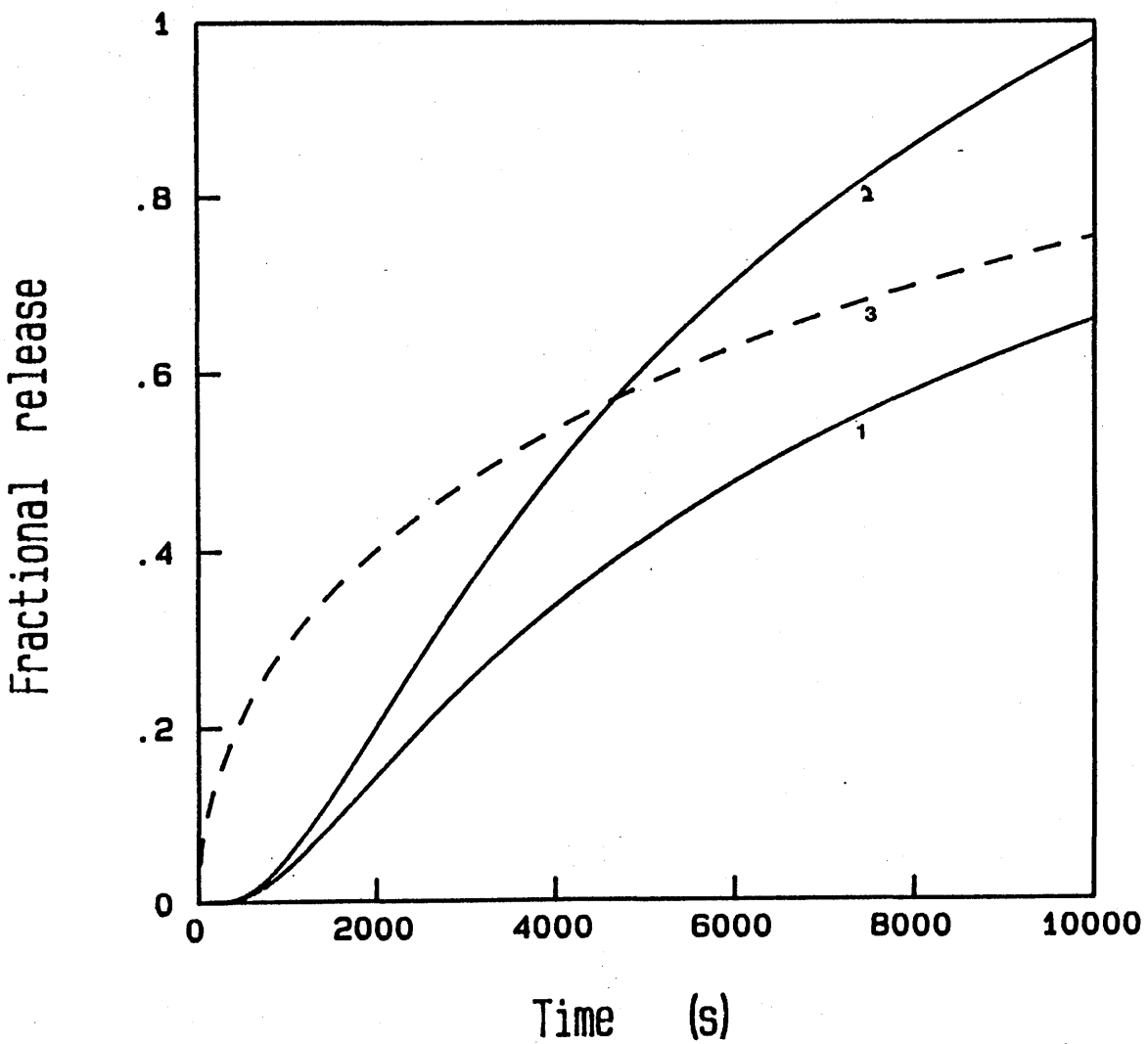
Fractional release
1
.8
.6
.4
.2
0
0
2000
4000
6000
8000
10000
Time (s)
2
3
1

TABLE 6.1.

Table of computed results for edge effects.

The edge effects were computed for a cylindrical disc membrane, exposed radius, r_e, 2.604cm, and diffusion coefficient $3.0x10^{-3}cm^2s^{-1}$, with a source concentration, c_{se}, 1M. The disc thickness 1, and total radius, r_o were varied to give several examples.

Radius ratio is $(r_o - r_e)/r_e$.

J_o, theoretical flux allowing no flow into the clamped volume.

J_e, simulated flux using the bond graph model for an edge effect.

J'_e predicted flux by analytical method of Barrer et al, (J of eqn(6.2), [3]).

cylinder length	radius ratio	J o	J e	J' e
6.67	0.118	4.5	5.5	5.5
6.67	0.486	4.5	8.0	7.7
10	0.118	3.0	3.7	3.7
10	0.486	3.0	5.7	5.54
13.33	0.486	2.25	4.45	4.33

TABLE 6.2.

Table of fractional release data, (q/q_o) compared for three different initial distributions of material, maximum loading 0.1M in all.

Parameters of sheet modelled were side 0.2cm, depth 0.2cm and diffusion coefficient $2.0 \times 10^{-7} cm^2 s^{-1}$. q_o is the amount of diffusant in sheet in uniformly loaded sheet at time zero, times are in seconds.

Column 1, data for release from edges of square sheet with initial uniform concentration at 0.1M into infinite bath calculated from analytical solution, eqn(5.10).

Column 2, data for sheet at 0.1M with isolated voids, (figs(6.8)).

Column 3, data for square sheet at zero with spots of 0.1M concentration, (figs(6.7)).

Column 4, data of columns 2 and 3 added using full precision of results.

Time(s)	1	2	3	Sum
250	0.153	0.146	0.005	0.151
500	0.213	0.196	0.016	0.212
750	0.257	0.230	0.027	0.257
1000	0.294	0.257	0.036	0.294
1250	0.325	0.281	0.044	0.325
1500	0.353	0.302	0.051	0.353
1750	0.378	0.321	0.057	0.378
2000	0.400	0.338	0.063	0.401
2250	0.421	0.354	0.068	0.422
2500	0.441	0.369	0.073	0.442
2750	0.459	0.383	0.078	0.460
3000	0.476	0.396	0.082	0.478
3250	0.493	0.408	0.086	0.494
3500	0.508	0.419	0.090	0.510
3750	0.523	0.430	0.094	0.524
4000	0.536	0.441	0.097	0.538
4250	0.550	0.451	0.101	0.552
4500	0.562	0.461	0.104	0.564
4750	0.575	0.470	0.107	0.577
5000	0.586	0.479	0.110	0.588

REFERENCES FOR CHAPTER SIX.

[1]. J.Crank. The Mathematics of Diffusion, Clarendon Press, Oxford, England (1959).

[2]. R.Paterson and P.Doran. J. Membrane Sci. **26**, (1986) 289.

[3] R.M. Barrer, J.A.Barrie and M.G.Rogers, Trans. Faraday Soc. **58**, (1962) 2473.

[4] J.C Jaeger and A.Beck. Brit. J. Appl. Physics. **6**, (1955) 15.

[5]. R.Paterson and Lutfullah. J. Membrane Sci. **23**, (1985) 59.

[6]. N.B. Graham, M.E. McNeill and A. Rashid. J. Controlled Release. **2**, (1985) 231.

CHAPTER SEVEN

A BOND GRAPH FOR THREE DIMENSIONAL DIFFUSION.

7.1 INTRODUCTION

Many important diffusion problems especially those in nature have total assymetry either in geometry or in diffusional properties. Even man made devices which have symmetrical design may be placed in environments which degrade the symmetry of the diffusional problem. The modelling of these systems requires theory for the description of diffusional flow in three dimensions. In this chapter a bond graph model for three dimensional diffusion is developed and tested for one simple case. On the basis of this bond graph it should be possible to address all diffusion phenomena.

7.2 DEVELOPMENT AND TESTING OF A THREE DIMENSIONAL BOND GRAPH.

The development of the bond graph for three dimensional diffusion is very similar to that described in detail for 2D systems in Chapter 5. Similarly to the bond graph model for the release from the edges of a plane sheet this new three dimensional bond graph is tested against the analytical solution of a simple example.

7.2.1 Three dimensional bond graph.

Any three dimensional shape is considered in this treatment as a three dimensional array of rectangular volume elements. These are the lumps of the 3D model and all flows within the system are planar. Diffusion through all six faces of each lump is now considered, (in the 2D model of a plane sheet only flows through four of the lump faces were simulated). Fig(7.1) shows the layout of the bond graph for this lump array and for clarity only the 1-

and 0- junctions with connecting power bonds have been shown. The broken line on this figure outlines the volume of a single lump. The capacitance of each volume element or lump is represented by a single capacitor located at the volume centre. Resistance to diffusion between the lump volume centres is represented by a resistor located on the faces between adjoining lumps. This graph may be regarded as a small portion of a much larger R-C network which extends in each direction and effectively models the Universe. This is a similar philosophy to that used in the development of the R-C plane model for 2D diffusion systems. By direct analogy with the 2D model, closed three dimensional diffusion systems may be defined within this bond graph by a (now three dimensional) wall of infinite resistances. This is an extremely powerful model as the system under study may be of any shape and the resistances to diffusion may be different in all directions.

The 0-junctions connecting the capacitors of each lump in the network are now 7-port devices as each lump has now 6 neighbours. Four of these are adjacent in the x and y directions, as in the two dimensional model, the other two are now above and below in the z direction. Therefore we need consider one other classification of resistor, that which accounts for resistance to flow parallel to the third, z axis. Following from the labelling used in the bond graph for two dimensional diffusion, these are classified as R′′′.

7.2.2 Characteristic state-space equations.

By defining the thermodynamic system under study as an isolated bond graph within the larger R-C network, it is ensured that every capacitor within the system has six neighbours and therefore a single characteristic state space equation may be applied to all.

To derive the state space equation for this model the R and C units are labelled in an analogous way to that employed for the 2D bond graph. The position of each of the capacitors is now given by a set of x, y, and z coordinates. The R′ and R′′ resistors are labelled relative to the grid defined by the capacitors as in the two dimensional model. R′ resistors are given the coordinates of the adjacent capacitor with the lowest y value, R′′ are labelled by the adjacent capacitor coordinates with the lowest x value. In a consistent manner, the R′′′ resistors have the coordinates of the adjacent capacitor with the lowest z value. This also translates into a computer algorithm with the minimum necessary array storage for the R, C, and q values.

It can be seen from fig(7.1) that this bond graph model may also be regarded as a network of R-C chains, running through the 3D matrix at right angles. By analogy with the 2D bond graph the flow into each capacitor is given as the sum of the net flows from each direction, eqn(7.1). This characteristic state space equation can be derived from a full analysis of the bond graph for three dimensional diffusion.

$$\dot{q}_{x,y,z} = -\left\{ \left(C^{-1}_{x,y,z} R''^{-1}_{x-1,y,z} + C^{-1}_{x,y,z} R''^{-1}_{x,y,z}\right) q_{x,y,z} + \left(\left(C^{-1}_{x-1,y,z} R''^{-1}_{x-1,y,z}\right) q_{x-1,y,z} + \left(C^{-1}_{x+1,y,z} R''^{-1}_{x,y,z}\right) q_{x+1,y,z}\right) \right\}$$

$$- \left\{ \left(C^{-1}_{x,y,z} R'^{-1}_{x,y-1,z} + C^{-1}_{x,y,z} R'^{-1}_{x,y,z}\right) q_{x,y,z} + \left(\left(C^{-1}_{x,y-1,z} R'^{-1}_{x,y-1,z}\right) q_{x,y-1,z} + \left(C^{-1}_{x,y+1,z} R'^{-1}_{x,y,z}\right) q_{x,y+1,z}\right) \right\}$$

$$- \left\{ \left(C^{-1}_{x,y,z} R'''^{-1}_{x,y,z-1} + C^{-1}_{x,y,z} R'''^{-1}_{x,y,z}\right) q_{x,y,z} + \left(\left(C^{-1}_{x,y,z-1} R'''^{-1}_{x,y,z-1}\right) q_{x,y,z-1} + \left(C^{-1}_{x,y,z+1} R'''^{-1}_{x,y,z}\right) q_{x,y,z+1}\right) \right\} \qquad (7.1)$$

This gives the flow into the capacitor $C_{x,y,z}$, as a function of the resistances (R), capacitances (C), and charges (q) of the six neighbouring lumps only. The braces in eqn(7.1) contain the net flow components from each direction, and so the analogy with the corresponding equation for the 2D bond graph, eqn(5.2), may be more

easily made. Despite the apparent complexity of this equation it may be restated in an identical form to the state space equations for the 1D and 2D models, eqn(7.2). (Compare with eqn(5.3).)

$$\dot{q}_{x,y,z} = \frac{dq_{x,y,z}}{dt} = -m_1 q_{x,y,z} + m_2 \qquad (7.2)$$

The coefficients m_1 and m_2 have yet more terms, eqns(7.3) and (7.4).

$$\begin{aligned} m_1 = \Big\{ & \left(C^{-1}_{x,y,z} R''^{-1}_{x-1,y,z} + C^{-1}_{x,y,z} R''^{-1}_{x,y,z}\right) \\ & + \left(C^{-1}_{x,y,z} R'^{-1}_{x,y-1,z} + C^{-1}_{x,y,z} R'^{-1}_{x,y,z}\right) \\ & + \left(C^{-1}_{x,y,z} R'''^{-1}_{x,y,z-1} + C^{-1}_{x,y,z} R'''^{-1}_{x,y,z}\right) \Big\} \end{aligned} \qquad (7.3)$$

$$\begin{aligned} m_2 = & \left(C^{-1}_{x-1,y,z} R''^{-1}_{x-1,y,z}\right) q_{x-1,y,z} \\ & + \left(C^{-1}_{x+1,y,z} R''^{-1}_{x,y,z}\right) q_{x+1,y,z} + \left(C^{-1}_{x,y-1,z} R'^{-1}_{x,y-1,z}\right) q_{x,y-1,z} \\ & + \left(C^{-1}_{x,y+1,z} R'^{-1}_{x,y,z}\right) q_{x,y+1,z} + \left(C^{-1}_{x,y,z-1} R'''^{-1}_{x,y,z-1}\right) q_{x,y,z-1} \\ & + \left(C^{-1}_{x,y,z+1} R'''^{-1}_{x,y,z}\right) q_{x,y,z+1} \end{aligned} \qquad (7.4)$$

By regarding the coefficients m_1 and m_2 as constant over a small step time increment H, we can immediately write down the updated charge in each capacitor x,y,z after

time H, $q^{H}_{x,y,z}$ by direct analogy with eqn(1.44), eqn(7.5). (See Section 1.3.8.)

$$q^{H}_{x,y,z} = \frac{m_2 - \exp(-Hm_1).(-m_1 q_{x,y} + m_2)}{m_1} \qquad (7.5)$$

This is an extremely important result since despite the apparent complexity of the state space equation, the numerical analysis based on the bond graph model can be decribed by a single exponential operator, eqn(7.5), equivalent to that used for the 1D and 2D models. This operator must now be moved around the three dimensional network of capacitors to obtain a new 3D concentration profile after time H. This cycle is repeated to produce an animation of the diffusion process in three dimensional space.

7.2.3 R and C values for a rectangular box.

Although any three dimensional shape may be modelled, it must be made up of an array of rectangular boxes since the volume elements of the N_x X N_y X N_z bond graph are of rectangular geometry. Therefore it is only necessary to formulate the R and C units in the 3D bond graph for a single rectangular system.

All flows between adjacent lump volumes are planar and therefore the resistances for this model are derived from the general equation for planar resistance in a Fickian model, eqn(2.9). The explicit definition of these in terms of system parameters follows directly from the example of the plane sheet model in Section 5.3.1. Eqns(7.6) to (7.8) give the resistances R′, R′′ and R′′′, for the three

dimensional bond graph and, as for the plane sheet model, these are functions of the system's dimensions; the length, width and depth of the box, l, w, and d respectively, and the degree of reticulation imposed in each direction, n_x, n_y and now n_z. D and α are, as elsewhere in this thesis, the diffusion and distribution coefficients respectively.

$$R' = \frac{n_z\, n_x\, w}{n_y D\, l\, d\, \alpha} \qquad (7.6)$$

$$R'' = \frac{n_z\, n_y\, l}{n_x D\, w\, d\, \alpha} \qquad (7.7)$$

$$R''' = \frac{n_x\, n_y\, d}{n_z D\, l\, w\, \alpha} \qquad (7.8)$$

Resistors on the faces of the box adjacent to an external well stirred solution have half the resistances of those on faces between lumps.

The capacitance of a single lump is, as for any Fickian model, the lump volume, v, scaled by the distribution coefficient, eqn(2.12). This may be related to the total volume of the rectangular box divided by the number of lumps used to model it, eqn(7.9).

$$C = \frac{\alpha\, l\, w\, d}{n_x n_y n_z} \qquad (7.9)$$

7.2.4 Simulation of diffusion from a cube into an infinite bath.

The simplest three dimensional problem which may be considered is the diffusion from an initially uniform concentration within a cube into an infinite bath, with release through all six faces. As this system is highly symmetric and the boundary conditions are simple, the analytical solution for release into an infinite bath is simply the cube of the analogous one dimensional problem, [1], [2], eqn(7.10).

$$\frac{q}{q_o} = 1 - \left(\sum_{k=0}^{\infty} \frac{8}{(2k+1)^2 \pi^2} \exp\left(\frac{D(2k+1)^2 \pi^2 t}{l^2} \right) \right)^3 \qquad (7.10)$$

Where q is once more the amount of diffusant released into the collecting bath at time t, as a fraction of initial loading in the cube, q_o. l is the length of side of the cube (l = w = d).

To validate this bond graph model of three dimensional diffusion the release from this system with these initial conditions was simulated. Due to symmetry it is necessary to simulate the release from only one of the eight corners of the cube. The system parameters of the plane sheet model in section 5.3.2 were used once more, that is a cube of side 0.2cm with diffusion coefficient $2.0 \times 10^{-7} cm^2 s^{-1}$. The initial set of q values were calculated

for a uniform initial loading, q_o, eqn(7.11).

$$q_{x,y,z} = \frac{q_o}{8\ n_x n_y n_z} \tag{7.11}$$

And for a cube $n_x = n_y = n_z$.

In an n_x X n_y X n_z model of release from the three faces of a corner there are $n_x.n_y + n_y.n_z + n_x.n_z$ lump faces contacting the external solution and therefore this number of collecting capacitors in the bond graph. A 30 X 30 X 30 lump model of this system has, by simple calculation, 29700 capacitors in total. The computational effort required to simulate these three dimensional diffusion problems is quite high.

A step time for integration, H, 0.1s was used. The simulated diffusion into the collecting bath, (calculated by summing the charges on the solution capacitors), is shown for the th degree of reticulation in fig(7.2). Fractional release (q/q_o) is plotted against time in seconds. The imposed points giving the analytical solution, eqn(7.10), [1], [2], agree with the 30 X 30 X 30 bond graph model to within 1%. This data is tabulated for closer inspection in table 7.1. (The subroutine for integration of the 3D state-space equations is included for example in the Appendix, Section A.4.)

The evolution of the concentration profiles within the system may also be obtained from the $q_{x,y,z}$ values. The illustration of these is an interesting graphics problem as the data is now four dimensional. The most likely method

for displaying these is by section through the system, although this has not been attempted here.

7.3 CONCLUSIONS.

The potential for application of this bond graph model to uncoupled diffusion phenomena is unlimited. The techniques illustrated in Chapters 3 to 6 for solving a variety of diffusion problems with 1D and 2D diffusional symmetry may also be incorporated into this model. Therefore the simulation of an equally extensive range of phenomena with total assymetry is now possible.

FIGURE 7.1.

Section of N_x X N_y X N_z network.

This shows one central lump with six neighbours. For clarity much detail has been ommited, with only the 1- and 0-junctions with connecting power bonds drawn.

The broken line encloses the volume of the central lump.

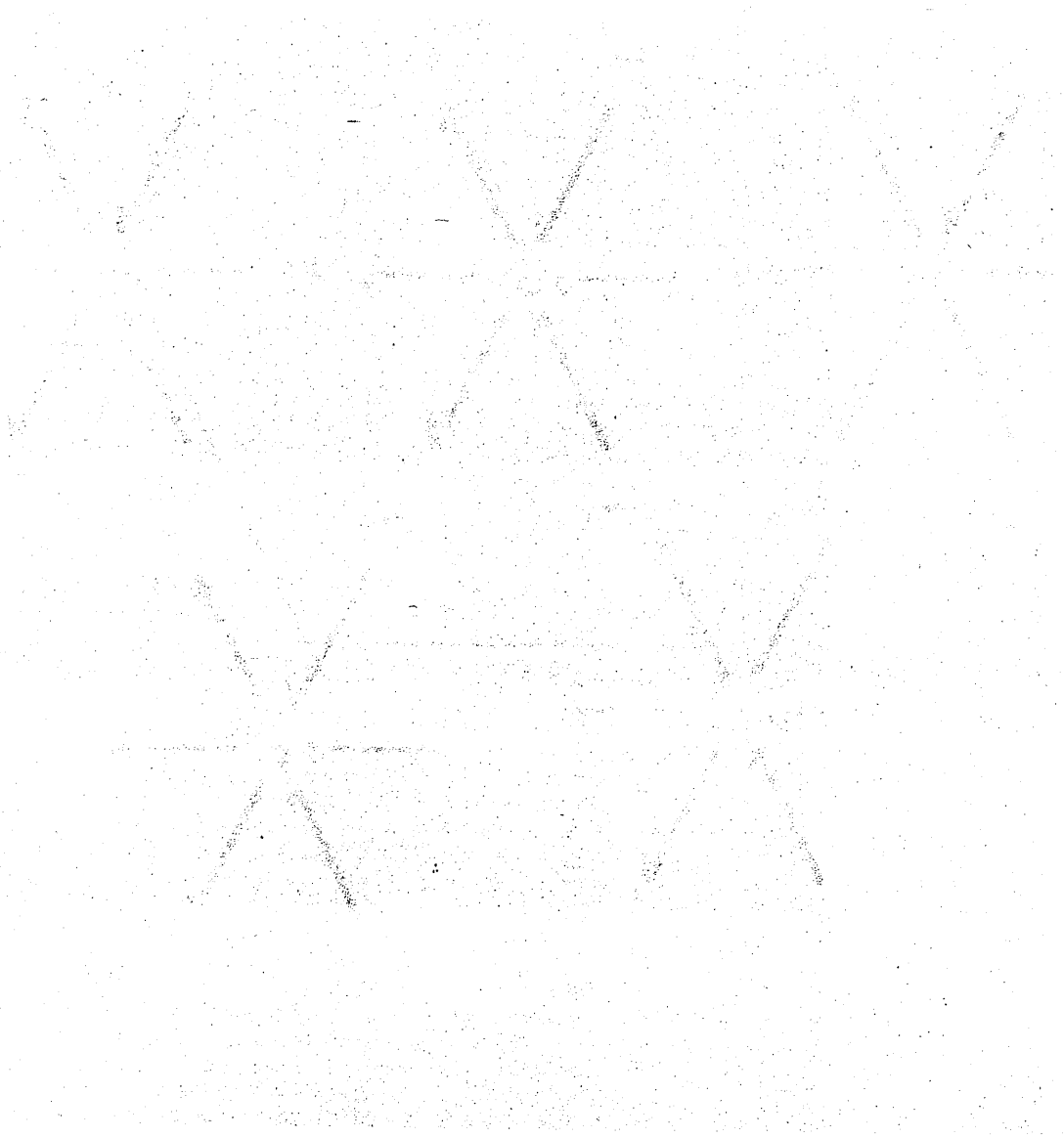

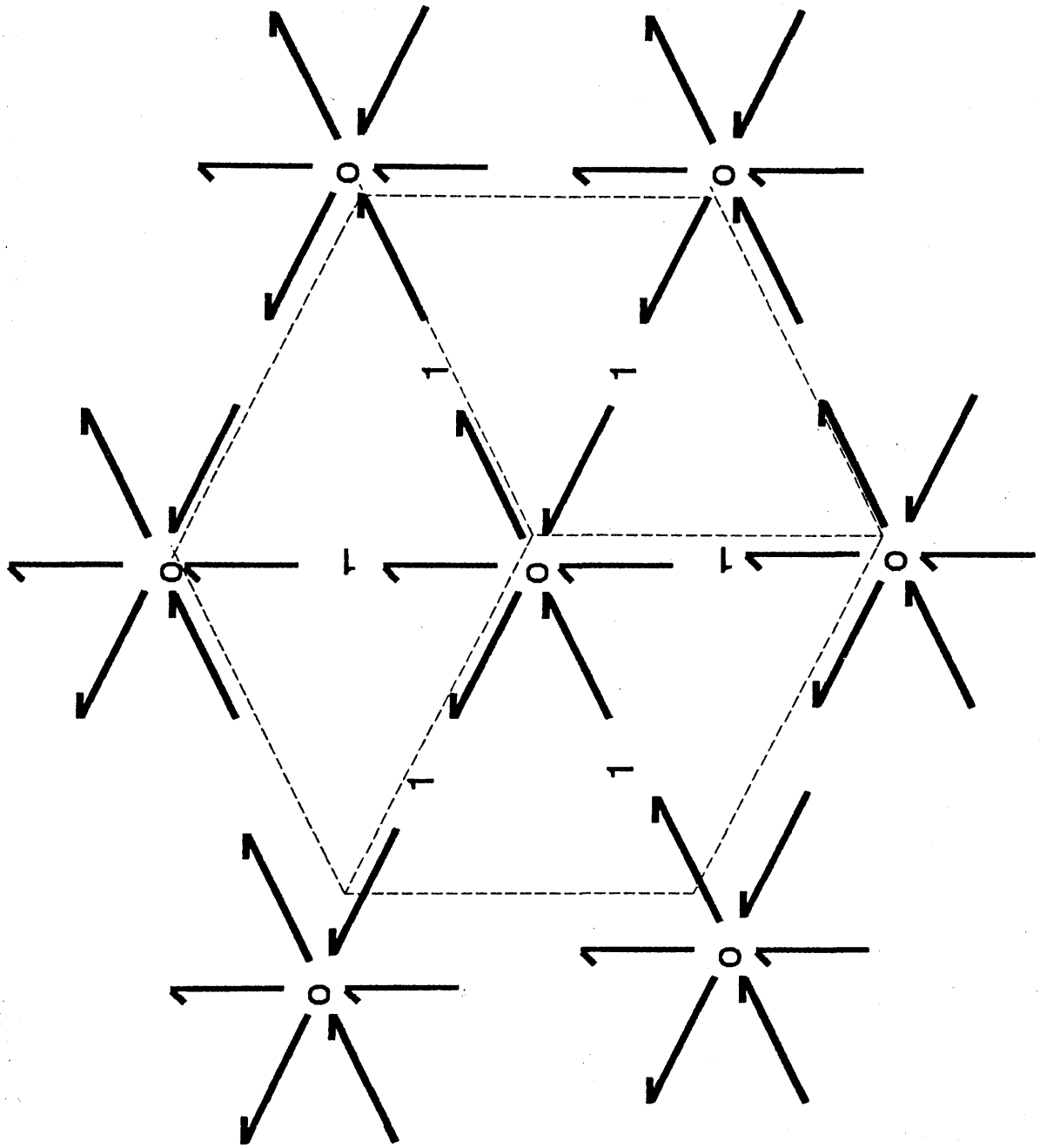

FIGURE 7.2.

Simulated efflux from all six faces of a cube.

Fractional release, q/q_o, plotted versus time in seconds. Three degrees of reticulation of the cube corner are compared to the analytical solution for release with infinite bath conditions, eqn(7.10) [1], [2]. Parameters of cube were: length of side, 1, 0.2cm and diffusion coefficient, D, $2.0 \times 10^{-7} cm^2 s^{-1}$. A step time of H, 0.1s was used in each case.

Points, analytical solution.

Less than 1% disparity is shown between 30 X 30 X 30 lump bond graph model and the mathematical prediction for release. Data presented in table(7.1).

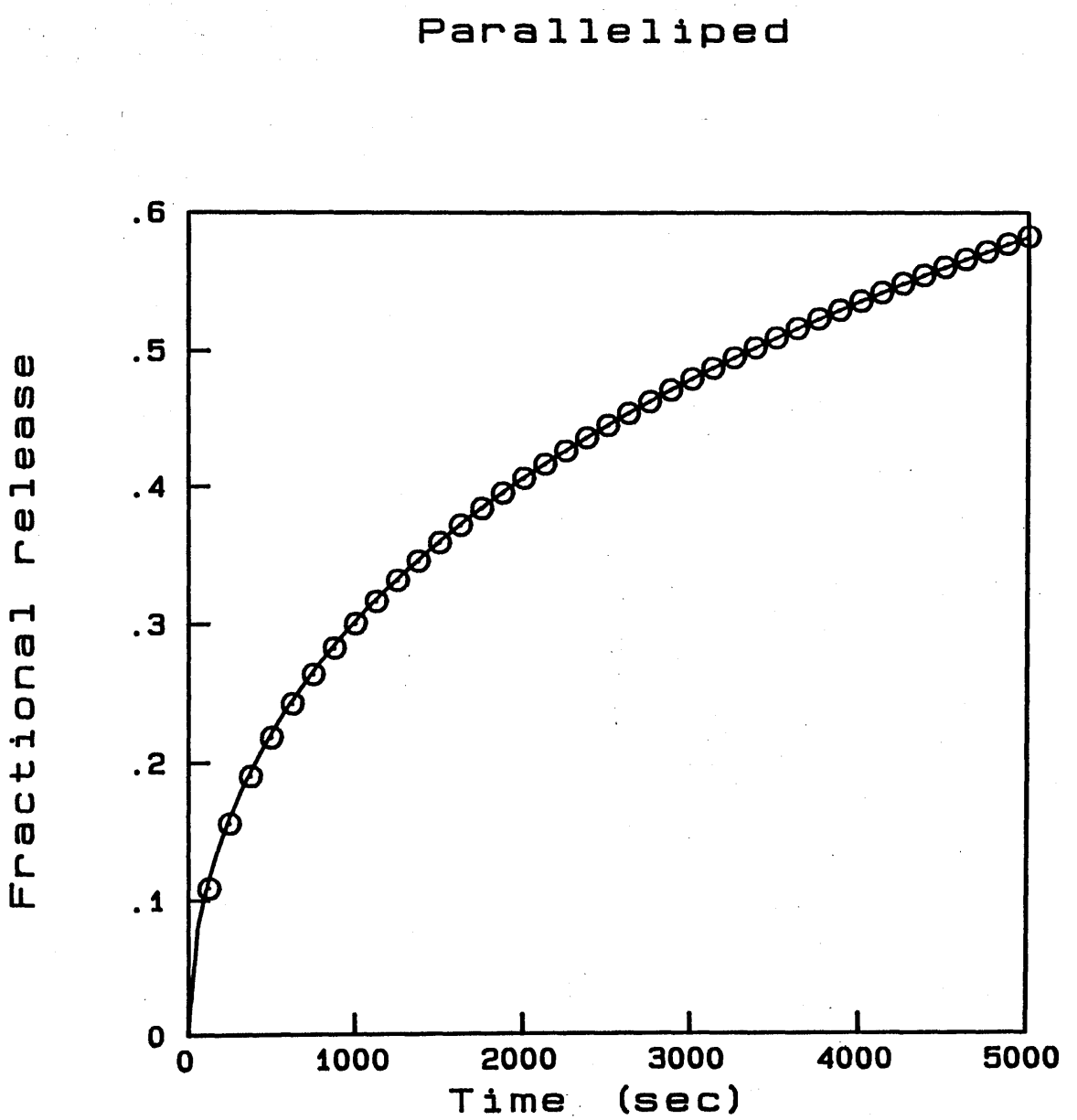
Paralleliped
Fractional release
.6
.5
.4
.3
.2
.1
0
0
1000
2000
3000
4000
5000
Time (sec)

TABLE 7.1

Comparison of bond graph results for release from all faces of a cube into an infinite bath with analytical solution, eqn(7.10), [1], [2]. (Data for fig(7.1).)

Fractional release (q/q_o) at time (s) is tabulated for 30 X 30 X 30 lump model of cube corner. Parameters of cube were: length of side 0.2cm and diffusion coefficient, D, $2.0x10^{-7}cm^2s^{-1}$. A step time for integration H, equal 0.1s was used.

Time(s)	Analytical	Simulation
200	0.138	0.133
400	0.192	0.189
600	0.232	0.230
800	0.265	0.264
1000	0.294	0.293
1200	0.319	0.319
1400	0.342	0.342
1600	0.363	0.363
1800	0.382	0.383
2000	0.400	0.401
2200	0.417	0.418
2400	0.433	0.434
2600	0.448	0.449
2800	0.463	0.464
3000	0.476	0.478
3200	0.489	0.491
3400	0.502	0.503
3600	0.514	0.516
3800	0.525	0.527
4000	0.536	0.538
4200	0.547	0.549
4400	0.557	0.559
4600	0.567	0.569
4800	0.577	0.579
5000	0.586	0.589

REFERENCES FOR CHAPTER SEVEN

[1] H.S.Carslaw and J.C.Jaeger. Conduction of Heat in Solids. Clarendon Press, Oxford, England (1959).

[2] J.Crank, The Mathematics of Diffusion, Clarendon Press, Oxford, England (1959).

APPENDIX.

FORTRAN LISTINGS.

A.1 Program for uni-divalent ion exchange simulation.

```
      PROGRAM UNIDIV
C-------------------------------------------------------------C
C    Ion-exchange bead model with limited bath conditions     C
C        ZB = 1,   ZA = 2,  ie UNIvalent, DIValent            C
C-------------------------------------------------------------C
C----------------C
C   Set up data  C
C----------------C
      IMPLICIT DOUBLE PRECISION (A - H, O - Z)
C... Shared areas of memory
      COMMON /BLOCK1/ QCAP, C, R, CBAR
      COMMON /BLOCK2/ NCAPS
      COMMON /BLOCK3/ INF
      COMMON /SYSPR1/ RADIUS, D, DBARA, DBARB, RDAB
      COMMON /SELECT/ DKAB
      COMMON /VALENC/ IZA, IZB
      COMMON /FIXEDC/ DNEGW

      PARAMETER (  PI = 3.14159265358979D+00, LMPMAX = 50,
     *             THIRD = 3.33333333333333D-01  )
C... Variables
      DOUBLE PRECISION QCAP(1:LMPMAX), C(1:LMPMAX),
     *                 R(1:LMPMAX), D(1:LMPMAX)
      CHARACTER FNAME*12, ANS*1
      INTEGER*4 NST
      INCLUDE 'C:®PROGRAMS®FORTPROG®IBMFIL.INC'
C
C---------------------C
C   Begin execution   C
C---------------------C
C... Format statements
  28  FORMAT (A)
  20  FORMAT (1PD25.17)
  21  FORMAT (I11)
C
C... Give meaningful names to some of the format statements
      ASSIGN 20 TO IDUB
      ASSIGN 21 TO ITGR
C... File name length
      ASSIGN 28 TO ICHAR
C
C... Display program information
      CALL DISPLY( '       PROGRAM FOR UNI-DIVALENT EXCHANGE'          )
      CALL DISPLY( '         ION A IS THE DIVALENT SPECIES'            )
      CALL DISPLY( 'CHARGES ARE WRITTEN OUT IN UNITS OF EQUIVALENCE' )
      CALL DISPLY( '  Exchange is from the A form to the B form'       )
      CALL DISPLY( ' The bead is initially entirely in the A form'    )
C
C... Concentration of fixed charges, (mmol per ml, ie molar)
      CALL DISPLY('ENTER CONCENTRATION OF FIXED CHARGE (mmol/cm3) : ')
      READ (5,*) CBAR
C... Sign of fixed charge
C 91  CALL DISPLY('ENTER SIGN OF FIXED CHARGE ( 1 / -1 ) : ')
C     READ (5,*) NEGW
C     IF ( ( NEGW * NEGW ) .NE. 1 ) GOTO 91
C     DNEGW = DBLE( - NEGW )
C
      DNEGW = 1.0D+00
C
C... Valencies
C     CALL DISPLY( 'ENTER VALENCY OF ION A : ')
```

```
C      READ (5,*) IZA
C      CALL DISPLY( 'ENTER VALENCY OF ION B : ')
C      READ (5,*) IZB
       IZA = 2.0D+00
       IZB = 1.0D+00
C
C... Radius of bead (cm)
       CALL DISPLY('RADIUS OF SPHERE (cm) : ')
       READ (5,*) RADIUS
C
C... Diffusion coefficient of ion a (cm squared per second)
       CALL DISPLY('DIFFUSION COEFFICIENT OF A IN BEAD (cm2/sec) : ')
       READ (5,*) DBARA
C... Diffusion coefficient of ion b (cm squared per second)
       CALL DISPLY('DIFFUSION COEFFICIENT OF B IN BEAD (cm2/sec) : ')
       READ (5,*) DBARB
C
C... Volume of collecting capacitor (cm cubed)
       CALL DISPLY('VOLUME OF LIMITED BATH (cm3) : ')
       READ (5,*) VOUT
C
C... Concentration of ion b in bath (molar)
       CALL DISPLY(
     *       'CONCENTRATION OF ION B IN THIS VOLUME (mmol/cm3) : ')
       READ (5,*) CBATH
C
C... Selectivity coefficient
       CALL DISPLY('THE SELECTIVITY COEFFICIENT IS CBARA')
       CALL DISPLY(' TIMES CB DIVIDED BY CBARB TIMES CA')
       CALL DISPLY('       ENTER VALUE : ')
       READ (5,*) DKAB
C
C... Number of lumps in model (must include the core also)
       CALL DISPLY('NUMBER OF LUMPS REQUIRED (The core is lump 1) : ')
       READ (5,*) NLUMPS
C... Total number of capacitors must include the collector
       NCAPS = NLUMPS + 1
C
C... File name to hold details of model
       CALL DISPLY('GIVE DETAILS FILE A NAME : ')
       READ (5,ICHAR) FNAME
C... Add directory path
       INF = IPATH // FNAME
C
C... Work out this value to save computing it later
       RDAB = 1.0D+00 / (DBARA * DBARB)
C
C... Total capacitance of bead
       TOTC = 4.0D+00 * PI * RADIUS * RADIUS * RADIUS * THIRD
C
       CALL DISPLY( 'Read in charges from a Q file (Y/N) ? ')
       READ (*,ICHAR) ANS
       IF (ANS.EQ.'Y'.OR.ANS.EQ.'y') THEN
         CALL DISPLY( 'Give Q filename : ')
         READ (*,ICHAR) FNAME
         OUTF = OPATH // FNAME
C...    Read charge profile, time and original loading
         CALL READLQ(OUTF,TIME,QB0)
         CALL DISPLY('Initial loading found to be : ')
         WRITE (6,*) QB0
       ELSE
         TIME = 0.0D+01
C...    Set initial charges, amount of b in bead at time zero
```

```
        QBBAR0 = 0.0D+00
C...    Convert concentration of b ib bath (mmol/ml) to charge (mmol)
        QB0 = CBATH * VOUT
C...    Set initial charges of ion b (mmol)
  11     DO 48 I=1, NLUMPS
  48       QCAP(I) = QBBAR0
         QCAP(NCAPS) = QB0
         CALL DISPLY('CHARGES ALL SET UP AND READY FOR SIMULATION')
       END IF
C
C... Compute R, C and individual D values in spherical model
      CALL RCBED2(NLUMPS,VOUT,QB0)
C
C... Record details on the specified file.
      OPEN (UNIT = 8, FILE = INF, ERR = 1010)
C... Be compatible with two dimensional models
      WRITE (8,ITGR) NLUMPS
      WRITE (8,ITGR) 1
      WRITE (8,IDUB) RADIUS
      WRITE (8,IDUB) DKAB
      WRITE (8,IDUB) DBARA
      WRITE (8,IDUB) DBARB
      WRITE (8,IDUB) TOTC
      WRITE (8,IDUB) VOUT
      WRITE (8,ITGR) NLUMPS
      WRITE (8,ITGR) 1
      CLOSE (8)
C
C... Step time (s)
      CALL DISPLY('STEP TIME FOR INTEGRATION : ')
      READ (5,*) H
C... Number of steps
      CALL DISPLY('NUMBER OF STEPS IN INTEGRATION : ')
      READ (5,*) NST
C... Number of steps between output to file
      CALL DISPLY('NUMBER OF STEPS BETWEEN OUTPUT TO FILE : ')
      READ (5,*) INC
C... The file to write the simulated charges to
      CALL DISPLY('GIVE OUTPUT FILE A NAME : ')
      READ (5,ICHAR) FNAME
C... Add directory path
      OUTF = OPATH // FNAME
C
C... Call integration proceedure (variable diffusion coefficient)
      CALL VARDP2(TIME,NST,H,INC,OUTF)
      STOP
C----------------------C
C    Error handling    C
C----------------------C
 1010 WRITE (6,1015) INF
 1015 FORMAT (1H1,'ERROR WHILST OPENING ',A30)
C... This is non standard
      PAUSE
      STOP
      END


      SUBROUTINE DISPLY(MESSGE)
C------------------------C
C  Output to the screen  C
C------------------------C
      CHARACTER MESSGE*(*)
   1  FORMAT (1H ,A)
```

```
      WRITE (6,1) MESSGE
      RETURN
      END


      SUBROUTINE RCBED2(NLUMPS,VOUT,QBO)
C-------------------------------------------------------------------C
C     Computes initial and updates R and C values for a sphere      C
C     D values must be given as inverse                             C
C     Also ZA = 2,   ZB = 1  is assumed                             C
C -------------------------------------------------------------------C
C-------------------C
C    Set up data    C
C-------------------C
C
      IMPLICIT DOUBLE PRECISION (A - H, O - Z)
C
      COMMON /BLOCK1/ QCAP, C, R, CBAR
      COMMON /BLOCK2/ NCAPS
      COMMON /SYSPR1/ RADIUS, D, DBARA, DBARB, RDAB
      COMMON /SELECT/ DKAB
      COMMON /VALENC/ IZA, IZB
      COMMON /FIXEDC/ DNEGW
      SAVE
C
      PARAMETER (   PI=3.14159265358979D+00,   LMPMAX = 50,
     *              THIRD=3.33333333333333D-01   )
C
C...  Set dimension for maximum of LMPMAX lumps.
      DOUBLE PRECISION QCAP(1:LMPMAX), C(1:LMPMAX),
     *                 R(1:LMPMAX), D(1:LMPMAX)
C
C-----------------------C
C    Begin execution    C
C-----------------------C
C
C... Declare reciprocal cube root as an inline function
      RCBRT(DI) = (1.0D+00 / (DI ** THIRD))
C
  1   FORMAT (A)
      IF ((IZA.NE.2).OR.(IZB.NE.1)) THEN
        WRITE (6,1) 'ERROR IN CHARGE VALUES FOR RCBED2'
        RETURN
      END IF
      DNL = DBLE(NLUMPS)
      RCNL = RCBRT(DNL)
      RVOUT = 1.0D+00 / VOUT
C
C... Make the valencies double precision for future use
      ZA = DBLE(IZA)
      ZB = DBLE(IZB)
      ZA2 = ZA * ZA
      ZB2 = ZB * ZB
C
C... Total volume of bead
      TOTC = 4.0D+00 * PI * (RADIUS ** 3.0D+00) / 3.0D+00
      RSC = DNL / TOTC
C
C... Remember initial B in collecting volume (ZB=1)
      ZBCBO = QBO * RVOUT
C
C... Set the capacitances
      DO 32 I=1, NLUMPS
```

```
 32     C(I) = RSC
C
      PAR = 4.0D+00 * PI * RADIUS * RCNL
C
C-----------------------------C
C   Subsequent entry point    C
C-----------------------------C
      ENTRY NEWRSP(NLUMPS)
C
C... Get the updated Diffusion coefficients of lumps in a sphere
      CALL NEWDSP(NLUMPS,ZA,ZB,ZA2,ZB2)
C
C... Compute new R values, lots of reciprocal cube roots
      DO 12 I=1, NLUMPS-1
        DI = DBLE(I)
        PA = RCBRT(DI - 5.0D-01) * D(I)
        PB = RCBRT(DI) * (D(I+1) - D(I))
        PC = RCBRT(DI + 5.0D-01) * D(I+1)
 12     R(I) = PAR / (PA + PB - PC)
C... Get the last value which has less terms
      R(NLUMPS) = PAR / (D(NLUMPS) * (RCBRT(DNL-5.0D-01) - RCBRT(DNL)))
C
C... Concentration of ion b in external solution (ZB = 1)
      ZBCB = QCAP(NCAPS) * RVOUT
      ZACA = ZBCB0 - ZBCB
      IF (ZACA.GT.0.0D+00) THEN
        U2 = ZBCB  /  ZACA
        U1 = DNEGW * CBAR / ZACA
        CALL LQADRT(DKAB,U2,-U1,ALPHA)
      ELSE
        ALPHA = CBAR / ZBCB0
      END IF
C     -----------------
C     -  Capacitance  -
C     -----------------
C... Inverse capacitance calculated for collector from
C...          alpha  /  Vout
      C(NCAPS) = ALPHA * RVOUT
      RETURN
      END


      SUBROUTINE LQADRT(A,B,C,ROOT1)
C... Returns largest root only
      IMPLICIT DOUBLE PRECISION (A - H, O - Z)
      RTWOA = 1.0D+00 / (2 * A)
      TEMP = SQRT( (B * B) - (4 * A * C) )
      ROOT1 = (-B + TEMP) * RTWOA
      ROOT2 = (-B - TEMP) * RTWOA
      IF (ROOT2 .GT. ROOT1)  ROOT1 = ROOT2
      RETURN
      END


      SUBROUTINE NEWDSP(NLUMPS,ZA,ZB,ZA2,ZB2)
C-------------------------------------------------------------C
C    Ion-exchange subroutine for finding mutual D values    C
C-------------------------------------------------------------C
C-------------------C
C    Set up data    C
C-------------------C
      IMPLICIT DOUBLE PRECISION (A - H, O - Z)
```

```
      COMMON /BLOCK1/ QCAP, C, R, CBAR
      COMMON /SYSPR1/ RADIUS, D, DBARA, DBARB, RDAB
      COMMON /FIXEDC/ DNEGW
      SAVE

C... Note  RDAB = (DBARA * DBARB) ** -1   ie reciprocal of DA times DB
C... DNEGW = - W where W equals the sign of the fixed charges
      PARAMETER (  LMPMAX=50  )

C... Set dimension for maximum of LMPMAX lumps.
      DOUBLE PRECISION QCAP(1:LMPMAX), C(1:LMPMAX),
     *                 R(1:LMPMAX), D(1:LMPMAX)
C
C----------------------C
C    Begin execution   C
C----------------------C
C... Compute concentrations and then mutual
C... D values (reciprocals) for each lump.
      DO 1 I=1, NLUMPS
        CONCB = QCAP(I) * C(I)
        CONCA = ((DNEGW * CBAR) - (ZB * CONCB)) / ZA
        CONCA = ZA2 * CONCA
        CONCB = ZB2 * CONCB
        D(I) = ( (DBARA * CONCA) + (DBARB * CONCB) )
     *       * RDAB / (CONCA + CONCB)
  1     CONTINUE
C
      RETURN
      END


      SUBROUTINE VARDP2(TIME,NST,H,INC,OUTF)
C-------------------------------------------------------------------C
C  This subroutine applies the definite integral to differntial    C
C  equations of type                                                C
C        dq(i)/dt   =   coeff(i,1)q(i-1)                            C
C        - coeff(i,2)q(i)   + coeff(i,3)q(i+1)   + par(nc)          C
C-------------------------------------------------------------------C
C-----------------C
C   Set up data   C
C-----------------C
      IMPLICIT DOUBLE PRECISION (A - H, O - Z)
      COMMON /BLOCK1/ QCAP,C,R,QZER
      COMMON /BLOCK2/ NCAPS
      COMMON /BLOCK3/ INF
      COMMON /VALENC/ IZA, IZB
      SAVE
      PARAMETER (NDB=1,NDT=50,ZERO=0.0D+01,NDTM1=49,NDBP1=2)
      DIMENSION QCAP(NDB:NDT),C(NDB:NDT),R(NDB:NDT), CFRONT(NDBP1:NDT),
     1          CBACK(NDB:NDTM1), QBACK(NDB:NDTM1),
     2          RFRONT(NDBP1:NDT), QFRONT(NDBP1:NDT),
     3          COEFF(NDB:NDT,1:3), PAR(NDB:NDT)
C
C... Set Qfront(i) = Qcap(i-1) from i=2 up to 50
C... Set also Qback(i) = Qcap(i+1) from i=1 to 49
C... same for the R and C values
      EQUIVALENCE (QCAP, QFRONT), (QCAP(2), QBACK),
     1            (C, CFRONT), (C(2), CBACK),
     2            (R, RFRONT)
      INTEGER*4 NST
      INCLUDE 'C:®PROGRAMS®FORTPROG®IBMFIL.INC'

C--------------------C
```

```
C   Begin execution   C
C---------------------C
  20  FORMAT (1PD25.17)
  21  FORMAT (I11)
  22  FORMAT (A30)
      ASSIGN 20 TO IDUB
      ASSIGN 21 TO ITGR
C
C... Set following parameters for output compatibility with other routines
      DATA NEDGE /0/
      PER = ZERO
      ZB = DBLE(IZB)
C
C... Number of lumps does not include collector
      NLUMPS = NCAPS - 1
C
C... Output run details to file
      OPEN (UNIT = 8, FILE = OUTF, ERR = 1010)
      WRITE (8,22) INF
      WRITE (8,ITGR) NST
      WRITE (8,IDUB) H
      WRITE (8,ITGR) INC
      WRITE (8,IDUB) QZER
      WRITE (8,IDUB) PER
      WRITE (8,ITGR) NEDGE
C
C... Compute number of times that output will be sent to file
      NSAVE = NINT(REAL(NST) / REAL(INC))
C... Time increment that this corresponds to
      TINC = DBLE(INC) * H
C
C...  Loop for each write to file
      DO 2 KK=1 , NSAVE
C
C...    Loop for number of steps between output
        DO 5 K=1, INC
C
C...      Calculate coefficients in differential eqn (see header notice)
C
C...      In front of q(i-1)
          DO 10 I=2, NCAPS
 10         COEFF(I,1) = CFRONT(I) * RFRONT(I)
C
C...      In front of q(i)
          DO 11 I=2, NLUMPS
 11         COEFF(I,2) = ( C(I) * RFRONT(I) ) + ( C(I) * R(I) )
          COEFF(1,2) = C(1) * R(1)
          COEFF(NCAPS,2) = C(NCAPS) * RFRONT(NCAPS)
C
C...      In front of q(i+1)
          DO 12 I=1, NLUMPS
 12         COEFF(I,3) = CBACK(I) * R(I)
C
C...      Pseudo constant
          PAR(1) = COEFF(1,3) * QBACK(1)
          DO 30 NC=2, NLUMPS
 30         PAR(NC) = ( COEFF(NC,1) * QFRONT(NC) )
     +                + ( COEFF(NC,3) * QBACK(NC) )
          PAR(NCAPS) = ( COEFF(NCAPS,1) * QFRONT(NCAPS) )
C
C...      Integrate flow for each capacitor (see differential equation)
          DO 3 NC=1, NCAPS
            FLOWT = PAR(NC) - ( QCAP(NC) * COEFF(NC,2) )
```

```
            IF ( ABS(FLOWT) .GT. ZERO ) THEN
              FNEW = FLOWT * EXP( -H * COEFF(NC,2) )
C...          Update charge
              QCAP(NC) = ( PAR(NC) - FNEW ) / COEFF(NC,2)
            END IF
  3         CONTINUE
C
C...      Update C and R values for sphere, this is an entry point
          CALL NEWRSP(NLUMPS)
C
C...      Next step
  5       CONTINUE
C
C...    Update time, output to file and then next block of times
        TIME = TIME + TINC
        WRITE (8,IDUB) TIME
        DO 2 NC=1, NCAPS
  2       WRITE (8,IDUB) QCAP(NC) * ZB
C
      CLOSE (8)
      RETURN
C-------------------C
C   Error handling  C
C-------------------C
 1010 WRITE (6,1015) OUTF
 1015 FORMAT (1H1,'ERROR WHILST OPENING ',A31)
      PAUSE
      STOP
      END
C
      SUBROUTINE READLQ(OUTF,TIME,QTOT)
      COMMON /BLOCK1/ QCAP, C, R, QBEG
      COMMON /BLOCK2/ NCAPS
      PARAMETER (NX=50)
      DOUBLE PRECISION QCAP(1:NX), TIME,
     * C(1:NX), R(1:NX), QBEG, QTOT
      INCLUDE 'C:®PROGRAMS®FORTPROG®IBMFIL.INC'
      OPEN (UNIT=9,FILE=OUTF,STATUS='OLD')
      READ (9,*) TIME
      READ (9,*) (QCAP(I), I=1, NCAPS)
C...  Sum charges
      QTOT = 0.0D+00
      DO 1 I=1, NCAPS
  1     QTOT = QTOT + QCAP(I)
      CLOSE (9)
      RETURN
      END
```

A.2 Program for swelling hydrogel simulations.

```
      PROGRAM TWHPF
C...  Release from swelling hydrogel simulation.
      IMPLICIT DOUBLE PRECISION (A - H, O - Z)
      COMMON /BLOCK1/ QCAP,C,R,QZER
      COMMON /BLOCK2/ NCAPS
      COMMON /BLOCK3/ INF
      COMMON /SWLPR1/ D,WC,XC,DMAX,DMIN
      COMMON /SYSPR1/ UNLEN,SCOEFF,AREA,CLOC
      COMMON /RATES/ RATE1,RATE2,HT
      EXTERNAL DPROWC, PFPRO
      DIMENSION QCAP(1:70),C(1:70)
     1,R(1:70),D(1:70),WC(0:140),XC(0:140)
      CHARACTER FNAME1*12 , FNAME2*12, ANS*1
      INCLUDE 'C:®PROGRAMS®FORTPROG®IBMFIL.INC'
C
C////////////////////////////////////////////////////////////////////////

C...  Initial parameters
C...  Minimum diffusion coefficient
      DMIN = 1.0D-17
C...  Time for system to reach half swollen state
      HT = 7200.0D+00
C...  Swelling coefficient
      SCOEFF = 2.0D+00
C...  Dry length
      CLEN  = .28D+00
C...  Dry area
      AREA = 2.75D+00
C...  Collecting capacitance
      COUT = 1.0D+03
      DCOEFF = DMIN
      NCOL = 1
C////////////////////////////////////////////////////////////////////////

C
      CALL DISPLY('NUMBER OF LUMPS REQUIRED ? ')
      READ (5,*) NLUMPS
C
C////////////////////////////////////////////////////////////////////////

C...  Calculate rest of parameters
      DNL = DBLE(NLUMPS) * 2.0D+00
      NCAPS = NLUMPS + 1
      NLT2 = NLUMPS * 2
      C(NCAPS) = 1.0D+00 / COUT
C...  Local capacitance of a lump
      CLOC = AREA * CLEN / DNL
C...  Diffusional path length of a dry lump
      UNLEN = CLEN / DNL
      WC(NLT2) = 1.0D+00
      XC(0) = 0.0D+00
C...  Guess at the rates
      RATE1 = CLEN * 5.0D-01 / HT
      RATE2 = 1.0D+00 / HT
C////////////////////////////////////////////////////////////////////////

C
  6   FORMAT (A12)
      CALL DISPLY('FILE NAME TO WRITE THESE DETAILS TO ? ')
      READ (5,6) FNAME1
      INF = IPATH//FNAME1
      CALL DISPLY('CREATING DETAILS FILE PLEASE WAIT')
      OPEN (UNIT = 7 , FILE = INF , ERR = 1000
     *  , STATUS = 'NEW' )
      NLY = 1
```

```
 15   WRITE (7,*) NLUMPS
      WRITE (7,*) NLY
      WRITE (7,*) CLEN
      WRITE (7,*) AREA
      WRITE (7,*) SCOEFF
      WRITE (7,*) DCOEFF
      WRITE (7,*) HT
      WRITE (7,*) COUT
      WRITE (7,*) NLUMPS
      WRITE (7,*) NCOL
      CLOSE (7)
 21   CALL PROEXP(WC(NLT2),SWLEN,SWAREA)
      SWLEN = SWLEN * DNL
      CSWELL = SWAREA * SWLEN
      CALL DISPLY('Incidentally fully swollen parameters are :')
      WRITE(6,78) SWLEN
 78   FORMAT (1H ,'Length of system : ',1PD25.17)
      WRITE(6,79) SWAREA
 79   FORMAT (1H ,'Area of system : ',1PD25.17)
      WRITE (6,80) CSWELL
 80   FORMAT (1H ,'Volume of system : ',1PD25.17)
      CALL DISPLY('NAME OF OUTPUT FILE ? ')
      READ (5,6) FNAME2
      OUTF = OPATH//FNAME2
      CALL DISPLY('INITIAL CHARGE IN SHEET ? ')
      READ (5,*) QZER
C...  Charge up with twice the required amount and avoid having to double
      QBEG = QZER / DBLE(NLUMPS)
      DO 9 NC=1 , NLUMPS
  9      QCAP(NC) = QBEG
      CALL DISPLY('NUMBER OF INCREMENTS IN TIME ? ')
      READ (5,*) NST
      CALL DISPLY('SIZE OF STEP TIME ? ')
      READ (5,*) H
      CALL DISPLY('HOW MANY STEP TIMES BETWEEN THE ')
      CALL DISPLY('RESULTS SAVED ON DISK ? ')
      READ (5,*) INC
C
      NL2 = NLT2 - 1
      TIME = 0.0D+01
C...  Hydrogel modified diffusion coefficient
      CALL DPROWH(NL2,NLUMPS)
      CALL NEWPOS(NLUMPS)
      CALL INTSW2(TIME,NST,H,INC,OUTF,DPROWH,PFPRO)
C
      CALL DISPLY('INTEGRATION COMPLETED')
      STOP
C
 1000 CALL DISPLY('WARNING '//INF//' EXISTS ALREADY')
 1013 CALL DISPLY('WRITE OVER (Y/N) ? ')
      READ (*,1015) ANS
 1015 FORMAT (A1)
      IF (ANS.EQ.'Y'.OR.ANS.EQ.'y') THEN
         OPEN (UNIT = 7 , FILE = INF)
         GOTO 15
      ELSE IF (ANS.EQ.'N'.OR.ANS.EQ.'n') THEN
         GOTO 21
      ELSE
         GOTO 1013
      END IF
      END

      SUBROUTINE INTSW1(TIME,NST,H,INC,OUTF,DFUN,WCFUN)
```

```
C...  This subroutine applies the definite integral .
C
      IMPLICIT DOUBLE PRECISION (A - H, O - Z)
      COMMON /BLOCK1/ QCAP,C,R,QZER
      COMMON /BLOCK2/ NCAPS
      COMMON /BLOCK3/ INF
      PARAMETER (NDB=1,NDT=70,ZERO=0.0D+01)
      DIMENSION QCAP(NDB:NDT),C(NDB:NDT),R(NDB:NDT)
     1,COEFF(NDB:NDT,1:3),PAR(NDB:NDT)
      LOGICAL FGTZ
      INCLUDE 'C:®PROGRAMS®FORTPROG®IBMFIL.INC'
C
  20  FORMAT (1PD25.17)
  21  FORMAT (I11)
  22  FORMAT (A30)
      ASSIGN 20 TO IDUB
      ASSIGN 21 TO ITGR
      DATA NEDGE,FSIGN /0,1.0D+00/
      PER = ZERO
      TINC = DBLE(INC) * H
      NLUMPS = NCAPS - 1
      NL2 = (NLUMPS * 2) - 1
C
C*****************************************************C
C***  Open and write initial data to output file  ***C
C*****************************************************C
      OPEN (UNIT = 8, FILE = OUTF, ERR = 1010)
      WRITE (8,22) INF
      WRITE (8,ITGR) NST
      WRITE (8,IDUB) H
      WRITE (8,ITGR) INC
      WRITE (8,IDUB) QZER
      WRITE (8,IDUB) PER
      WRITE (8,ITGR) NEDGE
      NSAVE = NINT(REAL(NST) / REAL(INC))
      DO 2 KK=1 , NSAVE
       DO 5 K=1, INC
C...    C and R are given as their inverse.
C...    R values are labelled from 1 and not zero!
        DO 10 I=2, NCAPS
 10      COEFF(I,1) = C(I-1) * R(I-1)
        DO 11 I=2, NLUMPS
 11      COEFF(I,2) = (C(I)*R(I-1)) + (C(I)*R(I))
        COEFF(1,2) = C(1) * R(1)
        COEFF(NCAPS,2) = C(NCAPS) * R(NLUMPS)
        DO 12 I=1, NLUMPS
 12      COEFF(I,3) = C(I+1) * R(I)
C...    Taking the QCAP values at the last step time
C...    calculate the constants PAR(NC); COEFF(NC,2)
C...    is the coeffecient before QCAP(NC) already calculated.
        PAR(1) = COEFF(1,3)*QCAP(2)
        DO 30 NC=2, NLUMPS
 30      PAR(NC) = (COEFF(NC,1)*QCAP(NC-1)) + (COEFF(NC,3)*QCAP(NC+1))
        PAR(NCAPS) = (COEFF(NCAPS,1)*QCAP(NLUMPS))
C
        DO 3 NC=1, NCAPS
C...     Calculate the flow at this time.
         FLOWT = PAR(NC) - (QCAP(NC) * COEFF(NC,2))
         FNEW = FLOWT * EXP(-H*COEFF(NC,2))
         QCAP(NC) = (PAR(NC) - FNEW) / COEFF(NC,2)
  3     CONTINUE
        CALL WCFUN(TIME,NL2)
        CALL DFUN(NL2,NLUMPS)
```

```
        CALL NEWPOS(NLUMPS)
  5     CONTINUE
        TIME = TIME + TINC
        WRITE (8,IDUB) TIME
        WRITE (8,IDUB) QCAP(NCAPS)
  2    CONTINUE
       CLOSE (8)
       RETURN
 1010 WRITE (6,1015) OUTF
 1015 FORMAT (1H1,'ERROR WHILST OPENING ',A31)
       PAUSE
       STOP
       END

       SUBROUTINE INTSW2(TIME,NST,H,INC,OUTF,DFUN,WCFUN)
C...   This subroutine applies the definite integral .
C
       IMPLICIT DOUBLE PRECISION (A - H)
       IMPLICIT DOUBLE PRECISION (O - Z)
       COMMON /BLOCK1/ QCAP,C,R,QZER
       COMMON /BLOCK2/ NCAPS
       COMMON /BLOCK3/ INF
       DIMENSION QCAP(1:70),C(1:70),R(1:70)
      1,COEFF(1:70,1:3),PAR(1:70)
       PARAMETER (ZERO=0.0D+01)
       INCLUDE 'C:®PROGRAMS®FORTPROG®IBMFIL.INC'
C
  20   FORMAT (1PD25.17)
  21   FORMAT (I11)
  22   FORMAT (A30)
       ASSIGN 20 TO IDUB
       ASSIGN 21 TO ITGR
       DATA NEDGE,FSIGN /0,1.0D+00/
       PER = ZERO
       TINC = DBLE(INC) * H
       NCM1 = NCAPS - 1
       NL2 = (NCM1 * 2) - 1

C
C*****************************************************C
C***  Open and write initial data to output file  ***C
C*****************************************************C
       OPEN (UNIT = 8, FILE = OUTF, ERR = 1010)
       WRITE (8,22) INF
       WRITE (8,ITGR) NST
       WRITE (8,IDUB) H
       WRITE (8,ITGR) INC
       WRITE (8,IDUB) QZER
       WRITE (8,IDUB) PER
       WRITE (8,ITGR) NEDGE
       WRITE (8,IDUB) TIME
       DO 7 I=1, NCAPS
   7    WRITE (8,IDUB) QCAP(I)
       NSAVE = NINT(REAL(NST) / REAL(INC))
       DO 2 KK=1 , NSAVE
        DO 5 K=1, INC
C...     C and R are given as their inverse.
C...     R values are labelled from 1 and not zero!
         DO 10 I=2, NCAPS
 10       COEFF(I,1) = C(I-1) * R(I-1)
         DO 11 I=2, NCM1
 11       COEFF(I,2) = (C(I)*R(I-1)) + (C(I)*R(I))
         COEFF(1,2) = C(1) * R(1)
```

```
        COEFF(NCAPS,2) = C(NCAPS) * R(NCM1)
        DO 12 I=1, NCM1
 12      COEFF(I,3) = C(I+1) * R(I)
C...    Taking the QCAP values at the last step time
C...    calculate the constants PAR(NC); COEFF(NC,2)
C...    is the coeffecient before QCAP(NC) already calculated.
        PAR(1) = COEFF(1,3)*QCAP(2)
        DO 30 NC=2, NCM1
         PAR(NC) = (COEFF(NC,1)*QCAP(NC-1))
     *             + (COEFF(NC,3)*QCAP(NC+1))
 30      CONTINUE
        PAR(NCAPS) = (COEFF(NCAPS,1)*QCAP(NCM1))
C
        DO 3 NC=1, NCAPS
C...     Calculate the flow at this time.
         FLOWT = PAR(NC) - (QCAP(NC) * COEFF(NC,2))
         FNEW = FLOWT * EXP(-H*COEFF(NC,2))
         QCAP(NC) = (PAR(NC) - FNEW) / COEFF(NC,2)
  3     CONTINUE
        CALL WCFUN(TIME,NL2)
        CALL DFUN(NL2,NCM1)
        CALL NEWPOS(NCM1)
  5    CONTINUE
       TIME = TIME + TINC
       WRITE (8,IDUB) TIME
       DO 6 I=1, NCAPS
  6     WRITE (8,IDUB) QCAP(I)
  2   CONTINUE
      CLOSE (8)
      RETURN
 1010 WRITE (6,1015) OUTF
 1015 FORMAT (1H1,'ERROR WHILST OPENING ',A31)
      PAUSE
      STOP
      END

      SUBROUTINE DPROWH(NL2,NLUMPS)
C...  Hydrogel type variable diffusion.
      IMPLICIT DOUBLE PRECISION (A - H, O - Z)
      COMMON /SWLPR1/ D,WC,XC,DMAX,DMIN
      COMMON /BLOCK2/ NCAPS
      DIMENSION D(1:70),WC(0:140),XC(0:140)
      I = 0
      DO 1 J=1, NL2, 2
        I = I + 1
        D(I) = ((WC(J) * 6.51) - 1.86D+00) * 1.0D-06
   1    IF (D(I).LT.0.0D+00) D(I) = DMIN
      D(NCAPS) = D(NLUMPS)
      RETURN
      END

      SUBROUTINE PROEXP(WC,XN,AR)
C-------------------------------------------------------C
C WC, water content fraction, XN, computed position,
C AR, computed average area of lump.
C     Works out the individual swellings for each dimension
C     on the basis of a proportional expansion
C-------------------------------------------------------C
      IMPLICIT DOUBLE PRECISION (A-H, O-Z)
C-----------------------------------------C
C X, present x position, SCOEFF, swelling
C coefficient, AREA, area of sheet, CLOC local
C capacitance.
```

```
C-----------------------------------------------C
      COMMON /SYSPR1/ X,SCOEFF,AREA,CLOC
      THIRD = 1.0D+00 / 3.0D+00
      Y = SQRT(AREA)
      SM1 = SCOEFF - 1.0D+00
C...  WC is input XN and AR are returned
C-----------------------------------------------C
C          Subsequent entry point               C
C                                               C
      ENTRY NEWDMS(WC,XN,AR)
      IF (WC.GT.0.0D+00) THEN
       VRATIO = 1.0D+00 + (WC * SM1)
       ALPHA = (VRATIO ** THIRD) - 1.0D+00
       XN = X + (ALPHA * X)
       AR = (Y + (ALPHA * Y)) ** 2.0D+00
      ELSE
       XN = X
       AR = AREA
      END IF
      RETURN
      END

      SUBROUTINE NEWPOS(NLUMPS)
      IMPLICIT DOUBLE PRECISION (A - H, O - Z)
      COMMON /BLOCK1/ QCAP,C,R,QZER
      COMMON /SWLPR1/ D,WC,XC,DMAX,DMIN
      COMMON /SYSPR1/ UNLEN,SCOEFF,AREA,CLOC
      DIMENSION QCAP(1:70),C(1:70)
     1,R(1:70),D(1:70),WC(0:140),XC(0:140)
C...  Establish origin at centre of system finding first RHS edge at XN
      CALL NEWDMS(WC(1),XN,AR)
      C(1) = 1.0D+00 / (XN * AR)
      XC(2) = XN
      CREM = XN
      XC(1) = XN * 5.0D-01
      ARL = AR
      DO 1 I=2, NLUMPS
       NN = 2 * I
       N = NN - 1
       CALL NEWDMS(WC(N),XN,AR)
C...   Individual capacitances calculated from swelling at centre
       C(I) = 1.0D+00 / (XN * AR)
C...   Calculate position of RHS edge of lump (add on length)
       XC(NN) = XN + CREM
       CREM = XC(NN)
C...   Calculate position of lump centre
       XC(N) = XC(NN) - (XN * 5.0D-01)
       CL = XC(N) - XC(N-2)
C...   Calculate resistance at LHS by averaging
       AVARD2 = (ARL + AR) * 2.5D-01
       R(I-1) = AVARD2 * (D(I) + D(I-1)) / CL
  1    ARL = AR
      R(NLUMPS) = AR * D(NLUMPS) / (XC(NN) - XC(N))
      RETURN
      END
```

A.3 Program for simulation of diffusion from limited cylinder.

```
      PROGRAM CYLINT
C...  Cylindrical matrix may be constructed for
C...  integration here or for another routine.
      IMPLICIT DOUBLE PRECISION (A - H)
      IMPLICIT DOUBLE PRECISION (O - Z)
      COMMON /BLOCK1/ QCAP,C,RH,RV,SEFF
      COMMON /BLOCK2/ NCAPS,XCAP,YCAP,NSOUR
      COMMON /BLOCK3/ INF
      COMMON /BLOCK4/ NEDGE
      CHARACTER FNAME*12,
     * INF*30, OUTF*31, ANS*1
      DOUBLE PRECISION QCAP(0:50,0:50,0:1)
     *,RH(0:50,0:50),RV(0:50,0:50),C(0:50,0:50)
      INTEGER X,Y
      INTEGER XCAP(1:2500),YCAP(1:2500)
      NEDGE = 0
      WRITE (*,30)
  30  FORMAT (1H1,'PROGRAM CYLINT COMPILED 1/4/1987')
  1   WRITE (*,2)
  2   FORMAT (1H ,'ARE MATRIX DETAILS STORED IN FILE (Y/N) ? ')
      READ (*,3) ANS
  3   FORMAT (A1)
      IF (ANS.EQ.'N'.OR.ANS.EQ.'n') THEN
         WRITE (*,4)
  4      FORMAT (1H ,'DETAILS FILE TO BE CREATED')
         WRITE (*,5)
  5      FORMAT (1H ,'GIVE FILE NAME ? ')
         READ (*,6) FNAME
         INF = 'C:®RESULTS®INDATA®'//FNAME
C...     Create cylindrical model from parameters.
C
         CALL CDETB
C
      ELSE IF (ANS.EQ.'Y'.OR.ANS.EQ.'y') THEN
         WRITE (*,7)
  7      FORMAT (1H1,'FILE NAME OF MATRIX DETAILS ? ')
         READ (*,6) FNAME
  6      FORMAT (A12)
         INF = 'C:®RESULTS®INDATA®'//FNAME
C...     Read in the details of the model.
         CALL READET
C
      ELSE
         GOTO 1
      END IF
      WRITE (*,8)
  8   FORMAT (1H ,'GIVE OUTPUT FILE A NAME ')
      READ (*,6) FNAME
      OUTF = 'C:®RESULTS®OUTDATA®'//FNAME
      WRITE (*,16)
 16   FORMAT (1H ,'NUMBER OF INCREMENTS IN TIME ? ')
      READ (*,*) NSTEPS
      WRITE (*,17)
 17   FORMAT (1H ,'SIZE OF STEP TIME ? ')
      READ (*,*) H
      WRITE (*,18)
 18   FORMAT (1H ,'HOW MANY STEP TIMES BETWEEN THE ')
      WRITE (*,19)
 19   FORMAT (1H ,'RESULTS SAVED ON DISK ? ')
      READ (*,*) INC
```

```
C
 11    WRITE (6,9)
  9    FORMAT (1H ,'READ Q VALUES FROM A QFILE ? ')
       ANS = ' '
       READ (5,3) ANS
       IF (ANS.EQ.'Y'.OR.ANS.EQ.'y') THEN
        WRITE (6,10)
 10     FORMAT (1H ,'GIVE FILE NAME : ')
        READ (5,6) FNAME
        CALL READQ(FNAME,TIME)
       ELSE IF (ANS.EQ.'N'.OR.ANS.EQ.'n') THEN
        TIME = 0.0D+01
       END IF
C
       CALL MATHIN(TIME,NSTEPS,H,INC,OUTF)
C
       WRITE (*,20)
  20   FORMAT (1HO,'INTEGRATION COMPLETED')
       STOP
       END


       SUBROUTINE MATHIN(TIME,NST,H,INC,OUTF)
C-------------------------------------------------C
C  This subroutine applies the definite integral  C
C  R and C values are supplied as their inverse.  C
C-------------------------------------------------C
C-----------------C
C   Set up data   C
C-----------------C
C
       IMPLICIT DOUBLE PRECISION (A - H, O - Z)
C
C... Shared areas of memory
       COMMON /BLOCK1/ QCAP,C,RH,RV,SEFF
       COMMON /BLOCK2/ NCAPS,XCAP,YCAP,NDUMY
       COMMON /BLOCK3/ INF
       COMMON /BLOCK4/ NEDGE
C
       DOUBLE PRECISION QCAP(0:50,0:50,0:1),CR(1:2500)
      *,RH(0:50,0:50),RV(0:50,0:50),C(0:50,0:50),EXC(1:2500)
C
       INTEGER XCAP(1:2500),YCAP(1:2500)
C
       INTEGER X, Y, XP1, YP1, XM1, YM1
C
C... Include IBM type files (replace for other computers)
       INCLUDE 'C:®PROGRAMS®FORTPROG®IBMFIL.INC'
C
C---------------------C
C   Begin execution   C
C---------------------C
C
    10 FORMAT (1PD25.17)
    11 FORMAT (I11)
    12 FORMAT (A30)
       ASSIGN 10 TO IDUB
       ASSIGN 11 TO ITGR
C
       PERIOD = 0.0D+00
       DATA NOW, LAST /0, 1/
C
       OPEN (UNIT = 8 , FILE = OUTF , ERR = 1010)
```

```
      WRITE (8,12) INF
      WRITE (8,ITGR) NST
      WRITE (8,IDUB) H
      WRITE (8,ITGR) INC
      WRITE (8,IDUB) SEFF
      WRITE (8,IDUB) PERIOD
      WRITE (8,ITGR) NEDGE
      WRITE (8,IDUB) TIME
      WRITE (8,IDUB) ( QCAP(XCAP(NC),YCAP(NC),NOW), NC=1, NCAPS )
C
C---------------------------------------C
C CR coefficients (time independant here) C
C---------------------------------------C
      DO 20 NC=1, NCAPS
C
         X = XCAP(NC)
         Y = YCAP(NC)
C
     0   CR(NC) = RV(X,Y-1) * C(X,Y)
     1          + RH(X-1,Y) * C(X,Y)
     2          + RH(X,Y) * C(X,Y)
     3          + RV(X,Y) * C(X,Y)
C
         EXC(NC) = EXP(-H * CR(NC))
C
 20      CR(NC) = 1.0D+00 / CR(NC)
C
C...  Set up loop for each step time.
      NSAVE = NST / INC
C
      TINC = H * DBLE(INC)
C
      DO 2 K=1, NSAVE
C
         DO 3 KK=1, INC
C
C...        Swap time indexes
            NOW = 1 - NOW
            LAST = 1 - LAST
C
C...        Set up loop for each capacitor.
            DO 3 NC=1 , NCAPS
C
C...           Get x and y coordinates of capacitor
               X = XCAP(NC)
               Y = YCAP(NC)
C
C...           Compute x and y coordinates around it
               XP1 = X + 1
               YP1 = Y + 1
               XM1 = X - 1
               YM1 = Y - 1
C
C...           Calculate pseudo-constant
C
     0         B =  ( QCAP(X,YM1,LAST) * RV(X,YM1) * C(X,YM1) )
     1           +  ( QCAP(XM1,Y,LAST) * RH(XM1,Y) * C(XM1,Y) )
     2           +  ( QCAP(XP1,Y,LAST) * RH(X,Y)   * C(XP1,Y) )
     3           +  ( QCAP(X,YP1,LAST) * RV(X,Y)   * C(X,YP1) )
C
C...           New charge at this step time
C
  3            QCAP(X,Y,NOW) = ( B * CR(NC) * (1.0D+00 - EXC(NC)) )
```

```
     1                        + ( QCAP(X,Y,LAST) * EXC(NC) )
C
C...      Increment time parameter for writing out
          TIME = TIME + TINC
          WRITE (8,IDUB) TIME
C
C...      Write all charges out with implied DO loop
  2       WRITE (8,IDUB) ( QCAP(XCAP(NC),YCAP(NC),NOW), NC=1, NCAPS)
C
       RETURN
C-------------------C
C  Error handling  C
C-------------------C
 1010 WRITE (*,1015) OUTF
 1015 FORMAT (1H1,'ERROR WHILST OPENING ',A31)
       PAUSE
       STOP
       END


       SUBROUTINE READQ(QFILE,TIME)
       COMMON /BLOCK1/ QCAP, C, RH, RV, QBEG
       COMMON /BLOCK2/ NCAPS, XCAP, YCAP, NCOL
       DOUBLE PRECISION QCAP(0:50,0:50,0:1), TIME,
      * C(0:50,0:50), RH(0:50,0:50), RV(0:50,0:50)
       INTEGER XCAP(1:2500), YCAP(1:2500)
       CHARACTER QFILE*12
       INCLUDE 'C:®PROGRAMS®FORTPROG®IBMFIL.INC'
       OUTF = OPATH // QFILE
       CALL DISPLY('READING FROM '// OUTF)
       OPEN (UNIT=9,FILE=OUTF,STATUS='OLD')
       READ (9,*) TIME
       DO 1 I=1, NCAPS
  1     READ (9,*) QCAP(XCAP(I),YCAP(I),0)
       CLOSE (9)
       RETURN
       END


       SUBROUTINE CDETB
C...   Limited cylinder.
       IMPLICIT DOUBLE PRECISION (A - H, O - Z)
       COMMON /BLOCK1/ QCAP,C,RH,RV,QBEG
       COMMON /BLOCK2/ NCAPS,XCAP,YCAP,NCOL
       COMMON /BLOCK3/ INF
       DOUBLE PRECISION QCAP(0:50,0:50,0:1)
      1,RH(0:50,0:50),RV(0:50,0:50),C(0:50,0:50)
      2,VRES(1:50)
       INTEGER XCAP(1:2500),YCAP(1:2500)
      1,XRV(1:2500),XRH(1:2500)
      2,YRV(1:2500),YRH(1:2500)
       INTEGER X,Y
       CHARACTER INF*30,ANS*1
       LOGICAL WRFIL
       PARAMETER (ONE=0.1D+01,ZERO=0.0D+01,DINF=1.0D+40)
       DATA NC,NRV,NRH /0,0,0/
       PI = DACOS(-(ONE))
       WRITE (*,1)
  1    FORMAT (1H ,'NUMBER OF LUMPS IN X DIRECTION ? ')
       READ (*,*) NLX
       WRITE (*,2)
  2    FORMAT (1H ,'NUMBER OF RADIAL LUMPS IN Y (INCLUSIVE OF CORE ? ')
       READ (*,*) NLY
```

```
      BX = DBLE(NLX) * 2.0D+00
      BY = DBLE(NLY)
      WRITE (*,3)
    3 FORMAT (1H ,'LENGTH OF CYLINDER ? ')
      READ (*,*) CLEN
      WRITE (*,4)
    4 FORMAT (1H ,'RADIUS OF CYLINDER ? ')
      READ (*,*) RAD
      WRITE (*,5)
    5 FORMAT (1H ,'DIFFUSION COEFFICIENT OF MATERIAL ? ')
      READ (*,*) DCOEFF
      WRITE (*,6)
    6 FORMAT (1H ,'C FOR EACH COLLECTOR ? ')
      READ (*,*) VOUT
      COUT = ONE / VOUT
      AREA =  PI * (RAD * RAD)
C...  Compute vertica1 resistance from core edge outwards.
      PDC = 0.4D+01 * PI * DCOEFF * CLEN
      DO 12 I=1, NLY-1, 1
         DI = DBLE(I)
         VRES(I) = PDC / (DLOG((DI+5.0D-01)/(DI-5.0D-01))*BX)
   12 CONTINUE
      DI = DBLE(NLY)
      VRES(NLY) = PDC / (DLOG(DI / (DI-5.0D-01)) * BX)
C...  Compute individua1 capacitances.
      CMAT = BY * BX / (AREA * CLEN)
C...  Two types of horizonta1 resitance.
      HRES = DCOEFF * AREA * BX / (CLEN * BY)
      HRFED = HRES * 0.2D+01
      WRITE (*,13)
   13 FORMAT (1H ,'INITIAL MATRIX CHARGE ? ')
      READ (*,*) QBEG
      QZER = QBEG / (BX * BY)
C...  Set up coordinates and capacitances of the
C...  integrab1e capacitors within matrix .
      DO 14 KY=1, NLY
         DO 14 KX=1, NLX
            NC = NC + 1
            XCAP(NC) = KX
            YCAP(NC) = KY
            C(KX,KY) = CMAT
            QCAP(KX,KY,0) = QZER
   14 CONTINUE
      NMAT = NC
C...  Set up for co11ecting capacitors.
      DO 15 KY=1, NLY
         NC = NC + 1
         XCAP(NC) = NLX+1
         YCAP(NC) = KY
         C(NLX+1,KY) = COUT
   15 CONTINUE
      DO 35 KX=1, NLX
         NC = NC + 1
         XCAP(NC) = KX
         YCAP(NC) = NLY + 1
         C(KX,NLY+1) = COUT
   35 CONTINUE
      NCAPS = NC
      NCOL = NC - NMAT
C...  Set up for sources (non-integrab1e), and for
C...  convenience set the charges at this stage to the effort.
      DO 16 KY=1, NLY+1
         NC = NC + 1
```

```
         XCAP(NC) = 0
         YCAP(NC) = KY
         C(0,KY) = ONE
         QCAP(0,KY,0) = ZERO
         QCAP(0,KY,1) = ZERO
 16   CONTINUE
      NSOUR = 0
C...  Set up for reducing flow equation at edges.
      DO 17 KX=1, NLX+1
         NC = NC + 1
         XCAP(NC) = KX
         YCAP(NC) = 0
         C(KX,0) = ONE
         QCAP(KX,0,0) = ZERO
         QCAP(KX,0,1) = ZERO
 17   CONTINUE
      DO 18 KX=1, NLX
         NC = NC + 1
         XCAP(NC) = KX
         YCAP(NC) = NLY + 2
         C(KX,NLY+2) = ONE
         QCAP(KX,NLY+1,0) = ZERO
         QCAP(KX,NLY+1,1) = ZERO
 18   CONTINUE
      DO 19 KY=1, NLY
         NC = NC + 1
         XCAP(NC) = NLX + 2
         YCAP(NC) = KY
         C(NLX+2,KY) = ONE
         QCAP(NLX+2,KY,0) = ZERO
         QCAP(NLX+2,KY,1) = ZERO
 19   CONTINUE
      NC = NC + 1
      XCAP(NC) = NLX + 1
      YCAP(NC) = NLY + 1
      C(NLX+1,NLY+1) = ONE
      QCAP(NLX+1,NLY+1,0) = ZERO
      QCAP(NLX+1,NLY+1,1) = ZERO
      NUMEXTRA = NC - NSOUR - NCAPS
C...  Set up for vertical resistors.
C...  To stop vertical diffusion beyond Y=0.
      DO 20 KX=1, NLX+1
         NRV = NRV + 1
         XRV(NRV) = KX
         YRV(NRV) = 0
         RV(KX,0) = ZERO
 20   CONTINUE
C...  Vertical diffusion within matrix.
      DO 21 KX=1, NLX
         DO 21 KY=1, NLY
            NRV = NRV + 1
            XRV(NRV) = KX
            YRV(NRV) = KY
            RV(KX,KY) = VRES(KY)
 21   CONTINUE
C...  Diffusion vertically between collectors not considered.
C...  For large sinks this is no problem.
      DO 22 KY=1, NLY
         NRV = NRV + 1
         XRV(NRV) = NLX + 1
         YRV(NRV) = KY
         RV(NLX+1,KY) = ZERO
 22   CONTINUE
```

```
C...  Stop diffusion beyond y=NLY+1
      DO 23 KX=1, NLX
         NRV = NRV + 1
         XRV(NRV) = KX
         YRV(NRV) = NLY + 1
         RV(KX,NLY+1) = ZERO
 23   CONTINUE
C...  Now horizontal resistors.
      DO 24 KX=1, NLX-1
         DO 24 KY=1, NLY
            NRH = NRH + 1
            XRH(NRH) = KX
            YRH(NRH) = KY
            RH(KX,KY) = HRES
 24   CONTINUE
C...  Those on horizontal edge
         DO 25 KY=1, NLY
            NRH = NRH + 1
            XRH(NRH) = NLX
            YRH(NRH) = KY
            RH(NLX,KY) = HRFED
 25   CONTINUE
C...  Stop diffusion beyond collectors.
      DO 26 KY=1, NLY
         NRH = NRH + 1
         XRH(NRH) = NLX + 1
         YRH(NRH) = KY
         RH(NLX+1,KY) = ZERO
 26   CONTINUE
C...  No Diffusion from Y=0
      DO 40 KY=1, NLY
         NRH = NRH + 1
         XRH(NRH) = 0
         YRH(NRH) = KY
         RH(0,KY) = ZERO
 40   CONTINUE
C...  Diffusion through collectors on top side
      DO 41 KX=0, NLX
         NRH = NRH + 1
         XRH(NRH) = KX
         YRH(NRH) = NLY + 1
         RH(KX,NLY+1) = ZERO
 41   CONTINUE
      WRITE (*,27)
 27   FORMAT (1H ,'CREATING DETAILS FILE PLEASE WAIT')
      OPEN (UNIT = 7, FILE = INF, ERR = 1000
     *, STATUS = 'NEW' )
 28   WRITE (7,*) NLX
      WRITE (7,*) NLY
      WRITE (7,*) CLEN
      WRITE (7,*) AREA
      WRITE (7,*) RAD
      WRITE (7,*) DCOEFF
      WRITE (7,*) SOLUB
      WRITE (7,*) COUT
      WRITE (7,*) NMAT
      WRITE (7,*) NCOL
 36   DO 29 NC=1, NCAPS
         X = XCAP(NC)
         Y = YCAP(NC)
         WRITE (7,*) XCAP(NC)
         WRITE (7,*) YCAP(NC)
 29      WRITE (7,*) ONE / C(X,Y)
```

```
      WRITE (7,*) NRH
      DO 30 N=1, NRH
         X = XRH(N)
         Y = YRH(N)
         WRITE (7,*) XRH(N)
         WRITE (7,*) YRH(N)
         IF (RH(X,Y).GT.ZERO) THEN
          WRITE (7,*) ONE / RH(X,Y)
         ELSE
          WRITE (7,*) DINF
         END IF
30    CONTINUE
      WRITE (7,*) NRV
      DO 31 N=1, NRV
         X = XRV(N)
         Y = YRV(N)
         WRITE (7,*) XRV(N)
         WRITE (7,*) YRV(N)
         IF (RV(X,Y).GT.ZERO) THEN
          WRITE (7,*) ONE / RV(X,Y)
         ELSE
          WRITE (7,*) DINF
         END IF
31    CONTINUE
      WRITE (7,*) NSOUR
      DO 32 N=NCAPS+1, NCAPS+NSOUR
         WRITE (7,*) XCAP(N)
         WRITE (7,*) YCAP(N)
32    CONTINUE
      WRITE (7,*) NUMEXTRA
      DO 33 M=N, N+NUMEXTRA-1
         WRITE (7,*) XCAP(M)
         WRITE (7,*) YCAP(M)
33    CONTINUE
      CLOSE (UNIT = 7, STATUS = 'KEEP')
      RETURN
1000  WRITE (*,1005) INF
1005  FORMAT (1H1,'WARNING ',A30,' EXISTS ALREADY')
1013  WRITE (*,1010)
1010  FORMAT (1H ,'WRITE OVER (Y/N) ? ')
      READ (*,10) ANS
 10   FORMAT (A1)
      IF (ANS.EQ.'Y'.OR.ANS.EQ.'y') THEN
         OPEN (UNIT = 7, FILE = INF)
         GOTO 28
      ELSE IF (ANS.EQ.'N'.OR.ANS.EQ.'n') THEN
         RETURN
      ELSE
         GOTO 1013
      END IF
      END
```

A.4 Subroutine for integration of three dimensional state-space equation.

```
      SUBROUTINE THRMAT(TIME,NST,H,INC,OUTF)
C...  (Records total collecting charge)
C...  Three D reciprocal R, C values required
C...  Non-zero flows only are considered
      IMPLICIT DOUBLE PRECISION (A - H, O - Z)
      COMMON /BLOCK1/ QCAP,C,RX,RY,RZ,SEFF
      COMMON /BLOCK2/ NCAPS,XCAP,YCAP,ZCAP,NCOL
      COMMON /BLOCK3/ INF
      DOUBLE PRECISION QCAP(0:12,0:12,0:12,0:1),CR(1:1331)
     1,RX(0:12,0:12,0:12),RY(0:12,0:12,0:12),C(0:12,0:12,0:12)
     2,RZ(0:12,0:12,0:12)
      INTEGER XCAP(1:1331),YCAP(1:1331),ZCAP(1:1331)
      INTEGER X,Y,Z
      CHARACTER OUTF*31
      CHARACTER INF*30
      PARAMETER (ZERO=0.0D+01)
C
   10 FORMAT (1PD25.17)
   11 FORMAT (I11)
   12 FORMAT (A30)
      ASSIGN 10 TO IDUB
      ASSIGN 11 TO ITGR
      PER = ZERO
      NEDGE = 0
      OPEN (UNIT = 8, FILE = OUTF, ERR = 1010)
      WRITE (8,12) INF
      WRITE (8,ITGR) NST
      WRITE (8,IDUB) H
      WRITE (8,ITGR) INC
      WRITE (8,IDUB) SEFF
      WRITE (8,IDUB) PER
      WRITE (8,ITGR) NEDGE
      DATA NOW,LAST,FSIGN /0,1,1.0D+00/
      NCMC = NCAPS - NCOL
      NSAVE = NST / INC
C
C...  Work out the CR coefficients which are (here)
C...  time independant.
      DO 20 NC=1, NCAPS
        X = XCAP(NC)
        Y = YCAP(NC)
        Z = ZCAP(NC)
        CR(NC) = (RY(X,Y-1,Z) * C(X,Y,Z))
     1  + (RX(X-1,Y,Z) * C(X,Y,Z)) + (RX(X,Y,Z) * C(X,Y,Z))
     2  + (RY(X,Y,Z) * C(X,Y,Z)) + (RZ(X,Y,Z) * C(X,Y,Z))
     3  + (RZ(X,Y,Z-1) * C(X,Y,Z))
 20   CONTINUE
C...  Set up loop for each step time.
      DO 6 KK=1, NSAVE
        DO 2 K=1, INC
C...      Increment time for new loop.
          TIME = TIME + H
C...      Exchange the values of NOW and LAST
          NCH = NOW
          NOW = LAST
          LAST = NCH
C...      Set up loop for each capacitor.
          DO 2 NC=1 , NCAPS
            X = XCAP(NC)
            Y = YCAP(NC)
```

```
            Z = ZCAP(NC)
C...        Calculate the constants QCR in the
C...        ordinary first-order differential equation .
            QCR = ( QCAP(X,Y-1,Z,LAST) * RY(X,Y-1,Z) * C(X,Y-1,Z) )
     1      + ( QCAP(X-1,Y,Z,LAST) * RX(X-1,Y,Z) * C(X-1,Y,Z) )
     2      + ( QCAP(X,Y,Z-1,LAST) * RZ(X,Y,Z-1) * C(X,Y,Z-1) )
     3      + ( QCAP(X+1,Y,Z,LAST) * RX(X,Y,Z) * C(X+1,Y,Z) )
     3      + ( QCAP(X,Y+1,Z,LAST) * RY(X,Y,Z) * C(X,Y+1,Z) )
     4      + ( QCAP(X,Y,Z+1,LAST) * RZ(X,Y,Z) * C(X,Y,Z+1) )
C...        Calculate the flow at time T .
            FLOWT = QCR - (QCAP(X,Y,Z,LAST) * CR(NC))
C...        Record the sign of flow at time T .
            FSIGN = SIGN (FSIGN,FLOWT)
            FLOWT = ABS(FLOWT)
C...        Full Differential equation applies .
            FNEW = SIGN((FLOWT * EXP(-H*CR(NC))), FSIGN)
  2         QCAP(X,Y,Z,NOW) = (QCR - FNEW) / CR(NC)
C...     Save on file
         Q = ZERO
         DO 5 NC=NCMC+1, NCAPS
           X = XCAP(NC)
           Y = YCAP(NC)
           Z = ZCAP(NC)
  5        Q = Q + QCAP(X,Y,Z,NOW)
         WRITE (8,IDUB) TIME
  6      WRITE (8,IDUB) Q
       RETURN
 1010  WRITE (*,1015) OUTF
 1015  FORMAT (1H1,'ERROR WHILST OPENING ',A31)
       PAUSE
       STOP
       END
```